Regional Geoid Modelling by the Least Squares Modified Hotine Formula Using Gridded Gravity Disturbances

SILJA MÄRDLA

TTÜ
PRESS

TALLINN UNIVERSITY OF TECHNOLOGY
School of Engineering
Department of Civil Engineering and Architecture
Road Engineering and Geodesy Research Group

This thesis was accepted for the defence of the degree of Doctor of Philosophy in Engineering on November 17, 2017.

Supervisor: Prof. Artu Ellmann
                    Road Engineering and Geodesy Research Group,
                    Tallinn University of Technology, Estonia

Opponents: Prof. Martin Vermeer
                    Department of Built Environment, Aalto University, Finland

                    Prof. Riccardo Barzaghi
                    Department of Civil and Environmental Engineering,
                    Politecnico di Milano, Italy

Defense of the thesis: December 13, 2017 at 12:30 in room NRG-226

Declaration:

Hereby I declare that this doctoral thesis, my original investigation and achievement, submitted for the doctoral degree at Tallinn University of Technology has not earlier been submitted for doctoral or equivalent academic degree.

Silja Märdla

Piirkondlik geoidi modelleerimine vähimruutude meetodil modifitseeritud Hotine valemiga kasutades võrgustatud raskuskiirenduse hälbeid

SILJA MÄRDLA

TTÜ
KIRJASTUS

Table of Contents

Abstract

A geoid model serves as a conversion surface between conventional sea level referred heights and modern GNSS-derived geodetic heights that are referred to the Earth ellipsoid. A regional geoid model is commonly computed by the modified Stokes formula from gridded gravity anomalies and its accuracy evaluated by comparison to co-located GNSS/levelling points.

This thesis investigates preparation of gravity grids, geoid modelling by the alternative Hotine formula and geoid model validation in marine areas. All the case studies concern the Nordic-Baltic region in Europe, while the findings are applicable in any regional geoid modelling task elsewhere.

Despite satellite derived gravity field products being available globally, continuous efforts to improve and revise terrestrial gravity data are able to improve regional geoid models in the order of centimetres, especially in coastal areas.

Gravity grids can be computed from irregularly spaced point data by the remove-interpolate-restore process. For the remove step, gravity reduction to Complete Bouguer Anomalies and Residual Terrain Model Anomalies are compared. Although the residual gravity field properties are found to be rather different, the resulting gravity grids are numerically similar. Triangulation, nearest neighbour, spline based and statistical (Least Squares Collocation and Kriging) interpolation methods are compared to investigate their suitability for gravity gridding. It is found that in case of inaccurate data, steep gradients and data gaps, statistical interpolation can provide the most realistic representation of the gravity field while spline based methods are to be avoided.

Equations are derived for the least squares modification of Hotine's formula and the corresponding additive corrections. The expressions and resulting geoid models are compared to the traditional Stokes counterparts. Although numerical results are similar, the benefit of using the Hotine formula lies in its use of gravity disturbances as input.

Marine geoid validation by GNSS positioning on the sea (ice) is described, tested and found to be usable at the 5 to 10 cm geoid model accuracy level. *In situ* GNSS positioning is also shown to be useful for sea surface topography determination.

The findings of this thesis contribute toward improvement in regional geoid modelling accuracy.

Keywords: *gravity, disturbance, gridding, geoid, Hotine, least squares modification, additive corrections, LSMHA*

Märdla, S. (2017) **Piirkondlik geoidi modelleerimine vähimruutude meetodil modifitseeritud Hotine valemiga kasutades võrgustatud raskuskiirenduse hälbeid**. Doktoritöö, Tallinna Tehnikaülikool.

Kokkuvõte

Geoidi mudeli abil saab teisendada tänapäevaseid Maa ellipsoidi suhtes mõõdetud geodeetilisi kõrgusi klassikalisteks merepinnast lähtuvateks kõrgusteks ja vastupidi. Tavaliselt arvutatakse piirkondlik geoidi mudel modifitseeritud Stokes'i valemi abil võrgustatud raskuskiirenduse anomaaliatest ning selle täpsust hinnatakse võrdluses GNSS/nivelleerimispunktidega.

Väitekiri uurib raskuskiirenduse võrgustike arvutamist, alternatiivse Hotine valemi abil geoidi modelleerimist ja geoidimudeli täpsuse hindamist merealadel. Kõik empiirilised uuringud on tehtud Põhja- ja Baltimaade piirkonnas, samas on tulemused rakendatavad geoidi modelleerimisülesannetele ka mujal.

Hoolimata sellest, et satelliitmõõdistused pakuvad globaalset raskuskiirenduse andmestikku, on maapealsete raskuskiirenduse andmete täiendamise ja revideerimise abil siiski võimalik piirkondlikke geoidimudeleid mitmete sentimeetrite võrra täpsustada, seda eriti rannikualadel.

Raskuskiirenduse võrgustikke saab ebakorrapäraselt paigutatud punktadmetest arvutada eemalda-interpoleeri-taasta (*remove-interpolate-restore*) protsessi abil. Võrreldakse reljeefiparandiga Bouguer anomaaliate (*Complete Bouguer Anomaly*) ja jääkpinnamudeli anomaaliate (*Residual Terrain Model Anomaly*) kasutamist eemalda-etapis. Kuigi jääkanomaaliaväljade omadused osutuvad üpris erinevaks, on saadud raskuskiirenduse võrgustikud numbriliselt sarnased. Võrreldakse ka triangulatsiooni, lähima naabri, splainipõhiseid ja statistilisi (vähimruutude kollokatsioon ja Kriging) interpoleerimismeetodeid, et uurida nende sobivust raskuskiirenduse andmete võrgustamiseks. Leitakse, et ebatäpsete andmete, järskude kallete ja andmelünkade korral võib kõige realistlikuma raskuskiirenduse välja mudeli saada statistilise interpoleerimise abil ning vältida tuleb splainipõhiseid meetodeid.

Tuletatakse valemid vähimruutude meetodil Hotine valemi modifitseerimiseks ning vastavate summeeritavate parandite arvutuseks. Valemeid ja neist arvutatud geoidimudeleid võrreldakse klassikaliste Stokes'i ekvivalentidega. Kuigi numbrilised tulemused on sarnased, räägib Hotine valemi kasuks raskuskiirenduse hälvete kasutamine sisendina.

Kirjeldatakse ja katsetatakse meregeoidi kontrollimist mere(jää)l tehtud GNSS mõõdistuse abil. Meetod osutub kasutatavaks 5-10 cm täpsusega geoidi kontrollimiseks. Samuti osutub merepinna GNSS mõõdistus kasutatavaks merepinna topograafia määramiseks.

Käesoleva doktoritöö tulemused aitavad kaasa piirkondliku geoidi modelleerimise täpsuse paranemisele.

Märksõnad: *raskuskiirendus, hälve, võrgustamine, geoid, Hotine, vähimruutude meetodil modifitseerimine, summeeritavad parandid, LSMHA*

Acknowledgements

First of all, I would like to thank my supervisor Artu Ellmann for offering me the opportunity to dive into the academic world, for guiding and pushing me through the first five years of this experience. From the very beginning he has taught me to document all my work in publications. He has encouraged me to participate in conferences and meetings, never without a presentation of course. And he has worked hard to ensure financial support throughout my studies. Not to mention the countless hours spent on reviewing and helping on my work.

Second, I am extremely grateful for my unofficial supervisors Jonas Ågren and Tõnis Oja.

Jonas shared his knowledge and work on practical geoid modelling that is poured into Fortran programs and Shell scripts, carefully explaining every little detail on the way. Knowing well that more questions will arise and arrive by e-mail. He has often taken the time to explain basic book knowledge in simple words, over and over again, until I seem to understand.

Tõnis has taken me on fun field trips, introduced me to gravity data processing, dragged me into using GMT (a script based mapping tool) and LaTeX (a method of text processing) that make scientific work so easy and difficult at once. He has taught me to try, tune and compare a load of options available before selecting a specific method or parameter.

Third, the NKG community as a whole has offered me support and inspiration. From day one I was accepted as part of it, the only question after my first presentation was: "Will we be seeing more of you?" Many thanks to Gabriel Strykowski, Rene Forsberg, Mirjam Bilker-Koivula, Harli Jürgenson and others for this.

Last but not least, I am grateful for my family and friends for supporting me in my PhD studies. My husband Mikk has taken care of our kids, listened to the keyboard clicking and my complaining. My mother has reminded me that good science needs to fit on five pages. My friends politely smile and nod when they listen to my answers about the topic and progress of my PhD.

Silja Märdla
November, 2017

DAR9085
- the European Commission (EC) Lifelong Learning programme Erasmus
- the Nordplus framework programme AGES "Access to Geodetic Education for Society"
- OÜ Geosoft and Trimble Inc.
- The Estonian Union of Geodesists

The figures of this thesis and constituting papers have been generated by the free and open source Generic Mapping Tools (Wessel et al. 2013) and Autodesk AutoCad (Autodesk Inc. 2017) using a student license.

Abbreviations

The following abbreviations are used in the thesis:

ARP - Antenna Reference Point
BIM - Building Information Model
BLS - Biased Least Squares
BSCD - Baltic Sea Chart Datum
BVP - Boundary Value Problem
CBA - Complete Bouguer Anomaly
d/o - degree and order
DTM - Digital Terrain Model
EGD - Estonia Gravity Database
EGG - European Gravimetric Geoid
EGS - Estonian Geological Survey
ETRF - European Terrestrial Reference Frame
EVRF - European Vertical Reference Frame
EVRS - European Vertical Reference System
FAMOS - Finalising Surveys for the Baltic Motorways of the Sea
GEOMED - Geoid Estimation in the Mediterranean Area
GGM - Global Geopotential Model
GMT - Generic Mapping Tools
GoF - Gulf of Finland
GNSS - Global Navigation Satellites System
IFB - Ice Freeboard
IMU - Inertial Measurement Unit
ISL - Instantaneous Sea Level
KTH - KTH Royal Institute of Technology (Kungliga Tekniska Högskolan)
LS - Least Squares
LSC - Least Squares Collocation
LSMHA - Least Squares Modification of Hotine's Formula with Additive corrections
LSMSA - Least Squares Modification of Stokes's Formula with Additive corrections
LVD - Local Vertical Datum
MES - Mean Earth Sphere
MSE - Mean Square Error
MSS - Mean Sea Surface
NKG - Nordic Geodetic Commission (Nordiska Kommissionen för Geodesi)
NVD - National Vertical Datum
OLS - Optimum Least Squares
RCR - Remove-Compute-Restore
RIR - Remove-Interpolate-Restore

RMS - Root Mean Square
RTM - Residual Terrain Model
RTMA - Residual Terrain Model Anomaly
SST - Sea Surface Topography
SD - Standard Deviation
ULS - Unbiased Least Squares
WG - Wong & Gore

Symbols

The symbols used in the thesis include (references to pages containing their defining equations are given in parenthesis):

a	semi-major axis of the Earth ellipsoid
a_{kr}	coefficients of the linear system of equations constructed for the determination of modification parameters s_n (p. 56)
b_n^*	augmented modification parameters b_n (p. 55)
c	scale coefficient (p. 55)
c_n^2	gravity signal degree variances
dc_n^2	GGM error degree variances
h	geodetic height
h_{kr}	coefficients of the linear system of equations constructed for the determination of modification parameters s_n (p. 56)
h_{ARP}	ellipsoidal height of the antenna reference point
h_{ISL}	ellipsoidal height of the instantaneous sea level (p. 82)
h_{MSS}	ellipsoidal height of the mean sea surface (p. 82)
n	spherical harmonic degree
m	spherical harmonic order
p_n	coefficient related to σ_n^2 (p. 54)
r	geocentric radius
s_n^*	augmented modification parameters s_n
C_n	coefficient related to gravity signal and error degree variances (p. 56)
C_{nm}	spherical harmonic coefficient
E_{nk}	function of the limiting radius ψ_0 (p. 54)
G	gravitational constant
GM	gravitational mass constant
L	modification limit
M	maximum limit for the use of GGM
H	levelled height
H^{N}	normal height (p. 22)
H^{O}	orthometric height (p. 22)

H_{ARP}	antenna reference point height
H_{IFB}	ice freeboard height
H_{ISL}	instantaneous sea level height
H_{SST}	sea surface topography height (p. 83)
$H(\psi)$	the Hotine function (p. 25, 54, 72)
$H^L(\psi)$	the modified Hotine function (p. 54)
N	geoid height (p. 24, 25, 54)
$\widetilde{N}$	approximate geoid (p. 24, 53, 54)
$\widehat{N}$	geoid estimator (p. 51, 57)
N_{GNSS}	GNSS derived geoid height (p. 82)
N_{GR}	gravimetric geoid height
$P_n(\cos \psi)$	Legendre polynomials of spherical harmonic degree n
Q_n	unmodified truncation coefficients (p. 54)
Q_n^L	modified truncation coefficients (p. 54)
R	mean Earth radius
R_{nk}	function of the limiting radius ψ_0 (p. 54)
$S(\psi)$	the Stokes function (p. 24, 54)
$S^L(\psi)$	the modified Stokes function (p. 54)
Y_{nm}	fully normalized spherical harmonic
γ	normal gravity at the ellipsoid
δ_{kr}	Kronecker delta (p. 56)
δg	gravity disturbance (p. 25)
δg^{BP}	gravitational effect of the Bouguer plate
δg_n^{GGM}	GGM-derived Laplace harmonics of gravity disturbance
δg^{RTM}	RTM correction
δg^{TC}	terrain correction
$\left(\delta\widetilde{N}\right)^2$	expected global mean square error of the geoid estimator $\widetilde{N}$ (p. 55)
$\left(\delta\widetilde{N}\right)^2_{\text{GGM}}$	expected global mean square error of the geoid estimator $\widetilde{N}$ due to GGM errors (p. 55)
$\left(\delta\widetilde{N}\right)^2_{\text{T}}$	expected global mean square error of the geoid estimator $\widetilde{N}$ due to terrestrial gravity data errors (p. 55)
$\left(\delta\widetilde{N}\right)^2_{\text{TR}}$	expected global mean square error of the geoid estimator $\widetilde{N}$ due to truncation (p. 55)
δN_{ATM}	combined atmospheric correction for a geoid model (p. 58)
δN_{COMB}	combined topographic correction for a geoid model (p. 57)
δN_{DWC}	combined downward continuation correction for a geoid model (p. 57)
δN_{ELL}	combined ellipsoidal correction for a geoid model (p. 58)
$\delta\zeta_{\text{ATM}}$	combined atmospheric correction for a quasigeoid model (p. 58)

$\delta\zeta_{\text{DWC}}$	combined downward continuation correction for a quasigeoid model (p. 57)
$\delta\zeta_{\text{ELL}}$	combined ellipsoidal correction for a quasigeoid model (p. 58)
Δg	gravity anomaly (p. 24)
Δg^{CBA}	Complete Bouguer Anomaly
Δg^{GGM}	GGM-derived gravity anomaly
Δg_n^{GGM}	GGM-derived Laplace harmonics of gravity anomaly
Δg^{RTMA}	Residual Terrain Model anomaly (p. 38)
ζ	quasigeoid height / height anomaly (p. 22)
$\widehat{\zeta}$	quasigeoid estimator (p. 52, 57)
ζ^0	approximate value for height anomaly
θ	geocentric co-latitude
λ	geocentric longitude
ρ	topographic density
ρ_{A}	atmospheric density
σ	unit sphere
σ_0	spherical cap
σ_n^2	terrestrial gravity error degree variances
ψ	spherical distance between computation and integration points
ψ_0	spherical distance corresponding to the cap size σ_0

List of publications

The following peer reviewed papers (indexed by the Scopus database), presented here to fulfil the requirements for the PhD degree of Tallinn University of Technology, are an inseparable part of this thesis:

Paper A Märdla, S., Ellmann, A., Ågren, J., and Sjöberg, L. E. (2017). Regional Geoid Computation by Least Squares Modified Hotine's Formula with Additive Corrections. *Journal of Geodesy*, pp 1-18. DOI: 10.1007/s00190-017-1061-7.

Paper B Märdla, S., Ågren, J., Strykowski, G., Oja, T., Ellmann, A., Forsberg, R., Bilker-Koivula, M., Omang, O., Paršeliūnas, E., Liepinš, I., and Kaminskis, J. (2017). From Discrete Gravity Survey Data to a High-Resolution Gravity Field Representation in the Nordic-Baltic Region. *Marine Geodesy* 40(6), pp. 416-453. DOI: 10.1080/01490419.2017.1326428.

Paper C Märdla, S., Ellmann, A., Oja, T., and Jürgenson, H. (2015). Improving and Validating Gravity Data Over Ice-Covered Marine Areas. In: *IAG 150 Years: Proceedings of the 2013 IAG Scientific Assembly, Potsdam, Germany, 1-6 September, 2013.* Ed. by C. Rizos and P. Willis. International Association of Geodesy Symposia 143. Potsdam, Germany: Springer International Publishing, pp. 263-270. ISBN: 978-3-319-24603-1. DOI: 10.1007/1345_2015_163.

Paper D Märdla, S., Oja, T., Ellmann, A., and Jürgenson, H. (2014). Modelling the Influence of Terraced Landforms to the Earth's Gravity Field. In: *Gravity, Geoid and Height Systems.* Ed. by U. Marti. International Association of Geodesy Symposia 141. Venice, Italy: Springer International Publishing, pp. 157-162. ISBN: 978-3-319-10836-0. DOI: 10.1007/978-3-319-10837-7_20.

Paper E Liibusk, A., Talvik, S., Ellmann, A., and Oja, T. (2014). Determining Regional Sea Surface Topography by GNSS Surveys on Ice. In: *Proceedings of the IEEE/OES Baltic International Symposium, May 27-29.* Tallinn, Estonia, pp. 1-9. DOI: 10.1109/BALTIC.2014.6887847.

Author's contribution to the publications

The author of this thesis contributed to the publications listed by:

Paper A deriving the majority of the equations presented; conducting the case study (using modified Fortran programs and Shell scripts originally developed by Dr. Jonas Ågren); performing the analysis and writing the manuscript in cooperation with all the co-authors. The idea for developing the LSMHA procedure presented was proposed by the supervisor Prof. Artu Ellmann.

Paper B assisting Dr. Gabriel Strykowski, Dr. Jonas Ågren and MSc. Tõnis Oja to prepare and analyse the NKG gravity database; collecting the methods of gravity reduction and interpolation previously used by co-authors, mainly by Dr. Jonas Ågren and MSc. Tõnis Oja; varying their computation parameters and testing these in a special case study; analysing the results and writing the manuscript in cooperation with all the co-authors, especially with Prof. Artu Ellmann, Dr. Jonas Ågren and MSc. Tõnis Oja.

Paper C participating in field work organized by MSc. Tõnis Oja; processing GNSS data; analysing the results; composing the publication in cooperation with all the co-authors. The idea of using GNSS positioning of gravity data for geoid validation was proposed by the supervisor prof. Artu Ellmann. Gravity data was processed by MSc. Tõnis Oja.

Paper D testing the methods suggested by MSc. Tõnis Oja; analysing the results and composing the publication in cooperation with all the co-authors.

Paper E processing the GNSS data for the point-wise survey; analysing and comparing the SST surfaces; contributing to parts of the manuscript text. The GNSS profiles were processed and final surface comparisons made by Dr. Aive Liibusk.

Relevant presentations in international conferences

Additional reading to the academic publications listed above is offered by the following presentations in international conferences, referred to by their bold Roman numerals:

I   Märdla, S., Ellmann, A., Ågren, J., and Sjöberg, L. E. (2017). Regional Geoid Computation by Least Squares Modified Hotine's Formula with Additive Corrections. In: *Joint Scientific Assembly of the International Association of Geodesy (IAG) and International Association of Seismology and Physics of the Earth's Interior (IASPEI), July 30 to August 4.* Kobe, Japan. DOI: 10.13140/RG.2.2.29154.63682.

II   Ågren, J., Schwabe, J., Strykowski, G., Forsberg, R., Liebsch, G., Förste, C., Barthelmes, F., Bilker-Koivula, M., Ellmann, A., and Märdla, S. (2017). Overview of the FAMOS Efforts to Improve the Baltic Sea Geoid Model by New Marine Gravity Measurements. In: *Joint Scientific Assembly of the International Association of Geodesy (IAG) and International Association of Seismology and Physics of the Earth's Interior (IASPEI), July 30 to August 4.* Kobe, Japan. DOI: 10.13140/RG.2.2.34378.67521.

III   Varbla, S., Ellmann, A., Märdla, S., and Gruno, A. (2017). Assessment of Marine Geoid Models by Ship-Borne GNSS Profiles. In: *The 10th International Conference "Environmental Engineering", April 27-28.* Vilnius, Lithuania. DOI: 10.13140/RG.2.2.32537.11365.

IV   Ågren, J., Strykowski, G., Bilker-Koivula, M., Omang, O., Märdla, S., Forsberg, R., Ellmann, A., Oja, T., Liepinš, I., Paršeliūnas, E., Kaminskis, J., Sjöberg, L. E., and Valsson, G. (2016). The NKG2015 Gravimetric Geoid Model for the Nordic-Baltic Region. In: *1st Joint Commission 2 and IGFS Meeting International Symposium on Gravity, Geoid and Height Systems, 19-23 September* Thessaloniki, Greece. DOI: 10.13140/RG.2.2.20765.20969.

V   Märdla, S., Ågren, J., Strykowski, G., Oja, T., Ellmann, A., Forsberg, R., Bilker-Koivula, M., Omang, O., Paršeliūnas, E., Liepinš, I., Kaminskis, J., and Sjöberg, L. E. (2016). From Discrete Gravity Survey Data to a High-Resolution Gravity Field Representation in the Nordic-Baltic Region. In: *1st Joint Commission 2 and IGFS Meeting International Symposium on Gravity, Geoid and Height Systems, 19-23 September.* Thessaloniki, Greece. DOI: 10.13140/RG.2.2.31906.32967.

VI   Ågren, J., Strykowski, G., Bilker-Koivula, M., Omang, O., Märdla, S., Oja, T., Liepiņš, I., Paršeliūnas, E., Forsberg, R., Kaminskis, J., Ellmann, A., Sjöberg, L., and Valsson, V. (2015). On the Development of the New Nordic Gravimetric Geoid Model NKG2015. In: *26th International Union of Geodesy and Geophysics (IUGG) General Assembly, June 22-July 02.* Prague, Czech Republic. DOI: 10.13140/RG.2.2.14121.49761.

VII   Märdla, S., Ellmann, A., Oja, T., and Ågren, J. (2015). Improving Regional Gravity Field and Geoid Modelling by Various Use of Global Geopotential Models. In: *26th International Union of Geodesy and Geophysics (IUGG) General Assembly, June 22- July 02.* Prague, Czech Republic. DOI: 10.13140/RG.2.2.25398.60481.

VIII   Märdla, S., Oja, T., and Ellmann, A. (2014). Investigations towards the NKG2014 Geoid Model in Estonia. In: *Nordic Geodetic Commission (NKG) General Assembly, September 1-5.* Gothenburg, Sweden. DOI: 10.13140/RG.2.2.34232.85766.

IX   Talvik, S., Ellmann, A., Oja, T., and Jürgenson, H. (2014). Analysing Methods of Detailed Gravity Field Modelling from Terrestrial Data. In: *European Geosciences Union (EGU) General Assembly, April 27 to May 2.* Vienna, Austria. DOI: 10.13140/RG.2.2.28813.03047.

X   Talvik, S., Ellmann, A., Oja, T., and Jürgenson, H. (2014). Analysing Methods of Detailed Gravity Field Modelling from Terrestrial Data. In: *European Geosciences Union (EGU) General Assembly, April 27 to May 2.* Vienna, Austria. DOI: 10.13140/RG.2.2.12035.81448.

XI   Oja, T. and Talvik, S. (2014). Estonian Gravity Data. In: *Nordic Geodetic Commission (NKG) Working Group of Geoid and Height Systems meeting, March 11-12.* Gävle, Sweden. DOI: 10.13140/RG.2.2.10744.75521.

XII   Oja, T., Bloom, A., Talvik, S., Jürgenson, H., and Ellmann, A. (2013). Relative Gravity Measurements on Ice-Covered Water Bodies. In: *International Association of Geodesy (IAG) Scientific Assembly, September 1-6.* Potsdam, Germany. DOI: 10.13140/RG.2.2.27974.16965.

XIII   Talvik, S., Oja, T., Jürgenson, H., Ellmann, A., and Bloom, A. (2013). Gravity Data in Estonia. In: *Nordic Geodetic Commission (NKG) Science Week, March 12-14.* Reykjavik, Iceland. DOI: 10.13140/RG.2.2.23937.15204.

XIV   Talvik, S., Oja, T., Ellmann, A., and Jürgenson, H. (2012). Modelling the Influence of Terraced Landforms to the Earth's Gravity Field. In: *International Symposium on Gravity, Geoid and Height Systems, October 9-12.* Venice, Italy. DOI: 10.13140/RG.2.2.15967.97444.

1   Introduction

1.1   Geoid model and its purpose

Geoid is an equipotential surface of the Earth's gravity field, best reflected in the nature by the ocean surface. Due to the Earth's rotation and inhomogeneities in its masses, the geoid is irregular. Its shape is described by its height N with respect to a global reference ellipsoid, nowadays the GRS-80 (Moritz 2000). Geoid heights N vary in the range of $\pm 100\,\text{m}$ globally, from 15 to 50 m in the Nordic-Baltic region and from 16 to 21 m in Estonia.

The geoid height can be determined from measurements of gravity acceleration on the Earth. To obtain a global coverage of gravity surveys, dedicated satellite missions such as CHAMP (Reigber et al. 2002), GRACE (Tapley et al. 2004) and GOCE (Drinkwater et al. 2003) have been conducted. As a result, series of global geoid models have been computed and made available in e.g. Barthelmes and Köhler (2016). These are accurate to the level of 1 to 2 cm at spectral resolutions of about 100 km (Denker 2013). However, high-resolution (in the order of 1 km) geoid models are needed for practical applications.

To compute high-resolution geoid models, the satellite derived gravity data need to be augmented by accurate and densely acquired terrestrial gravity data. Due to global (un)availability of terrestrial data and the computational burden, such geoid models only cover a specific area of interest. These regional geoid models can have resolutions down to about a kilometre. The scientific community has presently set the goal for high-resolution geoid modelling accuracy at the 5 to 10 mm level (e.g. Ågren and Sjöberg 2014). However, the current accuracy of regional geoid models is at the 1 to 10 cm level or worse due to insufficient gravity data coverage or complicated geoid modelling conditions (i.e. rough terrain). See e.g. Featherstone et al. (2010), Abbak et al. (2012), and Wang et al. (2017) for examples of geoid modelling accuracy achieved in different parts of the world.

A geoid model and its temporal variations allow to study and explain various natural phenomena such as the internal structure of the Earth and continuous physical processes like hydrological mass variations, ice melt in Greenland or Antarctica, isostasy, postglacial rebound, etc.

Besides containing information on the Earth's structure and geodynamic processes, geoid models have a very practical purpose, see Fig. 1. Knowing the geoid height N, it is possible to convert modern GNSS (Global Navigation Satellites System) derived geodetic heights h referring to the ellipsoid to conventional sea level referred (orthometric) heights H^{O} by:

$$H^{\text{O}} = h - N \tag{1}$$

Sea level referred heights (often used for the national vertical datum) are customarily obtained by levelling, which is labour intensive. Using GNSS po-
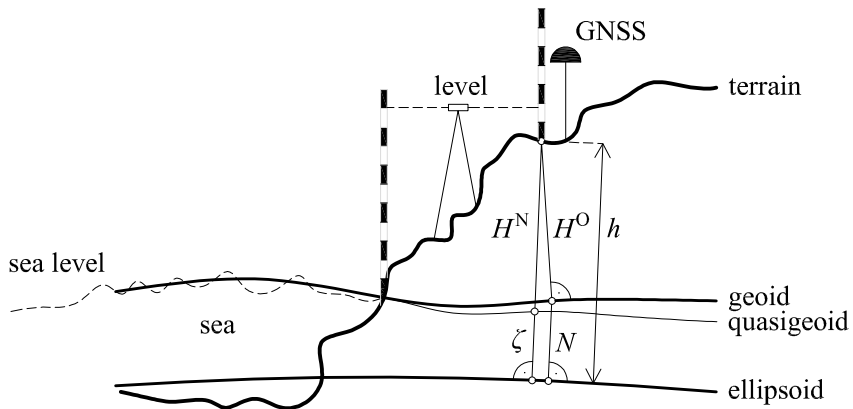
Figure 1: Height reference surfaces

sitioning for heighting is time and labour efficient. The latter also requires non-sophisticated expertise from the user.

The current geoid modelling accuracy of 1 to 10 cm is largely sufficient for the purposes of height conversion in hand-held GNSS devices and some land survey-ing purposes, such as measurements in open mines, soil volume determination, cadastral surveys, some construction surveys etc. However, geodetic GNSS re-ceivers and processing algorithms have potential for height determination at the cm level accuracy. Hence the current target of 5 to 10 mm in geoid modelling accuracy which would be able to support high precision GNSS positioning.

With increasing use of GNSS, the modern solution (used in e.g. Canada, see Véronneau and Huang 2016) to the problem of height conversion to and from conventional sea level referred height values is to discard the nationwide geodetic levelling network that needs maintenance and establish a geoid based national height system. Such a decision again clearly sets high accuracy requirements on geoid modelling.

Admittedly, GNSS itself may lack the required accuracy due to physical lim-itations (atmosphere, signal reflections from surrounding obstacles, mechanical constraints in antenna and clock construction, etc.) and data processing methods that attempt to consider the physical problems (combination of different frequen-cies, use of reference stations etc.), for an overview see e.g. Langley et al. (2017). Nevertheless, GNSS as a system is also constantly improving.

Accurate height values are important not only to geodesists actually determin-ing these, but also to the society. The design, construction and exploitation of the built environment largely relies on the correct locations of its parts. Buildings, roads, bridges and technical utilities need to fit together with each other and the surrounding landscape, especially when it comes to discharging liquids (drains, sewage). Therefore, a large part of engineering tasks depend on exact height de-termination.

Although for now, most specialised construction surveys remain a task for conventional geodetic tools, GNSS is often used for establishing local reference networks. Existence of an accurate geoid model allows to discard conventional resource demanding geodetic traverses that are necessary for the establishment of a local reference network at a construction site. Use of GNSS speeds up the work of a geodesist, thus reducing the fraction of construction funds spent on geodesy. Such solutions for geodetic engineering tasks are especially beneficial for the construction and maintenance of nation-wide objects such as roads, railways, technical utility networks, communication cables etc.

There is an increasing trend of digitizing construction modelling through BIM (Building Information Model), requiring more and more surveying based input (the geometric properties of the objects), thus increasing the demand for accurate, yet fast, positioning by GNSS methods.

Also, topographic surveying at the construction design stage could entirely be based on GNSS technology, at least in the open field. With the development of technology and increased speed of measurements, larger areas could be covered with accurate positioning data.

In addition to the construction sector, the shipping industry is also a large user of accurate GNSS positioning. The required marine geoid modelling accuracy is also at the level of a few cm, especially nearby ports and fairways with critical depth threshold.

1.2   Quasigeoid, fitted geoid

A geoid model serves thus as a height conversion surface between ellipsoidal and orthometric heights. The orthometric height is measured along the plumb line (tangent to the gravity vector), from the geoid to the point of interest. Besides orthometric heights H^O, there are other height types used, namely the normal height H^N. Normal heights are measured along the normal of the reference ellipsoid, see Heiskanen and Moritz (1967, Sect. 8-3) or Vaníček et al. (2012) for further explanation.

The differences between ellipsoidal heights h and normal heights H^N are called height anomalies ζ. In analogy to the geoid model, these can be reflected in a quasigeoid (i.e. height anomaly) model, see Fig. 1. Although a quasigeoid is not an equipotential surface as the geoid, its position can similarly be determined from gravity data. A normal height system is used in most European countries, including Estonia.

National or local vertical datums (NVDs or LVDs) often refer to a historic mean sea level value that does not necessarily correspond exactly to the surface of the geoid. Therefore, for use as a height conversion surface, the gravimetric geoid model can be fitted to the vertical datum. This conversion can be a one-dimensional vertical shift, but also a more complicated polynomial surface in case of distorted height systems.

For practical purposes most countries have established an official fitted geoid model corresponding to the height system(s) in use. In Estonia, the current geoid model is the EST-GEOID2011 (Ellmann et al. 2011, RT I, 3 2011) which is based on the corresponding GRAV-GEOID2011 gravimetric geoid model. The entire Nordic-Baltic region is covered by the NKG (Forsberg et al. 2004) and the EGG (Denker 2016) regional gravimetric geoid models. Such regional models can be used for height system unification, scientific purposes and other regional tasks, but also as national reference surfaces (after fitting to individual NVDs, if necessary).

1.3 Geoid modelling

Geoid modelling represents a boundary value problem (BVP) whereby a boundary shape (geoid) is to be determined from boundary values (gravity derived quantities) that refer to the boundary surface (Heiskanen and Moritz 1967).

In particular, the input data to geoid modelling can be gravity anomaly Δg values. Surface (also called free-air) gravity anomaly is the difference of the measured gravity value g_P (at point P at the height H_P above the geoid) and the normal gravity generated by the reference ellipsoid (*ibid.*, Eq. 8-7):

$$\Delta g_P = g_P - \gamma_{H_P} \tag{2}$$

where the normal gravity γ_{H_P} is evaluated at the height H_P above the reference ellipsoid (Molodensky 1945), using standard formulae (e.g. Moritz 2000).

In spherical approximation, a geoid model can be obtained from gravity anomaly values by the Stokes (1849) formula:

$$N = \frac{R}{4\pi\gamma} \iint_\sigma S(\psi)\Delta g d\sigma \tag{3}$$

where R is the mean Earth radius, γ is the normal gravity on the reference ellipsoid, σ is the unit sphere, i.e. the globe. The Stokes function $S(\psi)$ is defined as:

$$S(\psi) = \sum_{n=2}^{\infty} \frac{2n+1}{n-1} P_n(\cos\psi) \tag{4}$$

where ψ is the spherical distance between the computation point P and the integration point Q; $P_n(\cos\psi)$ are the Legendre polynomials of spherical harmonic degree n, see Heiskanen and Moritz (1967, Eq. 1-57').

Notice that Eq. 3 requires global integration of gravity anomalies. For regional geoid modelling it is modified so as to combine the integration of terrestrial gravity data Δg from within a spherical cap σ_0 (the near zone contribution) with the far zone contribution from a global geopotential model (GGM) as (Sjöberg 2003b, Eq. 7):

$$\widetilde{N} = \frac{R}{4\pi\gamma} \iint_{\sigma_0} S^L(\psi)\Delta g d\sigma + \frac{R}{2\gamma} \sum_{n=2}^{M} b_n \Delta g_n^{\text{GGM}} \tag{5}$$

where b_n are arbitrary modification parameters, Δg_n^{GGM} are the GGM-derived Laplace harmonics of Δg (Heiskanen and Moritz 1967, p. 97), M is the spherical harmonic degree up to which the GGM is used, S^L is the modified Stokes function and L the corresponding degree of modification.

There are certain requirements that need to be considered before the application of Eq. 3 in geoid modelling, resulting in a number of corrections to the input gravity data or Eq. 5 itself, see Sect. 4.1 for details.

In contemporary gravity surveys, point heights are determined by GNSS with respect to the ellipsoid. Knowing the ellipsoidal height of a gravity survey point allows to compute an alternative residual gravity quantity, the gravity disturbance δg. It is defined as the difference between the observed gravity g_P and the normal gravity γ_P at the same point in space (*ibid.*, Eq. 2-142):

$$\delta g_P = g_P - \gamma_P \tag{6}$$

While gravity disturbances can be converted to gravity anomalies using an existing geoid model, they can also be used for geoid modelling directly by the Hotine formula (Hotine 1969, Eq. 29.53):

$$N = \frac{R}{4\pi\gamma} \iint_\sigma H(\psi)\delta g d\sigma \tag{7}$$

where $H(\psi)$ is the Hotine function defined as (*ibid.*, Eq. 29.17):

$$H(\psi) = \sum_{n=0}^{\infty} \frac{2n+1}{n+1} P_n(\cos\psi) \tag{8}$$

Notice that, in contrast to the Stokes function, the summation in Eq. 8 can start from $n = 0$. In practical computations, the zero and first degree harmonics can often be neglected since the origin of the geodetic system is conventionally placed in the mass centre of the Earth and the adopted normal gravity field is generated by the mass equal to the actual mass of the Earth.

Use of gravity disturbances in conjunction with the Hotine formula in regional geoid modelling will be investigated in Chapter 4. The advantage of gravity disturbances compared to the anomalies is that a previously existing geoid model is not needed for geoid determination in case the survey points are positioned by GNSS.

1.4 Gravity gridding

Evaluation of the Stokes or Hotine integral requires the input gravity anomalies or disturbances to form a regular grid of rectangular or trapezoid like cells (except for e.g. the Santos and Escobar 2004 study that uses Voronoi polygons). However, it is not possible to conduct field surveys of gravity acceleration on a regular grid. Instead, measurements are constrained to locations accessible with a gravimeter,

which is an extremely sensitive and thus fragile instrument. Accordingly, a regular gravity anomaly or disturbance grid needs to be deduced by interpolation from the point-wise gravity data collected.

Most interpolation algorithms demand the phenomenon described by the point data to be homogeneous and regarded as a spatial stochastic process. That is, stationarity (constant mean over the area of interest and position independent covariance) and isotropy (independence of direction of the spatial dependence) have to be assumed, see e.g. the discussion in Darbeheshti and Featherstone (2009).

Neither the gravity values measured nor the surface gravity anomalies or disturbances satisfy the above conditions too well. However, a Remove-Interpolate-Restore (RIR) process can be used to perform the interpolation on a more suitable field. That is, gravity values can be reduced prior to interpolation and a corresponding restoration process applied on the regular grid to yield a gravity anomaly or disturbance grid. Various options exist both for gravity reduction and for interpolation. Combinations of some popular reduction and interpolation methods will be investigated in Chapter 3 to evaluate their suitability and quality in various conditions.

Geoid modelling is one application for gravity (anomaly) grids, which are also needed for other geosciences. For example, different gravity anomalies (free-air, simple Bouguer, complete Bouguer, slab-residual, mantle Bouguer etc., see e.g. Hackney and Featherstone 2003, Radhakrishna et al. 2008) are used in two- or three-dimensional inverse as well as forward modelling by various techniques to interpret variations in mass and density that reflect the structure of solid Earth. Gravity field derivatives such as gradients also reveal density contrasts (Elkins 1951). Numerous contributions similar to Mandal et al. (2015), Baptiste et al. (2016), and Klitzke et al. (2016) etc. describe and interpret the gravity field and geophysical features of specific regions.

1.5   Validation of geoid models

Gravimetric geoid models obtained by Eq. 5 can be validated by comparison to GNSS/levelling points i.e. the difference of the ellipsoidal height h determined by GNSS and the levelled height H.

For such a comparison, sufficiently accurate co-located GNSS/levelling points are needed. Obtaining a nation-wide coverage of such points with a distribution comparable to typical gravimetric geoid model resolution is not economically feasible. Therefore, the accuracy of gravimetric geoid models is judged by the distribution and statistics of discrepancies on the available points, see an example over Estonia on Fig. 2.

Using such comparisons, it is important to keep in mind that, due to inaccuracies of height data, vertical land motion, etc. the control GNSS/levelling data themselves can contain errors, see e.g. Lysaker et al. (2007).

Although GNSS/levelling validation is widely used in regional geoid mod-
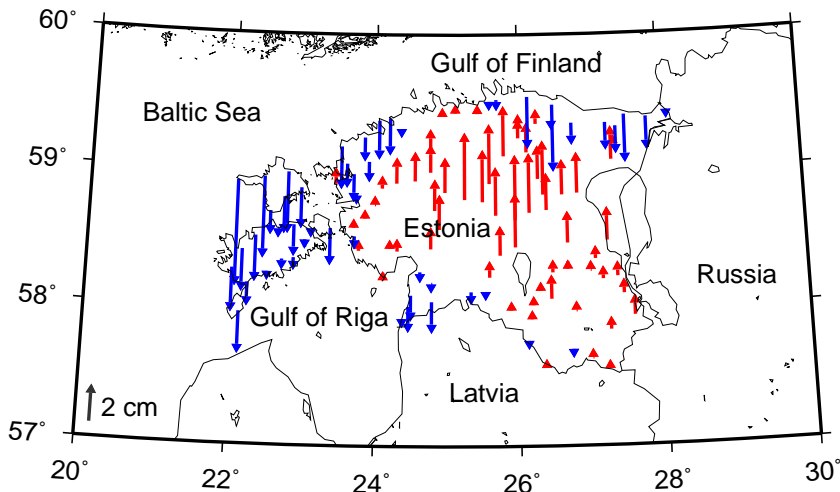
Figure 2: GNSS/levelling evaluation of the GRAV-GEOID2011 model (after removal of the mean difference; min: −5.7 cm; max: 3.6 cm; SD: 1.69 cm)

elling, it is not possible over marine areas due to data unavailability. For marine geoid validation, alternative methods are therefore needed, one of which is proposed in Chapter 5.

1.6 Geoid modelling in the Nordic-Baltic region

All the case studies of this thesis are conducted in the Nordic-Baltic region in Europe, embedding the Nordic (Finland, Sweden, Norway, Denmark, Iceland) and Baltic (Estonia, Latvia, Lithuania) countries, parts of Russia, Belarus, Poland and Germany, the Baltic Sea, North Sea and a large portion of the Arctic Ocean, see Fig. 3. In particular, Estonia is a country of about $45\,000\,km^2$, topographic elevations from 0 to 320 m and a coastline of a few thousand kilometres, including islands.

The Nordic-Baltic is a heterogeneous region covering both land and marine areas. Norway has a rugged terrain with deep fjords and heights exceeding 2 km while in Denmark and the Baltic countries the topographic heights only reach a few hundred metres, see Fig. 3. The quality and coverage of gravity data vary from satisfactory (e.g. Estonia) to sparse and inaccurate over some marine areas, see Fig. 6 on p. 36.

There are currently two geoid modelling projects active in the Nordic-Baltic area: the NKG geoid modelling project and the FAMOS project.

The Nordic Geodetic Commission (NKG) has a history of regional geoid modelling in the Nordic-Baltic area. The succession of NKG geoid models include NKG-86 (Tscherning and Forsberg 1986), NKG-89 (Forsberg 1991), NKG-96 (Forsberg et al. 1997), NKG2002 and NKG2004 (Forsberg et al. 2004).
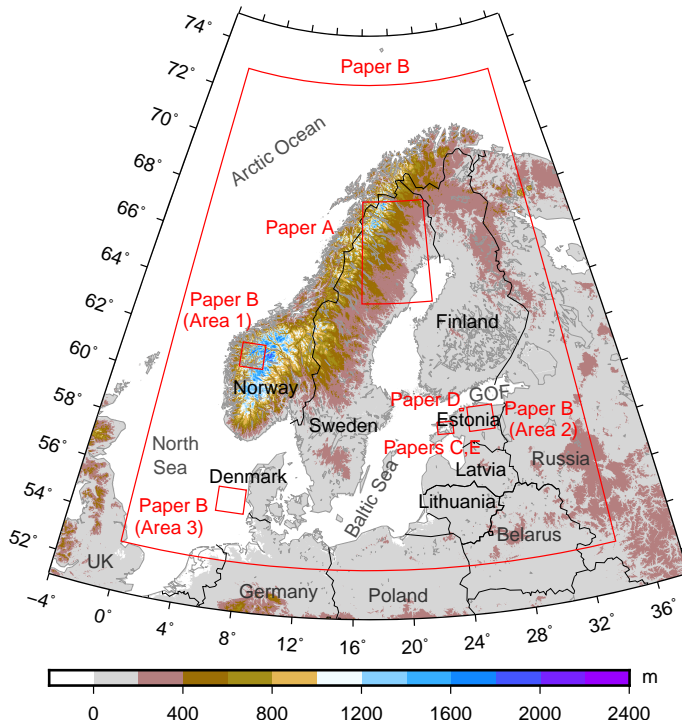
Figure 3: Terrain elevations in the Nordic-Baltic region of interest and specific areas studied in the **Papers**

In 2011 the NKG Working Group of Geoid and Height Systems (NKG WG-GHS 2017) started a project to compute and publish a new NKG geoid model covering the area of 53 to 73° N, 0 to 34° E. It was decided to treat geodetic reference systems and epochs as rigorously as possible. Dozens of geoid models were computed by many computation centres by their method(s) of selection using exactly the same input data. Following their analysis, the most suitable methods were selected for the computation of the NKG2015 geoid model.

See the relevant presentations, especially **IV** to **XIII**, for information on the contribution of the Estonian computation centre and specifically the author of this thesis to the NKG geoid modelling project. Notice however, that there are many aspects to this project that are not discussed in the present thesis, for example unification of reference systems (including conventions for permanent tides), compilation of GNSS/levelling or DTM data, selection of final geoid modelling methods etc. These essential aspects of any geoid modelling exercise are discussed in Ågren (2013) and upcoming publications.

The NKG2015 geoid model is available at ISG (2015), its main characteristics are described in **IV**.

Estonia is not officially part of the NKG association. Co-operation with the NKG community has nevertheless been active in the past decade. As a coun-

try, Estonia stands to benefit from the scientific and practical experience that the NKG community has to offer. This particular project of regional geoid modelling allows Estonia to investigate many theoretical and practical aspects of geoid modelling, that would need tackling in national efforts anyway, in co-operation with the NKG. Another important benefit of international cooperation is the possibility of data exchange, especially since geoid modelling requires data from at least a hundred kilometres surrounding the area of interest.

Another ongoing project related to geoid modelling in the Nordic-Baltic area of interest is the international FAMOS (Finalising Surveys for the Baltic Motorways of the Sea) Odin project (VEU16013). Activity 2 of this project aims at adopting a new vertical reference level for the Baltic Sea, the Baltic Sea Chart Datum (BSCD) 2000. The focus of this project is thus on marine geoid modelling. More specifically, gravity data will be surveyed and validated over parts of the Baltic Sea with the aim of computing a highly accurate and quality controlled marine geoid model. See **II** for current progress of the project. An example of a FAMOS marine gravity campaign can also be found in Varbla et al. (2017b).

1.7 Motivation and objectives

The underlying motivation of this thesis was largely the author's participation in the NKG geoid modelling project described in the previous section. Practical geoid modelling is not a straight forward task with a standard work flow to follow. Instead, there are numerous options in each stage of the process. Such tasks contain data collection, extensive analysis, gravity gridding, selection of an appropriate GGM and its parameters, selection of geoid modelling methods, inclusion of relevant corrections etc.

In this thesis, some specific aspects of gravity field and geoid modelling efforts made in a particular region will be documented. However, the findings are generally not area specific. Instead, these can be useful in any regional geoid modelling task. In addition to individual countries continuously improving their height reference surfaces, there has been international collaboration on regional geoid modelling, for example within the frames of the GEOMED2 (Barzaghi et al. 2017) project or in the International Association of Geodesy (IAG) for the EGG family of geoid models (Denker 2013, 2016).

It is important to notice, however, that the present thesis does not describe the NKG geoid model nor its computational aspects (a dedicated publication is currently under preparation), but reports upon the scientific research conducted to support the project activities.

In the present thesis, the following topics are studied:
- Preparation of gravity grids (**Papers B**, **C** and **D**)
- Geoid modelling methods (**Paper A**)
- Marine geoid validation and applications (**Papers C** and **E**)

While there is ample scientific literature available concerning modification of the Stokes formula and other methodological aspects of geoid modelling (see the references in Chapter 4), the gravity data analysis and preparation is often performed without much documentation. Positive exceptions being Gil and Rodríguez-Caderot (1998), Hinze et al. (2005), Jekeli et al. (2009), Martín et al. (2009), Saleh et al. (2013), and Véronneau (2013) where regional scale gravity data analysis is reported in. Yet, the methodological possibilities available for preparation of a high quality gravity grid are ample. Accordingly, these are analysed and compared in this thesis.

Use of the Stokes formula has been the traditional method for regional geoid modelling with dozens of variations. The alternative Hotine formula has also been used before. However, the specific approach called the Least Squares Modification of Stokes's formula (Sjöberg 1984, 1991, 2003b) with Additive corrections (Sjöberg 2003a) had not yet been fully implemented to the Hotine formula before this thesis.

As mentioned in Sect. 1.5, an alternative to gravimetric geoid validation by comparison to GNSS/levelling points is needed in marine areas. In this thesis, the feasibility of marine geoid validation by direct GNSS positioning "on the geoid" is investigated.

The general aim of this thesis is to analyse the improvements needed in gravity data coverage, gravity gridding and geoid modelling methods to achieve target accuracy of 5 to 10 mm in regional geoid modelling. Therefore, both theoretical and data related aspects of gravity gridding and geoid modelling are considered. In particular, the objectives are:

- to collect and analyse the Nordic-Baltic gravity data (**Papers B**, **C** and **D**)
- to select an optimal method of gravity gridding in a specific area (**Paper D**) or in a large heterogeneous area (**Paper B**)
- to introduce a new geoid modelling method that fully implements the least squares modifications of Stokes's formula with additive corrections to the Hotine formula (**Paper A**)
- to investigate use of GNSS surveys for marine geoid validation (**Paper C**) and sea surface topography determination (**Paper E**)

The present thesis does not aim to deliver a practical product usable for industrial height conversion. Therefore, only gravimetric geoid modelling is discussed: fitting of gravimetric geoid models to NVDs or LVDs is considered to be outside the scope of this study. However, the results of this study do allow for improvement over existing geoid products in the Nordic-Baltic, but also other regions.

1.8 Outline

For the readers' convenience, the specific studies will be introduced and discussed in the logical sequence they would come up in practical geoid modelling tasks. Apart from the Introduction and Discussion, each chapter of this thesis describes a specific task, methods involved in solving the problem and related findings of the corresponding studies.

The theoretical findings presented in the studies making up this thesis are verified in the Nordic-Baltic region, sometimes focusing on a particular part of the area with specific characteristics. The text of this thesis, as some of the constituting papers, intentionally turns some additional attention to Estonia. It is used as an example for explaining geoid modelling problems and related findings, for illustrating the relevance of the studies presented.

Chapter 1 has briefly explained the basics of regional geoid modelling and provided the motivation and objectives of the thesis. Chapters 2 and 3 report upon methods of gravity data analysis and gridding respectively. Chapter 4 concentrates on geoid modelling methods, specifically implementing the least squares modifications of Stokes's formula to the Hotine formula. Chapter 5 is a brief investigation of relations between the geoid and various sea levels in order to use GNSS positioning for marine geoid validation. Chapter 6 summarises the findings of the present thesis together with a discussion and suggestions for future research.

2 Gravity data analysis

Practical geoid modelling requires extensive data collection and analysis: in addition to gravity data, a digital terrain model (DTM) and a GNSS/levelling database for evaluation are needed. Even the best of methodological improvements become futile in practice if there is no adequate data to work with.

In this section, the process of collecting and analysing the necessary gravity data (together with relevant meta data, most importantly uncertainty estimates) will be described. The methods introduced can be of reference in projects elsewhere, for example the ongoing EGG and GEOMED2 research mentioned earlier.

All the case studies of this thesis are conducted within (parts of) the Nordic-Baltic area. For geoid modelling in the area of 53 to 73° N, 0 to 34° E, terrestrial gravity data from 51 to 75° N, −4 to 38° E are used. Gravity data in the NKG database have been cleaned and updated by the participating nations, see **Paper B**. In this thesis, the Estonian gravity data are also used to illustrate some of the processing tasks encountered. Similar procedures have been applied in the other countries involved before inclusion of national data into the updated NKG database.

In addition, the $3'' \times 3''$ DTM called NKG DEM 2014 and the NKG GNSS/levelling database with 2538 points are used. The GNSS and levelling data have been transformed to ETRF2000 (European Terrestrial Reference Frame) epoch 2000.0 and EVRF2007 (European Vertical Reference Frame) respectively.

If not specified otherwise, these are the data used in this thesis and the constituting papers.

2.1 Updating the Estonian Gravity Database

The basis for accurate gravity data collection is a high quality gravity network. Oja (2012) introduces the realisation of the national gravity system GV-EST established for Estonia. Revision and transformation of existing gravity data over Estonia has been ongoing, see Jürgenson (2003), Ellmann et al. (2009), and Jürgenson et al. (2011). Meantime, new gravity surveys have been conducted, e.g. Nikolenko (2010), Oja and Pihlak (2010), Oja (2011), Türk et al. (2011), and Pehlak (2014).

Starting the current studies, the initial task was to establish a new structured database where all the existing gravity data together with meta data could be collected, see the Estonian Gravity Database (EGD) report (Talvik and Oja 2014) and related plans presented in **XIII**. Similar work of generating and verifying meta data is ongoing also on the global level, see Vergos et al. (2017).

After collection and cleaning of existing and recently acquired gravity data (Fig. 4), the resulting data were compared to those used in the modelling of GRAV-GEOID2011, see **IX**, **X**, **XI**. From initial analysis it was found that the more recent gravity data can change the resulting geoid model significantly: in
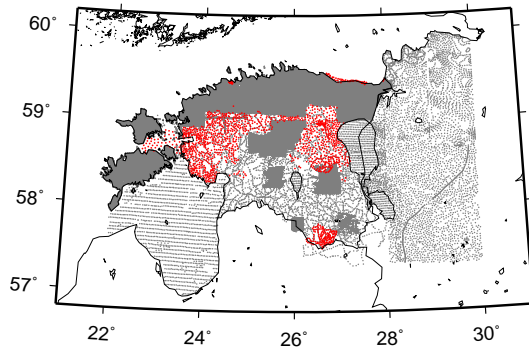
Figure 4: The updated EGD (data collected after 2011 in red)
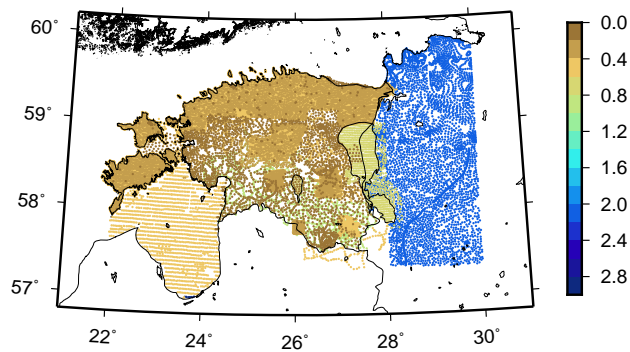
Figure 5: The EGD coloured according to error estimates

central and West Estonia but also near the terraced coast in the NE the geoid change can reach ± 2 cm which is well beyond the target accuracy of 5 to 10 mm set in regional geoid modelling.

Such a significant improvement in estimated geoid model accuracy illustrates the importance of continuing terrestrial gravity data collection and regional geoid modelling efforts in the era of dedicated satellite missions providing global gravity field and geoid products with increasingly high resolution and accuracy.

It was also clear that some specific areas need additional attention. As a result, gravity data were specially collected and analysed nearby a terraced area (**Paper D**) and on ice covered water bodies (**Paper C**).

A special effort was needed to analyse the Estonian Geological Survey (EGS) gravity data consisting of about 130 000 points, mostly over North Estonia (Talvik et al. 2014c). These had previously been digitized and transformed to the modern reference level, see e.g. All and Gromov (2007) and other similar reports. However, some meta data, such as data collection epoch and estimated accuracy level (0.2, 0.3 or 0.5 mGal) had to be newly gathered from the original reports. This information was later used in data filtering, see Sect. 3.3 and **Paper B**.

As a result, the Estonian gravity database contains about 143 000 points with

error estimates from 0.1 to 3 mGal, see Fig. 5.

2.2 Gravity surveys on ice

Geoid is a rather smooth surface where the long wavelength features dominate. Accordingly the geoid height at a specific point is largely affected by the gravity field in its surroundings, hence the original Stokes formula embedding global integration. Therefore, gravity data from nearby coastal areas (and more specifically, possible systematic errors in it) contribute to the mainland geoid model significantly (**Paper B**).

Unfortunately, gravity surveys are considerably more complicated over marine areas, especially nearby the coast where the quality of satellite altimetry derived gravity data degrades. The possible alternatives include marine gravimetry, airborne gravimetry and, where possible, surveys on marine ice. The latter are investigated in **Paper C**.

Previous attempts of ice gravity surveys are reported by Lehmuskoski and Mäkinen (1978), Ugalde et al. (2006), Engberg et al. (2011), Oja et al. (2011), and Ågren et al. (2014). The problems associated with gravity surveys on ice include weight of equipment on ice; gravimeter tilting due to snow compaction and ice melting; direct wind impact on the gravimeter; considerable ice oscillation, see **XII**, Kiviniemi (1975), Lehmuskoski and Mäkinen (1978).

Gravity surveys over the Väinameri Basin in West Estonia are described in **Paper C**. Attention is also given to vertical positioning of the gravity points. The efficiency and accuracy of rapid static and kinematic GNSS surveys for the purpose of positioning on ice (i.e. in relatively remote areas) is analysed. Contrary to surveys on land, (vertical) position differences on revisited points reflect not only GNSS inaccuracies but also motion of the ice sheet in tact with the sea level.

The ice gravity surveys serve not only the purpose of obtaining new data but also to validate and transform existing data. For example, the sea bottom gravity data of Gulf of Riga and the airborne gravimetry tracks over Väinameri are validated in Oja et al. (2011) and **Paper C** respectively.

Considering the recent experience described above, the achievable accuracy of gravity surveys on marine or lake ice is estimated to be ± 0.15 mGal, i.e. comparable to terrestrial gravity surveys.

2.3 Updating the NKG gravity database

For the purpose of the NKG geoid modelling project, the (already existing) NKG gravity database was also thoroughly modernised, see **Paper B** for some details. It contains data from within the area of 52 to 74° N, −2 to 36° E, also acting as a part of the future FAMOS gravity database.

Most importantly, each participating country is responsible for the data concerned, hence the careful compilation of the Estonian gravity database, described
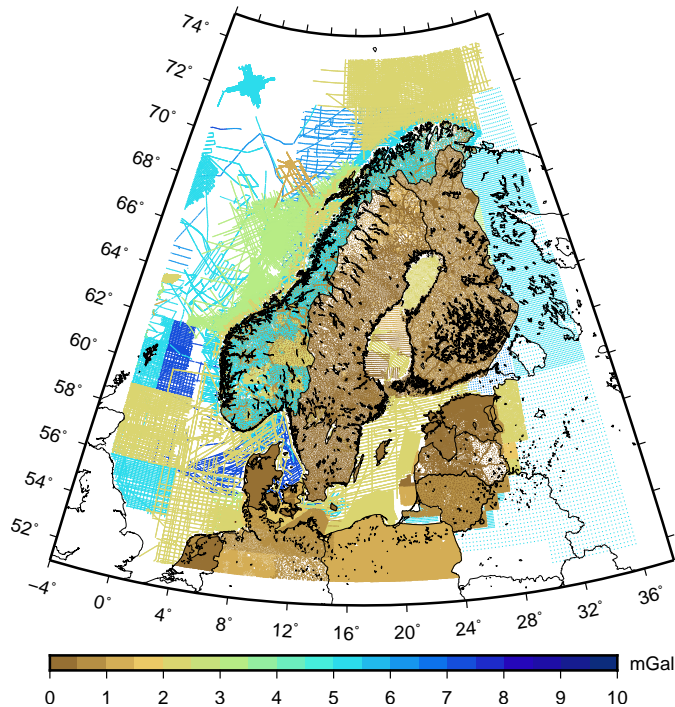
Figure 6: The NKG gravity point data coloured according to *a priori* error estimates (figure from **Paper B**). Notice that the colour scale differs from that used in Fig. 5.

in Sect. 2.1. Each data point comes with a corresponding uncertainty estimate, some carefully estimated to represent the actual quality of the observations, some (usually those of older data) less so.

After initial database compilation, the NKG gravity data were analysed by the participating computation centres to treat missing, overlapping or outlier data, see **VII** and **VIII**. The final database contains over half a million gravity points with *a priori* error estimates from 0.1 to 7.0 mGal originating from terrestrial, marine and airborne gravity surveys (Fig. 6).

After compilation and analysis of gravity data using the methods described in this chapter, the next task of gravity gridding necessary for geoid modelling can be proceeded to.

3 Gravity gridding

For input to geoid modelling by the Stokes (Eq. 3) or Hotine formula (Eq. 7), a grid of free-air anomalies or disturbances is needed. Gravity surveys yield point values of gravity acceleration, which are reduced to surface (free-air) gravity anomaly Δg point values by Eq. 2 (or disturbances δg by Eq. 6). Compared to the initial gravity values, the free-air anomaly field is reduced in magnitude. However, it can still be quite rough and correlated with height, thus not very suitable for high quality interpolation, unless sampled extremely densely (e.g. 10 values per km^2, according to Janák and Vaníček 2005).

As mentioned in the Introduction, gravity grids can be obtained from surveyed point data through the remove-interpolate-restore process. However, for both the reduction of gravity data and interpolation, there are numerous methods available. Accordingly, **Papers B** and **D** investigate gravity anomaly gridding in detail to find a combination of methods and computation parameters that results in the highest quality gravity anomaly grid. The findings of these analysis are also directly applicable for gravity disturbance gridding, as the two residual gravity quantities (and data sets) share the same properties.

First, the methods (criteria) used in assessing gravity grids are discussed in Sect. 3.1. Some widespread reduction, data filtering and interpolation methods are then evaluated in Sections 3.2, 3.3 and 3.4 respectively. Sect. 3.5 discusses the importance of area specifics in the selection of gridding methods. The overall quality of gravity gridding and resulting geoid models is discussed in Sections 3.6 and 3.7.

3.1 Methods for assessment of gravity grids

First, criteria for the best quality grid need to be decided upon. Intuitively, one would think that a grid with the smallest residuals with respect to the original point data would be the optimum solution. This would certainly be so in case of perfectly distributed flawless gravity data. However, survey data inevitably contain measurement errors and voids. Therefore, under some circumstances, a grid with larger residuals may in reality reflect the physical nature of the gravity field better.

The focus of current research is on geoid modelling. In such a case, the quality of the resulting geoid model offers additional means for validation of the gravity grids. Preliminary geoid models can be computed from gravity grids obtained by different methods. Each of these can then be evaluated by comparison to GNSS/levelling points to determine gravity gridding methods yielding the highest quality geoid models.

In this thesis, either quick geoid modelling by the Generic Mapping Tools (GMT, Wessel et al. 2013) sub-program *grdfft* (in case of **X**, **IX**) or more accurate methods similar to those used in the computation of the NKG2015 model (in case

of **Paper B**) are used for such preliminary geoid computation intended for gravity grid validation.

3.2 Gravity reduction

3.2.1 Reduction methods

Most of the high frequency information contained in the surface gravity values is due to topography. Although most of it is removed by the free-air reduction, there are a number of possibilities for further reduction of gravity anomalies. Out of these, the reduction to Complete Bouguer anomalies (CBA, sometimes also called Refined Bouguer anomalies) and to Residual Terrain Model anomalies (RTMA) is investigated in **Paper B**. Both are well known and widespread gravity reduction methods, albeit with different physical meaning.

The Complete Bouguer anomalies Δg^{CBA} are obtained from the free-air anomalies Δg (Eq. 2) by:

$$\Delta g^{\text{CBA}} = \Delta g - \delta g^{\text{BP}} + \delta g^{\text{TC}} \tag{9}$$

where the second term δg^{BP} represents the gravitational effect of the Bouguer plate (Heiskanen and Moritz 1967, Eq. 3-19) and the third term δg^{TC} the terrain correction (*ibid.*, Eq. 3-21).

The Residual Terrain Model anomalies Δg^{RTMA} are obtained by:

$$\Delta g^{\text{RTMA}} = \Delta g - \Delta g^{\text{GGM}} - \delta g^{\text{RTM}} \tag{10}$$

where the second term Δg^{GGM} is the gravity anomaly from a GGM evaluated to a suitable maximum degree and order (d/o) and δg^{RTM} is the RTM correction (Forsberg 1984). The RTM correction is similar to the terrain correction δg^{TC}, representing the gravitational effect of topography above a reference surface.

Possible alternatives to CBA and RTMA include mainly isostatic anomalies such as the Airy-Heiskanen or the Pratt-Hayford reduction that could be quite smooth over land or marine areas respectively (e.g. Novák et al. 2016).

Additional corrections to describe the gravitational effect of atmosphere or ice are also discussed in **Paper B**. The atmospheric correction cannot exceed 0.87 mGal and is thus relatively small. The ice correction is relevant only in areas where the gravity surveys are conducted on an ice sheet – i.e. over glaciers.

3.2.2 Evaluation of reduction methods

First, the effect of neglecting the terrain correction δg^{TC} from Eq. 9 on resulting geoid models is discussed. In mountainous areas reaching about 2 km in elevation, the resulting gravity grid and geoid model are clearly biased with deviations reaching decimetres (in Norway). Deviations in the order of metres were noticed in a similar experiment in the Rocky Mountains (Janák and Vaníček 2005). By
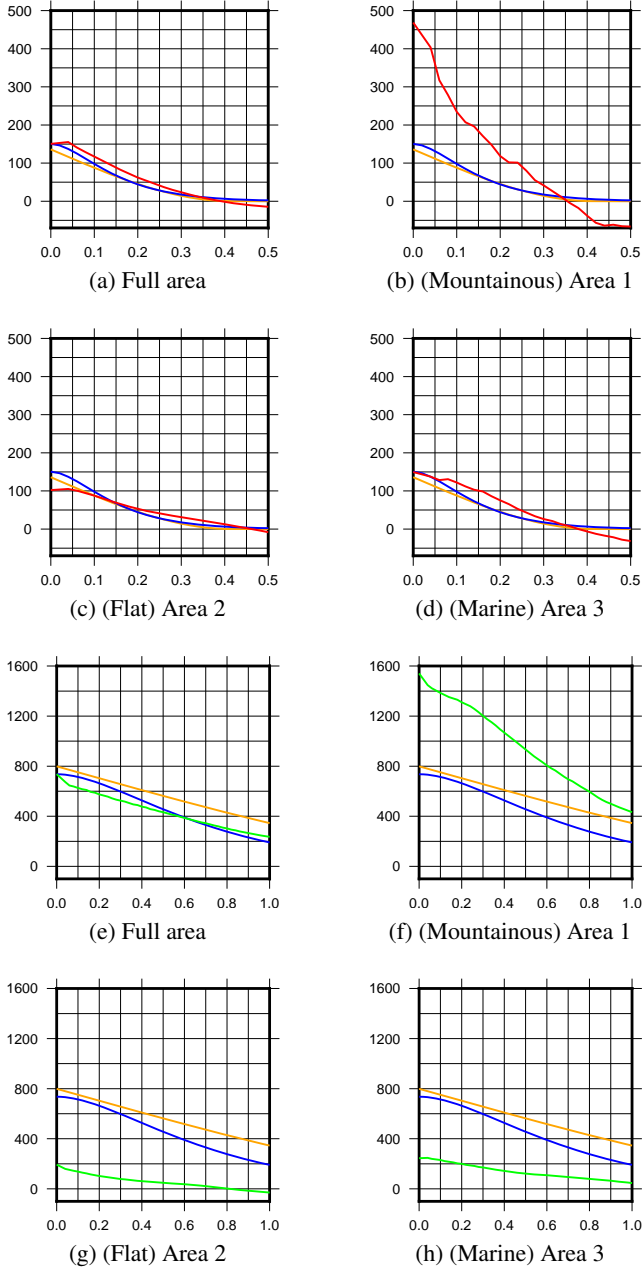
Figure 7: Covariance functions for the RTMA (a to d) and CBA (e to h) anomalies in different areas, see Fig. 3 for their locations* (figure from **Paper B**)

*The red or green lines depict the empirical covariance function, blue line the second order Markov and orange line the spherical model. Spherical distance [°] and variance [mGal^2] are represented on the horizontal and vertical axis respectively.

analogy, similar problems can be expected when neglecting the RTM correction δg^{RTM} in Eq. 10.

Another parameter that can be varied is the maximum d/o used for evaluation of Δg^{GGM} in Eq. 10. **Paper B** compares the maximum limit (300) of a satellite-only GGM to another reasonable choice of 240 degrees. The corresponding difference of the two gravity grids and the resulting geoid models is rather insignificant: over the study area of **Paper B** the standard deviation is 0.44 mGal and 0.6 mm, respectively. The absolute maximum deviation in the resulting geoid models is 1.4 cm.

The covariance analysis performed in **Paper B** (see Fig. 7) illustrates the different characteristics of the CBA or RTMA field. First of all, the variance of the RTMA field is much smaller than that of the CBA field, see the different scale of Figs. 7a to 7d compared to Figs. 7e to 7h.

Table 2 of **Paper B** also lists the estimated correlation lengths for the full NKG area and the specific study areas (Area 1 – mountainous, Area 2 – flat, Area 3 – marine). In general, the correlation lengths are two to three times smaller for the RTMA and vary much less between areas with different characteristics than those for the CBA. While the theoretical covariance model for RTMA fits the empirical values rather well in the flat and marine area at least, that of CBA under- or overestimates the spatial correlation in all of the test areas.

From the above analysis it would seem that the RTMA are more suitable for interpolation, at least by statistical methods that make use of spatial correlation information in the form of a covariance model, but also by other methods, as the RTMA field is "more predictable".

However, the case study of **Paper B** does not confirm this conclusion. The differences of reduced point values from the grid values (Table 4 of **Paper B**) are very similar for both reduction schemes, neither of the methods showing significantly smaller RMS (Root Mean Square) or extreme values. Comparing the final surface anomaly grid to the original surface anomaly values, only the grid computed via RTMA using the LSC interpolation (see Sect. 3.4) shows about 10 % better RMS values in the overall and mountainous area statistics.

The two reduction methods have different physical meaning, but the resulting surface gravity anomaly grids show a similar fit to the input data. Based on the case study results, it is therefore difficult to prefer either of the reduction methods. A reason to prefer the RTM anomalies for gravity data gridding could be their properties of shorter, more uniform correlation length and smaller variability (as discussed above) that are theoretically more suitable for interpolation.

3.3 Data filtering before interpolation

For practical implementation of many interpolation algorithms, the scattered point data should first be low-pass filtered or averaged according to the grid step of the final grid to reduce cluttering (or high frequency information) that results in
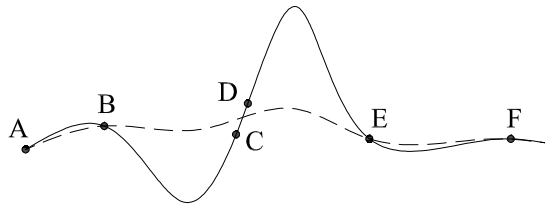
Figure 8: Illustration of aliasing in gravity gridding: aliased (solid line) and desired (dashed line) result

aliasing, see e.g. Smith and Wessel 1990.

The aliasing effects are different depending on the interpolation method. For an algorithm considering also the estimated accuracy of data points, the situation can be illustrated with the following example depicted on Fig. 8. There are two points C and D with a small error estimate close by each other and other points further away, the error estimates of these do not particularly matter. The interpolation surface tries to follow the points C and D that it considers highly accurate. As a result, the surface undulates between points B and E. If one of the points C or D in fact contained a larger error than their error estimate allows, then the desired surface should not pass through both of these points and the undulation should not be present. However, if points C and D were either filtered (i.e. one of the two removed) or averaged before interpolation, the desired smooth surface would have been obtained.

3.3.1 Filtering methods

Again, there are a number of ways to generate a point cloud corresponding to the selected grid step from the total number of observations. The GMT (a popular tool used in geosciences) sub-program *surface* intended for interpolation suggests the use of their *blockmean*, *blockmedian* or *blockmode* algorithms. In addition, such averaging can be performed using unit or realistic weights (for example the inverse of given error estimates squared).

An alternative to (weighted) averaging is the process of filtering. For example, one step (according to accuracy estimates) and two step (according to survey epoch, then estimated accuracy) filtering were attempted with the Estonian Geological Survey data collected over a longer time period (1968-2008) with different accuracy (**IX**, **X**, **XI**). See Fig. 9 for an illustration of a filtering result, whereby points with smaller error estimates have been preferred over those with a larger error estimate.
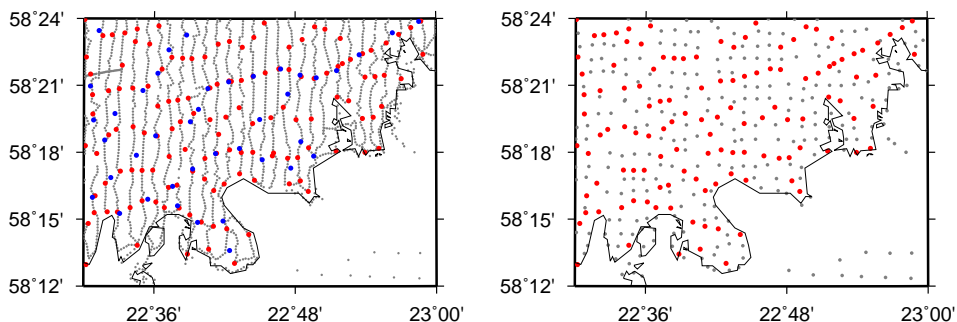
Figure 9: Gravity data before (left) and after (right) filtering according to error estimates (red – 0.2 mGal, gray – 0.3 mGal, blue – 0.5 mGal)

3.3.2 Evaluation of filtering methods

Preliminary geoid modelling by the simplified *grdfft* method is used to evaluate the effect of using these different averaging or filtering options, see **X** and **IX**. Over Estonia the differences between geoid heights obtained from gravity data averaged by *blockmean* or filtered according to uncertainty estimates remain within a few millimetres.

The effect of using realistic weights instead of unit weights in the *blockmean* process is local: it is noticeable within a distance of about 10 km around some specific computation points. In case of the Estonian data, the maximum difference between preliminary geoid models are in the order of 2 cm. While in general such local effects are rather harmless, they could have an adverse effect on GNSS/levelling evaluations if a control point happens to be in an area where the geoid modelling result has a large dependency on the weighting scheme used in gravity gridding.

It can be concluded that in a flat area densely covered with gravity data, such as Estonia, any of the above data filtering methods usually yield satisfactory geoid modelling results. For a generalisation, additional analysis in other areas would be beneficial.

3.4 Interpolation

In practice, the reduced gravity data are still somewhat non-stationary, anisotropic (see e.g. Schwarz and Lachapelle 1980, Goad et al. 1984) and contain unavoidable observation errors. However, they should now be much more suitable for interpolation. As the next step, an interpolation method best suitable for the specific characteristics of the residual gravity field is needed.

A number of interpolation methods are described and tested in **Papers B** and **D**, see Table 2. Most available interpolation tools fit in one of the categories listed in Table 2. In addition to the specific parameters given in Table 2, most algorithms

Table 2: Interpolation methods and tools used

Method	Parameters	Tool
triangulation	-	GMT *triangulate*
	-	Matlab[1] *griddata*
splines in tension	manual tension factor	GMT *surface*
	automatic tension factor	GMT *sphinterpolate*
nearest neighbour	search radius, number of sectors	GMT *nearneighbor*
statistical	covariance function or (semi)variogram	Gravsoft[2] (LSC) Surfer[3] (Kriging)

[1] MathWorks Inc (2017); [2] Forsberg and Tscherning (2008); [3] Golden Software LLC (2016)

can also make use of individual error estimates. However, in the present study, individual error estimates are only used with the LSC interpolation method.

3.4.1 Interpolation methods

Triangulation methods (used in **Paper D**) form triangles between data points, allowing for sharp edges and gradients in the field. Although the gravity field itself can not host such brake-lines that form on triangle sides, the triangulation methods can still be useful in areas of larger gravity field variations, such as the terraced area treated in the case study of **Paper D**.

The nearest neighbour algorithm (used in **Paper D**) depends on the specific search radius and data requirements per sector that need to be selected beforehand. An attempt to secure a high quality interpolation by setting strict requirements on the number and distribution of data points per sector can result in the algorithm being unable to estimate a value to many grid nodes due to lack of data. However, the four sector interpolation used in the terraced study area of **Paper D** yields rather good results.

Spline based methods (used in Papers **B** and **D**) form smooth surfaces, which should be able to reflect the nature of the gravitational potential field well. Depending on specific tension parameters, the spline surface formed can host extrema that do not coincide with data points (e.g. is able to represent a maximum value at the bottom of a valley in case survey points exist only at sides of the valley) and each data point is not necessarily passed through (allowing for measurement errors), see Smith and Wessel (1990). While the GMT *surface* algorithm demands that the tension factor determining the amount of undulation allowed in the spline surface be selected beforehand, the *sphinterpolate* algorithm allows for automatic determination of tension factors according to local gradients.

Statistical interpolation methods (used in **Paper B**) such as Kriging (Krige

1951) and Least Squares Collocation (LSC, e.g. Moritz 1980) base their estimates on *a priori* information about the spatial correlation of the data. The spatial dependence information is provided in the form of a covariance or semi-variogram model (see e.g. Isaaks and Srivastava 1989, p. 55), which is usually estimated from the survey data.

3.4.2 Evaluation of interpolation methods

The case study of **Paper B** shows that (at least with the selected parameters) both of the spline based methods tend to follow the input data rather closely, meaning the input values differ from the resulting grid surface very little. In general, this is a satisfactory result. However, such an "exact" surface does not consider the possibility of data points containing errors. Thus, in some cases, for example in areas of low quality gravity data (over Russia and the Atlantic Ocean), some other interpolation method could generate a physically more meaningful surface.

Another important aspect with the spline based methods is their behaviour in data gaps that are often present in marine areas. The case study of **Paper B** demonstrates that spline based algorithms can generate erratic maxima (in the order of 100 mGal) in data gaps. Unnecessary undulation can also appear nearby steep gradients elsewhere (Fig. 14 of **Paper B**). Also, their behaviour can be extremely noisy around and between track-wise (e.g. marine gravity) data (Fig. 15b of **Paper B**).

The LSC interpolation results of **Paper B** demonstrate the specific aspects of such a statistical method used in conjunction with individual error estimates. In areas of low quality gravity data, the interpolation results are rather smooth with the residuals to input data reflecting the estimated large observation errors. Therefore, these larger residuals (compared to the spline based methods used) should not be interpreted as errors of the interpolation process.

The case study of **Paper B** also demonstrates the importance of supplying realistic error estimates as these determine the smoothness of the resulting surface. If the error estimates are unrealistic, it could be better to discard them.

Due to the underlying covariance model, the LSC interpolation provides rather realistic results without unnecessary undulation nearby steep gradients and data gaps (Figs. 14 and 15 of **Paper B**). It tends to disregard a single value that stands out from the surrounding gravity field (Fig. 14 of **Paper B**), this being positive if the value is erroneous and negative if representing the actual signal.

Based on the experience described above, it can be concluded that in most areas of high quality gravity data all of the tested interpolation algorithms are able to generate a good quality gravity grid; nearby inaccurate gravity data, steep gradients and data gaps the spline based methods are better avoided; statistical interpolation provides realistic results thanks to the underlying covariance model; and unrealistic error estimates are better discarded.

3.5 Area specific and generic selection of gridding methods

The extent and specific characteristics of the research area can play a role in the selection of gravity gridding methods. It may be that the method working best in one area is not suitable in another area.

Paper D investigates gravity gridding in a very specific area containing terraced landforms, probably favouring methods that allow for more rapid changes in the gravity field model than necessary in most areas. In addition to terrain features, the distribution and accuracy of available data certainly plays a role in which method suits the particular area best.

Complementary to **Paper D** investigating an area with specific characteristics, **Paper B** attempts to generalise the task to a very large heterogeneous area. The particular study area of **Paper B** covering the Nordic and Baltic countries is extremely varying in terms of terrain, data coverage and quality, thus representing and illustrating most situations that will be met in gravity gridding tasks. The following discussion relevant to the NKG study area illustrates the importance of the area-dependent characteristics.

Figure 7 (on p. 39) depicts empirical covariance functions estimated for the full NKG study area or particular case study areas of **Paper B** representing a mountainous, flat or marine area. The difference of these covariance functions illustrates how varying even the reduced gravity field characteristics can be. These plots and Table 2 of **Paper B** reveal that the estimated correlation length of reduced gravity anomalies can vary two to three times between areas with different characteristics.

Since **Paper B** aims to use a common method and parameters of gravity gridding over all of the heterogeneous area, a single covariance model is fitted to the empirical values representing the entire NKG area. Such an "average" model is far from being optimum in the mountainous area (Figs. 7b and 7f). However, in case of the RTM anomaly, the average covariance function is also representative for the flat (Fig. 7c) and marine areas (Fig. 7d). In other words, interpolation parameters selected for the entire area should also be suitable for such flat or marine areas and therefore a reasonable interpolation result can be expected there.

The majority of geoid signal power is embedded in the long wavelengths. Although gravity gridding and geoid modelling can be relatively straight forward in a flat area covered with high quality data (such as Estonia), the estimated geoid height values are easily affected by methodological choices selected according to the needs of a larger, heterogeneous area (in this case the entire NKG area). For example, in Estonia it would not be so harmful to interpolate the surface gravity anomalies directly, but computing a geoid model with such a grid over the entire NKG area can result in a 10 cm tilt in the geoid model over Estonia (**VIII**).

The same problem of the gravity field having variable characteristics is also met when processing satellite altimetry data, see Knudsen (2005). Estimation and comparison of gravity field characteristics (over Canada) is also reported in

Schwarz and Lachapelle (1980). Both of these publications attempt to find a way to automatically vary related computational parameters according to specifics of the area. Goad et al. (1984) reports upon the differences in variance and correlation length values for the Bouguer anomalies (see Sec. 3.2.1) over the United States.

3.6 Resolution of gravity grids

The gravity grids used for input to geoid modelling generally have the same resolution as the geoid model (typically about 1 km by 1 km). As demonstrated in **Paper D**, the gravity field itself can contain signal with an even shorter wavelength. This should be kept in mind when using the gravity grid products initially generated for geoid modelling for other purposes (e.g. calculation of levelling corrections, see Talvik 2014, or the various other uses in geosciences shortly described in the Introduction).

The relatively low resolution gravity grids used for input in geoid modelling could also be limiting the accuracy of resulting geoid models. The example of a terraced area treated in **Paper D** shows that the short wavelength gravitational signal of the terrace is not represented in a typical gravity grid used for geoid modelling. Although the gravitational signal of a terrace is very local in the perpendicular direction of the terrace, the terrace can stretch for long distances (hundreds of kilometres), possibly causing a systematic error in geoid modelling from such a low resolution gravity grid omitting the terrace's signal.

However, no significant improvement (compared to direct interpolation on the required resolution) in grid quality is noticed when interpolation is performed on a higher resolution grid which is later averaged to the required grid step. In other words, to benefit from a higher resolution gravity grid able to represent more detail, the geoid model also needs to be computed on a higher resolution grid (**Paper D**).

3.7 Overall gridding quality

In the analysis of gravity gridding methods reported above, a number of extreme examples and study areas were considered. Leaving these aside, it can be said that all of the methods described are equally plausible for many practical gravity gridding tasks. Under this assumption, the uncertainty stemming from the use of different gridding approaches can be illustrated by the standard deviation of the test grids of **Paper B** in each grid cell, see Fig. 10.

Thus, gravity gridding accuracy better than 0.5 mGal can only be expected in flat areas with high-quality gravity data such as Denmark and Estonia, while the accuracy is limited to around 1 mGal in areas with slightly lower quality gravity data (Latvia and Lithuania) or higher terrains such as Sweden and Finland. Due
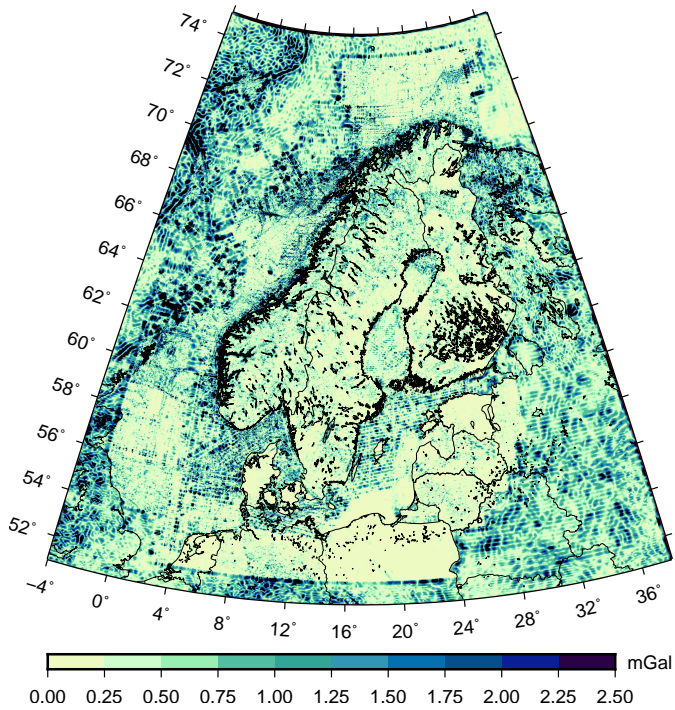
Figure 10: Estimation of gravity grid uncertainty over the NKG study area stemming from different gridding methods and options (figure from **Paper B**)
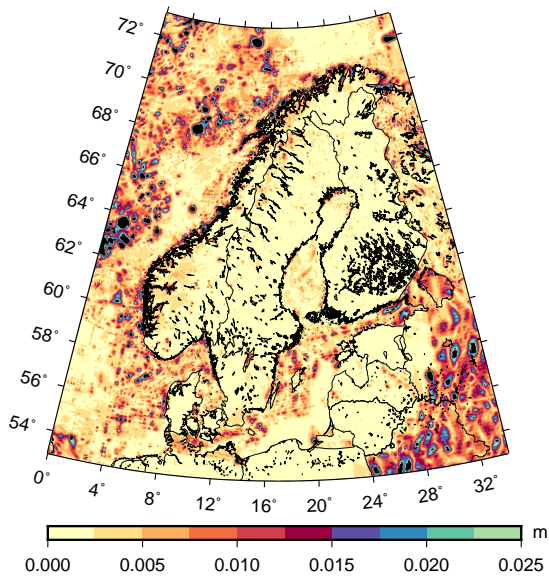
Figure 11: Estimation of geoid modelling uncertainty over the NKG study area stemming from gravity gridding methods and options (figure from **Paper B**)

to sparse data tracks, the marine areas are affected most by the choice of gridding methods.

Analogous analysis can be extended to estimate the uncertainty of geoid modelling, see Fig. 11. From the gravity gridding point of view, geoid model accuracy of 5 mm can be expected over most of the Nordic-Baltic dry land. Disqualifying the spline based interpolation methods, it is possible to compute a geoid model with an accuracy of 1 cm over most of the Baltic Sea (except the Eastern part of Gulf of Finland). Therefore, in view of the desired 5-mm accuracy geoid model, the data situation and gridding approaches still need some improvement in the Nordic-Baltic area.

The Nordic-Baltic research area offers an overview of expected gridding results due to its rather heterogeneous topography and data coverage. However, the results presented can only be of general reference to other similar computations elsewhere as the final grid is strongly dependent on the local situation – gravity data coverage and distribution, topography, bathymetry, glaciers etc.

In the context of geoid modelling, and the present thesis, the high quality gravity anomaly or disturbance grid obtained by (one of) the methods described in this chapter serves as input to the next step: the geoid modelling itself.

4 Geoid modelling

The basics of regional geoid modelling by the Stokes and Hotine formula were described in the Introduction. Sections 4.1 and 4.2 add some details about existing geoid modelling methods in order to provide a framework for presenting and evaluating the new method in Sections 4.3 to 4.9.

4.1 Additional considerations in regional geoid modelling

Recall that for regional geoid modelling the Stokes formula is modified so as to combine terrestrial gravity data with global geopotential models, see the Introduction. Numerous methods to modify the Stokes formula exist, for a recent overview see Featherstone (2013, Appendix A). In general, these can be divided into deterministic and stochastic modifications.

Deterministic modification methods, such as Molodenskii et al. (1962), Wong and Gore (1969), Meissl (1971), Heck and Grüninger (1987), Vaníček and Kleusberg (1987), Vaníček and Sjöberg (1991), Featherstone et al. (1998), and Evans and Featherstone (2000), aim at reducing the truncation error by imposing suitable, preselected limits on the integration kernel and its modification.

In contrast to deterministic methods, stochastic methods (e.g. Sjöberg 1980, Wenzel 1983) make use of estimated gravity signal and error spectra to balance the relative contribution of the GGM and terrestrial gravity observations. In particular, three stochastic modification methods of the Stokes formula proposed in Sjöberg (1984, 1991, 2003b) minimize the truncation error, the influence of erroneous terrestrial gravity data and geopotential coefficients in the least squares (LS) sense. The principles of these LS modifications are used for deriving the new geoid modelling method in Sec. 4.3.

Application of the Stokes formula assumes fulfilment of certain requirements (see e.g. Martinec 1998a), specifically the following.

First, the Stokes formula is valid only if the potential field is harmonic outside the geoid, meaning no masses are allowed above the geoid surface. In reality there are terrain and atmospheric masses above the geoid, violating the harmonicity condition. These are therefore artificially "removed" for the computation, yielding thus various topographic and atmospheric corrections, see e.g. Martinec (*ibid.*, Sect. 1.2) for further explanation.

Second, the input gravity quantities (boundary values) need to refer to the geoid instead of their initial surveyed position on top of the topography. These are therefore analytically "downward continued" (DWC) to the geoid surface, resulting in the DWC correction, see e.g. Martinec (1996).

Third, the geoid is considered as a sphere when formulating the boundary conditions regarding the Earth's gravity potential. In reality, the Earth and the geoid resemble an ellipsoid. The error made by such a spherical approximation can be accounted for by an ellipsoidal correction, see Sjöberg (2004) and the
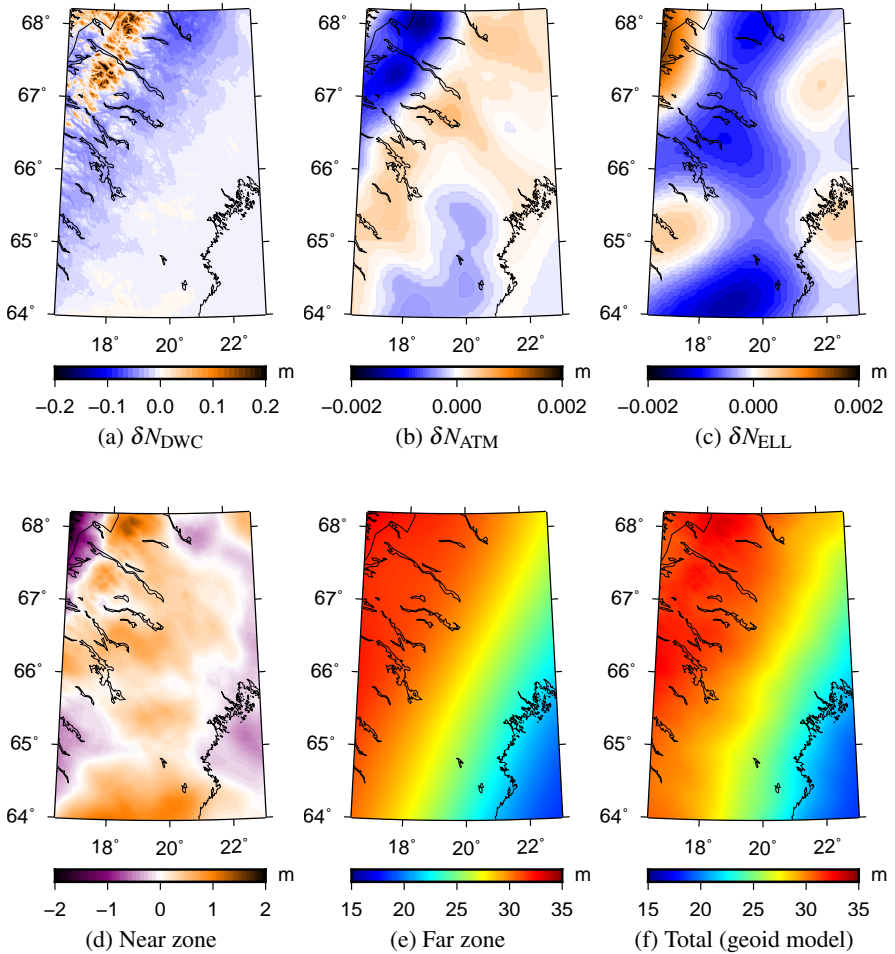
Figure 12: Partial contributions to a LSMSA geoid estimator (modified figure from **Paper A**)

references therein.

In general, there are two approaches to consider the aforementioned corrections: the remove-compute-restore (RCR) and the KTH approach (the latter refers to the KTH Royal Institute of Technology in Sweden, the affiliation of Prof. Lars E. Sjöberg).

In the RCR geoid modelling approach the surface gravity anomalies are reduced before input in the modified Stokes formula. The direct effects for which the reduction occurs are restored upon the geoid height as indirect effects, see e.g. Ellmann and Vaníček (2007). The RCR method is used by e.g. Vaníček and Kleusberg (1987), Vaníček and Sjöberg (1991), Forsberg (1993), Vaníček et al. (1995), Forsberg and Tscherning (1997), Omang and Forsberg (2000), and Sansò
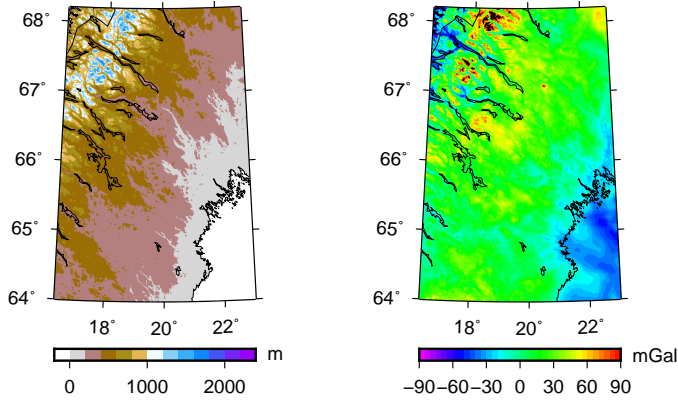
Figure 13: Terrain elevations (left) and gravity disturbance values (right) in the case study area of **Paper A**

and Sideris (2013).

In the alternative KTH approach (summarized in Sjöberg 2003a), the surface gravity anomalies (Eq. 2) are directly used as the integral argument. The direct and indirect effects of downward continuation, topographic, atmospheric and ellipsoidal corrections can then jointly be applied as combined (additive) corrections to the approximate geoid height obtained by the Stokes integration. A geoid model value $\widehat{N}$ is obtained by adding the approximate geoid estimator $\widetilde{N}$ of Eq. 5 and the corresponding corrections:

$$\widehat{N} = \widetilde{N} + \delta N_{\text{COMB}} + \delta N_{\text{DWC}} + \delta N_{\text{ATM}} + \delta N_{\text{ELL}} \tag{11}$$

where δN_{COMB} is the combined topographic effect (Sjöberg 1995, 1997, 2000), δN_{DWC} is the combined downward continuation effect (Sjöberg 2003c), δN_{ATM} is the combined atmospheric effect (Sjöberg 1999, 2001) and δN_{ELL} is the combined ellipsoidal effect (Sjöberg 2003d, 2004).

Compared to the RCR approach, the computational effort is reduced by combining the computation of the direct and indirect effect, see Sjöberg (2003a, Sec. 9.2). Also, as opposed to the RCR method, the magnitude of each correction directly reflects the error made in geoid modelling by neglecting that particular effect.

Used in conjunction with the least squares modifications of Sjöberg (1984, 1991, 2003b), the geoid modelling approach of Eq. 11 is called the method of Least Squares Modification of Stokes's formula with Additive Corrections (LSMSA).

Figure 12 illustrates contributions of the individual terms in Eq. 11 to the final geoid model in the study area of **Paper A** (see Fig. 13 for characteristics of the area). Most of the long wavelength geoid signal originates from the far zone (Fig. 12e) and the medium to short wavelength signal from the near zone (Fig.

51

12d). The DWC correction (Fig. 12a) also adds significant signal in the order of decimetres (in areas with an elevation of about 2 km) while the contribution of atmospheric (Fig. 12b) and ellipsoidal (Fig. 12c) corrections could be numerically below centimetre.

The approximate geoid $\widetilde{N}$ can also be used for quasigeoid (i.e. height anomaly) determination by:

$$\widehat{\zeta} = \widetilde{N} + \delta\zeta_{DWC} + \delta\zeta_{ATM} + \delta\zeta_{ELL} \tag{12}$$

where $\delta\zeta_{DWC}$, $\delta\zeta_{ATM}$ and $\delta\zeta_{ELL}$ are the corresponding DWC, atmospheric and ellipsoidal corrections for quasigeoid determination.

Examples of the LSMSA approach being used for regional geoid computation include Ellmann (2005c), Kiamehr (2006), Daras (2008), Ågren et al. (2009b), Ulotu (2009), Abdalla and Fairhead (2011), Abdalla and Tenzer (2011), Abbak et al. (2012), Sjöberg et al. (2015), Kuczynska-Siehien et al. (2016), and Ågren et al. (2016). The two approaches (RCR and KTH) are compared in e.g. Ågren (2004, Chapter 7 and 9) and Ågren et al. (2009a). Computer code for LS modifications is provided in Ellmann (2005a) and Abbak and Ustun (2015).

LSMSA is the method that will be implemented to the Hotine formula to yield the new geoid modelling method presented in this thesis.

4.2   Geoid modelling by the Hotine formula

Although use of the modified Stokes formula is more widespread, the Hotine formula has also been used for geoid determination, mostly from airborne gravimetry (e.g. Novák and Heck 2002, Novák et al. 2003, Alberts and Klees 2004, Serpas and Jekeli 2005, Sjöberg and Eshagh 2009), but also from altimetry (e.g. Zhang 1998) and land gravimetry (e.g. Kirby 2003).

Analogously to the Stokes formula, modifications to the Hotine formula have been presented in e.g. Jekeli (1979), Jekeli (1980), Sjöberg (1986), Guan and Li (1991), Sjöberg and Nord (1992), Vaníček et al. (1992), Zhang (1998), Novák (2003), Novák et al. (2003), Sjöberg and Eshagh (2009) and summarized in Featherstone (2013).

Featherstone (*ibid.*, Sec. 4.5) demonstrates the application of LS modification to Hotine's formula in the special case of no truncation (see also Sjöberg 2003b, Sec. 4). However, this study (also in **Paper A**) is the first to comprehensively adapt the particular least squares modification methods presented in Sjöberg (1984, 1991, 2003b) to the Hotine formula. That is, equations are presented for the biased, unbiased and optimum LS modification of Hotine's formula. Also, additive corrections for geoid and quasigeoid determination are developed analogously to Sjöberg (2003a) to fully implement the LSMSA principles to the Hotine formula. Correspondingly, the regional geoid modelling procedure developed in **Paper A** is called the Least Squares Modification of Hotine's formula with Additive Corrections (LSMHA).

Together, Tables 3 to 7 summarize and compare the complete LSMSA and LSMHA methods intended for geoid and quasigeoid computation.

4.3 Geoid modelling by the least squares modified Hotine formula

In analogy to the LSMSA geoid modelling method described in Sec. 4.1, a geoid model computed by the LSMHA approach is obtained by adding the approximate geoid estimator $\widetilde{N}$ and the additive corrections as in Eq. 11 (or Eq. 12 for the quasigeoid). This time, however, the approximate geoid estimator is computed from the modified Hotine formula, see Eq. 13 below. Accordingly, the expressions of additive corrections also need to be adapted to the use of Hotine's formula, see Sections 4.5 to 4.8 below.

The approximate geoid estimator $\widetilde{N}$ combines the near zone and the far zone gravity contributions analogously to Eq. 5:

$$\widetilde{N} = \frac{R}{4\pi\gamma} \iint_{\sigma_0} H^L(\psi)\delta g d\sigma + \frac{R}{2\gamma} \sum_{n=0}^{M} b_n \delta g_n^{\text{GGM}} \tag{13}$$

where $H^L(\psi)$ is the modified Hotine function, δg are terrestrial gravity disturbance values, δg_n^{GGM} are the GGM-derived Laplace harmonics of δg and b_n are again arbitrary modification parameters.

Equation 13 can equivalently be written in its spectral form as (analogously to Sjöberg 2003a, Eq. 8a):

$$\widetilde{N} = \frac{R}{4\pi\gamma} \sum_{n=0}^{\infty} \left(\frac{2}{n+1} - Q_n^L - s_n^* \right) \delta g_n^T + \frac{R}{2\gamma} \sum_{n=0}^{M} b_n \delta g_n^{\text{GGM}} \tag{14}$$

with

$$s_n^* = \begin{cases} s_n, & \text{if } 0 \leq n \leq L \\ 0, & \text{otherwise} \end{cases} \tag{15}$$

where Q_n^L are modified truncation coefficients and s_n are modification parameters. The modified truncation coefficients Q_n^L are computed from the modification parameters s_n and the unmodified (Molodensky-type) truncation coefficients Q_n adapted for the Hotine function, see Table 3. The latter can be evaluated by recursive relations given in Jekeli (1979, Appendix A or C) or Guan and Li (1991, p. 87).

For comparison, Table 3 presents equations and their components for geoid modelling by the modified Stokes and Hotine formula.

Different modifications to the Hotine formula are applied through selecting appropriate modification parameters s_n and b_n so as to minimize errors of the geoid estimator. Table 5 presents the necessary equations derived for the computation of the s_n and b_n parameters for the biased, unbiased and optimum least squares modifications to the Hotine formula (denoted as BLS, ULS and OLS respectively). Notice that even though these equations look exactly the same as the

Table 3: Comparison of the modified Stokes and Hotine formula and their components (the symbols are explained in text or the symbol list on p. 13)

Stokes	Hotine
$N = \dfrac{R}{4\pi\gamma} \iint_{\sigma} S(\psi)\Delta g\, d\sigma$	$N = \dfrac{R}{4\pi\gamma} \iint_{\sigma} H(\psi)\delta g\, d\sigma$
$S(\psi) = \displaystyle\sum_{n=2}^{\infty} \dfrac{2n+1}{n-1} P_n(\cos\psi)$	$H(\psi) = \displaystyle\sum_{n=0}^{\infty} \dfrac{2n+1}{n+1} P_n(\cos\psi)$
$\widetilde{N} = \dfrac{R}{4\pi\gamma} \iint_{\sigma_0} S^L(\psi)\Delta g^T d\sigma$ $+ \dfrac{R}{2\gamma} \displaystyle\sum_{n=2}^{M} b_n \Delta g_n^{\mathrm{GGM}}$	$\widetilde{N} = \dfrac{R}{4\pi\gamma} \iint_{\sigma_0} H^L(\psi)\delta g^T d\sigma$ $+ \dfrac{R}{2\gamma} \displaystyle\sum_{n=0}^{M} b_n \delta g_n^{\mathrm{GGM}}$
$S^L(\psi) = S(\psi) -$ $- \displaystyle\sum_{n=2}^{L} \dfrac{2n+1}{2} s_n P_n(\cos\psi)$	$H^L(\psi) = H(\psi) -$ $\displaystyle\sum_{n=0}^{L} \dfrac{2n+1}{2} s_n P_n(\cos\psi)$
$\widetilde{N} = \dfrac{R}{4\pi\gamma} \displaystyle\sum_{n=0}^{\infty} \left(\dfrac{2}{n-1} - Q_n^L - s_n^* \right) \Delta g_n$ $+ \dfrac{R}{2\gamma} \displaystyle\sum_{n=2}^{M} b_n \Delta g_n^{\mathrm{GGM}}$	$\widetilde{N} = \dfrac{R}{4\pi\gamma} \displaystyle\sum_{n=0}^{\infty} \left(\dfrac{2}{n+1} - Q_n^L - s_n^* \right) \delta g_n$ $+ \dfrac{R}{2\gamma} \displaystyle\sum_{n=0}^{M} b_n \delta g_n^{\mathrm{GGM}}$
$s_n^* = \begin{cases} s_n, & \text{if } 0 \le n \le L \\ 0, & \text{otherwise} \end{cases}$	
$\Delta g_n^{\mathrm{GGM}} = \dfrac{GM}{a^2} \displaystyle\sum_{n=2}^{\infty} (n-1)\left(\dfrac{a}{r}\right)^{n+2} \times$ $\times \displaystyle\sum_{m=-n}^{n} C_{nm} Y_{nm}$	$\delta g_n^{\mathrm{GGM}} = \dfrac{GM}{a^2} \displaystyle\sum_{n=0}^{\infty} (n+1)\left(\dfrac{a}{r}\right)^{n+2} \times$ $\times \displaystyle\sum_{m=-n}^{n} C_{nm} Y_{nm}$
$Q_n^L(\psi_0) = Q_n(\psi_0) - \displaystyle\sum_{k=0}^{L} E_{nk} s_k = Q_n(\psi_0) - \displaystyle\sum_{k=0}^{L} \dfrac{2k+1}{2} R_{nk} s_k$	
R_{nk} from Paul (1973)	
$Q_n(\psi_0)$ from Paul (1973)	$Q_n(\psi_0)$ from Jekeli (1979)
$p_n = \dfrac{2\sigma_n^2}{n-1}$	$p_n = \dfrac{2\sigma_n^2}{n+1}$

Table 4: Expected global mean square error of the geoid estimator for the modified Stokes and Hotine formula (the symbols are explained in text or the symbol list on p. 13)

	Stokes	Hotine
$\left(\delta\widetilde{N}\right)^2$	$\left(\delta\widetilde{N}\right)^2_{\text{TR}} + \left(\delta\widetilde{N}\right)^2_{\text{T}} + \left(\delta\widetilde{N}\right)^2_{\text{GGM}}$	
$\left(\delta\widetilde{N}\right)^2_{\text{TR}}$	$c^2 \sum\limits_{n=0}^{\infty} \left(b_n^* - s_n^* - Q_n^L\right)^2 c_n^2$	
$\left(\delta\widetilde{N}\right)^2_{\text{T}}$	$c^2 \sum\limits_{n=2}^{\infty} \left(\dfrac{2}{n-1} - s_n^* - Q_n^L\right)^2 \sigma_n^2$	$c^2 \sum\limits_{n=0}^{\infty} \left(\dfrac{2}{n+1} - s_n^* - Q_n^L\right)^2 \sigma_n^2$
$\left(\delta\widetilde{N}\right)^2_{\text{GGM}}$	$c^2 \sum\limits_{n=0}^{M} b_n^2 dc_n^2$	
	$b_n^* = \begin{cases} b_n, & \text{if } 0 \leq n \leq M \\ 0, & \text{otherwise} \end{cases}$	
c	$\dfrac{R}{2\gamma}$	
c_n^2	$c_{n,\Delta g}^2$	$c_{n,\delta g}^2$
σ_n^2	$\sigma_{n,\Delta g}^2$	$\sigma_{n,\delta g}^2$
dc_n^2	$dc_{n,\Delta g}^2$	$dc_{n,\delta g}^2$

Table 5: Modification parameters for the biased (BLS), unbiased (ULS) and optimum (OLS) least squares modifications, valid for both the Stokes and Hotine formula (the symbols are explained in text or the symbol list on p. 13)

	BLS	ULS	OLS
b_n	s_n	$s_n + Q_n^L$	$\dfrac{(s_n + Q_n^L)c_n^2}{(c_n^2 + dc_n^2)}$
s_r	$\displaystyle\sum_{r=0}^{L} a_{kr}s_r = h_k, k = 0,1,2,...,L$		
$a_{kr} = a_{rk}$	$\displaystyle\sum_{n=0}^{\infty} E_{nk}E_{nr}(\sigma_n^2 + c_n^2) + \\ + \delta_{kr}(\sigma_r^2 + dc_r^2) - E_{kr}\sigma_k^2 - E_{rk}\sigma_r^2$	$\displaystyle\sum_{n=0}^{\infty} E_{nk}E_{nr}C_n + \delta_{kr}C_r - E_{kr}C_k - E_{rk}C_r$	
h_k	$p_k - Q_k\sigma_k^2 + \displaystyle\sum_{n=0}^{\infty} \left[Q_n(\sigma_n^2 + c_n^2) - p_n \right] E_{nk}$	$p_k - Q_kC_k + \displaystyle\sum_{n=0}^{\infty} (Q_nC_n - p_n) E_{nk}$	
C_n		$\sigma_n^2 + \begin{cases} dc_n^2, & \text{if } n \leq M \\ c_n^2, & \text{if } n > M \end{cases}$	$\sigma_n^2 + \begin{cases} c_n^2 dc_n^2/(c_n^2 + dc_n^2), & \text{if } n \leq M \\ c_n^2, & \text{if } n > M \end{cases}$
	$\delta_{kr} = \begin{cases} 1, & \text{if } k = r \\ 0, & \text{otherwise} \end{cases}$		

Table 6: Computation of the additive corrections for the modified Stokes and Hotine formula (the symbols are explained in text or the symbol list on p. 13)

	Stokes	Hotine
$\widehat{N}$	$\widetilde{N} + \delta N_{\mathrm{COMB}} + \delta N_{\mathrm{DWC}} + \delta N_{\mathrm{ATM}} + \delta N_{\mathrm{ELL}}$	
$\widehat{\zeta}$	$\widetilde{N} + \delta\zeta_{\mathrm{DWC}} + \delta\zeta_{\mathrm{ATM}} + \delta\zeta_{\mathrm{ELL}}$	
$\delta N_{\mathrm{COMB}}(\mathrm{P})$	$-\dfrac{2\pi G\rho}{\gamma}\left(H_{\mathrm{P}}^2 + \dfrac{2}{3}\dfrac{H_{\mathrm{P}}^3}{r_{\mathrm{P}}}\right)$	
$\delta N_{\mathrm{DWC}}(\mathrm{P})$	$\delta N_{\mathrm{DWC}}^{(1)}(\mathrm{P}) + \delta N_{\mathrm{DWC}}^{\mathrm{L}(1),\mathrm{far}}(\mathrm{P}) + \delta N_{\mathrm{DWC}}^{\mathrm{L}(2)}(\mathrm{P})$	
$\delta N_{\mathrm{DWC}}^{(1)}(\mathrm{P})$	$\dfrac{\Delta g(\mathrm{P})}{\gamma}H_{\mathrm{P}} + 3\dfrac{\zeta_{\mathrm{P}}^0}{r_{\mathrm{P}}}H_{\mathrm{P}} - \dfrac{1}{2\gamma}\left.\dfrac{\partial \Delta g}{\partial r}\right|_{\mathrm{P}} H_{\mathrm{P}}^2$	$\dfrac{\delta g(\mathrm{P})}{\gamma}H_{\mathrm{P}} + \dfrac{\zeta_{\mathrm{P}}^0}{r_{\mathrm{P}}}H_{\mathrm{P}} - \dfrac{1}{2\gamma}\left.\dfrac{\partial \delta g}{\partial r}\right|_{\mathrm{P}} H_{\mathrm{P}}^2$
$\delta N_{\mathrm{DWC}}^{\mathrm{L}(1),\mathrm{far}}(\mathrm{P})$	$\dfrac{R}{2\gamma}\displaystyle\sum_{n=2}^{M}(s_n + Q_n^L)\left[\left(\dfrac{R}{r_{\mathrm{P}}}\right)^{n+2} - 1\right]\Delta g_n^{\mathrm{GGM}}(\mathrm{P})$	$\dfrac{R}{2\gamma}\displaystyle\sum_{n=0}^{M}(s_n + Q_n^L)\left[\left(\dfrac{R}{r_{\mathrm{P}}}\right)^{n+2} - 1\right]\delta g_n^{\mathrm{GGM}}(\mathrm{P})$
$\delta N_{\mathrm{DWC}}^{\mathrm{L}(2)}(\mathrm{P})$	$\dfrac{R}{4\pi\gamma}\displaystyle\iint_{\sigma_0} S^L(\psi)\left[\left.\dfrac{\partial \Delta g}{\partial r}\right|_{\mathrm{Q}}(H_{\mathrm{P}} - H_{\mathrm{Q}})\right]d\sigma_{\mathrm{Q}}$	$\dfrac{R}{4\pi\gamma}\displaystyle\iint_{\sigma_0} H^L(\psi)\left[\left.\dfrac{\partial \delta g}{\partial r}\right|_{\mathrm{Q}}(H_{\mathrm{P}} - H_{\mathrm{Q}})\right]d\sigma_{\mathrm{Q}}$
$\delta\zeta_{\mathrm{DWC}}(\mathrm{P})$	$3\dfrac{\zeta_{\mathrm{P}}^0}{r_{\mathrm{P}}}H_{\mathrm{P}} + \delta N_{\mathrm{DWC}}^{\mathrm{L}(1),\mathrm{far}}(\mathrm{P}) + \delta N_{\mathrm{DWC}}^{\mathrm{L}(2)}(\mathrm{P})$	

Table 7: Computation of the additive corrections for the modified Stokes and Hotine formula (continued)

	Stokes	Hotine
$\delta N_{\text{ATM}}(\text{P})$ $\approx \delta\zeta_{\text{ATM}}(\text{P})$	$-\dfrac{2\pi RG\rho_{\text{A}}}{\gamma}\displaystyle\sum_{n=0}^{M}\left(\dfrac{2}{n-1}-s_n-Q_n^L\right)H_n(\text{P})-$ $-\dfrac{2\pi RG\rho_{\text{A}}}{\gamma}\displaystyle\sum_{n=M+1}^{\infty}\left(\dfrac{2}{n-1}-\dfrac{n+2}{2n+1}Q_n^L\right)H_n(\text{P})$	$-\dfrac{2\pi RG\rho_{\text{A}}}{\gamma}\displaystyle\sum_{n=0}^{M}\left(\dfrac{2}{n+1}-s_n-Q_n^L\right)H_n(\text{P})-$ $-\dfrac{2\pi RG\rho_{\text{A}}}{\gamma}\displaystyle\sum_{n=M+1}^{\infty}\left(\dfrac{2}{n+1}-\dfrac{n+2}{2n+1}Q_n^L\right)H_n(\text{P})$
$\delta N_{\text{ELL}}(\text{P})$ $\approx \delta\zeta_{\text{ELL}}(\text{P})$	$\dfrac{R}{2\gamma}\displaystyle\sum_{n=0}^{\infty}\left(\dfrac{2}{n-1}-s_n^*-Q_n^L\right)\times$ $\left(\dfrac{a-R}{R}\Delta g_n^{\text{GGM}}(\text{P})+\dfrac{a}{R}\delta g_n^{\text{e}}\right)$	$\dfrac{R}{2\gamma}\displaystyle\sum_{n=0}^{\infty}\left(\dfrac{2}{n+1}-s_n^*-Q_n^L\right)\times$ $\left(\dfrac{a-R}{R}\delta g_n^{\text{GGM}}(\text{P})+\dfrac{a}{R}\delta g_n^{\text{e}}\right)$
δg_n^{e}	$\dfrac{e^2 GM}{2a}\displaystyle\sum_{m=-n}^{n}\{[3-(n+2)F_{nm}]C_{nm}-$ $-(n+1)G_{nm}C_{n-2,m}-(n+7)E_{nm}C_{n+2,m}\}Y_{nm}(\text{P})$	$\dfrac{e^2 GM}{2a}\displaystyle\sum_{m=-n}^{n}\{[3-(n+4)F_{nm}]C_{nm}-$ $-(5-n)G_{nm}C_{n+2,m}-(3n+7)E_{nm}C_{n-2,m}\}Y_{nm}(\text{P})$

original equations intended for use with the Stokes formula, some of the symbols used have a different definition.

To each set of s_n and b_n parameters corresponds a modified Hotine function H^L and modified truncation coefficients Q_n^L. Together, b_n and H^L determine the relative contribution of the far zone and the near zone gravity information to the particular geoid estimator, see Eq. 13. In fact, the modified truncation parameters Q_n^L work in conjunction with the corresponding s_n in such a way that the coefficients b_n become numerically very similar regardless of the modification method used.

For the unbiased modification, the truncation error is completely reduced up to degree M, hence the name. The biased and optimum LS estimators are slightly biased (c.f. Sjöberg 1991, 2003b). For the optimum method, this bias is small if the GGM-related error estimates are small below the limit of M. With the GGM-related errors becoming significant, for example by increasing the maximum degree M of the GGM used, the bias increases (see Table 8 on p. 78).

Importantly, being stochastic modifications, all of the presented LS modifications depend on estimated gravity signal and error properties. These are provided by the terrestrial gravity error degree variances σ_n^2, GGM error degree variances dc_n^2 and gravity signal degree variances c_n^2 which are used in the computation of the modification parameters s_n and b_n (see Table 5).

The gravity disturbance (signal or error) degree variances $d_{n,\delta g}^2$ can be expressed in terms of the gravity anomaly degree variances $d_{n,\Delta g}^2$ as (**Paper A**):

$$d_{n,\delta g}^2 = \frac{(n+1)^2}{(n-1)^2} d_{n,\Delta g}^2 \qquad (16)$$

revealing that the difference in anomaly and disturbance degree variances becomes smaller and approaches zero with increasing degree n. Alternatively, instead of adapting the gravity anomaly degree variances to gravity disturbance by the relation given in Eq. 16, standard models (similar to Kaula 1963 or Tscherning and Rapp 1974) can directly be constructed for the gravity disturbances.

4.4 Expected global error of geoid modelling

Means to evaluate the result of specific modifications to the Hotine formula is provided by the expected global mean square error (MSE) of the geoid estimator $\widetilde{N}$:

$$\left(\delta\widetilde{N}\right)^2 = \left(\delta\widetilde{N}\right)_{\mathrm{TR}}^2 + \left(\delta\widetilde{N}\right)_{\mathrm{T}}^2 + \left(\delta\widetilde{N}\right)_{\mathrm{GGM}}^2 \qquad (17)$$

where the partial contributions represent the error due to truncation, terrestrial data and the GGM respectively. See Table 4 for the computation of these partial contributions.

Equation 17 allows to find an estimate of the geoid model error that corresponds to the specific modification parameters s_n and b_n and the estimated gravity

signal and error properties described by the degree variance models of c_n^2, σ_n^2 and dc_n^2.

Under the assumption of equal degree variances (i.e. not using Eq. 16), the Hotine formula will yield a smaller expected global MSE than its Stokes's counterpart, see e.g. Sjöberg (1986, Sec. 4) and Guan and Li (1991, Fig. 1).

4.5 Additive corrections for the LS modified Hotine formula

Tables 6 and 7 present the necessary equations for the computation of the four additive corrections to geoid (Eq. 11) and quasigeoid (Eq. 12) modelling by the modified Hotine formula.

These additive corrections follow the same principles as those summarized in Sjöberg (2003a) for the Stokes formula. Accordingly they also have a similar magnitude to the Stokes counterparts presented on Fig. 12. For an illustration of their contributions to the (quasi)geoid model computed by the LSMHA method, see Fig. 3 of **Paper A**. Notice however, that Eq. 46 (and consequently Fig. 3f) of **Paper A** contains an error.

The following sections 4.6 to 4.8 of this thesis present details of the DWC and ellipsoidal correction that were not included in **Paper A** due to space limitations. The notation used in Sections 4.6 to 4.8 is deliberately kept similar to the original publications and therefore deviates slightly from that used in the rest of the thesis (and the symbol list on p. 13).

4.6 DWC correction for geoid modelling

In this section, the DWC correction for geoid modelling δN_{DWC} (in Eq. 11) corresponding to the LSMHA method will be derived similarly to the LSMSA version presented in Ågren (2004, Sec. 5.4.1). For a slightly different derivation, see Sjöberg (2003c) and Sjöberg and Bagherbandi (2017, Sect. 5.3).

The DWC effect at point P can be separated in two parts (anal. to Ågren 2004, Eq. 5.32):

$$\delta N_{\mathrm{DWC}}(\mathrm{P}) = \delta N_{\mathrm{DWC}}^{\mathrm{L}(1)}(\mathrm{P}) + \delta N_{\mathrm{DWC}}^{\mathrm{L}(2)}(\mathrm{P}) \tag{18a}$$

$$= \frac{c}{2\pi} \iint_{\sigma_0} H^L(\psi) \left[\delta g^*(\mathrm{Q}) - \delta g(r_{\mathrm{P}}, \mathrm{Q}) \right] d\sigma_{\mathrm{Q}}$$
$$+ \frac{c}{2\pi} \iint_{\sigma_0} H^L(\psi) \left[\delta g(r_{\mathrm{P}}, \mathrm{Q}) - \delta g(\mathrm{Q}) \right] d\sigma_{\mathrm{Q}} \tag{18b}$$

where $\delta g^*(\mathrm{Q})$ is the downward continued gravity disturbance of the running integration point Q; $r_{\mathrm{P}} = R + H_{\mathrm{P}}$; $\delta g(r_{\mathrm{P}}, \mathrm{Q})$ is the gravity disturbance of Q downward continued to the level of the computation point P; $c = R/2\pi$. The second term $\delta N_{\mathrm{DWC}}^{\mathrm{L}(2)}(\mathrm{P})$ represents the passage from the surface point Q to the level of point P and the first term $\delta N_{\mathrm{DWC}}^{\mathrm{L}(1)}(\mathrm{P})$ the remaining continuation down to sea level, see Fig. 14. These could also be called the terrain and Bouguer part of DWC, respectively.
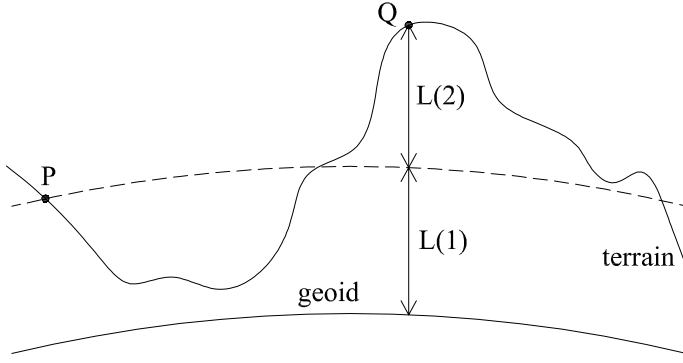
Figure 14: Separation of the DWC effect

The first term $\delta N_{\text{DWC}}^{\text{L(1)}}(\text{P})$ of Eq. 18a can be rewritten in terms of the difference between the total contribution and the far zone contribution as (anal. to Ågren 2004, Eq. 5.33):

$$
\delta N_{\text{DWC}}^{\text{L(1)}}(\text{P}) = \frac{c}{2\pi} \iint_{\sigma} H^L(\psi) \left[\delta g^*(\text{Q}) - \delta g(r_{\text{P}},\text{Q}) \right] d\sigma_{\text{Q}}
$$
$$
- \frac{c}{2\pi} \iint_{\sigma-\sigma_0} H^L(\psi) \left[\delta g^*(\text{Q}) - \delta g(r_{\text{P}},\text{Q}) \right] d\sigma_{\text{Q}} \tag{19a}
$$
$$
= \frac{c}{2\pi} \iint_{\sigma} H(\psi) \left[\delta g^*(\text{Q}) - \delta g(r_{\text{P}},\text{Q}) \right] d\sigma_{\text{Q}}
$$
$$
- c \sum_{n=0}^{\infty} \left(s_n^* + Q_n^L \right) \left[1 - \left(\frac{R}{r_{\text{P}}} \right)^{n+2} \right] \delta g_n(\text{P}) \tag{19b}
$$
$$
= \delta N_{\text{DWC}}^{(1)}(\text{P}) + \delta N_{\text{DWC}}^{\text{L(1),far}}(\text{P}) \tag{19c}
$$

The infinite series in the second term $\delta N_{\text{DWC}}^{\text{L(1),far}}(\text{P})$ of Eq. 19c can in practice be computed by a GGM evaluated up to maximum degree M:

$$
\boxed{\delta N_{\text{DWC}}^{\text{L(1),far}}(\text{P}) = c \sum_{n=0}^{M} \left(s_n^* + Q_n^L \right) \left[\left(\frac{R}{r_{\text{P}}} \right)^{n+2} - 1 \right] \delta g_n(\text{P})} \tag{20}
$$

Next, an approximate expression will be derived for $\delta N_{\text{DWC}}^{(1)}(\text{P})$ (the first term of Eq. 19c) representing downward continuation from point level to sea level for the original Hotine formula, anal. to Sjöberg (2003c). For this, $\delta g(r_{\text{P}},\text{Q})$ is approximated by the first three terms of its Taylor series (anal. to Ågren 2004, Eq. 5.37):

$$
\delta g(r_{\text{P}},\text{Q}) \approx \delta g^*(\text{Q}) + \left. \frac{\partial \delta g}{\partial r} \right|_{\text{Q}}^{*} H_{\text{P}} + \frac{1}{2} \left. \frac{\partial^2 \delta g}{\partial r^2} \right|_{\text{Q}}^{*} H_{\text{P}}^2 \tag{21}
$$

Since

$$\delta g(\mathrm{P}) = \sum_{n=0}^{\infty} \frac{n+1}{R} \left(\frac{R}{r_{\mathrm{P}}} \right)^{n+2} T_n(\mathrm{P}) \tag{22}$$

where $T_n(\mathrm{P})$ are the Laplace harmonics of the disturbing potential (Heiskanen and Moritz 1967, Eq. 2-152), we have

$$\left. \frac{\partial \delta g}{\partial r} \right|_{\mathrm{P}} = - \sum_{n=0}^{\infty} \frac{(n+1)(n+2)}{R^2} \left(\frac{R}{r_{\mathrm{P}}} \right)^{n+3} T_n(\mathrm{P}) \tag{23}$$

and

$$\left. \frac{\partial^2 \delta g}{\partial r^2} \right|_{\mathrm{P}} = \sum_{n=0}^{\infty} \frac{(n+1)(n+2)(n+3)}{R^3} \left(\frac{R}{r_{\mathrm{P}}} \right)^{n+4} T_n(\mathrm{P}) \tag{24}$$

Substituting the Taylor series of Eq. 21 into $\delta N_{\mathrm{DWC}}^{(1)}(\mathrm{P})$ (Eq. 19b) yields (anal. to Ågren 2004, Eq. 5.41):

$$\begin{aligned}
\delta N_{\mathrm{DWC}}^{(1)}(\mathrm{P}) &= - \frac{c}{2\pi} \iint_{\sigma} H(\psi) \left(\left. \frac{\partial \delta g}{\partial r} \right|_{\mathrm{Q}}^{*} H_{\mathrm{P}} + \frac{1}{2} \left. \frac{\partial^2 \delta g}{\partial r^2} \right|_{\mathrm{Q}}^{*} H_{\mathrm{P}}^2 \right) \\
&= \frac{1}{\gamma_0} \sum_{n=0}^{\infty} \left[\frac{n+2}{R} H_{\mathrm{P}} - \frac{(n+2)(n+3)}{2R^2} H_{\mathrm{P}}^2 \right] T_n(\mathrm{P})
\end{aligned} \tag{25}$$

where γ_0 is the normal gravity at the ellipsoid.

Since

$$\frac{n+2}{R} = \frac{n+1}{R} + \frac{1}{R} \tag{26}$$

and

$$\frac{(n+2)(n+3)}{2R^2} = \frac{(n+2)(n+1)}{2R^2} + \frac{2(n+1)}{2R^2} + \frac{2}{2R^2} \tag{27}$$

then

$$\delta N_{\mathrm{DWC}}^{(1)}(\mathrm{P}) =$$

$$= \frac{1}{\gamma_0} \sum_{n=0}^{\infty} \left\{ \left[\frac{n+1}{R} + \frac{1}{R} \right] H_{\mathrm{P}} - \left[\frac{(n+2)(n+1)}{2R^2} + \frac{n+1}{R^2} + \frac{1}{R^2} \right] H_{\mathrm{P}}^2 \right\} T_n(\mathrm{P}) \tag{28a}$$

$$= \frac{\delta g^*(\mathrm{P})}{\gamma_0} H_{\mathrm{P}} + \frac{1}{R} \frac{T^*(\mathrm{P})}{\gamma_0} H_{\mathrm{P}} + \frac{1}{2\gamma_0} \left. \frac{\partial \delta g}{\partial r} \right|_{\mathrm{P}}^{*} H_{\mathrm{P}}^2 - \left[\frac{\delta g^*}{R\gamma_0} + \frac{T^*(\mathrm{P})}{\gamma_0 R^2} \right] H_{\mathrm{P}}^2 \tag{28b}$$

As shown by Sjöberg (2003c), the last term of Eq. 28b can safely be neglected. Thus

$$\delta N_{\mathrm{DWC}}^{(1)}(\mathrm{P}) = \frac{\delta g^*(\mathrm{P})}{\gamma_0} H_{\mathrm{P}} + \frac{1}{R} \frac{T^*(\mathrm{P})}{\gamma_0} H_{\mathrm{P}} + \frac{1}{2\gamma_0} \left. \frac{\partial \delta g}{\partial r} \right|_{\mathrm{P}}^{*} H_{\mathrm{P}}^2 \tag{29}$$

Since the downward continued height anomaly is defined as

$$\zeta_{\mathrm{P}}^* = \frac{T^*(\mathrm{P})}{\gamma_0} \tag{30}$$

then (anal. to Ågren 2004, Eq. 5.42)

$$\delta N_{\text{DWC}}^{(1)}(\text{P}) = \frac{\delta g^*(\text{P})}{\gamma_0} H_{\text{P}} + \frac{\zeta_{\text{P}}^*}{R} H_{\text{P}} + \frac{1}{2\gamma_0} \frac{\partial \delta g}{\partial r}\bigg|_{\text{P}}^* H_{\text{P}}^2 \tag{31}$$

Notice that, compared to the original equation intended for the Stokes formula, the factor 3 is not present in the second term of Eq. 31.

The downward continued height anomaly ζ_{P}^* of Eq. 30 can be expanded into a Taylor series at the point P by (anal. to Sjöberg 2003c, Eq. 7):

$$\zeta_{\text{P}}^* = \sum_{k=0}^{\infty} \frac{(-H_{\text{P}})^k}{k!} \frac{\partial^k \zeta}{\partial H^k}\bigg|_{\text{P}} \approx \zeta_{\text{P}} - H_{\text{P}} \frac{\partial \zeta}{\partial H}\bigg|_{\text{P}} \tag{32}$$

The correct height anomaly at P is given by the Bruns' formula (anal. to *ibid.*, Eq. 4):

$$\zeta_{\text{P}} = \frac{T_{\text{P}}}{\gamma} \tag{33}$$

where γ is the normal gravity at the telluroid. By differentiating Eq. 33 with respect to H at the point P:

$$\frac{\partial \zeta}{\partial H}\bigg|_{\text{P}} = \frac{1}{\gamma}\left(\frac{\partial T}{\partial H}\bigg|_{\text{P}} - \frac{1}{\gamma}\frac{\partial \gamma}{\partial H}\bigg|_{\text{P}} T_{\text{P}}\right) = \frac{1}{\gamma}\left(\delta g(\text{P}) - \frac{2}{R}T_{\text{P}}\right) = -\frac{\Delta g(\text{P})}{\gamma} \tag{34}$$

the following is arrived at (Ågren 2004, Eq. 5.43):

$$\zeta_{\text{P}}^* \approx \zeta_{\text{P}} + \frac{\Delta g(\text{P})}{\gamma} H_{\text{P}} \tag{35}$$

Since (anal. to *ibid.*, Eq. 5.44):

$$\delta g^*(\text{P}) = \delta g(\text{P}) - \frac{\partial \delta g}{\partial r}\bigg|_{\text{P}} H_{\text{P}} \tag{36}$$

and

$$\frac{1}{\gamma_0} = \frac{1}{\gamma}\left(1 - 2\frac{H_{\text{P}}}{r_{\text{P}}}\right) \tag{37}$$

and

$$\frac{1}{R} = \frac{1}{r_{\text{P}}}\left(1 + \frac{H_{\text{P}}}{r_{\text{P}}}\right) \tag{38}$$

the first part of $\delta N_{\text{DWC}}^{(1)}(\text{P})$ given in Eq. 31 becomes:

$$\frac{\delta g^*(\text{P})}{\gamma_0} H_{\text{P}} = \left[\frac{\delta g(\text{P})}{\gamma_0} - \frac{1}{\gamma_0}\frac{\partial \delta g}{\partial r}\bigg|_{\text{P}} H_{\text{P}}\right] H_{\text{P}} \tag{39a}$$

$$= \frac{1}{\gamma}\delta g(\text{P})H_{\text{P}} - \frac{2}{\gamma}\frac{H_{\text{P}}^2}{r_{\text{P}}}\delta g(\text{P}) - \frac{1}{\gamma}\frac{\partial \delta g}{\partial r}\bigg|_{\text{P}} H_{\text{P}}^2 + 2\gamma\frac{H_{\text{P}}}{r_{\text{P}}}\frac{\partial \delta g}{\partial r}\bigg|_{\text{P}} H_{\text{P}}^2 \tag{39b}$$

The second and fourth term of Eq. 39b can be omitted. Thus

$$\frac{\delta g^*(P)}{\gamma_0} H_P = \frac{1}{\gamma} \delta g(P) H_P - \frac{1}{\gamma} \left.\frac{\partial \delta g}{\partial r}\right|_P H_P^2 \tag{40}$$

Due to Eqs. 35 and 38, the second term of $\delta N_{\mathrm{DWC}}^{(1)}(P)$ given in Eq. 31 becomes:

$$\frac{\zeta_P^*}{R} H_P = \frac{1}{r_P} \left[1 + \frac{H_P}{r_P}\right] \left[\zeta_P H_P + \frac{\Delta g(P)}{\gamma} H_P^2\right] \tag{41a}$$

$$= \zeta_P \frac{H_P}{r_P} + \frac{\Delta g(P)}{\gamma} \frac{H_P^2}{r_P} + \zeta_P \frac{H_P^2}{r_P^2} + \frac{\Delta g(P)}{\gamma} \frac{H_P^3}{r_P^2} \tag{41b}$$

The last two terms of Eq. 41b can again be neglected. Also for $H = 5(8)$ km (Sjöberg 2003c, Sec. 3):

$$\left|\frac{H^2 \Delta g}{\gamma r}\right| \leq 1(3)\mathrm{mm} \tag{42}$$

which allows to neglect also the second term of Eq. 41b. Thus:

$$\frac{\zeta^*}{R} H_P = \zeta_P \frac{H_P}{r_P} \tag{43}$$

Assuming

$$\left.\frac{\partial \delta g}{\partial r}\right|_P^* \approx \left.\frac{\partial \delta g}{\partial r}\right|_P \tag{44}$$

the third part of $\delta N_{\mathrm{DWC}}^{(1)}(P)$ given in Eq. 31 becomes:

$$\frac{1}{2\gamma_0} \left.\frac{\partial \delta g}{\partial r}\right|_P^* H_P^2 = \frac{1}{2\gamma} \left.\frac{\partial \delta g}{\partial r}\right|_P H_P^2 - \frac{1}{\gamma} \left.\frac{\partial \delta g}{\partial r}\right|_P \frac{H_P^3}{r_P} \tag{45}$$

where the last term can be omitted (as it is in the order H^3), thus

$$\frac{1}{2\gamma_0} \left.\frac{\partial \delta g}{\partial r}\right|_P^* H_P^2 = \frac{1}{2\gamma} \left.\frac{\partial \delta g}{\partial r}\right|_P H_P^2 \tag{46}$$

Adding the three parts (Eqs. 40, 43 and 46) of $\delta N_{\mathrm{DWC}}^{(1)}(P)$ (Eq. 31) together, the following practical formula is arrived at:

$$\boxed{\delta N_{\mathrm{DWC}}^{(1)}(P) = \frac{\delta g(P)}{\gamma} H_P + \zeta_P \frac{H_P}{r_P} - \frac{1}{2\gamma} \left.\frac{\partial \delta g}{\partial r}\right|_P H_P^2} \tag{47}$$

which is similar to that intentended for use with the Stokes formula, except that the factor 3 is not present in the second term.

Next, the other part of the downward continuation effect given in Eq. 18a is concentrated on, i.e.

$$\delta N_{\text{DWC}}^{\text{L(2)}}(\text{P}) = \frac{c}{2\pi} \iint_{\sigma_0} H^L(\psi) \left(\delta g(r_{\text{P}}, \text{Q}) - \delta g(\text{Q}) \right) d\sigma_{\text{Q}} \tag{48}$$

In anal. to Ågren (2004, Eq. 5.50):

$$\delta g(r_{\text{P}}, \text{Q}) - \delta g(\text{Q}) = \left. \frac{\partial \delta g}{\partial r} \right|_{\text{Q}} (H_{\text{P}} - H_{\text{Q}}) \tag{49}$$

which leads to

$$\delta N_{\text{DWC}}^{\text{L(2)}}(\text{P}) = \frac{c}{2\pi} \iint_{\sigma_0} H^L(\psi) \left[\left. \frac{\partial \delta g}{\partial r} \right|_{\text{Q}} (H_{\text{P}} - H_{\text{Q}}) \right] d\sigma_{\text{Q}} \tag{50}$$

Equations 47, 20 and 50 together make up the practical equation for the computation of downward continuation correction $\delta N_{\text{DWC}}(\text{P})$ presented in **Paper A** and Table 6.

4.7 DWC correction for quasigeoid modelling

In this section, the DWC correction for quasigeoid modelling $\delta \zeta_{\text{DWC}}$ (in Eq. 11) corresponding to the LSMHA method will be derived similarly to the LSMSA version presented in Ågren (*ibid.*, Sec. 9.5.1).

The quasigeoid height ζ at the surface point P is given by (anal. to *ibid.*, Eq. 9.15):

$$\zeta(\text{P}) = \frac{R}{4\pi\gamma} \iint_{\sigma} H(\psi) \left[\delta g + \sum_{i=1}^{\infty} g_i(r_{\text{P}}, \text{Q}) \right] d\sigma_{\text{Q}} \tag{51}$$

where the Molodensky series $\sum_{i=1}^{\infty} g_i(r_{\text{P}}, \text{Q})$ represents the downward or upward continuation of the gravity disturbances to the sea level surface through the computation point P.

Considering that the sphere through P has a radius of $r_{\text{P}} = R + H_{\text{P}}$, the height anomaly becomes (anal. to *ibid.*, Eq. 9.16):

$$\zeta(\text{P}) = \frac{r_{\text{P}}}{4\pi\gamma} \iint_{\sigma} H(\psi) \left[\delta g + \sum_{i=1}^{\infty} g_i(r_{\text{P}}, \text{Q}) \right] d\sigma_{\text{Q}} \tag{52}$$

where γ is again the normal gravity at the telluroid.

Combining computations from terrestrial and GGM data (anal. to *ibid.*, Eq. 9.17):

$$\begin{aligned}
\zeta(\text{P}) = &\frac{r_{\text{P}}}{4\pi\gamma} \iint_{\sigma_0} H^L(\psi) \left[\delta g + \sum_{i=1}^{\infty} g_i(r_{\text{P}}, \text{Q}) \right] d\sigma_{\text{Q}} \\
&+ \frac{r_{\text{P}}}{2\gamma} \sum_{n=0}^{M} (s_n + Q_n^L) \left(\frac{R}{r_{\text{P}}} \right)^{n+2} \delta g_n^{\text{GGM}}
\end{aligned} \tag{53}$$

The factor r_P/γ can be approximated as (anal. to Ågren 2004, Eq. 9.18):

$$\frac{r_P}{\gamma} \approx \frac{R}{\gamma_0}\left(1+\frac{H_P}{r_P}\right)\left(1+2\frac{H_P}{r_P}\right) \approx \frac{R}{\gamma_0}\left(1+3\frac{H_P}{r_P}\right) \tag{54}$$

Substituting this into Eq. 53:

$$\begin{aligned}
\zeta(P) = {} & \frac{R}{4\pi\gamma_0}\iint_{\sigma_0} H^L(\psi)\left[\delta g + \sum_{i=1}^{\infty} g_i(r_P,Q)\right]d\sigma_Q \\
& + \frac{R}{2\gamma_0}\sum_{n=0}^{M}\left(s_n+Q_n^L\right)\left(\frac{R}{r_P}\right)^{n+2}\delta g_n^{GGM} + 3\frac{H_P}{r_P}\zeta_P^0
\end{aligned} \tag{55}$$

where ζ_P^0 is an approximate value for height anomaly. Rewriting this with the first term separated into the δg term and the g_i term; the second term separated into the usual GGM term and what is left of it:

$$\begin{aligned}
\zeta(P) = {} & \frac{R}{4\pi\gamma_0}\iint_{\sigma_0} H^L(\psi)\delta g\, d\sigma_Q + \frac{R}{4\pi\gamma_0}\iint_{\sigma_0} H^L(\psi)\sum_{i=1}^{\infty} g_i(r_P,Q)d\sigma_Q \\
& + \frac{R}{2\gamma_0}\sum_{n=0}^{M}\left(s_n+Q_n^L\right)\delta g_n^{GGM} + \frac{R}{2\gamma_0}\sum_{n=0}^{M}\left(s_n+Q_n^L\right)\left[\left(\frac{R}{r_P}\right)^{n+2}-1\right]\delta g_n^{GGM} \\
& + 3\frac{H_P}{r_P}\zeta_P^0
\end{aligned} \tag{56}$$

Rearranging the terms in Eq. 56:

$$\begin{aligned}
\zeta(P) = {} & \frac{R}{4\pi\gamma_0}\iint_{\sigma_0} H^L(\psi)\delta g\, d\sigma_Q + \frac{R}{2\gamma_0}\sum_{n=0}^{M}\left(s_n+Q_n^L\right)\delta g_n^{GGM} \\
& + \frac{R}{4\pi\gamma_0}\iint_{\sigma_0} H^L(\psi)\sum_{i=1}^{\infty} g_i(r_P,Q)d\sigma_Q \\
& + \frac{R}{2\gamma_0}\sum_{n=0}^{M}\left(s_n+Q_n^L\right)\left[\left(\frac{R}{r_P}\right)^{n+2}-1\right]\delta g_n^{GGM} \\
& + 3\frac{H_P}{r_P}\zeta_P^0
\end{aligned} \tag{57}$$

Since (anal. to *ibid.*, Eq. 5.52)

$$\sum_{i=1}^{\infty} g_i(r_P,Q) = \delta g(r_P,Q) - \delta g(Q) \tag{58}$$

66

then Eq. 57 can be written as (anal. to *ibid.*, Eq. 9.20):

$$
\zeta(P) = \frac{R}{4\pi\gamma_0} \iint_{\sigma_0} H^L(\psi)\delta g \, d\sigma_Q + \frac{R}{2\gamma_0} \sum_{n=0}^{M} \left(s_n + Q_n^L\right) \delta g_n^{\text{GGM}}
$$

$$
+ \frac{R}{4\pi\gamma_0} \iint_{\sigma_0} H^L(\psi) \left[\delta g(r_P, Q) - \delta g(Q)\right] d\sigma_Q
$$

$$
+ \frac{R}{2\gamma_0} \sum_{n=0}^{M} \left(s_n + Q_n^L\right) \left[\left(\frac{R}{r_P}\right)^{n+2} - 1\right] \delta g_n^{\text{GGM}} \tag{59}
$$

$$
+ 3\frac{H_P}{r_P} \zeta_P^0
$$

where the first line is the spherical geoid estimator of Eq. 13, the second line is equal to $\delta N_{\text{DWC}}^{L(2)}(P)$ (Eq. 50), the third line is equal to $\delta N_{\text{DWC}}^{L(1),\text{far}}(P)$ (Eq. 20) and the fourth line shares the factor $\frac{H_P}{r_P}\zeta_P^0$ with $\delta N_{\text{DWC}}^{(1)}(P)$ (Eq. 47). From comparison with the DWC effects for geoid computation given by Eqs. 50, 20 and 47:

$$
\begin{aligned}
\delta\zeta_{\text{DWC}}(P) &= \delta\zeta_{\text{DWC}}^{(1)}(P) + \delta\zeta_{\text{DWC}}^{L(1),\text{far}}(P) + \delta\zeta_{\text{DWC}}^{L(2)}(P) \\
&= \delta\zeta_{\text{DWC}}^{(1)}(P) + \delta N_{\text{DWC}}^{L(1),\text{far}}(P) + \delta N_{\text{DWC}}^{L(2)}(P)
\end{aligned} \tag{60}
$$

i.e.

$$
\boxed{\delta\zeta_{\text{DWC}}(P) = 3\frac{H_P}{r_P}\zeta_P^0 + \delta N_{\text{DWC}}^{L(1),\text{far}}(P) + \delta N_{\text{DWC}}^{L(2)}(P)} \tag{61}
$$

which is the downward continuation correction for quasigeoid computations $\delta\zeta_{\text{DWC}}(P)$ presented in **Paper A** and Table 6.

4.8 Ellipsoidal correction

In this section, the ellipsoidal correction for geoid modelling $\delta N_{\text{ELL}} \approx \delta\zeta_{\text{ELL}}$ (in Eq. 11) corresponding to the LSMHA method will be derived similarly to the LSMSA version presented in Sjöberg and Bagherbandi (2017, Sect. 5.5), see also Sjöberg (2003e) and Sjöberg (2004).

4.8.1 Components of the ellipsoidal correction

The original Hotine formula (Eq. 7) written as

$$
N^0 = \frac{R}{4\pi\gamma} \iint_{\sigma} H(\psi)\delta g \, d\sigma \tag{62}
$$

would provide the correct geoid height if:
  – the Earth's topography and atmosphere were disregarded (or accounted for separately, which is assumed when deriving the ellipsoidal correction);

67
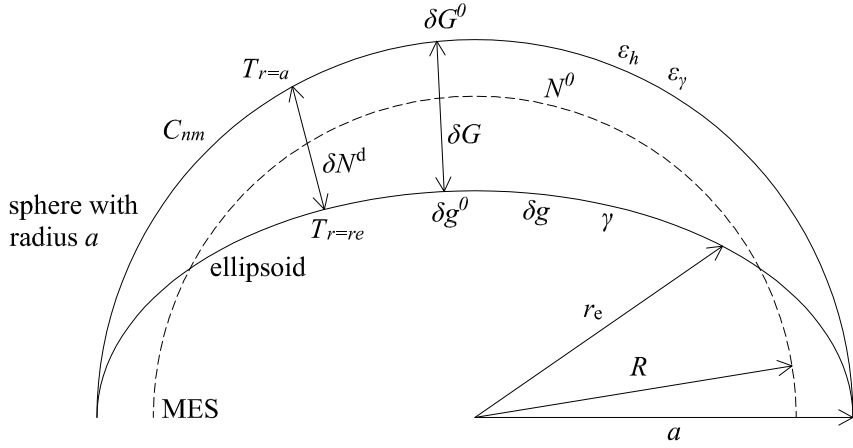
Figure 15: The ellipsoidal correction

- the gravity disturbances δg would refer to the mean Earth sphere (MES) of radius R;
- δg would satisfy the boundary value condition, i.e. be consistent with the fundamental equation of physical geodesy (Heiskanen and Moritz 1967, p. 88):

$$\delta g^0 = -\frac{\partial T}{\partial r} \tag{63}$$

To make the Hotine formula consistent:
- integration is carried out on the sphere of radius a instead of the MES of radius R;
- the original gravity disturbance (assumed to be downward continued to the sea level approximated by the reference ellipsoid of radius r_e) is corrected by δG so as to be consistent with the spherical approximation of the Hotine formula on the sphere of radius a;
- the disturbing potential T obtained from the Hotine integration on the sphere of radius a is downward continued to the geoid (approximated by the reference ellipsoid of radius r_e)

The ellipsoidal correction corresponding to these three actions can be expressed as (Sjöberg and Bagherbandi 2017, Eq. 5.97):

$$\delta N_e^0 = kN^0 + \frac{a}{4\pi\gamma}\iint_\sigma H(\psi)\delta G d\sigma - \delta N^d \tag{64}$$

where $k = (a-R)/R$ is a scale factor augmenting N^0 to the sphere of radius a, the second term represents Hotine integration of the gravity disturbance correction δG on the sphere of radius a and the last term δN^d represents the DWC of the disturbing potential, see Fig. 15. Specific equations for these terms will be derived below.

4.8.2 Gravity disturbance correction δG

The original gravity disturbance δg needs two corrections to become δg^0 which is consistent with the boundary condition: the ellipsoidal correction due to the difference between the derivative of the potential T with respect to the plumb line and the radial derivative (ε_h) and the ellipsoidal correction due to upward continuation of the normal gravity field from the reference ellipsoid to the Earth's surface (ε_γ):

$$\delta g^0 = \delta g - \varepsilon_h - \varepsilon_\gamma \tag{65}$$

To order e^2 (Cruz 1986):

$$\varepsilon_h = e^2 \sin\theta \cos\theta \frac{\partial T}{a\partial\theta} \tag{66}$$

and

$$\varepsilon_\gamma = e^2 \frac{T}{a}(3\cos^2\theta - 2) \tag{67}$$

where e is the ellipsoidal flattening and θ is the co-latitude of the computation point; ε_h and ε_γ are computed at $r = a$.

Since δg^0 refers to the ellipsoid, it needs to be upward continued to the sphere of radius a for the integration by Hotine's formula (anal. to Sjöberg and Bagherbandi 2017, Eq. 5.96a):

$$\delta G^0 = \delta g^0 + (a - r_e)\left(\frac{\partial\delta g^0}{\partial r}\right)_{r=a} \tag{68}$$

Using the following first order approximation for the ellipsoidal radius

$$r_e = a\sqrt{1 - e^2\cos^2\theta} \approx a - ae^2\frac{\cos^2\theta}{2} \tag{69}$$

Eq. 68 becomes:

$$\delta G^0 = \delta g^0 + \frac{ae^2\cos^2\theta}{2}\left(\frac{\partial\delta g^0}{\partial r}\right)_{r=a} \tag{70}$$

The total correction δG to the original gravity disturbance δg is thus:

$$\delta G = \delta G^0 - \delta g \tag{71}$$

From Eq. 65:

$$\delta g = \delta g^0 + \varepsilon_h + \varepsilon_\gamma \tag{72}$$

Inserting Eq. 70 and Eq. 72 into Eq. 71, the following expression is obtained for the gravity disturbance correction δG (anal. to *ibid.*, Eq. 5.96b):

$$\delta G = \frac{ae^2\cos^2\theta}{2}\left(\frac{\partial\delta g^0}{\partial r}\right)_{r=a} - e^2\sin\theta\cos\theta\left(\frac{\partial T}{a\partial\theta}\right)_{r=a} - e^2\frac{T_{r=a}}{a}(3\cos^2\theta - 2) \tag{73}$$

4.8.3 Relevant relations for the spherical harmonics

These relations will be used for representing the ellipsoidal correction as a harmonic series in Sect. 4.8.4.

The spherical harmonic Y_{nm} is defined so that the orthogonality relations apply (Heiskanen and Moritz 1967, Eq. 1-68):

$$\frac{1}{4\pi} \iint_{\sigma} Y_{nm} Y_{kl} d\sigma = \begin{cases} 1, & \text{if } n = k \text{ and } m = l \\ 0, & \text{otherwise} \end{cases} \tag{74}$$

where σ is the unit sphere.

The following relations from Moritz (1980), Martinec (1998b) or Claessens (2005) apply:

$$\cos^2 \theta Y_{nm} = E_{nm} Y_{n+2,m} + F_{nm} Y_{nm} + G_{nm} Y_{n-2,m} \tag{75}$$

$$\sin \theta \cos \theta \frac{\partial}{\partial \theta} Y_{nm} = A_{nm} Y_{n+2,m} + B_{nm} Y_{nm} + D_{nm} Y_{n-2,m} \tag{76}$$

where the harmonic coefficients A_{nm} to G_{nm} are given as (Sjöberg 2004, Appendix):

$$A_{nm} = \frac{n}{2n+3} \sqrt{\frac{[(n+1)^2 - m^2][(n+2)^2 - m^2]}{(2n+1)(2n+5)}} \tag{77a}$$

$$B_{nm} = -\frac{n(n+1) - 3m^2}{(2n-1)(2n+3)} \tag{77b}$$

$$D_{nm} = -\frac{n+1}{2n-1} \sqrt{\frac{[(n-1)^2 - m^2](n^2 - m^2)}{(2n-3)(2n+1)}} \tag{77c}$$

$$E_{nm} = \frac{1}{2n+3} \sqrt{\frac{[(n+1)^2 - m^2][(n+2)^2 - m^2]}{(2n+1)(2n+5)}} \tag{77d}$$

$$F_{nm} = \frac{2n(n+1) - 6m^2}{3(2n-1)(2n+3)} + \frac{1}{3} \tag{77e}$$

$$G_{nm} = \frac{1}{2n-1} \sqrt{\frac{[(n-1)^2 - m^2](n^2 - m^2)}{(2n-3)(2n+1)}} \tag{77f}$$

From their definition it follows that the coefficients are related by:

$$A_{nm} = n E_{nm} \tag{78}$$

$$2B_{nm} = 1 - 3F_{nm} \tag{79}$$

$$D_{nm} = -(n+1) G_{nm} \tag{80}$$

The following summation relations apply (*ibid.*, Eq. 21):

$$\sum_n A_{n\pm2,m} Y_{nm} = \sum_n A_{nm} Y_{n\mp2,m} \tag{81}$$

4.8.4 The ellipsoidal correction as a harmonic series

The disturbing potential (Heiskanen and Moritz 1967, Eq. 2-137) is represented by the following series (as in Sjöberg and Bagherbandi 2017, Eq. 5.98):

$$T = \frac{GM}{a} \sum_{n=0}^{\infty} \left(\frac{a}{r}\right)^{n+1} \sum_{m=-n}^{n} C_{nm} Y_{nm}(\theta, \lambda) \tag{82}$$

where GM is the gravitational mass constant; r, θ and λ represent the geocentric radius, co-latitude and longitude respectively; a is the semi-major axis of the Earth ellipsoid; C_{nm} is the harmonic coefficient of the disturbing potential related to the bounding sphere of radius a and the fully normalized spherical harmonic Y_{nm}.

In the following, the abbreviated notation of

$$\sum_{n,m} = \sum_{n=0}^{\infty} \sum_{m=-n}^{n} \tag{83}$$

will often be used. Also, where not specified otherwise, Y_{nm} refers to the computation point P with the coordinates θ and λ, i.e. $Y_{nm} = Y_{nm}(P) = Y_{nm}(\theta, \lambda)$.

Following Eq. 82, gravity disturbance is expressed by spherical harmonics as (Heiskanen and Moritz 1967, p. 97):

$$\delta g^0 = -\frac{\partial T}{\partial r} = \frac{GM}{a^2} \sum_{n=0}^{\infty} (n+1) \left(\frac{a}{r}\right)^{n+2} \sum_{m=-n}^{n} C_{nm} Y_{nm}(\theta, \lambda) \tag{84}$$

Taking the radial derivative of Eq. 84:

$$\frac{\partial \delta g^0}{\partial r} = -\frac{GM}{a^3} \sum_{n,m} \left(\frac{a}{r}\right)^{n+3} (n+1)(n+2) C_{nm} Y_{nm} \tag{85}$$

Accordingly

$$T_{r=a} = \frac{GM}{a} \sum_{n,m} C_{nm} Y_{nm} \tag{86}$$

and

$$\delta G^0 = -\left(\frac{\partial T}{\partial r}\right)_{r=a} = \frac{GM}{a^2} \sum_{n,m} (n+1) C_{nm} Y_{nm} \tag{87}$$

and

$$\left(\frac{\partial \delta g^0}{\partial r}\right)_{r=a} = -\frac{GM}{a^3} \sum_{n,m} (n+1)(n+2) C_{nm} Y_{nm} \tag{88}$$

Considering the following property of Legendre polynomials (*ibid.*, Eq. 1-73)

$$(2n+1) P_n(\cos \psi) = \sum_{m=-n}^{n} Y_{nm}(P) Y_{nm}(Q) \tag{89}$$

71

the Hotine function (Eq. 8) can be represented in its spectral form as:

$$H(\psi) = \sum_{n=0}^{\infty} \frac{1}{n+1} \sum_{m=-n}^{n} Y_{nm}(P)Y_{nm}(Q) \tag{90}$$

where P and Q represent the computation and integration point respectively. From the orthogonality relations of Eq. 74 it follows that:

$$\frac{1}{4\pi} \sum_{n,m} Y_{nm}(P)Y_{nm}(Q)d\sigma = 1 \tag{91}$$

Inserting the spectral forms of $\left(\frac{\partial \delta g^0}{\partial r}\right)_{r=a}$ (Eq. 88) and $T_{r=a}$ (Eq. 86) into the gravity disturbance correction δG (Eq. 73):

$$\delta G = \frac{ae^2 \cos^2 \theta}{2} \times -\frac{GM}{a^3} \sum_{n,m} (n+1)(n+2)C_{nm}Y_{nm}$$

$$- e^2 \sin \theta \cos \theta \left(\frac{\partial}{a\partial \theta}\right) \times \frac{GM}{a} \sum_{n,m} C_{nm}Y_{nm} \tag{92}$$

$$- e^2 \frac{1}{a}(3\cos^2 \theta - 2) \times \frac{GM}{a} \sum_{n,m} C_{nm}Y_{nm}$$

Simplifying:

$$\delta G = -\frac{e^2 GM}{2a^2} \sum_{n,m} \Big[(n+1)(n+2)C_{nm}\cos^2 \theta Y_{nm}+$$

$$+2\sin \theta \cos \theta \frac{\partial}{\partial \theta} C_{nm}Y_{nm} + 6\cos^2 \theta C_{nm}Y_{nm} - 4C_{nm}Y_{nm}\Big]$$

$$= -\frac{e^2 GM}{2a^2} \sum_{n,m} \Big[(n^2+3n+8)C_{nm}\cos^2 \theta Y_{nm}+ \tag{93}$$

$$+2\sin \theta \cos \theta \frac{\partial}{\partial \theta} C_{nm}Y_{nm} - 4C_{nm}Y_{nm}\Big]$$

Using Eqs. 75 and 76:

$$\delta G = -e^2 \frac{GM}{2a^2} \sum_{n,m} \times$$

$$\times \Big[(n^2+3n+8)(E_{nm}Y_{n+2,m}+F_{nm}Y_{nm}+G_{nm}Y_{n-2,m})C_{nm}+ \tag{94}$$

$$+ 2(A_{nm}Y_{n+2,m}+B_{nm}Y_{nm}+D_{nm}Y_{n-2,m})C_{nm} - 4Y_{nm}C_{nm}\Big]$$

Using Eqs. 78, 79 and 80:

$$\delta G = -e^2 \frac{GM}{2a^2} \sum_{n,m} \times$$

$$\times \Big\{(n^2+3n+8)(E_{nm}Y_{n+2,m}+F_{nm}Y_{nm}+G_{nm}Y_{n-2,m})C_{nm}+ \tag{95}$$

$$+ [2nE_{nm}Y_{n+2,m}+(1-3F_{nm})Y_{nm}-2(n+1)G_{nm}Y_{n-2,m}]C_{nm}$$

$$-4Y_{nm}C_{nm}\Big\}$$

Simplifying:

$$\delta G = e^2 \frac{GM}{2a^2} \sum_{n,m} \times$$
$$\times \left\{ -(n^2+5n+8)E_{nm}C_{nm}Y_{n+2,m} - (n^2+3n+5)F_{nm}C_{nm}Y_{nm} - \right.$$
$$\left. -(n^2+n+6)G_{nm}C_{nm}Y_{n-2,m} + 3Y_{nm}C_{nm} \right\} \tag{96}$$

Using the summation relations of Eq. 81, the following expression for δG is arrived at (anal. to Sjöberg and Bagherbandi 2017, Eq. 5.100):

$$\delta G = e^2 \frac{GM}{2a^2} \sum_{n,m} Y_{nm} \times$$
$$\times \left\{ \left[3 - \left(n^2+3n+5\right) F_{nm} \right] C_{nm} - \left(n^2+n+6\right) G_{nm}C_{n+2,m} - \right.$$
$$\left. - \left(n^2+5n+8\right) E_{nm}C_{n-2,m} \right\} \tag{97}$$

i.e. the Laplace series for the correction δG is:

$$\delta G = \sum_{n=0}^{\infty} \delta G_n \tag{98}$$

with

$$\delta G_n = e^2 \frac{GM}{2a^2} \sum_{m=-n}^{n} Y_{nm} \times$$
$$\times \left\{ \left[3 - \left(n^2+3n+5\right) F_{nm} \right] C_{nm} - \left(n^2+n+6\right) G_{nm}C_{n+2,m} - \right.$$
$$\left. - \left(n^2+5n+8\right) E_{nm}C_{n-2,m} \right\} \tag{99}$$

Considering the spectral forms of the Hotine function (Eq. 90) and δG (Eq. 98), the second term of Eq. 64 becomes:

$$\frac{a}{4\pi\gamma} \iint_{\sigma} H(\psi)\delta G d\sigma = \frac{a}{4\pi\gamma} \sum_{n=0}^{\infty} \frac{1}{n+1} \sum_{m=-n}^{n} Y_{nm}(P)Y_{nm}(Q)\delta G_n d\sigma \tag{100}$$

which in view of the orthogonality relations (Eq. 91) reduces to:

$$\frac{a}{4\pi\gamma} \iint_{\sigma} H(\psi)\delta G d\sigma = \frac{a}{\gamma} \sum_{n=0}^{\infty} \frac{1}{n+1}\delta G_n \tag{101}$$

Next, the spectral form of δN^{d} will be derived. Since (the Bruns' formula, Heiskanen and Moritz 1967, p. 85):

$$N = \frac{T}{\gamma} \tag{102}$$

the geoidal correction due to downward continuation from the sphere of radius a to the ellipsoid of radius r_{e} of the disturbing potential is represented by

$$\delta N^{\mathrm{d}} = (a - r_{\mathrm{e}}) \frac{1}{\gamma} \left(\frac{\partial T}{\partial r} \right)_{r=a} \tag{103}$$

Using the approximation of Eq. 69, Eq. 103 becomes:

$$\delta N^{\mathrm{d}} = ae^2 \frac{\cos^2 \theta}{2\gamma} \left(\frac{\partial T}{\partial r} \right)_{r=a} \tag{104}$$

Inserting the spectral form of $\left(\frac{\partial T}{\partial r} \right)_{r=a}$ (Eq. 87) into Eq. 104:

$$
\begin{aligned}
\delta N^{\mathrm{d}} &= e^2 a \frac{\cos^2 \theta}{2\gamma} \times \frac{GM}{a^2} \sum_{n,m} (n+1) C_{nm} Y_{nm} \\
&= \frac{e^2 GM}{2a\gamma} \sum_{n,m} (n+1) C_{nm} \cos^2 \theta Y_{nm}
\end{aligned}
\tag{105}
$$

Multiplying and dividing by $n+1$:

$$\delta N^{\mathrm{d}} = \frac{e^2 GM}{2a\gamma} \sum_{n=0}^{\infty} \frac{1}{n+1} \sum_{m=-n}^{n} (n+1)(n+1) C_{nm} \cos^2 \theta Y_{nm} \tag{106}$$

Using Eq. 75:

$$
\begin{aligned}
\delta N^{\mathrm{d}} = \frac{e^2 GM}{2a\gamma} \sum_{n=0}^{\infty} \frac{1}{n+1} \sum_{m=-n}^{n} (n+1)(n+1) C_{nm} \times \\
\times (E_{nm} Y_{n+2,m} + F_{nm} Y_{nm} + G_{nm} Y_{n-2,m})
\end{aligned}
\tag{107}
$$

Considering the summation relations of Eq. 81 the following expression is arrived at (anal. to Sjöberg and Bagherbandi 2017, Eq. 5.101):

$$
\begin{aligned}
\delta N^{\mathrm{d}} = \frac{e^2 GM}{2a\gamma} \sum_{n=0}^{\infty} \frac{1}{n+1} \sum_{m=-n}^{n} (n^2 + 2n + 1) Y_{nm} \times \\
\times (E_{nm} C_{n-2,m} + F_{nm} C_{nm} + G_{nm} C_{n+2,m})
\end{aligned}
\tag{108}
$$

i.e. the Laplace series for δN^{d}:

$$\delta N^{\mathrm{d}} = \frac{1}{\gamma} \sum_{n=0}^{\infty} \delta T_n^{\mathrm{d}} \tag{109}$$

where

$$
\begin{aligned}
\delta T_n^{\mathrm{d}} = \frac{e^2 GM}{2a} \sum_{n=0}^{\infty} \frac{1}{n+1} \sum_{m=-n}^{n} (n^2 + 2n + 1) Y_{nm} \times \\
\times (E_{nm} C_{n-2,m} + F_{nm} C_{nm} + G_{nm} C_{n+2,m})
\end{aligned}
\tag{110}
$$

Inserting the individual parts (Eqs. 101 and 109) into Eq. 64, the spherical harmonic representation of the ellipsoidal correction is obtained (anal. to *ibid.*, Eq. 5.102):

$$\delta N_{\mathrm{e}}^0 = kN^0 + \frac{a}{\gamma} \sum_{n=0}^{\infty} \frac{1}{n+1} \delta G_n + \frac{1}{\gamma} \sum_{n=0}^{\infty} \delta T_n^{\mathrm{d}} \tag{111}$$

To simplify practical computations, the last two terms of Eq. 111 can be combined so that:

$$\delta N_{\mathrm{e}}^0 = kN^0 + \frac{a}{\gamma} \sum_{n=0}^{\infty} \frac{\delta g_n^{\mathrm{e}}}{n+1} \tag{112}$$

where

$$\delta g_n^{\mathrm{e}} = \delta G_n + \frac{n+1}{a} \delta T_n^{\mathrm{d}} \tag{113}$$

are the Laplace harmonics of the ellipsoidal correction to the gravity disturbance. From Eqs. 99 and 110:

$$\begin{aligned} \delta g_n^{\mathrm{e}} = e^2 \frac{GM}{2a^2} \sum_{n,m} Y_{nm} \times \\ \times \{[3 - (n+4)F_{nm}]C_{nm} - (5-n)G_{nm}C_{n+2,m} - (3n+7)E_{nm}C_{n-2,m}\} \end{aligned} \tag{114}$$

Notice that, in addition to the factors $(n+4)$, $(5-n)$ and $(3n+7)$ differing from the Stokes version (*ibid.*, Eq. 5.103b or Table 7), the indexes of GGM coefficients C_{nm} are also interchanged.

4.8.5 Ellipsoidal correction to the modified Hotine formula

The ellipsoidal correction (Eq. 112) can also be written in the space domain as (anal. to *ibid.*, Eq. 5.104):

$$\delta N_{\mathrm{e}}^0 = \frac{R}{4\pi\gamma} \iint_{\sigma} H(\psi) \left(k\delta g + \frac{a}{R} \delta g^{\mathrm{e}} \right) \tag{115}$$

where

$$\delta g^{\mathrm{e}} = \sum_{n=0}^{\infty} \delta g_n^{\mathrm{e}} \tag{116}$$

In case of the modified Hotine formula (Eq. 13) the ellipsoidal correction becomes (anal. to *ibid.*, Eq. 5.105):

$$\delta N_{\mathrm{ELL}} = \frac{R}{4\pi\gamma} \iint_{\sigma_0} H(\psi)^L \left(k\delta g + \frac{a}{R} \delta g^{\mathrm{e}} \right) \tag{117}$$

which can also be represented as the harmonic series

$$\delta N_{\mathrm{ELL}} = \frac{R}{2\gamma} \sum_{n=0}^{\infty} \left(\frac{2}{n+1} - s_n^* - Q_n^L \right) \left(k\delta g_n + \frac{a}{R} \delta g_n^{\mathrm{e}} \right) \tag{118}$$

which is the ellipsoidal correction for geoid or quasigeoid computations $\delta N_{\mathrm{ELL}}(\mathrm{P}) \approx \delta \zeta_{\mathrm{ELL}}(\mathrm{P})$ presented in **Paper A** and Table 7.

4.9 Comparison of LSMHA to LSMSA

Based on the case study of **Paper A**, the differences of the LSMHA procedure developed from the original LSMSA methods will now be discussed. A simple deterministic Wong & Gore (WG) type modification (Wong and Gore 1969) is also used for reference, since it has been used in many geoid modelling tasks.

All of the test computations were performed for the integration cap size of $\psi_0 = 2°$, using the GOCE data containing GO_CONS_GCF_2_DIR_R5 (Bruinsma et al. 2014) GGM model with $M = L$ and the modification limit of $L = 200$.

The modification limit L was selected according to expected global mean square error estimates for different limits L. Fortunately, provided that the limit L is sufficiently high to allow the GGM to contribute within the range of which it is considered to contain valuable information, the expected global RMS is not very sensitive to the actual modification limit selected. The weight of GGM contribution is automatically lowered for higher degrees, see Table 2 of **Paper A**.

For the LSMHA and LSMSA methods to be directly comparable, the zero and first degree harmonics are neglected and computations are started at $n = 2$.

4.9.1 Modification parameters

The s_n coefficients (starting from $n = 2$) for the deterministic WG type modification are presented in Fig. 16a. Those of the Stokes function are essentially computed from $\frac{2}{n-1}$, hence the s_n values steadily decrease from 2 to 0. In contrast, s_n coefficients associated with the Hotine function are essentially computed from $\frac{2}{n+1}$, starting the decrease from $\frac{2}{3}$.

Interestingly, the s_n coefficients of the BLS modification follow the WG coefficients very closely. While the WG and BLS s_n coefficients are steadily decreasing, those of ULS and OLS modification undulate, see Fig. 16b. For the same input parameters, the coefficients s_n of ULS and OLS are almost identical. Compared to the Stokes counterparts, the Hotine coefficients undulate with a larger amplitude.

The s_n parameters of the ULS or OLS modification of both Stokes's or Hotine's formula depend strongly on the numerical (regularization) method used to solve the linear system of equations defining these parameters (Ellmann 2005b; Ellmann 2004, Sec. 3.3). **Paper A** also demonstrates an alternative set of ULS s_n parameters that undulates violently (Fig. 4c of **Paper A**) which is very difficult to compare to the Stokes counterparts.

As discussed earlier, the b_n coefficients (Fig. 16c) are very similar for all of the modification methods. In fact, their values are close to $\frac{2}{n-1}$ or $\frac{2}{n+1}$ for the Stokes or Hotine formula respectively. Consequently, the Hotine b_n coefficients start from a smaller value than the Stokes counterparts. The second part of Eq. 13 reveals that smaller values of b_n result in a smaller contribution of the GGM coefficients to the geoid estimator (which can be counterbalanced by the gravity

(a) s_n coefficients for the WG (and BLS) modifications

(b) s_n coefficients for the ULS (and OLS) modifications

(c) Modification parameters b_n

(d) The original (solid), WG modified (dotted), LS modified (dashed) Hotine or Stokes function
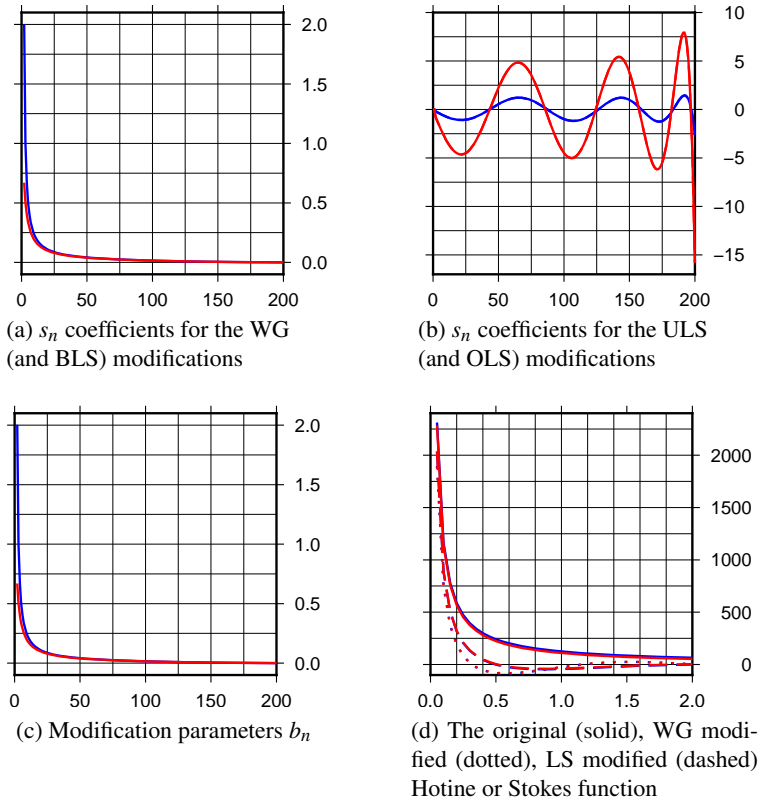
Figure 16: Modification parameters for Hotine's (red) or Stokes's (blue) function[*] (modified figure from **Paper A**)

[*]The horizontal axis of Fig. 16a to 16c depicts the degree n while that of Fig. 16d the spherical distance ψ

disturbance values differing from the anomaly values).

Behaviour of the modified Hotine function H^L (Fig. 16d) determining the terrestrial data contribution from within the spherical cap σ_0 also varies depending on the modification method used. Nevertheless, all of the least squares modifications presented, including BLS, follow the same curve that does not differ much from the Stokes counterparts.

4.9.2 The expected global mean square error

The expected global MSE of Eq. 17 can be used to compare the different geoid modelling methods. The total and partial contributions of the global root mean square (RMS) error are presented for the different modification methods of Stokes's and Hotine's formula in Table 8.

Table 8: The expected global RMS error of geoid modelling (based on different degree variance models for the Stokes and Hotine formula, see Eq. 16), units: mm (table from **Paper A**)

	n	Stokes				Hotine			
		WG	BLS	ULS	OLS	WG	BLS	ULS	OLS
$\left(\delta\widetilde{N}\right)^2_{\mathrm{TR}}$	$2...L$	0.00	0.20	0.00	0.04	0.00	0.24	0.00	0.04
	$L+1...\infty$	2.79	2.01	2.16	2.16	2.78	2.00	2.24	2.24
	$2...\infty$	2.79	2.02	2.16	2.16	2.78	2.02	2.24	2.24
$\left(\delta\widetilde{N}\right)^2_{\mathrm{T}}$	$2...L$	6.54	6.39	6.33	6.33	6.53	6.51	6.41	6.41
	$L+1...\infty$	8.66	8.67	8.67	8.67	8.66	8.67	8.67	8.67
	$2...\infty$	10.85	10.77	10.73	10.73	10.85	10.84	10.78	10.78
$\left(\delta\widetilde{N}\right)^2_{\mathrm{GGM}}$	$2...L$	1.74	1.77	1.80	1.80	1.73	1.73	1.77	1.77
	$L+1...\infty$	–	–	–	–	–	–	–	–
	$2...\infty$	1.74	1.77	1.80	1.80	1.73	1.73	1.77	1.77
$\left(\delta\widetilde{N}\right)^2$	$2...L$	6.76	6.63	6.58	6.58	6.76	6.74	6.65	6.65
	$L+1...\infty$	9.10	8.90	8.93	8.93	9.09	8.90	8.95	8.95
	$2...\infty$	**11.34**	**11.10**	**11.09**	**11.09**	**11.33**	**11.16**	**11.15**	**11.15**

Bold values represent the total expected error

All of the LS modifications of Hotine's formula yield very similar global error estimates. As the name suggests, the BLS modification yields a slightly larger truncation error (bias) for degrees $2-L$ than the ULS and OLS modifications that are numerically very similar to each other.

In the case study of **Paper A**, the LS modifications of Hotine's formula show a larger global RMS error than the Stokes counterparts. This result is dependent on the gravity disturbance degree variance models being determined by Eq. 16 from those of gravity anomalies. In practical computations, the gravity anomaly degree variances $d_{n,\Delta g}$ can safely be used also for computations by Hotine's formula as the global signal and error models are rough and in no way specific to gravity anomaly or disturbance, nor the region of study. Related quasigeoid model differences remain within a mm (standard deviation, SD) over the study area of **Paper A**.

4.9.3 Geoid contributions

As discussed earlier, the modification parameters b_n and s_n define the partial contributions of the near and far zone to the approximate geoid estimator. For example, over the study area of **Paper A** (see Fig. 13 on p. 51 for the area characteristics) the ULS modification of Hotine's formula yields a near zone contribution that is on average 7.8 cm smaller and a far zone contribution that is on average 7.1 cm

(a) Approximate geoid $\widetilde{N}$ · (b) DWC correction δN_{DWC} · (c) Geoid $\widehat{N}$ or quasigeoid $\widehat{\zeta}$
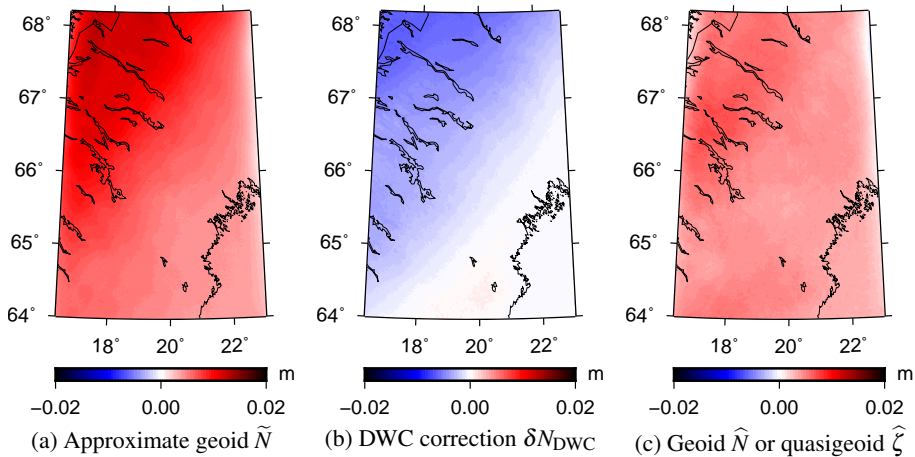
Figure 17: Differences of geoid contributions computed by the Stokes or Hotine formula (figures from **Paper A**)

larger than that of the corresponding Stokes formula. As a result, the approximate geoid models computed by the ULS modified Hotine's or Stokes's formula differ only by 3 mm (SD) with maximum differences of 1.3 cm occurring in the high topography regions in the NW, see Fig. 17a.

Contribution of the combined topographic effect is identical for the Hotine and Stokes formula. Differences in the atmospheric and ellipsoidal corrections are at the sub-millimetre level over the study area of **Paper A**. However, the DWC correction differences reach 7 mm, see Fig. 17b. Therefore, in many practical geoid modelling tasks, the additive corrections for the combined topographic, atmospheric and ellipsoidal effect meant for the Stokes formula can be used also for geoid modelling by the Hotine formula. However, the DWC effect is better computed by the appropriate equations developed for the Hotine formula.

Together with the additive corrections, the geoid and quasigeoid models for the study area of **Paper A** differ on average by 5 mm with a SD of 1 mm and the maximum differences reaching 8 mm in the mountainous area in NW, see Fig. 17c.

The results described may be dependent on the way input data was generated for the research presented in **Paper A**, that is, the gravity disturbances were computed from gravity anomalies using an existing geoid model. For an improved analysis on the differences of LSMHA from LSMSA, special data could be collected.

It is concluded that the differences described between using the Stokes or Hotine formula are marginal. They are smaller than the general geoid modelling accuracy which is currently at the level of a few mm in the most suitable areas (e.g. flat landscape) to centimetres in more challenging areas (e.g. rugged terrain).

Agreement between the numerical results obtained by the existing LSMSA and the newly developed LSMHA methods helps to confirm the correctness of the equations developed.

Although numerically the LSMHA procedure developed differs very little from the original LSMSA method, the benefit of using LSMHA stands in the use of gravity disturbances as input. As gravity surveys are nowadays accompanied with GNSS height positioning, disturbances can be obtained directly while the determination of anomalies (for input to the LSMSA method) is dependent on the quality of a previously existing geoid model.

5 Specifics of the marine geoid

Recall that the standard gravimetric geoid evaluation method of comparison to GNSS/levelling points is not possible over marine areas. Due to the long wavelength nature of the geoid, the lack of evaluation possibilities is not only a problem for marine geoid modelling, but also for nearby coastal areas where geoid modelling accuracy can easily suffer due to insufficient or inaccurate data coverage over the marine areas nearby.

As an alternative to the GNSS/levelling evaluation possible over land, several attempts of measuring the actual sea surface position (that reflects the geoid in the nature) by regular GNSS devices (Jürgenson et al. 2008, Liibusk and Ellmann 2015, Lavrov et al. 2016, Varbla et al. 2017b) or airborne laser scanning (Gruno et al. 2013, Julge et al. 2014) have been made. Although special GNSS buoys have also been used for sea level positioning (see e.g. André et al. 2013, Dawidowicz 2014, Lin et al. 2017 and references therein), their poor coverage is not comparable to the surveys referenced above.

However, in addition to the geoid, the instantaneous sea level (ISL) also reflects sea surface height variation due to tides, water velocity, temperature, salinity, currents, wind stress, atmospheric pressure, Coriolis force, water depth, bottom friction (Pugh 1987), river discharge and seabed topography (Dunn and Ridgway 2002, Merry and Vaníček 1983). Some of these effects are predictable by dedicated models (e.g. currents, tides, Coriolis force) while others (e.g. river discharge, waves) are more difficult to estimate, making it difficult to extract the actual geoid signal from the ISL.

To improve the possibilities of marine geoid validation, the problem of separating the ISL height provided by *in situ* GNSS measurements conducted on sea ice into geoid signal (**Paper C**) and the sum of the physical and meteorological effects described above (**Paper E**) is investigated.

In the specific area of the Väinameri basin studied in **Papers C** and **E**, the largest contributors to sea level deviation from the geoid are the water balance of the Baltic Sea (depending on river discharge and water transport through the Danish straights) and wind induced water convergence. Both of these can reach ± 1 to 2 m in extreme cases. Wind induced seiches – waves with a period of a few hours to about a day – can also contribute significantly. See Suursaar and Kullas (2009), Suursaar et al. (2006), Hünicke et al. (2015) and references therein for additional information.

5.1 Determination of sea level heights

The relations between various sea level heights and related reference surfaces are illustrated in Fig. 18. Using a GNSS receiver, the ellipsoidal height h_{ARP} of the antenna reference point (ARP) can be observed. The ellipsoidal height h_{ISL} of the instantaneous sea level is obtained from h_{ARP} by subtracting the antenna height
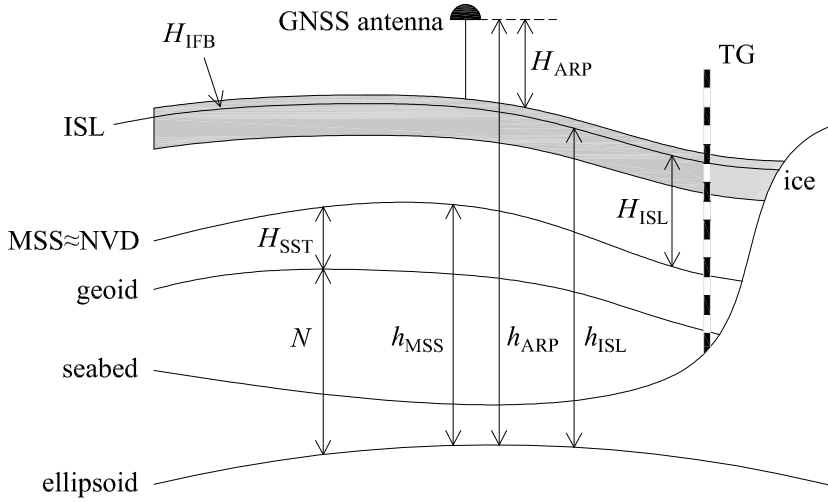
Figure 18: Relations of ice-tamed sea level heights (modified figure from **Paper E**)

H_{ARP} and the ice freeboard (IFB) height H_{IFB} recorded during the surveys:

$$h_{ISL} = h_{ARP} - H_{ARP} - H_{IFB} \tag{119}$$

The height H_{ISL} of the instantaneous sea level above the historic mean sea surface (MSS) can be estimated from nearby tide gauges (TG).

Unfortunately tide gauges are rare and located only on the coastline. The quality of H_{ISL} values estimated from TGs may therefore be rather unrepresentative for the actual survey point locations. Over larger open sea areas, satellite altimetry can be used instead. However, in coastal regions satellite altimetry availability and accuracy also degrades.

Using the value of H_{ISL}, the ellipsoidal height h_{MSS} of the mean sea surface is obtained:

$$h_{MSS} = h_{ISL} - H_{ISL} = h_{ARP} - H_{ARP} - H_{IFB} - H_{ISL} \tag{120}$$

h_{MSS} is what approximates the GNSS derived geoid height N_{GNSS} that can be used to evaluate the gravimetric geoid value N_{GR}. However, the mean sea surface actually reflects the geoid plus the sea surface topography (SST) height H_{SST}. For a more rigorous comparison, the GNSS derived geoid height can be computed as:

$$N_{GNSS} = h_{MSS} - H_{SST} = h_{ARP} - H_{ARP} - H_{IFB} - H_{ISL} - H_{SST} \tag{121}$$

SST is the time-average difference of the mean sea surface (or NVD) from the geoid height N due to the various physical and meteorological effects described in the beginning of this chapter. In general, there are four ways to estimate the SST:

– from satellite altimetry derived sea surface heights (e.g. Andersen 2010)

– from long-term oceanographic data (e.g. Carlsson 1998)
– from geodetic measurements of sea surface heights at tide gauges (e.g. Kakkuri and Poutanen 1997)
– from *in situ* sea surface measurements (see Eq. 122 below)

Out of these possibilities, only the SST models determined from oceanographic data are (relatively) independent of existing geoid models. For SST determination from the other sources listed, an existing geoid model is needed. The estimated accuracy of SST models (in the current Nordic-Baltic area of interest) is 5 cm at best, see the references given for each method. Also, the SST models estimated by the above listed methods differ in the time period concerned: while *in situ* measurements provide instantaneous information, the other models can (and usually do) contain information averaged over periods as long as decades.

For determination of SST from GNSS survey positions on ice, a scheme similar to Eq. 121 can be used:

$$H_{SST} = h_{ARP} - H_{ARP} - H_{IFB} - H_{ISL} - N_{GR} \qquad (122)$$

Both, Eq. 121 and 122 can be used for geoid or SST determination by GNSS surveys on board various (moving) platforms such as a car on ice (Liibusk and Ellmann 2015), a ship (Varbla et al. 2017b) or an aeroplane (Julge et al. 2014). Surveying from an aeroplane, the antenna height H_{ARP} is determined by laser scanning the sea surface.

Using a ship, the ice freeboard H_{IFB} is likely to be zero and the antenna height H_{ARP} can be measured at the port from the antenna reference point to the water level. For the best results it could be corrected to account for the ship's squat, roll and pitch when moving at different speeds in various wave conditions for example by using two or more GNSS receivers or an inertial measurement unit (IMU) similar to those used in airborne photogrammetry, see Lavrov et al. (2016) and the references provided therein.

5.2 Marine geoid validation

Paper C presents a case study whereby gravity data was collected on ice of the Väinameri basin in Estonia. The GNSS derived positions of these survey points are used to validate the gravimetric geoid model GRAV-GEOID2011. A simplified version of Eq. 121 is used:

$$N_{GNSS} = h_{ARP} - H_{ARP} - H_{ISL} - \Delta H \qquad (123)$$

where ΔH is the average difference between N_{GNSS} and N_{GR}.

Figure 19 depicts the GRAV-GEOID2011 model and its validation results. The standard deviation of N_{GNSS} minus N_{GR} is 3.6 cm. Although differences on adjacent points are similar and the results look promising, there are also large differences (negative values in the NW) that appear where the GNSS processing results by different methods varied up to 10 cm.
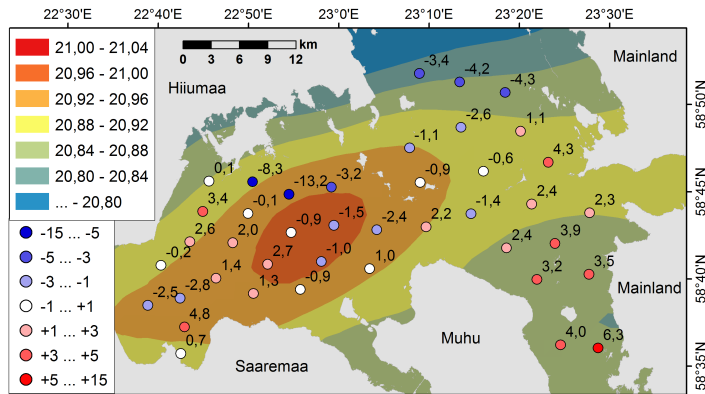
Figure 19: N_{GNSS} minus N_{GR} (in cm), depicted by the coloured circles explained in the bottom legend, together with the GRAV-GEOID2011 model (in metres), contoured according to the top legend (figure from **Paper C**)

Also, a NW to SE tilt of up to 10 cm can be observed in the validation results on the Eastern side. Considering the low accuracy of SST models, one was not used in the case study of **Paper C**. However various SST models (e.g. those presented in **Paper E**) for this specific area do reveal a similar NW to SE tilt that would improve the validation results, but only by 2 to 4 cm.

Considering that the GRAV-GEOID2011 gravimetric geoid model should be of rather high quality, the validation results are found to be too pessimistic. It is suspected that the surveyed GNSS heights may have a systematic error component in them.

Therefore it seems that the GNSS positioning methods used in **Paper C** are not accurate enough to improve marine geoid determination in this particular area. Nevertheless, high accuracy GNSS positioning on the sea ice could allow for direct marine geoid determination using the method described above.

5.3 Determination of sea surface topography

While the sea surface topography needs to be eliminated from the instantaneous sea level for geoid validation, SST could also be estimated from ISL by Eq. 122, as done in **Paper E**. In this case, a suitable geoid model is subtracted instead.

The case study conducted in **Paper E** concerns the same Väinameri area as in **Paper C**. SST surface models are computed from (parts of) the point-wise GNSS survey used in **Paper C** and the profile-wise GNSS surveys of Liibusk and Ellmann (2015).

Although the two surveys were carried out in different winter seasons, the average discrepancy between the profile wise SST values and the SST surface computed from the point values remains within ± 4.3 cm. Such a difference indicates the combined effect of inaccuracies in GNSS measurements and ice freeboard

estimates.

The GNSS derived SST model is compared to the global model DTU10MDT (Andersen 2010) derived from satellite altimetry and a regional SST model presented by Liibusk (2013) derived from annual sea level observations at nearby tide gauges. Clearly the resolution of the GNSS derived model is the highest, but all three models show a NW to SE slope (2 cm in the DTU10MDT, 4 cm in the annual and 6 cm in the GNSS derived model).

Relative differences between the models remain within 4...5 cm with the larger differences being observed in the Northern part of the Väinameri basin. A local SST anomaly not detectable by global models could exist in this area or the point wise GNSS survey values could contain a systematic error component.

The relative coincidence between SST models based on short-term (some days) and long-term (years of) sea surface observations is reasonable, remaining within the estimated accuracy of the measurements and the geoid model. Thus, the case study of **Paper E** demonstrates the possibility of using short-term GNSS measurements on ice in combination with instantaneous tide gauge data to determine SST surface tilts in coastal regions. Further out the coast, such measurements could provide SST models with similar accuracy but better resolution to long term (years of) satellite altimetry observations.

6 Conclusions and discussion

6.1 Conclusions

In this doctoral thesis, regional geoid modelling was investigated from the aspects of gravity data analysis and gridding, geoid modelling methods and specifics of the marine geoid. This was done by

- illustrating the possibilities available for gravity data analysis and improvement (Chapter 2);
- collecting and rigorously comparing widespread gravity gridding methods (Chapter 3);
- proposing a new geoid modelling method that uses gravity disturbances as input, comparing it to its existing counterpart that uses gravity anomalies (Chapter 4);
- proposing a method based on GNSS positioning on the sea for marine geoid validation and sea surface topography (SST) determination (Chapter 5);

The main results of this thesis can be summarized as follows:

- Continuous efforts to improve terrestrial gravity data quality and coverage are still needed in the era of dedicated satellite missions providing high quality gravity field products.
- Based on the NKG case study, it is difficult to prefer either the Bouguer type anomalies or the RTM anomalies for gravity reduction prior to interpolation. A reason to prefer the RTM anomalies could be their properties that are theoretically more suitable for interpolation.
- In most areas of high quality gravity data, all of the triangulation, nearest neighbour, spline based and statistical interpolation methods tested are able to generate a high quality gravity grid.
- Under more difficult conditions, such as nearby inaccurate gravity data, steep gradients and data gaps, statistical interpolation can provide the most realistic representation of the gravity field while the spline based methods are to be avoided.
- Interpolation can be improved by considering individual error estimates only if these are realistic.
- From the gravity gridding point of view, geoid model accuracy of 5 mm can be expected over most of the Nordic-Baltic dry land. Disqualifying the spline based interpolation methods, it is possible to compute a geoid model with an accuracy of 1 cm over most of the Baltic Sea (except the Eastern part of Gulf of Finland due to large data void).
- Considering the target accuracy of 5 to 10 mm in regional geoid modelling, the data situation and gridding approaches still need some improvement in the Nordic-Baltic area.
- The differences in the resulting geoid models between using the least

squares modifications and additive corrections with the traditional Stokes formula or the Hotine formula are marginal compared to the general geoid modelling accuracy. However, the partial contributions of the near and far zone do differ in the order of a decimetre in a study area with elevations up to 2 km.

– Although numerically similar to the existing LSMSA (Stokes) method, the benefit of the new LSMHA (Hotine) method lies in its use of gravity disturbances as input.

– The adaptation of the LSMSA to the new LSMHA approach in high accuracy geoid modelling requires the use of corresponding additive corrections, especially the DWC correction that differs significantly, while the atmospheric and ellipsoidal correction differences are not exceeding the current geoid modelling accuracy.

– Although the method of GNSS positioning on sea proposed for marine geoid validation did not particularly improve the geoid modelling situation over the Väinameri basin, it can still be useful for geoid validation at the 5 to 10 cm accuracy level.

– It is possible to use short-term GNSS measurements on sea in combination with instantaneous tide gauge data to determine SST surface tilts.

6.2   Relevance and novelty of the study

Accurate height positioning is essential to the functioning of the modern society living within a built environment in the globalised world. To provide fast and accurate hight positioning by GNSS methods, a geoid model with sufficient accuracy and resolution is needed. Countries have therefore invested into development of national geoid models that are constantly being improved. In addition to national models, regional geoid models serve to unify the height systems of neighbouring countries and fulfil many other scientific tasks.

Reaching target accuracy of 5 to 10 mm in regional geoid modelling demands continuous efforts in both data and methodological aspects. This thesis summarises the author's contribution to these efforts.

Both, gravity data analysis and gridding, are rarely reported upon in scientific literature. Hardly any of the data analysis methods described in Papers **B**, **C** and **D** are new in themselves, but they are reported in more detail than usually, so as to be of reference to other similar tasks worldwide.

The used gravity reduction and interpolation methods themselves are not new either. The value of related investigations reported in Papers **B** and **D** lies in the rigorous comparison of these both in theory and in case studies representing many of the possible situations that could occur in practical tasks.

From the references describing various modifications of the Stokes or Hotine formula (see Sections 4.1 and 4.2), it is clear that an ample number of approaches to regional geoid modelling already exist. The method of least squares modifica-

tion of the Stokes formula (Sjöberg 1984, 1991, 2003b) with additive corrections (Sjöberg 2003a), that uses gravity anomalies as input, has previously been shown to yield high quality results (e.g. in the NKG geoid modelling project). Therefore it was decided to adapt this approach to the Hotine formula that uses an alternative residual gravity quantity, the gravity disturbance, as input. With GNSS positioning providing the height information that allows to compute gravity disturbances instead of the anomalies, use of the Hotine formula in geoid modelling can only grow.

Although the Stokes and Hotine formula and modifications thereof look rather similar, the specific equations of the LSMHA approach needed deriving. Thanks to **Paper A** these are now concisely presented in an academic publication.

To the author's knowledge, the methods proposed in Papers **C** and **E** for geoid and SST determination from the instantaneous sea level height measured by *in situ* GNSS positioning with such a high spatial resolution have not been extensively used elsewhere. In view of the attempts to increase the accuracy of the Baltic Sea geoid within the FAMOS project, such an evaluation possibility could become useful, e.g. by evaluating marine geoid models by non-dedicated GNSS surveys on commercial ships sailing the Baltic Sea.

6.3 Discussion

Most scientific research regarding geoid modelling serves to improve practical geoid modelling products. Therefore, the following discussion concentrates on the latter.

The geoid modelling efforts made in the Nordic-Baltic region (and also globally) within the last five years have resulted in significant improvements of geoid models. As an example, these improvements can be quantified by looking at the difference of the current official gravimetric geoid model for Estonia (GRAV-GEOID2011) and the new NKG2015 model (Fig. 20).

The differences between GRAV-GEOID2011 and NKG2015 reach 14 cm. In comparison to the target accuracy of 5 to 10 mm, this is huge. Over mainland, the differences are smaller, remaining within ± 5 cm. Before discussing the specific reasons for such differences, both geoid models are evaluated by comparison to the same NKG GNSS/levelling data, see Fig. 2 on p. 27 and Fig. 21.

There are a number of features that can be spotted from the comparison and evaluation results. First, the large differences between GRAV-GEOID2011 and NKG2015 over the Eastern part of Gulf of Finland (GoF), that is, the negative values depicted in black on Fig. 20. It is an area of about $20\,000\,\mathrm{km}^2$ with no terrestrial (marine) gravity data. In the older model the GoF area was filled by gravity data from the high resolution EGM2008 (Pavlis et al. 2012) GGM model (Ellmann et al. 2011) while in the newer model it was filled by the satellite-only low-resolution GO_CONS_GCF_2_DIR_R5 (Bruinsma et al. 2013) model. Due to the geoid model containing strong long wavelength signal, systematic biases
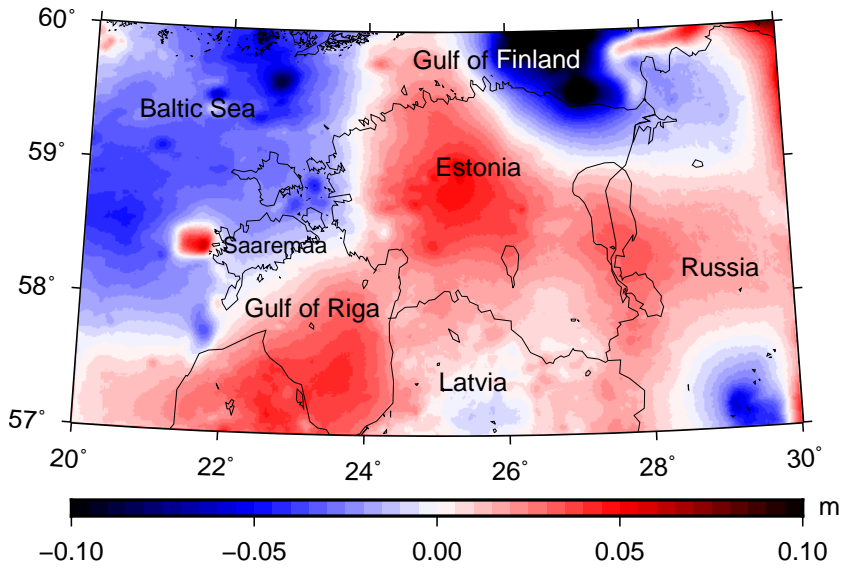
Figure 20: The NKG2015 geoid model minus the GRAV-GEOID2011 model (after removal of the mean difference)
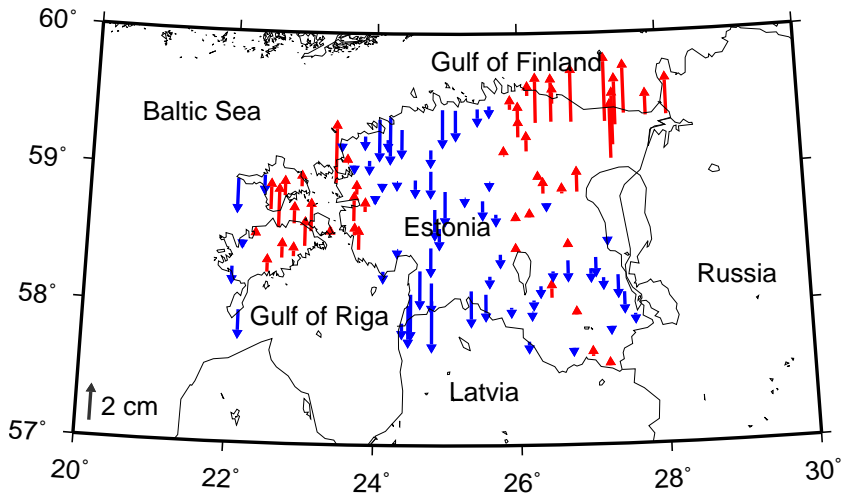

Figure 21: GNSS/levelling evaluation of the NKG2015 model (after removal of the mean difference; min: −2.8 cm; max: 3.7 cm; SD: 1.42 cm)

in gravity data over such a large area can seriously distort the geoid model over mainland as well. This could be one reason as to why the models differ relatively much also over mainland. The red rectangle West of Saaremaa (around 58.5° N, 22° E) is also caused by the differences of fill-in data.

Second, the GGM used for providing the far zone contribution (the right hand side of Eq. 5) is different. Not only the selection of the GGM model, but also the maximum limit M used in Eq. 5 has a strong effect on the long wavelength signal of the geoid model. This is likely the reason why large positive and negative difference areas (with a wavelength of about a 100 to 150 km) are visible on the comparison plot in Fig. 20.

Third, the effect of new gravity data being included to geoid modelling is visible in between mainland and the islands on the West (at the Väinameri Basin). Due to the long wavelength differences between geoid models being dominant, the other data related differences (see **IX**, **X**) are not very easy to spot. It can only be assumed though, that new data improve a geoid model rather than make it worse.

GNSS/levelling evaluation of the NKG2015 model (Fig. 21) suggests that it is rather accurate over most of Estonia with many discrepancies being below the cm level. In comparison, the GRAV-GEOID2011 evaluation (Fig. 2 on p. 27) shows much larger discrepancies over most of Estonia, except for the SE corner where their results are comparable and the NE where GRAV-GEOID2011 shows a better fit to GNSS/levelling data. The patterns of negative and positive discrepancies visible on the comparison plot (Fig. 20) are also apparent in the GRAV-GEOID2011 evaluation plot, leading to believe that in most parts the NKG2015 model really is an improvement over the older model (except for the NE part due to fill-in data in the GoF).

This thesis itself does not provide a geoid modelling product. However the findings can be used to compute a new geoid model for Estonia (or elsewhere). Computation of a new geoid model for Estonia is especially relevant in the light of adopting the new height system based on the European Vertical Reference System (EVRS) from January 2018.

The above discussion illustrates the improvement that can be expected in new geoid models thanks to the data related and scientific improvements to geoid modelling methods reported in this thesis.

6.4 Recommendations for further studies

The results of this study lead to several perspectives for future research:
- In addition to the Bouguer and RTM anomalies compared for suitability of interpolation, isostatic anomalies (see e.g. Novák et al. 2016) could be considered.
- Reduction of gravity anomalies before interpolation can certainly be improved, specifically by including bathymetry information. This would im-

prove the accuracy of gravity gridding in marine areas, especially in rugged coastline with fjords (such as Norway).

– One of the benefits of using the Hotine formula instead of the traditional Stokes version is that the zero and first degree spherical harmonics can directly be considered, i.e. the normal gravity field adopted does not have to correspond to the actual mass of the Earth and the origin of the geodetic reference system does not have to coincide with the mass centre of the Earth. Although all of the geoid modelling equations derived include also the zero and first degree harmonics, analysis of these was considered to be outside the scope of this study.

– The marine geoid validation attempts would benefit from better SST data, which could be provided by high-resolution (both in space and time) ocean forecast models such as Lagemaa et al. (2011) or those analysed in Golbeck et al. (2015).

– The empirical studies of this thesis were conducted over the Nordic-Baltic region which is heterogeneous in terms of terrain and data coverage, hosting also rather challenging areas such as Norway. Yet, there exist even more challenging areas in terms of poor data coverage (e.g. Russia) and heterogeneity (e.g. North America) or topography (e.g. the Himalayas).

– Data related improvements in the Nordic-Baltic region. While terrestrial data coverage is rather good over most of the Nordic-Baltic mainland, it can be poor over coastal and marine areas which has a strong effect on the marine geoid, but also on the geoid on land nearby the coast. Terrestrial gravity data collection is resource demanding, but fortunately significant improvements are expected from the marine gravity campaigns of the FAMOS project targeting the areas needing most attention.

References

Abbak, R. A., Sjöberg, L. E., Ellmann, A., and Ustun, A. (2012). "A Precise Gravimetric Geoid Model in a Mountainous Area with Scarce Gravity Data: A Case Study in Central Turkey". *Studia Geophysica et Geodaetica* 56 (4), pp. 909–927. DOI: 10.1007/s11200-011-9001-0.

Abbak, R. A. and Ustun, A. (2015). "A Software Package for Computing a Regional Gravimetric Geoid Model by the KTH Method". *Earth Science Informatics* 8 (1), pp. 255–265. DOI: 10.1007/s12145-014-0149-3.

Abdalla, A. and Fairhead, D. (2011). "A New Gravimetric Geoid Model for Sudan Using the KTH Method". *Journal of African Earth Sciences* 60 (4), pp. 213–221. DOI: 10.1016/j.jafrearsci.2011.02.012.

Abdalla, A. and Tenzer, R. (2011). "The Evaluation of the New Zealand's Geoid Model Using the KTH Method". *Geodesy and Cartography* 37 (1), pp. 5–14. DOI: 10.3846/13921541.2011.558326.

Ågren, J. (2004). "Regional Geoid Determination Methods for the Era of Satellite Gravimetry: Numerical Investigations Using Synthetic Earth Gravity Models". PhD thesis. Stockholm, Sweden: KTH Royal Institute of Technology.

Ågren, J. (2013). *Initial Specification of the NKG2014 Geoid Model Computation*. Internal Report. Nordic Geodetic Commission (NKG), Working Group of Geoid and Height Systems.

Ågren, J., Barzaghi, R., Carrion, D., Denker, H., Duquenne, H., Grigoriadis, V. N., Kiamehr, R., Sona, G., Tscherning, C. C., and Tziavos, I. N. (2009a). "Different Geoid Computation Methods Applied on a Test Dataset: Results and Considerations". In: *VII Hotine-Marussi Symposium on Mathematical Geodesy*. Rome, Italy, 6-10 June.

Ågren, J., Engberg, L. E., Alm, L., Dahlström, F., Engfeldt, A., and Lidberg, M. (2014). "Improving the Swedish Quasigeoid by Gravity Observations on the Ice of Lake Vänern". In: *Gravity, Geoid and Height Systems: Proceedings of the IAG Symposium GGHS 2012, October 9 - 12, 2012, Venice, Italy*. Vol. 141. International Association of Geodesy Symposia. Springer International Publishing, pp. 171–177. ISBN: 978-3-319-10836-0. DOI: 10.1007/978-3-319-10837-7_22.

Ågren, J., Schwabe, J., Strykowski, G., Forsberg, R., Liebsch, G., Förste, C., Barthelmes, F., Bilker-Koivula, M., Ellmann, A., and Märdla, S. (2017). "Overview of the FAMOS Efforts to Improve the Baltic Sea Geoid Model by New Marine Gravity Measurements". In: *Joint Scientific Assembly of the International Association of Geodesy (IAG) and International Association of Seismology and Physics of the Earth's Interior (IASPEI), July 30 to August 4*. Kobe, Japan. DOI: 10.13140/RG.2.2.34378.67521. **Presentation II**.

Ågren, J. and Sjöberg, L. E. (2014). "Investigation of Gravity Data Requirements for a 5 mm-Quasigeoid Model over Sweden". In: *Gravity, geoid and height systems: Proceedings of the IAG Symposium GGHS 2012, October 9 - 12,*

2012, Venice, Italy. Vol. 141. International Association of Geodesy Symposia. Springer International Publishing, pp. 143–150. ISBN: 978-3-319-10836-0. DOI: 10.1007/978-3-319-10837-7_18.

Ågren, J., Sjöberg, L. E., and Kiamehr, R. (2009b). "The New Gravimetric Quasigeoid Model KTH08 over Sweden". *Journal of Applied Geodesy* 3 (3), pp. 143–153. DOI: 10.1515/JAG.2009.015.

Ågren, J., Strykowski, G., Bilker-Koivula, M., Omang, O., Märdla, S., Forsberg, R., Ellmann, A., Oja, T., Liepinš, I., Paršeliūnas, E., Kaminskis, J., Sjöberg, L. E., and Valsson, G. (2016). "The NKG2015 Gravimetric Geoid Model for the Nordic-Baltic Region". In: *1st Joint Commission 2 and IGFS Meeting International Symposium on Gravity, Geoid and Height Systems, 19-23 September*. Thessaloniki, Greece. DOI: 10.13140/RG.2.2.20765.20969. **Presentation IV**.

Ågren, J., Strykowski, G., Bilker-Koivula, M., Omang, O., Märdla, S., Oja, T., Liepinš, I., Paršeliūnas, E., Forsberg, R., Kaminskis, J., Ellmann, A., Sjöberg, L. E., and Valsson, V. (2015). "On the Development of the New Nordic Gravimetric Geoid Model NKG2015". In: 26th International Union of Geodesy and Geophysics (IUGG) General Assembly, June 22- July 02. Prague, Czech Republic. DOI: 10.13140/RG.2.2.14121.49761. **Presentation VI**.

Alberts, B. and Klees, R. (2004). "A Comparison of Methods for the Inversion of Airborne Gravity Data". *Journal of Geodesy* 78 (1-2), pp. 55–65. DOI: 10.1007/s00190-003-0366-x.

All, T. and Gromov, O. (2007). *Geoloogilise Baaskaardi Tapa (6431) Lehe Gravimeetrilise Teemakihi Täiendamine [Complementing the Gravimetric Layer for the Tapa Sheet (6431) of the Geological Basemap]*. Report 7894. 30 pages. Tallinn: Eesti Geoloogiakeskus.

Andersen, O. B. (2010). "The DTU10 Global Gravity Field and Mean Sea Surface – Improvements in the Arctic". In: *Second International Symposium of the Gravity Field of the Earth (IGFS2)*. Fairbanks, Alaska.

André, G., Martín Míguez, B., Ballu, V., Testut, L., and Wöppelmann, G. (2013). "Measuring Sea Level with GPS-Equipped Buoys: A Multi-Instrument Experiment at Aix Island". *International Hydrographic Review* 10, pp. 27–38.

Autodesk Inc. (2017). *AutoCad*. URL: https://www.autodesk.eu/products/autocad/overview (visited on 11/08/2017).

Baptiste, J., Martelet, G., Faure, M., Beccaletto, L., Reninger, P.-A., Perrin, J., and Chen, Y. (2016). "Mapping of a Buried Basement Combining Aeromagnetic, Gravity and Petrophysical Data: The Substratum of Southwest Paris Basin, France". *Tectonophysics* 683, pp. 333–348. DOI: 10.1016/j.tecto.2016.05.049.

Barthelmes, F. and Köhler, W. (2016). "International Centre for Global Earth Models (ICGEM)". *Journal of Geodesy: The Geodesist's Handbook 2016* 90 (10). Ed. by H. Drewes, F. Kuglitsch, J. Adám, and S. Rózsa, pp. 1177–1180. DOI: 10.1007/s00190-016-0948-z.

Barzaghi, R., Vergos, G., Albertella, A., Carrion, D., Tziavos, I., Grigoriadis, V., Natsiopoulos, D., Bruinsma, S., Sylvain, B., Seoane, L., Reinquin, F., LeQuentrec-Lalancette, M.-F., Bonnefond, P., Knudsen, P., Andersen, O., Simav, M., Hasan, Y., Basic, T., Gil, A. J., Cazzaniga, N., and Vergos, G. S. (2017). "The GEOMED2 Project: Geoid Estimation in the Mediterranean Area". In: *Joint Scientific Assembly of the International Association of Geodesy (IAG) and International Association of Seismology and Physics of the Earth's Interior (IASPEI), July 30 to August 4*. Kobe, Japan. DOI: 10.13140/RG.2.2.24438.50244.

Bruinsma, S. L., Förste, C., Abrikosov, O., Lemoine, J.-M., Marty, J.-C., Mulet, S., Rio, M.-H., and Bonvalot, S. (2014). "ESA's Satellite-Only Gravity Field Model via the Direct Approach Based on All GOCE Data". *Geophysical Research Letters* 41 (21), 2014GL062045. DOI: 10.1002/2014GL062045.

Bruinsma, S. L., Förste, C., Abrikosov, O., Marty, J.-C., Rio, M.-H., Mulet, S., and Bonvalot, S. (2013). "The New ESA Satellite-Only Gravity Field Model via the Direct Approach". *Geophysical Research Letters* 40 (14), pp. 3607–3612. DOI: 10.1002/grl.50716.

Carlsson, M. (1998). "Mean Sea-level Topography in the Baltic Sea Determined by Oceanographic Methods". *Marine Geodesy* 21 (3), pp. 203–217. DOI: 10.1080/01490419809388136.

Claessens, S. J. (2005). "New Relations among Associated Legendre Functions and Spherical Harmonics". *Journal of Geodesy* 79 (6-7), pp. 398–406. DOI: 10.1007/s00190-005-0483-9.

Cruz, J. Y. (1986). *Ellipsoidal Corrections to Potential Coefficients Obtained from Gravity Anomaly Data on the Ellipsoid*. Report 371. The Ohio State University.

Daras, I. (2008). "Determination of a Gravimetric Geoid Model of Greece Using the Method of KTH". Master's thesis. KTH Royal Institute of Technology.

Darbeheshti, N. and Featherstone, W. E. (2009). "Non-Stationary Covariance Function Modelling in 2D Least-Squares Collocation". *Journal of Geodesy* 83 (6), pp. 495–508. DOI: 10.1007/s00190-008-0267-0.

Dawidowicz, K. (2014). "Sea Level Changes Monitoring Using GNSS Technology – a Review of Recent Efforts". *Acta Adriatica : international journal of Marine Sciences* 55 (2), pp. 145–161.

Denker, H. (2013). "Regional Gravity Field Modeling: Theory and Practical Results". In: *Sciences of Geodesy - II*. Ed. by G. Xu. Springer Berlin Heidelberg, pp. 185–291. ISBN: 978-3-642-27999-7. DOI: 10.1007/978-3-642-28000-9_5.

Denker, H. (2016). "A New European Gravimetric (Quasi)Geoid EGG2015". In: *1st Joint Commission 2 and IGFS Meeting International Symposium on Gravity, Geoid and Height Systems*. Thessaloniki, Greece, 19-23 September.

Drinkwater, M. R., Floberghagen, R., Haagmans, R., Muzi, D., and Popescu, A. (2003). "GOCE: ESA's First Earth Explorer Core Mission". *Space Science Reviews* 108 (1-2), pp. 419–432. DOI: 10.1023/A:1026104216284.

Dunn, J. R. and Ridgway, K. R. (2002). "Mapping Ocean Properties in Regions of Complex Topography". *Deep Sea Research Part I: Oceanographic Research Papers* 49 (3), pp. 591–604. DOI: 10.1016/S0967-0637(01)00069-3.

Elkins, T. (1951). "The Second Derivative Method of Gravity Interpretation". *Geophysics* 16 (1), pp. 29–50. DOI: 10.1190/1.1437648.

Ellmann, A. (2004). "The Geoid for the Baltic Countries Determined by the Least Squares Modification of Stokes' Formula". PhD thesis. Stockholm, Sweden: KTH Royal Institute of Technology.

Ellmann, A. (2005a). "Computation of Three Stochastic Modifications of Stokes's Formula for Regional Geoid Determination". *Computers & Geosciences* 31 (6), pp. 742–755. DOI: 10.1016/j.cageo.2005.01.008.

Ellmann, A. (2005b). "On the Numerical Solution of Parameters of the Least Squares Modification of Stokes' Formula". In: *A Window on the Future of Geodesy*. Ed. by P. D. F. Sansò. International Association of Geodesy Symposia 128. Springer Berlin Heidelberg, pp. 403–408. ISBN: 978-3-540-24055-6. DOI: 10.1007/3-540-27432-4_69.

Ellmann, A. (2005c). "Two Deterministic and Three Stochastic Modifications of Stokes's Formula: A Case Study for the Baltic Countries". *Journal of Geodesy* 79 (1-3), pp. 11–23. DOI: 10.1007/s00190-005-0438-1.

Ellmann, A., All, T., and Oja, T. (2009). "Towards Unification of Terrestrial Gravity Data Sets in Estonia". *Estonian Journal of Earth Sciences* 58 (4), pp. 229–245. DOI: 10.3176/earth.2009.4.02.

Ellmann, A., Oja, T., and Jürgenson, H. (2011). "Kosmosetehnoloogia rakendused geoidi ja gravitatsioonivälja täpsustamiseks Eesti alal [Application of space technologies to improve geoid and gravity field models over Estonia]". *Geodeet* 41, pp. 22–25.

Ellmann, A. and Vaníček, P. (2007). "UNB Application of Stokes–Helmert's Approach to Geoid Computation". *Journal of Geodynamics* 43 (2), pp. 200–213. DOI: 10.1016/j.jog.2006.09.019.

Engberg, L. E., Alm, L., Dahlström, F., Ågren, J., Engfeldt, A., and Lidberg, M. (2011). "Relative Gravity Measurements on the Ice of Lake Vänern". In: *Proceedings of the International Association of Geodesy (IAG) Reference Frame Sub-Commission for Europe (EUREF) Symposium, May 25-28*. Chisinau, Moldova.

Evans, J. D. and Featherstone, W. E. (2000). "Improved Convergence Rates for the Truncation Error in Gravimetric Geoid Determination". *Journal of Geodesy* 74 (2), pp. 239–248. DOI: 10.1007/s001900050282.

Featherstone, W. E. (2013). "Deterministic, Stochastic, Hybrid and Band-Limited Modifications of Hotine's Integral". *Journal of Geodesy* 87 (5), pp. 487–500. DOI: 10.1007/s00190-013-0612-9.

Featherstone, W. E., Evans, J. D., and Olliver, J. G. (1998). "A Meissl-Modified Vaníček and Kleusberg Kernel to Reduce the Truncation Error in Gravimetric Geoid Computations". *Journal of Geodesy* 72 (3), pp. 154–160. DOI: 10.1007/s001900050157.

Featherstone, W. E., Kirby, J. F., Hirt, C., Filmer, M. S., Claessens, S. J., Brown, N. J., Hu, G., and Johnston, G. M. (2010). "The AUSGeoid09 Model of the Australian Height Datum". *Journal of Geodesy* 85 (3), pp. 133–150. DOI: 10.1007/s00190-010-0422-2.

Forsberg, R. (1993). "Modelling the Fine-Structure of the Geoid: Methods, Data Requirements and Some Results". *Surveys in Geophysics* 14 (4-5), pp. 403–418. DOI: 10.1007/BF00690568.

Forsberg, R. (1984). *A Study of Terrain Reductions, Density Anomalies and Geophysical Inversion Methods in Gravity Field Modelling*. Report 355. The Ohio State University.

Forsberg, R. (1991). "A New High-Resolution Geoid of the Nordic Area". In: *Determination of the Geoid*. Ed. by R. H. Rapp and F. Sansò. International Association of Geodesy Symposia 106. Springer New York, pp. 241–250. ISBN: 978-0-387-97470-5. DOI: 10.1007/978-1-4612-3104-2_29.

Forsberg, R., Kaminskis, J., and Solheim, D. (1997). "Geoid of the Nordic and Baltic Region from Gravimetry and Satellite Altimetry". In: *Gravity, Geoid and Marine Geodesy*. Ed. by P. D. J. Segawa, P. D. H. Fujimoto, and P. D. S. Okubo. International Association of Geodesy Symposia 117. Springer Berlin Heidelberg, pp. 540–547. ISBN: 978-3-642-08328-0. DOI: 10.1007/978-3-662-03482-8_72.

Forsberg, R., Strykowski, G., and Solheim, D. (2004). "NKG-2004 Geoid of the Nordic and Baltic Area". In: *Proceedings on CD-ROM from the International Association of Geodesy*. Gravity, Geoid and Satellite Gravity Missions, Aug 30 - Sep 3, 2004. Porto, Portugal.

Forsberg, R. and Tscherning, C. C. (1997). "Topographic Effects in Gravity Field Modelling for BVP". In: *Geodetic Boundary Value Problems in View of the One Centimeter Geoid*. Ed. by P. D. F. Sansó and P. D. R. Rummel. Lecture Notes in Earth Sciences 65. Springer Berlin Heidelberg, pp. 239–272. ISBN: 978-3-540-62636-7. DOI: 10.1007/BFb0011707.

Forsberg, R. and Tscherning, C. C. (2008). *An Overview Manual for the GRAVSOFT Geodetic Gravity Field Modelling Programs. Second Edition.*

Gil, A. J. and Rodríguez-Caderot, G. (1998). "Processing Gravity Data in the Territory of Andalusia". *Marine Geodesy* 21 (1), pp. 81–89. DOI: 10.1080/01490419809388123.

Goad, C. C., Tscherning, C. C., and Chin, M. M. (1984). "Gravity Empirical Covariance Values for the Continental United States". *Journal of Geophysical Research: Solid Earth* 89 (B9), pp. 7962–7968. DOI: 10.1029/JB089iB09p07962.

Golbeck, I., Li, X., Janssen, F., Brüning, T., Nielsen, J. W., Huess, V., Söderkvist, J., Büchmann, B., Siiriä, S.-M., Vähä-Piikkiö, O., Hackett, B., Kristensen, N. M., Engedahl, H., Blockley, E., Sellar, A., Lagemaa, P., Ozer, J., Legrand, S., Ljungemyr, P., and Axell, L. (2015). "Uncertainty Estimation for Operational Ocean Forecast Products – a Multi-Model Ensemble for the North Sea and the Baltic Sea". *Ocean Dynamics* 65 (12), pp. 1603–1631. DOI: 10.1007/s10236-015-0897-8.

Golden Software LLC (2016). *Surfer*. URL: http://www.goldensoftware.com/products/surfer (visited on 01/09/2016).

Gruno, A., Liibusk, A., Ellmann, A., Oja, T., Vain, A., and Jürgenson, H. (2013). "Determining Sea Surface Heights Using Small Footprint Airborne Laser Scanning". In: *SPIE 8888, Remote Sensing of the Ocean, Sea Ice, Coastal Waters, and Large Water Regions 2013, 88880R, October 16, 2013*, pp. 1–13. DOI: 10.1117/12.2029189.

Guan, Z. and Li, Y. (1991). "The Determination of Oceanic Geoid Using Modified Hotine Integral". In: *Determination of the Geoid*. Ed. by R. H. Rapp and F. Sansò. International Association of Geodesy Symposia 106. Springer New York, pp. 86–94. ISBN: 978-0-387-97470-5. DOI: 10.1007/978-1-4612-3104-2_11.

Hackney, R. I. and Featherstone, W. E. (2003). "Geodetic versus Geophysical Perspectives of the 'Gravity Anomaly'". *Geophysical Journal International* 154 (1), pp. 35–43. DOI: 10.1046/j.1365-246X.2003.01941.x.

Heck, B. and Grüninger, W. (1987). "Modification of Stokes's Integral Formula by Combining Two Classical Approaches". In: *Proceedings of the XIX IUGG General Assembly*. Vol. 2. Vancouver, Canada, pp. 319–337.

Heiskanen, W. A. and Moritz, H. (1967). *Physical Geodesy*. San Francisco W. H. Freeman and Company.

Hinze, W., Aiken, C., Brozena, J., Coakley, B., Dater, D., Flanagan, G., Forsberg, R., Hildenbrand, T., Keller, G., Kellogg, J., Kucks, R., Li, X., Mainville, A., Morin, R., Pilkington, M., Plouff, D., Ravat, D., Roman, D., Urrutia-Fucugauchi, J., Véronneau, M., Webring, M., and Winester, D. (2005). "New Standards for Reducing Gravity Data: The North American Gravity Database". *Geophysics* 70 (4), J25–J32. DOI: 10.1190/1.1988183.

Hotine, M. (1969). *Mathematical Geodesy*. Rockville: US Environmental Science Services Administration.

Hünicke, B., Zorita, E., Soomere, T., Madsen, K. S., Johansson, M., and Suursaar, Ü. (2015). "Recent Change – Sea Level and Wind Waves". In: *Second Assessment of Climate Change for the Baltic Sea Basin*. Ed. by The BACC II Author Team. Regional Climate Studies. Springer, Cham, pp. 155–185. ISBN: 978-3-319-16005-4. DOI: 10.1007/978-3-319-16006-1_9.

Isaaks, E. H. and Srivastava, R. M. (1989). *Applied Geostatistics*. Oxford, New York: Oxford University Press. ISBN: 978-0-19-505013-4.

ISG (2015). *International Service for the Geoid: Baltic and Nordic Region (NKG2015)*. URL: http : / / www . isgeoid . polimi . it / Geoid / Europe / NordicCountries/nordic_baltic_countries_g.html (visited on 09/05/2017).

Janák, J. and Vaníček, P. (2005). "Mean Free-Air Gravity Anomalies in the Mountains". *Studia Geophysica et Geodaetica* 49 (1), pp. 31–42. DOI: 10.1007/s11200-005-1624-6.

Jekeli, C. (1979). *Global Accuracy Estimates of Point and Mean Undulation Differences, Gravity Anomalies, and Potential Coefficients*. Report 288. The Ohio State University.

Jekeli, C. (1980). "Comparison of Undulation Difference Accuracies Using Gravity Anomalies and Gravity Disturbances". *Bulletin géodésique* 54 (2), pp. 137–147. DOI: 10.1007/BF02521243.

Jekeli, C., Yang, H. J., and Kwon, J. H. (2009). "Using Gravity and Topography-Implied Anomalies to Assess Data Requirements for Precise Geoid Computation". *Journal of Geodesy* 83 (12), pp. 1193–1202. DOI: 10.1007/s00190-009-0337-y.

Julge, K., Gruno, A., Ellmann, A., Liibusk, A., and Oja, T. (2014). "Exploring Sea Surface Heights by Using Airborne Laser Scanning". In: *Proceedings of the IEEE/OES Baltic International Symposium, May 27-29*. Tallinn, Estonia, pp. 1–7. DOI: 10.1109/BALTIC.2014.6887853.

Jürgenson, H. (2003). "Eesti täppisgeoidi arvutus [Determination of Estonian Precision Geoid]". PhD thesis. Tartu, Estonia: Estonian University of Life Sciences.

Jürgenson, H., Liibusk, A., and Ellmann, A. (2008). "Geoid Profiles in the Baltic Sea Determined Using GPS and Sea Level Surface". *Geodezija ir Kartografija* 34 (4), pp. 109–115. DOI: 10.3846/1392-1541.2008.34.109-115.

Jürgenson, H., Türk, K., and Randjärv, J. (2011). "Determination and Evaluation of the Estonian Fitted Geoid Model EST-GEOID 2003". *Geodesy and Cartography* 37 (1), pp. 15–21. DOI: 10.3846/13921541.2011.558339.

Kakkuri, J. and Poutanen, M. (1997). "Geodetic Determination of the Surface Topography of the Baltic Sea". *Marine Geodesy* 20 (4), pp. 307–316. DOI: 10.1080/01490419709388111.

Kaula, W. M. (1963). "The Investigation of the Gravitational Fields of the Moon and Planets with Artificial Satellites". *Advances in Space Sciences and Technology* 5, pp. 210–226.

Kiamehr, R. (2006). "A Strategy for Determining the Regional Geoid by Combining Limited Ground Data with Satellite-Based Global Geopotential and Topographical Models: A Case Study of Iran". *Journal of Geodesy* 79 (10-11), pp. 602–612. DOI: 10.1007/s00190-005-0009-5.

Kirby, J. F. (2003). "On the Combination of Gravity Anomalies and Gravity Disturbances for Geoid Determination in Western Australia". *Journal of Geodesy* 77 (7-8), pp. 433–439. DOI: 10.1007/s00190-003-0334-5.

Kiviniemi, A. (1975). *Measurements of Wave Motion in the Ice Surface*. Report of the Finnish Geodetic Institute 75:4. Helsinki, Finland.

Klitzke, P., Sippel, J., Faleide, J. I., and Scheck-Wenderoth, M. (2016). "A 3D Gravity and Thermal Model for the Barents Sea and Kara Sea". *Tectonophysics*. Special Issue on GeoMod 2014 – Modelling in Geoscience 684, pp. 131–147. DOI: 10.1016/j.tecto.2016.04.033.

Knudsen, P. (2005). "Patching Local Empirical Covariance Functions – A Problem in Altimeter Data Processing". In: *A Window on the Future of Geodesy*. Ed. by F. Sansò. International Association of Geodesy Symposia 128. Springer, Berlin, Heidelberg, pp. 483–487. ISBN: 978-3-540-24055-6. DOI: 10.1007/3-540-27432-4_82.

Krige, D. G. (1951). "A Statistical Approach to Some Basic Mine Valuation Problems on the Witwatersrand". *Journal of the Southern African Institute of Mining and Metallurgy* 52 (6), pp. 119–139.

Kuczynska-Siehien, J., Lyszkowicz, A., and Birylo, M. (2016). "Geoid Determination for the Area of Poland by the Least Squares Modification of Stokes' Formula". *Acta Geodynamica et Geomaterialia* 13 (1), pp. 19–26. DOI: 10.13168/AGG.2015.0041.

Lagemaa, P., Elken, J., and Kõuts, T. (2011). "Operational Sea Level Forecasting in Estonia". *Estonian Journal of Engineering* 17 (4), pp. 301–331. DOI: 10.3176/eng.2011.4.03.

Langley, R. B., Teunissen, P. J. G., and Montenbruck, O. (2017). "Introduction to GNSS". In: *Springer Handbook of Global Navigation Satellite Systems*. Ed. by P. J. G. Teunissen and O. Montenbruck. Springer Handbooks. Springer, Cham, pp. 3–23. ISBN: 978-3-319-42926-7. DOI: 10.1007/978-3-319-42928-1_1.

Lavrov, D., Even-Tzur, G., and Reinking, J. (2016). "Expansion and Improvement of the Israeli Geoid Model by Shipborne GNSS Measurements". *Journal of Surveying Engineering* 143 (2), p. 04016022. DOI: 10.1061/(ASCE)SU.1943-5428.0000204.

Lehmuskoski, P. and Mäkinen, J. (1978). *Gravity Measurements on the Ice of the Bothnian Bay*. Publications of the Finnish Geodetic Institute 86. Helsinki, Finland.

Liibusk, A., Talvik, S., Ellmann, A., and Oja, T. (2014). "Determining Regional Sea Surface Topography by GNSS Surveys on Ice". In: *Proceedings of the IEEE/OES Baltic International Symposium, May 27-29*. Tallinn, Estonia, pp. 1–9. DOI: 10.1109/BALTIC.2014.6887847. **Paper E**.

Liibusk, A. (2013). "Precise Hydrodynamic Levelling Using Pressure Gauges with Application to Improvement of the Estonian National Levelling Network". PhD thesis. Tartu, Estonia: Estonian University of Life Sciences.

Liibusk, A. and Ellmann, A. (2015). "Validation of Marine Geoid Models by Profile-Wise GNSS Measurements on Ice Surface". *Marine Geodesy* 38 (4), pp. 314–326. DOI: 10.1080/01490419.2015.1037408.

Lin, Y.-P., Huang, C.-J., Chen, S.-H., Doong, D.-J., and Kao, C. C. (2017). "Development of a GNSS Buoy for Monitoring Water Surface Elevations in Estuaries and Coastal Areas". *Sensors* 17 (1). DOI: 10.3390/s17010172.

Lysaker, D. I., Omang, O. C. D., Pettersen, B. R., and Solheim, D. (2007). "Quasigeoid Evaluation with Improved Levelled Height Data for Norway". *Journal of Geodesy* 81 (9), pp. 617–627. DOI: 10.1007/s00190-006-0129-6.

Mandal, A., Gupta, S., Mohanty, W. K., and Misra, S. (2015). "Sub-Surface Structure of a Craton–mobile Belt Interface: Evidence from Geological and Gravity Studies across the Rengali Province–Eastern Ghats Belt Boundary, Eastern India". *Tectonophysics*. Special issue on comparative tectonic and dynamic analysis of cratons, orogens, basins, and metallogeny 662, pp. 140–152. DOI: 10.1016/j.tecto.2015.01.016.

Märdla, S., Ellmann, A., Oja, T., and Jürgenson, H. (2015a). "Improving and Validating Gravity Data Over Ice-Covered Marine Areas". In: *IAG 150 Years: Proceedings of the 2013 IAG Scientific Assembly, 1–6 September, 2013*. Ed. by C. Rizos and P. Willis. International Association of Geodesy Symposia 143. Potsdam, Germany: Springer International Publishing, pp. 263–270. ISBN: 978-3-319-24603-1. DOI: 10.1007/1345_2015_163. **Paper C**.

Märdla, S., Ågren, J., Strykowski, G., Oja, T., Ellmann, A., Forsberg, R., Bilker-Koivula, M., Omang, O., Paršeliūnas, E., Liepiņš, I., and Kaminskis, J. (2017a). "From Discrete Gravity Survey Data to a High-Resolution Gravity Field Representation in the Nordic-Baltic Region". *Marine Geodesy* 40 (6), pp. 416–453. DOI: 10.1080/01490419.2017.1326428. **Paper B**.

Märdla, S., Ågren, J., Strykowski, G., Oja, T., Ellmann, A., Forsberg, R., Bilker-Koivula, M., Omang, O., Paršeliūnas, E., Liepiņš, I., Kaminskis, J., and Sjöberg, L. (2016). "From Discrete Gravity Survey Data to a High-Resolution Gravity Field Representation in the Nordic-Baltic Region". In: *1st Joint Commission 2 and IGFS Meeting International Symposium on Gravity, Geoid and Height Systems, 19-23 September*. Thessaloniki, Greece. DOI: 10.13140/RG.2.2.31906.32967. **Presentation V**.

Märdla, S., Ellmann, A., Ågren, J., and Sjöberg, L. E. (2017b). "Regional Geoid Computation by Least Squares Modified Hotine's Formula with Additive Corrections". *Journal of Geodesy*, pp. 1–18. DOI: 10.1007/s00190-017-1061-7. **Paper A**.

Märdla, S., Ellmann, A., Ågren, J., and Sjöberg, L. E. (2017c). "Regional Geoid Computation by Least Squares Modified Hotine's Formula with Additive Corrections". In: *Joint Scientific Assembly of the International Association of Geodesy (IAG) and International Association of Seismology and Physics of the Earth's Interior (IASPEI), July 30 to August 4*. Kobe, Japan. DOI: 10.13140/RG.2.2.29154.63682. **Presentation I**.

Märdla, S., Ellmann, A., Oja, T., and Ågren, J. (2015b). "Improving Regional Gravity Field and Geoid Modelling by Various Use of Global Geopotential Models". In: 26th International Union of Geodesy and Geophysics (IUGG)

General Assembly, June 22- July 02. Prague, Czech Republic. DOI: 10.13140/ RG.2.2.25398.60481. **Presentation VII**.

Märdla, S., Oja, T., and Ellmann, A. (2014a). "Investigations towards the NKG2014 Geoid Model in Estonia". In: Nordic Geodetic Commission (NKG) General Assembly, September 1-5. Gothenburg, Sweden. DOI: 10.13140/RG. 2.2.34232.85766. **Presentation VIII**.

Märdla, S., Oja, T., Ellmann, A., and Jürgenson, H. (2014b). "Modelling the Influence of Terraced Landforms to the Earth's Gravity Field". In: *Gravity, Geoid and Height Systems*. Ed. by U. Marti. International Association of Geodesy Symposia 141. Venice, Italy: Springer International Publishing, pp. 157–162. ISBN: 978-3-319-10836-0. DOI: 10.1007/978-3-319-10837-7_20. **Paper D**.

Martinec, Z. (1996). "Stability Investigations of a Discrete Downward Continuation Problem for Geoid Determination in the Canadian Rocky Mountains". *Journal of Geodesy* 70 (11), pp. 805–828. DOI: 10.1007/BF00867158.

Martinec, Z. (1998a). *Boundary-Value Problems for Gravimetric Determination of a Precise Geoid*. Vol. 73. Lecture Notes in Earth Sciences. Springer, Berlin, Heidelberg. ISBN: 978-3-540-64462-0. DOI: 10.1007/BFb0010337.

Martinec, Z. (1998b). "Construction of Green's Function for the Stokes Boundary-Value Problem with Ellipsoidal Corrections in the Boundary Condition". *Journal of Geodesy* 72 (7-8), pp. 460–472. DOI: 10.1007/s001900050185.

Martín, A., Anquela, A. B., Padín, J., and Baselga, S. (2009). "Some Notes and Numerical Comparisons on Gravity Anomalies Interpolation". *Survey Review* 41 (312), pp. 201–215. DOI: 10.1179/003962609X390102.

MathWorks Inc (2017). *Matlab*. URL: https://se.mathworks.com/products/matlab. html (visited on 11/09/2017).

Meissl, P. (1971). *Preparations for the Numerical Evaluation of Second Order Molodensky-Type Formulas*. Report 163. The Ohio State University.

Merry, C. L. and Vaníček, P. (1983). "Investigation of Local Variations of Sea-surface Topography". *Marine Geodesy* 7 (1-4), pp. 101–126. DOI: 10.1080/ 15210608309379477.

Molodenskii, M., Eremeev, V., and Urkina, M. (1962). *Methods for Study of the External Gravitation Field and Figure of the Earth*. Transl. from Russian, Israel Program for Scientific Translations. Jerusalem, Israel.

Molodensky, M. S. (1945). "The Principal Problems of Geodetic Gravimetry (in Russian)". *TRUDY Ts NIIGAiK* 42.

Moritz, H. (1980). *Advanced Physical Geodesy*. England: Abacus Press. ISBN: 978-0-85626-195-4.

Moritz, H. (2000). "Geodetic Reference System 1980". *Journal of Geodesy* 74 (1), pp. 128–133. DOI: 10.1007/s001900050278.

Nikolenko, T. (2010). "Raskuskiirenduse Mõõtmine Ja Tasandamine Puhja–Rõngu–Tõrva Piirkonnas Aastatel 2009–2010 [Measurement and Adjustment of Gravity Acceleration in the Area of Puhja–Rõngu–Tõrva in 2009-2010]". Master's thesis. Tartu, Estonia: University of Life Sciences.

NKG WGGHS (2017). *The Nordic Geodetic Commission Working Group of Geoid and Height Systems*. URL: http://www.nordicgeodeticcommission.com/geoid-and-height-systems/ (visited on 09/14/2017).

Novák, P. (2003). "Geoid Determination Using One-Step Integration". *Journal of Geodesy* 77 (3-4), pp. 193–206. DOI: 10.1007/s00190-003-0314-9.

Novák, P. and Heck, B. (2002). "Downward Continuation and Geoid Determination Based on Band-Limited Airborne Gravity Data". *Journal of Geodesy* 76 (5), pp. 269–278. DOI: 10.1007/s00190-002-0252-y.

Novák, P., Kern, M., Schwarz, K.-P., Sideris, M. G., Heck, B., Ferguson, S., Hammada, Y., and Wei, M. (2003). "On Geoid Determination from Airborne Gravity". *Journal of Geodesy* 76 (9-10), pp. 510–522. DOI: 10.1007/s00190-002-0284-3.

Novák, P., Tenzer, R., Baghrebandi, M., Sjöberg, L. E., and Chen, W. (2016). "Isostatic Global Gravity Fields for Geodetic and Geophysical Applications". In: *1st Joint Commission 2 and IGFS Meeting International Symposium on Gravity, Geoid and Height Systems*. Thessaloniki, Greece, 19-23 September.

Oja, T. (2011). "Raskuskiirenduse Anomaalvälja Kerkest Luusika Kandis Ning Selle Mõjust Geoidile [The Uplift of Gravity Anomaly Field near Luusika and Its Impact on Geoid]". *Geodeet* 41, pp. 26–30.

Oja, T. (2012). "Gravity System and Network in Estonia". In: *Geodesy for Planet Earth. Proceedings of the 2009 IAG Symposium, August 31 - September 4, 2009, Buenos Aires, Argentina*. Ed. by S. Kenyon, M. Pacino, and M. Urs. International Association of Geodesy Symposia 136. Springer, Berlin, Heidelberg, pp. 315–322. ISBN: 978-3-642-20337-4. DOI: 10.1007/978-3-642-20338-1_38.

Oja, T., Bloom, A., Talvik, S., Jürgenson, H., and Ellmann, A. (2013). "Relative Gravity Measurements on Ice-Covered Water Bodies". In: International Association of Geodesy (IAG) Scientific Assembly, September 1-6. Potsdam, Germany. DOI: 10.13140/RG.2.2.27974.16965. **Presentation XII**.

Oja, T. and Pihlak, P. (2010). *Maa Raskuskiirenduse Uuringud Haanjas Aastatel 2008-2009 [Investigations of the Earth's Gravity in Haanja in 2008-2009]*. Geodeetiliste Tööde Aruanne. Tallinn, Estonia: Eesti Maa-amet.

Oja, T. and Talvik, S. (2014). "Estonian Gravity Data". In: Nordic Geodetic Commission (NKG) Working Group of Geoid and Height Systems meeting, March 11-12. Gävle, Sweden. DOI: 10.13140/RG.2.2.10744.75521. **Presentation XI**.

Oja, T., Türk, K., Ellmann, A., Gruno, A., Bloom, A., and Sulaoja, M. (2011). "Relative Gravity Surveys on Ice-Covered Water Bodies". In: *Environmental Engineering. The 8th International Conference. May 19–20, 2011, Vilnius, Lithuania*. Vilnius Gediminas Technical University press "Technika", pp. 1394–1401. ISBN: 978-9955-28-829-9.

Omang, O. C. D. and Forsberg, R. (2000). "How to Handle Topography in Practical Geoid Determination: Three Examples". *Journal of Geodesy* 74 (6), pp. 458–466. DOI: 10.1007/s001900000107.

Paul, M. K. (1973). "A Method of Evaluating the Truncation Error Coefficients for Geoidal Height". *Bulletin Géodésique* 110 (1), pp. 413–425. DOI: 10.1007/BF02521951.

Pavlis, N. K., Holmes, S. A., Kenyon, S. C., and Factor, J. K. (2012). "The Development and Evaluation of the Earth Gravitational Model 2008 (EGM2008)". *Journal of Geophysical Research: Solid Earth* 117 (B4), B04406. DOI: 10.1029/2011JB008916.

Pehlak, A.-L. (2014). "Gravimeetrilise Anomaalvälja Uuringud Tartu- Ja Võrumaal [Research on the Gravimetric Anomaly Field in Tartu and Võru Counties]". Master's thesis. Tartu, Estonia: University of Life Sciences.

Pugh, D. (1987). *Tides, Surges and Mean Sea-Level*. New York: John Wiley.

Radhakrishna, M., Lasitha, S., and Mukhopadhyay, M. (2008). "Seismicity, Gravity Anomalies and Lithospheric Structure of the Andaman Arc, NE Indian Ocean". *Tectonophysics* 460 (1–4), pp. 248–262. DOI: 10.1016/j.tecto.2008.08.021.

Reigber, C., Balmino, G., Schwintzer, P., Biancale, R., Bode, A., Lemoine, J.-M., König, R., Loyer, S., Neumayer, H., Marty, J.-C., Barthelmes, F., Perosanz, F., and Zhu, S. Y. (2002). "A High-Quality Global Gravity Field Model from CHAMP GPS Tracking Data and Accelerometry (EIGEN-1S)". *Geophysical Research Letters* 29 (14), pp. 37–1. DOI: 10.1029/2002GL015064.

RT I, 3 (2011). *Legal Acts of Estonia: Geodeetiline Süsteem, RT I, 28.10.2011, 3*. URL: https://www.riigiteataja.ee/akt/128102011003 (visited on 11/10/2016).

Saleh, J., Li, X., Wang, Y. M., Roman, D. R., and Smith, D. A. (2013). "Error Analysis of the NGS' Surface Gravity Database". *Journal of Geodesy* 87 (3), pp. 203–221. DOI: 10.1007/s00190-012-0589-9.

Sansò, F. and M. G. Sideris, eds. (2013). *Geoid Determination*. Vol. 110. Lecture Notes in Earth System Sciences. Springer, Berlin, Heidelberg. ISBN: 978-3-540-74699-7. DOI: 10.1007/978-3-540-74700-0.

Santos, N. P. dos and Escobar, I. P. (2004). "Discrete Evaluation of Stokes's Integral by Means of Voronoi and Delaunay Structures". *Journal of Geodesy* 78 (6), pp. 354–367. DOI: 10.1007/s00190-004-0402-5.

Schwarz, K. P. and Lachapelle, G. (1980). "Local Characteristics of the Gravity Anomaly Covariance Function". *Bulletin Géodésique* 54 (1), pp. 21–36. DOI: 10.1007/BF02521093.

Serpas, J. G. and Jekeli, C. (2005). "Local Geoid Determination from Airborne Vector Gravimetry". *Journal of Geodesy* 78 (10), pp. 577–587. DOI: 10.1007/s00190-004-0416-z.

Sjöberg, L. E. (1980). "Least Squares Combination of Satellite Harmonics and Integral Formulas in Physical Geodesy". *Gerlands Beitraege zur Geophysik* 89, pp. 371–377.

Sjöberg, L. E. (1984). "Least Squares Modification of Stokes' and Vening Meinesz' Formulas by Accounting for Truncation and Potential Coefficient Errors". *Manuscripta Geodaetica* 9, pp. 209–229.

Sjöberg, L. E. (1986). "The Modification of Stokes' and Hotine's Formulas: A Comparison". In: *Proc. of Int. Symp on Figure and Dynamics of the Earth, Moon, and Planets*. Prague, pp. 323–333.

Sjöberg, L. E. (1991). "Refined Least Squares Modification of Stokes Formula". *Manuscripta Geodaetica* 16, pp. 367–375.

Sjöberg, L. E. (1995). "The Total Terrain Effect in the Modified Stokes' Formula". In: *Gravity and Geoid – Proceedings of the Joint Symposium of the International Gravity Commission and the International Geoid Commission, Sep. 11-17, 1994, Graz, Austria*. Ed. by H. Sünkel and I. Marson. Vol. 113. International Association of Geodesy Symposia. Springer, Berlin, Heidelberg, pp. 616–623. ISBN: 978-3-540-59204-4. DOI: 10.1007/978-3-642-79721-7_65.

Sjöberg, L. E. (1997). "The Total Terrain Effect in Gravimetric Geoid Determinations". *Boll Geod Sci Aff* 56 (2), pp. 209–222.

Sjöberg, L. E. (1999). "The IAG Approach to the Atmospheric Geoid Correction in Stokes' Formula and a New Strategy". *Journal of Geodesy* 73 (7), pp. 362–366. DOI: 10.1007/s001900050254.

Sjöberg, L. E. (2000). "Topographic Effects by the Stokes–Helmert Method of Geoid and Quasi-Geoid Determinations". *Journal of Geodesy* 74 (2), pp. 255–268. DOI: 10.1007/s001900050284.

Sjöberg, L. E. (2001). "Topographic and Atmospheric Corrections of Gravimetric Geoid Determination with Special Emphasis on the Effects of Harmonics of Degrees Zero and One". *Journal of Geodesy* 75 (5-6), pp. 283–290. DOI: 10.1007/s001900100174.

Sjöberg, L. E. (2003a). "A Computational Scheme to Model the Geoid by the Modified Stokes Formula without Gravity Reductions". *Journal of Geodesy* 77 (7-8), pp. 423–432. DOI: 10.1007/s00190-003-0338-1.

Sjöberg, L. E. (2003b). "A General Model for Modifying Stokes' Formula and Its Least-Squares Solution". *Journal of Geodesy* 77 (7-8), pp. 459–464. DOI: 10.1007/s00190-003-0346-1.

Sjöberg, L. E. (2003c). "A Solution to the Downward Continuation Effect on the Geoid Determined by Stokes' Formula". *Journal of Geodesy* 77 (1-2), pp. 94–100. DOI: 10.1007/s00190-002-0306-1.

Sjöberg, L. E. (2003d). "Ellipsoidal Corrections to Order E2 of Geopotential Coefficients and Stokes' Formula". *Journal of Geodesy* 77 (3-4), pp. 139–147. DOI: 10.1007/s00190-003-0321-x.

Sjöberg, L. E. (2003e). "The Correction to the Modified Stokes Formula for an Ellipsoidal Earth". In: *Honoring the Academic Life of Petr Vanicek*. Ed. by M. Santos. UNB Technical Report 218. New Brunswick, Canada, pp. 99–110.

Sjöberg, L. E. (2004). "A Spherical Harmonic Representation of the Ellipsoidal Correction to the Modified Stokes Formula". *Journal of Geodesy* 78 (3), pp. 180–186. DOI: 10.1007/s00190-004-0378-1.

Sjöberg, L. E. and Bagherbandi, M. (2017). *Gravity Inversion and Integration - Theory and Applications in Geodesy and Geophysics*. Springer International Publishing. ISBN: 978-3-319-50298-4. DOI: 10.1007/978-3-319-50298-4.

Sjöberg, L. E. and Eshagh, M. (2009). "A Geoid Solution for Airborne Gravity Data". *Studia Geophysica et Geodaetica* 53 (3), pp. 359–374. DOI: 10.1007/s11200-009-0025-7.

Sjöberg, L. E., Gidudu, A., and Ssengendo, R. (2015). "The Uganda Gravimetric Geoid Model 2014 Computed by The KTH Method". *Journal of Geodetic Science* 5 (1). DOI: 10.1515/jogs-2015-0007.

Sjöberg, L. E. and Nord, T. (1992). "Geoidal Undulation Computation by Modifying Stokes's Kernel versus Hotine's Kernel from Gravity Anomalies". *Manuscripta Geodaetica* 17, pp. 135–140.

Smith, W. H. F. and Wessel, P. (1990). "Gridding with Continuous Curvature Splines in Tension". *GEOPHYSICS* 55 (3), pp. 293–305. DOI: 10.1190/1.1442837.

Stokes, G. G. (1849). "On the Variation of Gravity at the Surface of the Earth". In: Trans. Cambridge Philos. Soc. VIIII, pp. 672–695.

Suursaar, Ü., Jaagus, J., and Kullas, T. (2006). "Past and Future Changes in Sea Level near the Estonian Coast in Relation to Changes in Wind Climate". *Boreal Environment Research* 11, pp. 123–142.

Suursaar, Ü. and Kullas, T. (2009). "Meretase ja hoovused Eesti rannikumeres muutuva kliima tingimustes [Sea level and currents in the coastal waters of Estonia under changing wind regime]". In: *Kliimamuutuste mõju Eesti rannikule*. Ed. by A. Kont and H. Tõnisson. Vol. 11. Ökoloogia Instituudi publikatsioonid. Tallinn, Estonia: Tallinna Ülikooli Kirjastus, pp. 25–43. ISBN: 1736-5554.

Talvik, S. (2014). "Precise Levelling Data Processing near Terraced Landforms". *Geodesy and Cartography* 40 (2), pp. 51–57. DOI: 10.3846/20296991.2014.930247.

Talvik, S., Ellmann, A., Oja, T., and Jürgenson, H. (2014a). "Analysing Methods of Detailed Gravity Field Modelling from Terrestrial Data". In: European Geosciences Union (EGU) General Assembly, April 27 to May 2. Vienna, Austria. DOI: 10.13140/RG.2.2.28813.03047. **Presentation IX**.

Talvik, S., Ellmann, A., Oja, T., and Jürgenson, H. (2014b). "Analysing Methods of Detailed Gravity Field Modelling from Terrestrial Data". In: European Geosciences Union (EGU) General Assembly, April 27 to May 2. Vienna, Austria. DOI: 10.13140/RG.2.2.12035.81448. **Presentation X**.

Talvik, S. and Oja, T. (2014). *Eesti Gravimeetriline Andmebaas [The Estonian Gravity Database]*. Unpublished report. 27 pages. Tallinn, Estonia: Tallinn University of Technology, Estonian Land Board.

Talvik, S., Oja, T., Ellmann, A., and Jürgenson, H. (2012). "Modelling the Influence of Terraced Landforms to the Earth's Gravity Field". In: International Symposium on Gravity, Geoid and Height Systems, October 9-12. Venice, Italy. DOI: 10.13140/RG.2.2.15967.97444. **Presentation XIV**.

Talvik, S., Oja, T., Jürgenson, H., and Ellmann, A. (2014c). *Eesti Geoloogiakeskuse (EGK) raskuskiirenduse andmete filtreerimine [Filtering the Estonian Geological Survey (EGK) gravimetric data]*. Unpublished report. 35 pages. Tallinn, Estonia: Tallinn University of Technology, Estonian Land Board, Estonian University of Life Sciences.

Talvik, S., Oja, T., Jürgenson, H., Ellmann, A., and Bloom, A. (2013). "Gravity Data in Estonia". In: Nordic Geodetic Commission (NKG) Science Week, March 12-14. Reykjavik, Iceland. DOI: 10.13140/RG.2.2.23937.15204. **Presentation XIII**.

Tapley, B. D., Bettadpur, S., Watkins, M., and Reigber, C. (2004). "The Gravity Recovery and Climate Experiment: Mission Overview and Early Results". *Geophysical Research Letters* 31 (9), p. L09607. DOI: 10.1029/2004GL019920.

Tscherning, C. C. and Forsberg, R. (1986). "Geoid Determination in the Nordic Countries from Gravity and Height Data". In: *Bolletino Di Geodesia e Scienze Affini*. International Symposium on the Definition of the Geoid. Vol. XLVI. Florence, Italy, pp. 21–43.

Tscherning, C. C. and Rapp, R. H. (1974). *Closed Covariance Expressions for Gravity Anomalies, Geoid Undulations, and Deflections of the Vertical Implied by Anomaly Degree Variance Models*. Report 208. The Ohio State University.

Türk, K., Sulaoja, M., Oja, T., Ellmann, A., and Jürgenson, H. (2011). "Precise Gravity Surveys in South Estonia from 2009 to 2010". In: *Environmental Engineering. The 8th International Conference. May 19–20, 2011, Vilnius, Lithuania*. Vilnius Gediminas Technical University press "Technika", pp. 1499–1505. ISBN: 978-9955-28-829-9.

Ugalde, H. A., L'Heureux, E., Lachapelle, R., and Milkereit, B. (2006). "Measuring Gravity on Ice: An Example from Wanapitei Lake, Ontario, Canada". *GEOPHYSICS* 71 (3), J23–J29. DOI: 10.1190/1.2189387.

Ulotu, P. (2009). "Geoid Model of Tanzania from Sparse and Varying Gravity Data Density by the KTH Method". PhD thesis. Stockholm: KTH Royal Institute of Technology.

Vanícek, P., Changyou, Z., and Sjöberg, L. E. (1992). "A Comparison of Stokes's and Hotine's Approaches to Geoid Computation". *Manuscripta Geodaetica* 17, pp. 29–35.

Vaníček, P. and Kleusberg, A. (1987). "The Canadian Geoid – Stokesian Approach". *Manuscripta Geodaetica* 12, pp. 86–98.

Vaníček, P., Kingdon, R., and Santos, M. (2012). "Geoid versus Quasigeoid: A Case of Physics versus Geometry". *Contributions to Geophysics and Geodesy* 42 (1), pp. 101–118. DOI: 10.2478/v10126-012-0004-9.

Vaníček, P., Najafi, M., Martinec, Z., Harrie, L., and Sjöberg, L. E. (1995). "Higher-Degree Reference Field in the Generalized Stokes-Helmert Scheme for Geoid Computation". *Journal of Geodesy* 70 (3), pp. 176–182. DOI: 10.1007/BF00943693.

Vaníček, P. and Sjöberg, L. E. (1991). "Reformulation of Stokes's Theory for Higher than Second-Degree Reference Field and Modification of Integration Kernels". *Journal of Geophysical Research: Solid Earth* 96 (B4), pp. 6529–6539. DOI: 10.1029/90JB02782.

Varbla, S., Ellmann, A., Märdla, S., and Gruno, A. (2017a). "Assessment of Marine Geoid Models by Ship-Borne GNSS Profiles". In: The 10th International Conference "Environmental Engineering", April 27-28. Vilnius, Lithuania. DOI: 10.13140/RG.2.2.32537.11365. **Presentation III**.

Varbla, S., Ellmann, A., Märdla, S., and Gruno, A. (2017b). "Assessment of Marine Geoid Models by Ship-Borne GNSS Profiles". *Geodesy and Cartography* 43 (2), pp. 41–49. DOI: 10.3846/20296991.2017.1330771.

Vergos, G. S., Grigoriadis, V. N., Barzaghi, R., and Carrion, D. (2017). "IGFS Metadata for Gravity and Geoid. Structure, Build-up and Application Module". In: Joint Scientific Assembly of the International Association of Geodesy (IAG) and International Association of Seismology and Physics of the Earth's Interior (IASPEI), July 30 to August 4. Kobe, Japan. DOI: 10.13140/RG.2.2.23599.64161.

Véronneau, M. (2013). *The Helmert Gravity Grid Used for CGG2010*. Geodetic Survey Division, Natural Resources Canada, Ottawa, Canada (via Pers. Comm., 28.04.2016).

Véronneau, M. and Huang, J. (2016). "The Canadian Geodetic Vertical Datum of 2013 (CGVD2013)". *GEOMATICA* 70 (1), pp. 9–19. DOI: 10.5623/cig2016-101.

Wang, Y. M., Becker, C., Mader, G., Martin, D., Li, X., Jiang, T., Breidenbach, S., Geoghegan, C., Winester, D., Guillaume, S., and Bürki, B. (2017). "The Geoid Slope Validation Survey 2014 and GRAV-D Airborne Gravity Enhanced Geoid Comparison Results in Iowa". *Journal of Geodesy* 91 (10), pp. 1261–1276. DOI: 10.1007/s00190-017-1022-1.

Wenzel, H. G. (1983). "Geoid Computation by Least Squares Spectral Combination Using Integral Kernels". In: *Proceedings of the International Association of Geodesy General Meeting*. Tokyo, Japan, pp. 438–453.

Wessel, P., Smith, W. H. F., Scharroo, R., Luis, J., and Wobbe, F. (2013). "Generic Mapping Tools: Improved Version Released". *Eos, Transactions American Geophysical Union* 94 (45), pp. 409–410. DOI: 10.1002/2013EO450001.

Wong, L. and Gore, R. (1969). "Accuracy of Geoid Heights from Modified Stokes Kernels". *Geophysical Journal of the Royal Astronomical Society* 18 (1), pp. 81–91. DOI: 10.1111/j.1365-246X.1969.tb00264.x.

Zhang, C. (1998). "Estimation of Dynamic Ocean Topography in the Gulf Stream Area Using the Hotine Formula and Altimetry Data". *Journal of Geodesy* 72 (9), pp. 499–510. DOI: 10.1007/s001900050189.

Curriculum Vitae

Personal data

Name:	Silja Märdla (formerly Talvik)
Date and place of birth:	December 2, 1988, Tartu, Estonia
Nationality:	Estonian
E-mail address:	silja.mardla@ttu.ee,
	silja.mardla@gmail.com

Language skills

Language	Level
Estonian	Native
English	Fluent
French	Average
Russian	Average

Education

Graduation	Institution	Education
2012	Tallinn University of Technology	Transport Engineering specializing in Construction Geodesy, MSc.
2007	Schola Europaea Luxembourg	Secondary education
2004	Tallinna Arte Gümnaasium	Primary education

Special courses

Period	Course, location
September 3–7, 2012	NKG Autumn School, Finland
August 18–22, 2014	Least Squares Approach to Modelling the Geoid, Sweden

Professional employment

Period	Organization	Position
09.2012–…	Tallinn University of Technology	Early stage researcher, specialist
07–08.2011, 07–08.2010	OÜ ViaGeo	Construction geodesist
09.2008–04.2010	Eesti Kaardikeskus	Photogrammetry specialist
06–07.2009	REIB OÜ	Geodesist

Research mobility

Period	Receiving institution, objectives
November 11-16, 2013	DTU (Technical University of Denmark) Space, working on the NKG gravity database
November 17-21, 2014	Lantmäteriet, The Swedish Mapping, Cadastral and Land Registration Authority, practical geoid modelling

Supervised MSc. Theses

Elmi, L. (2014). "Fassaadide võrdlev mõõdistus tahhümeetria, maapealse fotogramm-meetria ja laserskaneerimisega [A comparative study of facade survey methods – tacheometry, terrestrial photogrammetry and laser scanning]". Superv. by Talvik, S., Ellmann, A. Master's thesis. Tallinn, Estonia: Tallinn University of Technology.

Lõhmus, H. (2014). "Terrestrilise laserskaneerimise kaasamine sildade koormuskatsetuste geodeetilistel uuringutel [Implementation of terrestrial laser scanning technology in geodetic observations at bridge load tests]". Superv. by Ellmann, A., Talvik S. Master's thesis. Tallinn, Estonia: Tallinn University of Technology.

Rebane, S. (2015). "Mittestandardsete hoonete rajamise geodeetiline teenindamine kaasaegsete mõõdistustehnoloogiate kaasamisega [Geodetic service of non-standard structures by incorporating modern surveying technologies]". Superv. by Kala V., Märdla S. Master's thesis. Tallinn, Estonia: Tallinn University of Technology.

Saarik, S. (2014). "Elektrontahhümeetrite ja laserskanneri kaugusmõõturi täpsuse hindamine [Assessment of the accuracy of total stations and laser scanner distance meters]". Superv. by Kala V., Talvik S. Master's thesis. Tallinn, Estonia: Tallinn University of Technology.

Talver, T. (2014). "Trigonomeetriline nivelleerimine ja laserskaneerimine teede külmakergete uurimisel [Determining road frost heave by trigonometric leveling and terrestrial laser scanning]". Superv. by Märdla S. Master's thesis. Tallinn, Estonia: Tallinn University of Technology.

Publications

Articles in peer-reviewed journals:

Kuusk, A., Lang, M., Märdla, S., and Pisek, J. (2015). "Tree Stems from Terrestrial Laser Scanner Measurements". *Forestry Studies / Metsanduslikud Uurimused* 63, pp. 44–55.

Lõhmus, H., Ellmann, A., Märdla, S., and Idnurm, S. (2017). "Terrestrial Laser Scanning for the Monitoring of Bridge Load Tests – Two Case Studies". *Survey Review*, pp. 1–15. DOI: 10.1080/00396265.2016.1266117.

Märdla, S., Ågren, J., Strykowski, G., Oja, T., Ellmann, A., Forsberg, R., Bilker-Koivula, M., Omang, O., Paršeliūnas, E., Liepinš, I., and Kaminskis, J. (2017a). "From Discrete Gravity Survey Data to a High-Resolution Gravity Field Representation in the Nordic-Baltic Region". *Marine Geodesy* 40 (6), pp. 416–453. DOI: 10.1080/01490419.2017.1326428. **Paper B**.

Märdla, S., Ellmann, A., Ågren, J., and Sjöberg, L. E. (2017b). "Regional Geoid Computation by Least Squares Modified Hotine's Formula with Additive Corrections". *Journal of Geodesy*, pp. 1–18. DOI: 10.1007/s00190-017-1061-7. **Paper A**.

Talvik, S. (2014). "Precise Levelling Data Processing near Terraced Landforms". *Geodesy and Cartography* 40 (2), pp. 51–57. DOI: 10.3846/20296991.2014.930247.

Varbla, S., Ellmann, A., Märdla, S., and Gruno, A. (2017). "Assessment of Marine Geoid Models by Ship-Borne GNSS Profiles". *Geodesy and Cartography* 43 (2), pp. 41–49. DOI: 10.3846/20296991.2017.1330771.

Articles in conference proceedings:

Julge, K., Eelsalu, M., Grünthal, E., Talvik, S., Ellmann, A., Soomere, T., and Tõnisson, H. (2014). "Combining Airborne and Terrestrial Laser Scanning to Monitor Coastal Processes". In: *Proceedings of the IEEE/OES Baltic International Symposium, May 27-29*. Tallinn, Estonia, pp. 1–10. DOI: 10.1109/BALTIC.2014.6887874.

Liibusk, A., Talvik, S., Ellmann, A., and Oja, T. (2014). "Determining Regional Sea Surface Topography by GNSS Surveys on Ice". In: *Proceedings of the IEEE/OES Baltic International Symposium, May 27-29*. Tallinn, Estonia, pp. 1–9. DOI: 10.1109/BALTIC.2014.6887847. **Paper E**.

Märdla, S., Ellmann, A., Oja, T., and Jürgenson, H. (2015). "Improving and Validating Gravity Data Over Ice-Covered Marine Areas". In: *IAG 150 Years: Proceedings of the 2013 IAG Scientific Assembly, 1–6 September, 2013*. Ed. by C. Rizos and P. Willis. International Association of Geodesy Symposia 143. Potsdam, Germany: Springer International Publishing, pp. 263–270. ISBN: 978-3-319-24603-1. DOI: 10.1007/1345_2015_163. **Paper C**.

Märdla, S., Oja, T., Ellmann, A., and Jürgenson, H. (2014). "Modelling the Influence of Terraced Landforms to the Earth's Gravity Field". In: *Gravity, Geoid and Height Systems*. Ed. by U. Marti. International Association of Geodesy Symposia 141. Venice, Italy: Springer International Publishing, pp. 157–162. ISBN: 978-3-319-10836-0. DOI: 10.1007/978-3-319-10837-7_20. **Paper D**.

Others:

Eelsalu, M., Ellmann, A., Julge, K., Märdla, S., and Soomere, T. (2014). "Rannaprotsesside anatoomia laserskaneerimise skalpelliga [Laser scanning anatomy of beach processes]". In: *Kaugseire Eestis*. Ed. by A. Aan and K. Narusk. Tallinn, Estonia: Keskkonnaagentuur, pp. 47–58.

Elmi, L., Märdla, S., and Ellmann, A. (2014). "Fassaadide võrdlev mõõdistus tahhümeetria, maapealse fotogramm-meetria ja laserskaneerimise teel [A comparative study of facade survey methods – tacheometry, terrestrial photogrammetry and laser scanning]". *Geodeet* 44, pp. 92–101.

Kala, V., Ellmann, A., and Märdla, S. (2015). *Kõrgem geodeesia. Polügonomeetria ja kõrgtäpne nivelleerimine.* Textbook. Tallinn, Estonia: TTÜ Kirjastus. ISBN: 978-9949-23-738-8.

Kangur, A., Märdla, S., Arumäe, T., Jürgenson, H., and Kask, P. (2015). "Üksikpuu Kõrguse Mõõtmine [Measuring the Height of a Single Tree]". *Eesti Mets* (2), pp. 34–39.

Saarik, S., Kala, V., and Märdla, S. (2014). "Elektrontahhümeetrite ja laserskanneri kaugusmõõturi täpsuse hindamine [Assessment of the accuracy of total stations and laser scanner distance meters]". *Geodeet* 44, pp. 76–82.

Talvik, S., Ellmann, A., and Oja, T. (2012a). "Maa Raskuskiirenduse Välja Mõjust Täppisnivelleerimise Tulemustele Klintastangu Näitel [Influence of the Earth's Gravity Field on the Results of Precise Levelling with Application to a Terrace]". *Geodeet* 42, pp. 19–22.

Talvik, S., Oja, T., and Ellmann, A. (2012b). "Astanguliste Pinnavormide Mõjust Maa Raskuskiirenduse Väljale Põhja-Eesti Klintranniku Näitel [Influence of Terraced Landforms to the Earth's Gravity Field with Application to the North-Estonian Klint]". *Geodeet* 42, pp. 10–18.

Elulookirjeldus

Isikuandmed

Ees- ja perekonnanimi: Silja Märdla (varem Talvik)
Sünniaeg ja -koht: 2. detsember 1988, Tartu, Eesti
Kodakondsus: Eesti
E-posti aadress: silja.mardla@ttu.ee,
     silja.mardla@gmail.com

Keelteoskus

Keel	Tase
Eesti	Emakeel
Inglise	Kõrgtase
Prantsuse	Kesktase
Vene	Kesktase

Hariduskäik

Lõpetamine	Õppeasutus	Haridus
2012	Tallinna Tehnikaülikool	Transpordiehitus spetsialiseerumisega ehitusgeodeesiale, MSc.
2007	Schola Europaea Luxembourg	Keskharidus
2004	Tallinna Arte Gümnaasium	Põhiharidus

Täiendusõpe

Aeg	Kursus, toimumispaik
3.–7. september 2012	NKG Sügiskool, Soome
18.-22. august 2014	Geoidi modelleerimine vähimruutude meetodil, Rootsi

Teenistuskäik

Aeg	Asutus	Amet
09.2012–...	Tallinna Tehnikaülikool	Nooremteadur, spetsialist
07–08.2011, 07–08.2010	OÜ ViaGeo	Ehitusgeodeet
09.2008–04.2010	Eesti Kaardikeskus	Fotogramm-meetria spetsialist
06–07.2009	REIB OÜ	Geodeet

Teadusvisiidid

Aeg	Vastuvõttev asutus, eesmärgid
11.-16. november 2013	DTU Space (Taani Tehnikaülikool), töö NKG raskuskiirenduse andmebaasiga
17.-21. november 2014	Lantmäteriet (Rootsi riigiasutus), praktiline geoidi modelleerimine

Juhendatud väitekirjade ja avaldatud teadusartiklite loetelu on toodud ingliskeelse CV juures.

Paper A

Märdla, S., Ellmann, A., Ågren, J., and Sjöberg, L. E. (2017). "Regional Geoid Computation by Least Squares Modified Hotine's Formula with Additive Corrections". *Journal of Geodesy*, pp. 1–18. DOI: 10.1007/s00190-017-1061-7. **Paper A**.

CrossMark

ORIGINAL ARTICLE

Regional geoid computation by least squares modified Hotine's formula with additive corrections

Silja Märdla[1] · **Artu Ellmann**[1] · **Jonas Ågren**[2] · **Lars E. Sjöberg**[3]

Abstract Geoid and quasigeoid modelling from gravity anomalies by the method of least squares modification of Stokes's formula with additive corrections is adapted for the usage with gravity disturbances and Hotine's formula. The biased, unbiased and optimum versions of least squares modification are considered. Equations are presented for the four additive corrections that account for the combined (direct plus indirect) effect of downward continuation (DWC), topographic, atmospheric and ellipsoidal corrections in geoid or quasigeoid modelling. The geoid or quasigeoid modelling scheme by the least squares modified Hotine formula is numerically verified, analysed and compared to the Stokes counterpart in a heterogeneous study area. The resulting geoid models and the additive corrections computed both for use with Stokes's or Hotine's formula differ most in high topography areas. Over the study area (reaching almost 2 km in altitude), the approximate geoid models (before the additive corrections) differ by 7 mm on average with a 3 mm standard deviation (SD) and a maximum of 1.3 cm. The additive corrections, out of which only the DWC correction has a numerically significant difference, improve the agreement between respective geoid or quasigeoid models to an average difference of 5 mm with a 1 mm SD and a maximum of 8 mm.

Keywords Geoid · Gravity anomaly · Gravity disturbance · Hotine · Quasigeoid · Stokes

✉ Silja Märdla
  silja.mardla@ttu.ee

1 Tallinn University of Technology, Tallinn, Estonia

2 Lantmäteriet, The Swedish Mapping, Cadastral and Land Registration Authority, Gävle, Sweden

3 KTH, Royal Institute of Technology, Stockholm, Sweden

1 Introduction

Traditionally, the geoid height N is determined from the global coverage of gravity anomaly Δg which is the difference of measured gravity values g_P (at point P at the height H_P above the geoid) and the normal gravity field generated by the reference ellipsoid (Heiskanen and Moritz 1967, Eq. 8-7). The normal gravity γ_Q is evaluated at the telluroid point Q at the height H_P above the reference ellipsoid (Molodensky 1945), using standard formulae, cf. Moritz (2000).

In spherical approximation, N can be determined by integrating gravity anomalies over the mean Earth sphere by using the Stokes formula (Stokes 1849). Fulfilment of certain requirements (i.e. the harmonicity of the potential field) that enable the application of the Stokes formula will be discussed in Sect. 3.

An alternative residual gravity quantity is the gravity disturbance δg defined as the difference between the observed gravity g_P and the normal gravity γ_P at the same point in space (Heiskanen and Moritz 1967, Eq. 2-142).

In traditional gravity surveys, heights referring to the geoid, or in practice, the national vertical datum, were obtained (by laborious levelling or less accurate methods like barometric heighting), yielding gravity anomaly values. In contemporary gravity surveys, direct positioning by GNSS (Global Navigation Satellite System) with respect to the ellipsoid is primarily used, yielding gravity disturbance values. Disturbances can be converted into anomalies (to be used for geoid modelling by the Stokes formula) using an existing geoid model, possibly introducing previous geoid model errors into new geoid modelling. However, as proposed by Hotine (1969, Eq. 29.53), the gravity disturbances can also be used directly for geoid modelling by the Hotine formula (Eq. 1).

The Hotine formula has been used for geoid determination from airborne gravimetry (e.g. Novák and Heck 2002; Novák et al. 2003; Alberts and Klees 2004; Serpas and Jekeli 2005; Sjöberg and Eshagh 2009),but also from altimetry (e.g. Zhang 1998) and land gravimetry (e.g. Kirby 2003). However, the traditional Stokes approach is still more widespread than the Hotine formula.

Studies applying the Hotine formula (e.g. Jekeli 1979, 1980; Sjöberg 1986b, 1989; Guan and Li 1991; Vaníček et al. 1992) have demonstrated that, in addition to the availability of gravity disturbances, there may be other reasons (including possibly higher accuracy in geoid modelling, see Sect. 7.2) to prefer the Hotine formula to the Stokes formula. However, both gravity anomalies and disturbances are affected by distortions in the respective height systems, especially in areas of vertical land motion (e.g. postglacial land uplift).

To reduce the truncation error introduced by limiting the integration to a spherical cap, the Stokes function can be modified, which was originally presented by Molodenskii et al. (1962). A number of alternative modifications of the Stokes formula have later been developed, for a recent overview, see e.g. Featherstone (2013, "Appendix A"). There are two main groups: deterministic and stochastic modifications of the Stokes formula.

Deterministic modification methods, such as Molodensky's and several others (e.g. Wong and Gore 1969; Meissl 1971; Heck and Grüninger 1987; Vaníček and Kleusberg 1987; Vaníček and Sjöberg 1991; Featherstone et al. 1998; Evans and Featherstone 2000), aim at reducing the truncation error by imposing suitable, preselected limits on the integration kernel and its modification. In contrast to deterministic methods, stochastic methods (e.g. Sjöberg 1980; Wenzel 1983) make use of estimated gravity signal and error spectra to balance relative data precision of the Global Geopotential Model (GGM) and terrestrial gravity observations. In particular, three stochastic modification methods of the Stokes formula proposed in Sjöberg (1984, 1991, 2003b) minimise the truncation error, the influence of erroneous terrestrial gravity data and geopotential coefficients in the least squares (LS) sense.

Reviews and comparisons of modifications to the Stokes formula can be found in e.g. Sjöberg (1986a), Sjöberg and Hunegnaw (2000), Nahavandchi and Sjöberg (2001), Ellmann (2004), Sjöberg and Featherstone (2004), Ågren (2004), Sjöberg (2005), Yildiz et al. (2012). Computer code for LS modifications is provided in Ellmann (2005a) and Abbak and Ustun (2015).

Many geoid modelling methods (Vaníček and Kleusberg 1987; Vaníček and Sjöberg 1991; Forsberg 1993; Vaníček et al. 1995; Forsberg and Tscherning 1997; Omang and Forsberg 2000; Ellmann and Vaníček 2007; Sansò and Sideris 2013) utilise the remove-compute-restore (RCR) approach, where the surface gravity anomalies are reduced prior to input

in the modified Stokes formula. The various direct effects for which the reduction occurs (downward continuation to sea level, ellipsoidal correction, removal of topographic and atmospheric masses or long wavelength features provided by a GGM) are restored upon the geoid height obtained from the Stokes integral as indirect effects.

Alternatively, Sjöberg (2003a) proposes to use the surface gravity anomalies as the integral argument. The direct and indirect effects of downward continuation, topographic, atmospheric and ellipsoidal corrections can then jointly be applied as combined corrections to the approximate geoid height obtained by the Stokes integration. Used in conjunction with the LS modification, this method is called the Least Squares Modification of Stokes's formula with Additive Corrections—LSMSA.

The main advantage of using such combined corrections is the reduced computational effort, see Sjöberg (2003a, Sect. 9.2). For example, there is no need for global integration (or a decision of a cut-off radius) for topographic corrections. Also, the magnitude of each combined correction directly reflects the error made by neglecting that particular effect.

Several corresponding LSMSA geoid models have been computed, e.g. by Ellmann (2005c), Kiamehr (2006), Daras (2008), Ågren et al. (2009b), Ulotu (2009), Abdalla and Fairhead (2011), Abdalla and Tenzer (2011), Abbak et al. (2012), Sjöberg et al. (2015), Kuczynska-Siehien et al. (2016), Ågren et al. (2016), achieving results compatible with GNSS/levelling control data down to about 3 cm and significantly better in countries of high quality geodetic infrastructure.

Modifications of Hotine's formula have been presented in e.g. Jekeli (1979, 1980), Sjöberg (1986b), Guan and Li (1991), Sjöberg and Nord (1992), Vaníček et al. (1992), Zhang (1998), Novák (2003), Novák et al. (2003), Sjöberg and Eshagh (2009) and summarised in Featherstone (2013).

Featherstone (2013, Sect. 4.5) demonstrated the application of LS modification to Hotine's formula in the special case of no truncation (see also Sjöberg 2003b, Sect. 4). The current contribution will comprehensively adapt the principle of LSMSA to Hotine's formula. Therefore, equations are developed for the biased, unbiased and optimum LS modification of Hotine's formula and the four additive corrections for both geoid and quasigeoid (c.f. Heiskanen and Moritz 1967, Sect. 8.3) computation. That is, the procedure of Least Squares Modification of Hotine's formula with Additive Corrections (LSMHA) is presented. Application of the LSMHA procedure for geoid or quasigeoid computation will be illustrated and compared to the LSMSA counterpart. For this, several regional (quasi)geoid models are computed and compared in a heterogeneous study area including marine and land parts.

This contribution is organised as follows. After the introduction, the general modification scheme and the specific LS

modifications of Hotine's formula are presented in Sect. 2. The four additive corrections for Hotine's formula are presented in Sect. 3. The estimation of gravity disturbance signal and error properties is discussed in Sect. 4. Sections 5 and 6 numerically verify the LSMHA quasigeoid computation scheme over the selected study area. Sect. 7 compares the LSMHA method to the LSMSA method, while Sect. 8 demonstrates the differences of resulting (quasi)geoid models over the study area. The contribution ends with conclusions and discussion about the LSMHA procedure developed.

2 Modification of Hotine's formula

2.1 General expressions

The Hotine formula (Hotine 1969, Eq. 29.53) reads:

$$N = \frac{R}{4\pi\gamma} \iint_\sigma H(\psi)\delta g \mathrm{d}\sigma \qquad (1)$$

where R is the mean Earth radius, γ is the normal gravity on the reference ellipsoid, σ is the unit sphere. H is the Hotine function defined as (Hotine 1969, Eq. 29.17):

$$H(\psi) = \sum_{n=0}^{\infty} \frac{2n+1}{n+1} P_n(\cos\psi) \qquad (2)$$

where ψ is the spherical distance between the computation and the integration point; $P_n(\cos\psi)$ are the Legendre polynomials of spherical harmonic degree n, c.f. Heiskanen and Moritz (1967, Eq. 1-57′).

The appearance of Stokes's formula and function are similar to those of Hotine, see e.g. Heiskanen and Moritz (1967, Eqs. 2-163b and 2-169).

Any modification of Hotine's formula is obtained by rewriting Eq. 1 as (analogously to Sjöberg 2003b, Eq. 3a):

$$N = \frac{R}{4\pi\gamma} \iint_\sigma H^L(\psi)\delta g \mathrm{d}\sigma + \frac{R}{2\gamma} \sum_{n=0}^{L} s_n \delta g_n \qquad (3)$$

where δg_n are the Laplace harmonics of δg defined analogously to Heiskanen and Moritz (1967, p. 97):

$$\delta g_n = \frac{2n+1}{4\pi} \iint_\sigma \delta g \, P_n(\cos\psi)\mathrm{d}\sigma \qquad (4)$$

or equivalently in spherical harmonic representation (Heiskanen and Moritz 1967, Eq. 2-153):

$$\delta g_n = \frac{GM}{a^2} \left(\frac{a}{r}\right)^{n+2} (n+1)$$
$$\sum_{m=0}^{n} \left\{ \overline{C}_{nm}\cos m\lambda + \overline{S}_{nm}\sin m\lambda \right\} \overline{P}_{nm}(\sin\overline{\phi}) \qquad (5)$$

where $\overline{P}_{nm}$ are the fully normalised Legendre functions (Heiskanen and Moritz 1967, Eq. 1-57), r, λ and $\overline{\phi}$ are the geocentric radius, longitude and latitude, respectively, $\overline{C}_{nm}$ and $\overline{S}_{nm}$ are the fully normalised spherical harmonic coefficients of the disturbing potential corresponding to the reference values of a and GM.

$H(\psi)^L$ is the modified Hotine function:

$$H(\psi)^L = H(\psi) - \sum_{n=0}^{L} \frac{2n+1}{2} s_n P_n(\cos\psi) \qquad (6)$$

where L is the selected maximum degree of modification and s_n are arbitrary modification parameters (also present in the last term of Eq. 3). The unmodified Hotine function $H(\psi)$ can be evaluated in its closed form by Hotine (1969, Eq. 29.17):

$$H(\psi) = \frac{1}{\sin(\psi/2)} - \ln\left(1 + \frac{1}{\sin(\psi/2)}\right) \qquad (7)$$

or

$$\widetilde{H}(\psi) = H(\psi) - 1 - \frac{3}{2}\cos\psi \qquad (8)$$

if degrees $n = 0$ and $n = 1$ are omitted (Jekeli 1979, "Appendix C").

Limiting the integration to a spherical cap σ_0 with radius $\psi_0 \neq 0$ centred around the computation point, Eq. 3 can equivalently be written as (anal. to Sjöberg 2003b, Eq. 5a):

$$N = \frac{R}{4\pi\gamma} \iint_{\sigma_0} H^L(\psi)\delta g \mathrm{d}\sigma + \frac{R}{2\gamma} \sum_{n=0}^{\infty} \left(Q_n^L + s_n^*\right)\delta g_n \quad (9)$$

where

$$s_n^* = \begin{cases} s_n, & \text{if } 0 \leq n \leq L \\ 0, & \text{otherwise} \end{cases} \qquad (10)$$

Equation 9 combines gravity disturbance data within the spherical cap around the computation point with the Laplace harmonics δg_n of the gravity disturbance. The representation of Eq. 9 is equivalent to Eq. 1. The modified truncation coefficients $Q_n^L(\psi_0)$ are a function of the integration radius and represent the geoid far-zone contribution (outside the cap σ_0):

$$Q_n^L(\psi_0) = Q_n^L = \int_{\psi_0}^{\pi} H^L(\psi) P_n(\cos \psi) \sin \psi \, d\psi \qquad (11a)$$

$$= Q_n(\psi_0) - \sum_{k=0}^{L} E_{nk} s_k \qquad (11b)$$

where $Q_n(\psi_0) = Q_n$ are the Molodensky-type truncation coefficients (Heiskanen and Moritz 1967, Eq. 7-34) adapted for the Hotine function:

$$Q_n = \int_{\psi_0}^{\pi} H(\psi) P_n(\cos \psi) \sin \psi \, d\psi \qquad (12)$$

and

$$E_{nk} = \frac{2k+1}{2} \int_{-1}^{\cos \psi_0} P_n(t) P_k(t) dt = \frac{2k+1}{2} R_{nk} \qquad (13)$$

In practical computations, the integral part R_{nk} of Eq. 13 is evaluated by recursive formulae given in Paul (1973). The truncation coefficients of Eq. 11 are evaluated by recursive relations given by either Jekeli (1979, "Appendix A") or Guan and Li (1991, p. 87). These are analogous to the so-called Molodensky truncation coefficients evaluated by either Paul (1973) or Hagiwara (1976).

Further, the true gravity disturbance δg is replaced by its estimate δg^{T} from terrestrial data and the spherical harmonic expansion of the gravity disturbance δg_n by its estimate $\delta g_n^{\mathrm{GGM}}$ as given by a GGM model evaluated to a finite maximum degree M (often $L = M$ is adopted). As a generalisation, arbitrary parameters b_n can be used for modification (in case of Eq. 9, $b_n = Q_n^L + s_n^*$). The resulting geoid estimator $\widetilde{N}$ is written as:

$$\widetilde{N} = \frac{R}{4\pi \gamma} \iint_{\sigma_0} H^L(\psi) \delta g^{\mathrm{T}} d\sigma + \frac{R}{2\gamma} \sum_{n=0}^{M} b_n \delta g_n^{\mathrm{GGM}} \qquad (14)$$

or equivalently in its spectral form as (c.f. Heiskanen and Moritz 1967, p. 97):

$$\widetilde{N} = \frac{R}{4\pi \gamma} \sum_{n=0}^{\infty} \left(\frac{2}{n+1} - Q_n^L - s_n^* \right) \delta g_n^{\mathrm{T}}$$

$$+ \frac{R}{2\gamma} \sum_{n=0}^{M} b_n \delta g_n^{\mathrm{GGM}} \qquad (15)$$

In contrast to the Stokes function, the summation in the Hotine function can start from $n = 0$. However, in practical computations, the zero and first degree harmonics can often be neglected since the origin of the geodetic system is conventionally placed in the mass centre of the Earth and the adopted normal gravity field is generated by the mass equal

to the actual mass of the Earth. In this case, the recursive relations for computing the truncation coefficients Q_n are given in Jekeli (1979, "Appendix C").

2.2 Error propagation

The main objective of modifying either Stokes's or Hotine's formula is to minimise the errors of the geoid estimator. Based on the spectral form of the true geoid height, the expected global mean square error (MSE) of the geoid estimator $\widetilde{N}$ can be written as (anal. to Sjöberg 2003b, Eq. 13):

$$\left(\delta \widetilde{N} \right)^2 = \left(\delta \widetilde{N} \right)_{\mathrm{TR}}^2 + \left(\delta \widetilde{N} \right)_{\mathrm{T}}^2 + \left(\delta \widetilde{N} \right)_{\mathrm{GGM}}^2 \qquad (16)$$

where

$$\left(\delta \widetilde{N} \right)_{\mathrm{TR}}^2 = \left(\frac{R}{2\gamma} \right)^2 \sum_{n=0}^{\infty} \left(b_n^* - s_n^* - Q_n^L \right)^2 c_n^2 \qquad (17a)$$

$$\left(\delta \widetilde{N} \right)_{\mathrm{T}}^2 = \left(\frac{R}{2\gamma} \right)^2 \sum_{n=0}^{\infty} \left(\frac{2}{n+1} - s_n^* - Q_n^L \right)^2 \sigma_n^2 \qquad (17b)$$

$$\left(\delta \widetilde{N} \right)_{\mathrm{GGM}}^2 = \left(\frac{R}{2\gamma} \right)^2 \sum_{n=0}^{M} b_n^2 dc_n^2 \qquad (17c)$$

and

$$b_n^* = \begin{cases} b_n, & \text{if } 0 \le n \le M \\ 0, & \text{otherwise} \end{cases} \qquad (18)$$

Equations 17a, 17b and 17c represent the error contribution due to truncation, terrestrial data and the GGM, respectively.

The following notation is used: σ_n^2 for terrestrial gravity error degree variances, dc_n^2 for GGM error degree variances and c_n^2 for gravity signal degree variances. Practical estimation of these is discussed in Sect. 4. These models are assumed to describe the gravity disturbance signal and error properties which are then propagated through Eq. 16 to find an estimate of the geoid model error that corresponds to the specific signal and error models selected.

Notice that Eqs. 17a and 17c differ from the Stokes counterparts only by the definition of the symbols used in them, while Eq. 17b differs also by the first term in the parenthesis.

Apparently, the expected global MSE is affected by the aforementioned variance models as well as by the modification conditions: choice of ψ_0, L and M. However, the key factor to minimise $\left(\delta \widetilde{N} \right)^2$ is a suitable selection of the parameters s_n. Different modifications to the Hotine formula are applied through selecting the b_n and s_n parameters. Specific modifications will be presented below.

2.3 The Wong and Gore type (WG) deterministic modification

The modification coefficients s_n of deterministic methods are invariant to input data error estimates. Reviews and comparisons of various aspects of the deterministic modification methods can be found, e.g. in Jekeli (1981), Heck and Grüninger (1987), Vaníček and Featherstone (1998), Featherstone et al. (1998), Featherstone (2003a).

In this contribution, a simple deterministic band-limited modification subtracting polynomial terms from the original function is used. For the Stokes function, it was presented by Wong and Gore (1969). It was first applied to the Hotine function by Vaníček et al. (1992), Sjöberg and Nord (1992) and also used by Novák and Heck (2002), Novák et al. (2003). For this modification the coefficients $b_n = s_n + Q_n^L$ with $s_n = 2/(n+1)$.

Although a deterministic modification does not require estimation of signal and error degree variances for determination of the modification parameters s_n, these are required to compute the expected global MSE by Eq. 16.

2.4 Stochastic least squares modification

The global MSE of $\widetilde{N}$ given by Eq. 16 is minimised by selecting appropriate LS modification parameters b_n and s_n. To obtain the modification parameters, Eq. 16 is differentiated with respect to each s_k ($k = 0, 1, 2, \ldots, L$) and equated to zero (anal. to Sjöberg 2003b, Eq. 15):

$$\frac{\partial \left(\delta \widetilde{N}\right)^2}{\partial s_k} = 2 \left(\frac{r}{2\gamma}\right)^2 \sum_{n=2}^{\infty} \left(\delta_{nk} + \frac{\partial Q_n^L}{\partial s_k}\right)$$
$$\times \left[\left(Q_n^L + s_n^*\right) C_n - p_n\right] = 0 \quad (19)$$

where δ_{nk} is the Kroenecker delta defined as:

$$\delta_{nk} = \begin{cases} 1, & \text{if } n = k \\ 0, & \text{otherwise} \end{cases} \quad (20)$$

and

$$p_n = \frac{2\sigma_n^2}{n+1} \quad (21)$$

C_n is constructed from signal and error degree variances, see Eqs. 28 and 29 below.

With Eq. 19, the following linear system of equations is arrived at (anal. to Sjöberg 2003b, Eq. 14b):

$$\sum_{r=0}^{L} a_{kr} s_r = h_k \quad (22)$$

where the coefficients a_{kr} and h_k can be expressed via Q_n, $E_{nk} = -\partial Q_n^L / \partial s_k$, c_n^2, $\mathrm{d}c_n^2$ and σ_n^2 (see Eqs. 26–31 below). The system of equations is then solved in the least squares sense for s_n.

Sjöberg (1984, 1991, 2003b) present three methods of LS modifications that differ in the choice of parameters b_n. The Biased LS (BLS) modification with

$$b_{n,\mathrm{BLS}} = s_n \quad (23)$$

the Unbiased LS (ULS) modification with

$$b_{n,\mathrm{ULS}} = s_n + Q_n^L \quad (24)$$

and the Optimum LS (OLS) modification with

$$b_{n,\mathrm{OLS}} = \left(s_n + Q_n^L\right) c_n^2 \Big/ \left(c_n^2 + \mathrm{d}c_n^2\right) \quad (25)$$

The choice of b_n dictates the contribution of the truncation error (bias) in the global MSE (Eq. 17a). For the unbiased modification, the truncation error is completely reduced up to degree M, hence the name. The biased and optimum LS estimators are slightly biased (c.f. Sjöberg 1991, 2003b). For the optimum method, this bias is small if the GGM-related errors $\mathrm{d}c_n^2$ are small below the limit of M. With the GGM-related errors becoming significant, for example by increasing the maximum degree M of the GGM used, the bias increases (cf. Table 2). The deterministic Wong and Gore method is also unbiased up to degree M.

For the optimum and unbiased method, the linear system of equations given in Eq. 22 is constructed as (anal. to Sjöberg 2003b, Eqs. 14c, 14d):

$$a_{kr} = a_{rk} = \sum_{n=0}^{\infty} E_{nk} E_{nr} C_n + \delta_{kr} C_r - E_{kr} C_k - E_{rk} C_r \quad (26)$$

$$h_k = p_k - Q_k C_k + \sum_{n=0}^{\infty} \left(Q_n C_n - p_n\right) E_{nk} \quad (27)$$

where for the optimum method:

$$C_{n,\mathrm{OLS}} = \sigma_n^2 + \begin{cases} c_n^2 \mathrm{d}c_n^2 / \left(c_n^2 + \mathrm{d}c_n^2\right), & \text{if } n \leq M \\ c_n^2, & \text{if } n > M \end{cases} \quad (28)$$

and the unbiased method:

$$C_{n,\mathrm{ULS}} = \sigma_n^2 + \begin{cases} \mathrm{d}c_n^2, & \text{if } n \leq M \\ c_n^2, & \text{if } n > M \end{cases} \quad (29)$$

For the biased LS modification, $M = L$ is required, Eq. 19 is slightly different, Eqs. 26 and 27 become (anal. to Sjöberg 1991, Eqs. 2.9a, 2.9b):

$$a_{kr,\text{BLS}} = a_{rk} = \sum_{n=0}^{\infty} E_{nk} E_{nr} \left(\sigma_n^2 + c_n^2 \right)$$
$$+ \delta_{kr} \left(\sigma_r^2 + \text{d}c_r^2 \right) - E_{kr}\sigma_k^2 - E_{rk}\sigma_r^2 \qquad (30)$$

$$h_{k,\text{BLS}} = p_k - Q_k \sigma_k^2$$
$$+ \sum_{n=0}^{\infty} \left[Q_n \left(\sigma_n^2 + c_n^2 \right) - p_n \right] E_{nk} \qquad (31)$$

Notice that Eqs. 26–31 differ from the Stokes counterparts presented in Sjöberg (2003b) by the definition of the symbols used in them.

2.5 Solution to the linear system of equations

The linear system of equations given in Eq. 22 can be written in matrix form as:

$$\mathbf{As} = \mathbf{h} \qquad (32)$$

Estimates $\hat{s}_n$ of the modification parameters s_n are then expressed as:

$$\hat{\mathbf{s}} = \mathbf{A}^{-1}\mathbf{h} \qquad (33)$$

However, for the optimum and unbiased LS modification, the system of equations given in Eq. 33 is ill-conditioned, see Ågren (2004, Sect. 3.2.3). To obtain a solution, a numerical method, such as Singular Value Decomposition (SVD), can be used instead of direct inversion of $\mathbf{A}$, see e.g. Ellmann (2005b) and Ellmann (2004, Sect. 3.3).

Depending on the numerical method used to solve the system of equations, the s_n coefficients can be very different. For each set of s_n, a corresponding set of Q_n^L are computed by Eq. 11b. The modified truncation coefficients Q_n^L counterbalance the values of s_n in such a way that the resulting b_n coefficients for different sets of s_n are very similar (see also Sect. 7.1).

3 Additive corrections

The application of Stokes's or Hotine's integral requires that no masses lay above the geoid surface approximated by radius R. The traditional remove-compute-restore method to fulfil this requirement is to reduce the surface gravity anomaly for forbidden masses, compute the co-geoid from the reduced gravity anomalies and correct the co-geoid by indirect effects (see e.g. Ellmann and Vaníček 2007 or Sjöberg 2003a, Sect. 2). An alternative method of geoid computation summarised by Sjöberg (2003a) is to compute an approximate geoid height from the original surface gravity

anomalies by Eq. 15 and add the necessary effects directly to the approximate geoid height as:

$$\overline{N} = \widetilde{N} + \delta N_{\text{COMB}} + \delta N_{\text{DWC}} + \delta N_{\text{ATM}} + \delta N_{\text{ELL}} \qquad (34)$$

where δN_{COMB} is the combined topographic effect, δN_{DWC} is the combined downward continuation (DWC) effect, δN_{ATM} is the combined atmospheric effect and δN_{ELL} is the combined ellipsoidal effect.

$\widetilde{N}$, the result of Eq. 15 can also be used for quasigeoid (i.e. height anomaly) modelling by:

$$\overline{\zeta} = \widetilde{N} + \delta\zeta_{\text{COMB}} + \delta\zeta_{\text{DWC}} + \delta\zeta_{\text{ATM}} + \delta\zeta_{\text{ELL}} \qquad (35)$$

where $\delta\zeta_{\text{COMB}}, \delta\zeta_{\text{DWC}}, \delta\zeta_{\text{ATM}}$ and $\delta\zeta_{\text{ELL}}$ are the corresponding combined, DWC, atmospheric and ellipsoidal corrections for quasigeoid determination.

The combined corrections corresponding to the Hotine function have been derived following the principles presented in Sjöberg (2003a) and the original publications referenced therein. These additive corrections will be presented for both geoid and quasigeoid computations in Sects. 3.1–3.4. Detailed derivations are omitted from this contribution to keep the representation concise.

3.1 Combined topographic effect

The combined topographic effect reflects the removal and restoration (by any method) of topographic masses from above the geoid, see e.g. Sjöberg and Bagherbandi (2017), Sect. 5.2. Since the combined topographic effect follows from the potential of removed topography and the Bruns formula (cf. Heiskanen and Moritz 1967, Eq. 2-144), it is the same for the Stokes or Hotine formula.

δN_{COMB} can be computed as (Sjöberg 2007, Eqs. 20 and 27):

$$\delta N_{\text{COMB}} = -\frac{2\pi G\rho}{\gamma} \left(H_P^2 + \frac{2}{3}\frac{H_P^3}{r_P} \right) \qquad (36)$$

For quasigeoid computations (Sjöberg 2000, Eq. 77):

$$\delta\zeta_{\text{COMB}} = 0 \qquad (37)$$

i.e. there is no combined topographic effect in the LS modified Hotine formula.

3.2 Combined downward continuation effect

The combined downward continuation effect for geoid computation is (anal. to Ågren et al. 2009b, Eq. 3, see also Ågren

2004, Sect. 5.4.1):

$$\delta N_{\text{DWC}}(P) = \delta N_{\text{DWC}}^{(1)}(P) + \delta N_{\text{DWC}}^{L(1),\text{far}}(P)$$
$$+ \delta N_{\text{DWC}}^{L(2)}(P) \quad (38)$$

$\delta N_{\text{DWC}}^{(1)}$ is the term for downward continuation from computation point level to sea level of the unmodified Hotine formula:

$$\delta N_{\text{DWC}}^{(1)}(P) = \frac{\delta g(P)}{\gamma} H_P + \frac{\zeta_P^0}{r_P} H_P - \frac{1}{2\gamma} \frac{\partial \delta g}{\partial r}\bigg|_P H_P^2 \quad (39)$$

where ζ_P^0 is an approximate value of the height anomaly ζ (usually $\zeta_P^0 \approx \tilde{N}$ is sufficient, see e.g. Ågren 2004, p. 120) and $\partial \delta g / \partial r$ is the vertical gradient of gravity disturbance computed analogously to Heiskanen and Moritz (1967, Eq. 2-217). Notice that, compared to the Stokes counterpart, the factor 3 is not present in the second term of Eq. 39.

$\delta N_{\text{DWC}}^{L(1),\text{far}}$ is the term for downward continuation from computation point level to sea level of the far-zone contribution of modified Hotine's formula:

$$\delta N_{\text{DWC}}^{L(1),\text{far}}(P)$$
$$= \frac{R}{2\gamma} \sum_{n=0}^{M} \left(s_n + Q_n^L \right) \left[\left(\frac{R}{r_P} \right)^{n+2} - 1 \right] \delta g_n^{\text{GGM}}(P)$$
$$(40)$$

$\delta N_{\text{DWC}}^{L(2)}$ is the term for downward continuation from the integration point level to the computation point level of modified Hotine's formula:

$$\delta N_{\text{DWC}}^{L(2)}(P)$$
$$= \frac{R}{4\pi\gamma} \iint_{\sigma_0} H^L(\psi) \left(\frac{\partial \delta g}{\partial r}\bigg|_Q (H_P - H_Q) \right) d\sigma_Q \quad (41)$$

where Q is the running point in the integral.

The combined downward continuation effect for quasi-geoid computation is (anal. to Ågren et al. 2009b, Eq. 9):

$$\delta \zeta_{\text{DWC}}(P) = \delta \zeta_{\text{DWC}}^{(1)}(P) + \delta \zeta_{\text{DWC}}^{L(1),\text{far}}(P) + \delta \zeta_{\text{DWC}}^{L(2)}(P)$$
$$= \delta \zeta_{\text{DWC}}^{(1)}(P) + \delta N_{\text{DWC}}^{L(1),\text{far}}(P) + \delta N_{\text{DWC}}^{L(2)}(P)$$
$$(42)$$

with

$$\delta \zeta_{\text{DWC}}^{(1)}(P) = 3 \frac{\zeta_P^0}{r_P} H_P \quad (43)$$

Notice that, similarly to the Stokes counterpart, the factor 3 is also present in $\delta \zeta_{\text{DWC}}^{(1)}$.

3.3 Combined atmospheric effect

The combined atmospheric effect reflects the removal and restoration of atmospheric masses. On the current accuracy level $\delta N_{\text{ATM}} \approx \delta \zeta_{\text{ATM}}$ (Ågren et al. 2009b) and the effect can be computed by (anal. to Sjöberg and Nahavandchi 2000, Eq. 41):

$$\delta N_{\text{ATM}}(P) \approx \delta \zeta_{\text{ATM}}(P)$$
$$= -\frac{2\pi R G \rho_A}{\gamma} \sum_{n=0}^{M} \left(\frac{2}{n+1} - s_n - Q_n^L \right) H_n(P)$$
$$- \frac{2\pi R G \rho_A}{\gamma} \sum_{n=M+1}^{\infty} \left(\frac{2}{n+1} - \frac{n+2}{2n+1} Q_n^L \right) H_n(P) \quad (44)$$

where ρ_A is the atmospheric density at sea level, G is the gravitational constant and H_n are the Laplace surface harmonics of the topographic height.

3.4 Combined ellipsoidal effect

The combined ellipsoidal effect accounts for the error (to order e^2 with e being the ellipticity of the reference ellipsoid) stemming from the spherical approximation of the Hotine formula. On the current accuracy level $\delta N_{\text{ELL}} \approx \delta \zeta_{\text{ELL}}$ (Ågren et al. 2009b) and the effect can be computed by (anal. to Sjöberg 2004):

$$\delta N_{\text{ELL}}(P) \approx \delta \zeta_{\text{ELL}}(P) = \frac{R}{2\gamma} \sum_{n=0}^{\infty} \left(\frac{2}{n+1} - s_n^* - Q_n^L \right)$$
$$\times \left(\frac{a-R}{R} \delta g_n^{\text{GGM}}(P) + \frac{a}{R} (\delta g_e)_n \right) \quad (45)$$

with

$$(\delta g_e)_n = \frac{e^2}{2a} \sum_{m=-n}^{n} \Big\{ [3 - (n-3)F_{nm}] T_{nm}$$
$$- (n+2)G_{nm} T_{n-2,m}$$
$$- (n+5)E_{nm} T_{n+2,m} \Big\} Y_{nm}(P) \quad (46)$$

where T_{nm} are the spherical harmonic coefficients for the disturbing potential. For the ellipsoidal coefficients F_{nm}, G_{nm} and E_{nm}, see Sjöberg (2004, "Appendix").

4 Degree variance models of data and their errors

In contrast to deterministic modifications, the stochastic methods aiming to minimise the truncation error and errors stemming from input data, depend on *a priori* or empirical

stochastic models describing the signal and error properties of the input data. Therefore, estimates for the gravity disturbance signal degree variances c_n^2, terrestrial error degree variances σ_n^2 and GGM error degree variances dc_n^2 need to be compiled.

Gravity anomaly signal degree variances can be based on standard models such as Kaula's rule (Kaula 1963) or the Tscherning and Rapp (1974) model, a more recent model, e.g. Rexer and Hirt (2015), but also on GGM models directly.

The gravity disturbance (signal or error) degree variances $d_{n,\delta g}^2$ can be expressed in terms of the gravity anomaly degree variances $d_{n,\Delta g}^2$ as:

$$d_{n,\delta g}^2 = \frac{(n+1)^2}{(n-1)^2} d_{n,\Delta g}^2 \tag{47}$$

Equation 47 follows from the relation between the Laplace harmonics of the disturbing potential and the gravity anomaly (Heiskanen and Moritz 1967, Eq. 2-155) or the gravity disturbance (Heiskanen and Moritz 1967, Eq. 2-153). As seen from Eq. 47, the difference in anomaly and disturbance degree variances becomes smaller and approaches zero with increasing degree n.

Notice that, instead of adapting the gravity anomaly degree variances to gravity disturbance by the relation given in Eq. 47, standard models corresponding to Kaula's rule or the Tscherning and Rapp (1974) model could directly be constructed for the gravity disturbances.

The signal and GGM error degree variances are usually estimated as global averages, not necessarily yielding estimates suitable for a specific region of study. However, if necessary, regionally adapted estimates (e.g. Heiskanen and Moritz 1967, Eq. 7-8) or empirical scaling factors can be used.

In principle, a possible correlation between terrestrial and GGM information can also be considered, see e.g. Sjöberg (1991), Sect. 4. However, this can generally be avoided by using appropriate modification limits. For instance, satellite-only GGMs have no correlation with terrestrial data.

Although the spectral models are only estimates and may be inaccurate, the choice of using stochastic modifications assumes that a coarse model should be preferred over neglecting the errors of terrestrial and gravity data completely (by not modifying the Stokes or Hotine formula) or deterministic modifications eliminating certain contributions (e.g. long wavelength information from terrestrial data) by selection. See also the discussion in Heck and Grüninger (1987).

5 Case study

The LSMHA method of geoid or quasigeoid computation described above will be numerically verified in a case study.

Alternative geoid models will be computed from gravity anomalies or disturbances using the different modification methods described above, thereby explaining the differences of geoid computation via various modifications of Stokes's or Hotine's formula.

5.1 Study area and input data

To verify the LSMHA quasigeoid modelling approach both in marine and land areas, a study area located in the North of Sweden, Europe was selected. This area was selected as the current research was conducted to support the Nordic Geodetic Commission (NKG) geoid modelling efforts (Ågren et al. 2016; ISG 2015) and the FAMOS project (FAMOS Consortium 2014) which aim at computing a geoid model over the Nordic–Baltic area. It also includes both high terrain and marine areas.

The target area with geographical limits of 64°–68.2° N, 16.4°–23° E includes a part of the Gulf of Botnia and terrain with elevations from 0 to 1900 m. The aim was to compute a quasigeoid model on a grid of 0.01° by 0.02° over the study area.

A gravity disturbance grid generated for the NKG geoid modelling project was used as terrestrial gravity information. The disturbance grid was generated from an anomaly grid using a quasigeoid model, i.e. it was not constructed from real gravity data with ellipsoidal heights.

For the current case study, the gravity disturbances were available on a grid of 0.01° by 0.02° over the target area (Fig. 2) and its surroundings extended by 2° from each side of the rectangular target area. Also, the digital terrain model (DTM, averaged to 0.002° by 0.004°, cf. Figure 1) and the GNSS/levelling database compiled for the NKG geoid project were used. The global topography was described by the SRTM30_PLUS (Becker et al. 2009) model. The GO_CONS_GCF_2_DIR_R5 (Bruinsma et al. 2014) model available from Barthelmes and Köhler (2016) was used as a reference GGM both in gravity gridding and geoid modelling. For more details on gravity gridding, see Märdla et al. (2017a).

5.2 Parameters of geoid computations

An approximate geoid model was computed by four modification methods of Hotine's formula: WG, BLS, ULS and OLS. For comparison, traditional Stokes's counterparts were also computed.

All of the test computations were performed for the integration cap size of $\psi_0 = 2°$, which was also used for the NKG2015 quasigeoid model. For other cap sizes, differences between Stokes's and Hotine's formula may vary, see also Jekeli (1980).
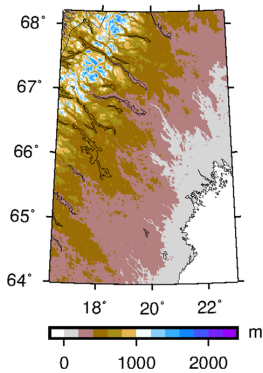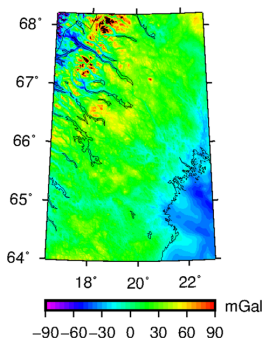
Fig. 1 Terrain elevations

Fig. 2 Gravity grid

The zero and first degree harmonics were omitted from computations by Hotine's formula by starting the summation at $n = 2$, using the corresponding Eq. 8 and truncation coefficients Q_n computed as in Jekeli (1979, "Appendix C"), thus making the results directly comparable to the Stokes counterparts. Correspondingly, the additive corrections of degrees $n = 0, 1$ were also neglected from geoid and quasigeoid computations.

The global RMS error (square root of MSE given by Eq. 16) was used to find appropriate modification limits L, see Sect. 5.2.1. The use of estimated global RMS error values for the selection of modification limits can yield geoid models with higher accuracy also with respect to GNSS/levelling control points. Nevertheless, it also requires that appropriate signal and error degree variance models be selected which is otherwise not necessary for deterministic modifications.

5.2.1 Modification limits

As often done in practice (e.g. Featherstone 2003b, Sect. 4.1), the Wong and Gore type modification was improved by allowing two modification limits $L1$ and $L2$ ($L1 \leq L2 \leq M$)

by which a transferring band from the Wong and Gore type modification to no modification can be created, i.e. the coefficients s_n were computed as:

$$s_{n,\text{WG}} = \begin{cases} \frac{2}{n+1}, & \text{if } n \leq L1 \\ \frac{2}{n+1} \times \frac{L2-n}{L2-L1}, & \text{if } L1 \leq n \leq L2 \\ 0, & \text{if } n \geq L2 \end{cases} \quad (48)$$

Table 1 illustrates the error contribution of different sources through different WG modification degrees $L1$ and $L2$. Judging by the total global RMS error, it would be optimal to use a combination of low $L1$ and high $L2$, thereby allowing a long span of degrees n for the transition from the GGM to the terrestrial data contribution (which is in fact automatically allowed by the LS modifications). Therefore, the limits of $L1 = 50$ and $L2 = 200$ were selected for the WG computations.

Although experience has shown that the WG solution improves with increasing cap size (Sjöberg 2005, Table 1), it was not the aim of the current study to find the optimum WG solution. Thus, integration cap size of $\psi_0 = 2°$ was also used for the WG modification.

The Wong and Gore type modification is often used in conjunction with the RCR geoid modelling method whereby the gravity data need to be reduced before input to the Stokes formula. However, notice that, by applying the modification the LSMSA way, the surface gravity anomalies are used for integration. The LSMSA method has been compared to RCR methods several times, see e.g. Ågren (2004), Chaps. 7 and 9; Ågren et al. (2009a), etc.

A shortcoming of using the deterministic WG modification is the effort needed to find appropriate modification limits. Finding a suitable modification limit for the LS modifications requires considerably less effort.

As seen from Table 2, provided that the limit L is sufficiently high to allow the GGM to contribute within the range of which it is considered to contain valuable information, the resulting expected global RMS is not very sensitive to the actual modification limit selected (the GGM contribution is automatically lowered for higher degrees). Consequently, the limit of $L = 200$ was selected for all of the LS modifications. Although not presented in detail in the current manuscript, many test computations performed during the NKG geoid modelling project have confirmed the suitability of such a limit in terms of expected global RMS and/or GNSS/levelling fit.

Note that the use of $L = 200$ in LS modifications implies that the data from the GGM can not be considered above $n = 200$ and for all of the lower degrees, the contribution of the GGM and terrestrial data is weighted according to the error models supplied.

The additive corrections were computed using the corresponding limit $M = L = 200$. For the computation of

Table 1 Expected global RMS of the WG type modifications for various modification limits $L1$ and $L2$, units: mm

$L2$	200				150			100		50
$L1$	200	150	100	50	150	100	50	100	50	50
$(\delta\widetilde{N})^2_{\mathrm{TR}}$	39.8	18.25	9.17	2.79	16.81	10.21	5.81	9.52	14.61	14.28
$(\delta\widetilde{N})^2_{\mathrm{T}}$	8.64	9.10	9.86	10.85	9.94	11.37	12.45	13.01	14.64	19.95
$(\delta\widetilde{N})^2_{\mathrm{GGM}}$	6.08	4.47	2.86	1.74	2.93	1.54	0.81	0.97	0.91	0.72
$(\delta\widetilde{N})^2$	41.18	20.88	13.77	11.34	19.75	15.36	13.76	16.15	20.70	24.55

Table 2 Expected global RMS of BLS modifications for various modification limits L, units: mm

L	150	200	250	300
$(\delta\widetilde{N})^2_{\mathrm{TR}}$	35.04	2.02	2.75	2.80
$(\delta\widetilde{N})^2_{\mathrm{T}}$	10.83	10.84	11.58	12.00
$(\delta\widetilde{N})^2_{\mathrm{GGM}}$	1.46	1.73	1.73	1.73
$(\delta\widetilde{N})^2$	36.71	11.16	12.02	12.44

the combined atmospheric effect, the spherical harmonic expansion of the global topographic elevation was truncated to the maximum degree of $n = 720$ as in Ågren et al. (2009b), see also Sjöberg (2003c, Table 2).

5.2.2 Degree variance models

As discussed in Sect. 4, the application of stochastic modifications to the Stokes or Hotine formula depends on *a priori* knowledge of gravity signal and error properties provided in the form of degree variances. Since the study area overlaps, spectral models similar to Ågren et al. (2009b, Table 1) were used for the case study of this contribution. For the used degree variance plots, see Märdla et al. (2017b).

The gravity anomaly signal degree variances $c_{n,\Delta g}$ were constructed by the Tscherning and Rapp (1974) model scaled by 0.5^2. Such rescaling increases the model fit to GGM signal degree variances most from degree 10 to 40. The GGM error degree variances $dc_{n,\Delta g}$ as published for the GO_CONS_GCF_2_DIR_R5 GGM model were used without rescaling. The terrestrial gravity error degree variances $\sigma_{n,\Delta g}$ were constructed as a combination of the reciprocal distance (RD) and white noise (WN) models with the following parameters: standard deviation of 0.5 mGal and correlation length of $0.25°$ for RD, standard deviation of 1 mGal and Nyquist degree of 3960 for the WN part.

In this contribution, the gravity disturbance degree variances were derived by Eq. 47 from those of gravity anomaly. However, in practical computations, the gravity anomaly degree variances $d_{n,\Delta g}$ can safely be used also for computations by Hotine's formula as the signal and error models are rough and in no way specific to gravity anomaly or dis-

turbance, nor the region of study. Related quasigeoid model differences remain within a mm (standard deviation, SD) over the current study area.

6 Illustration of the LSMHA computation scheme

The LSMHA (quasi)geoid computation scheme is illustrated by the contributions of different computational steps. Figure 3 depicts these for the Unbiased LSMHA.

Figures 3a–d depict the partial contributions of the downward continuation effect to the geoid and quasigeoid model (Eqs. 38 and 42, respectively). In quasigeoid computation, over the given study area the $\delta\zeta^{L(2)}_{\mathrm{DWC}}$ part dominates the DWC correction with values from -6 to 11 cm together with $\delta\zeta^{L(1),\mathrm{far}}_{\mathrm{DWC}}$ with negative values up to -5 cm. In geoid computation, $\delta N^{(1)}_{\mathrm{DWC}}$ is also significant, with values reaching up to 36 cm.

Figures 3e and f depict the contribution of the combined atmospheric (Eq. 44) and ellipsoidal (Eq. 45) effect, respectively. Both are in the order of a few mm, thus negligible in many practical cases.

Figure 3g depicts the contribution of the near zone (first part of Eq. 14), i.e. the terrestrial gravity data from within the spherical cap σ_0, while Fig. 3h depicts the contribution of the far zone (second part of Eq. 14), i.e. long wavelength information provided by the GGM.

Finally, Figure 3i depicts the resulting quasigeoid model $\overline{\zeta}$ of Eq. 35, i.e. the sum of the near zone, far-zone and the additive correction contribution.
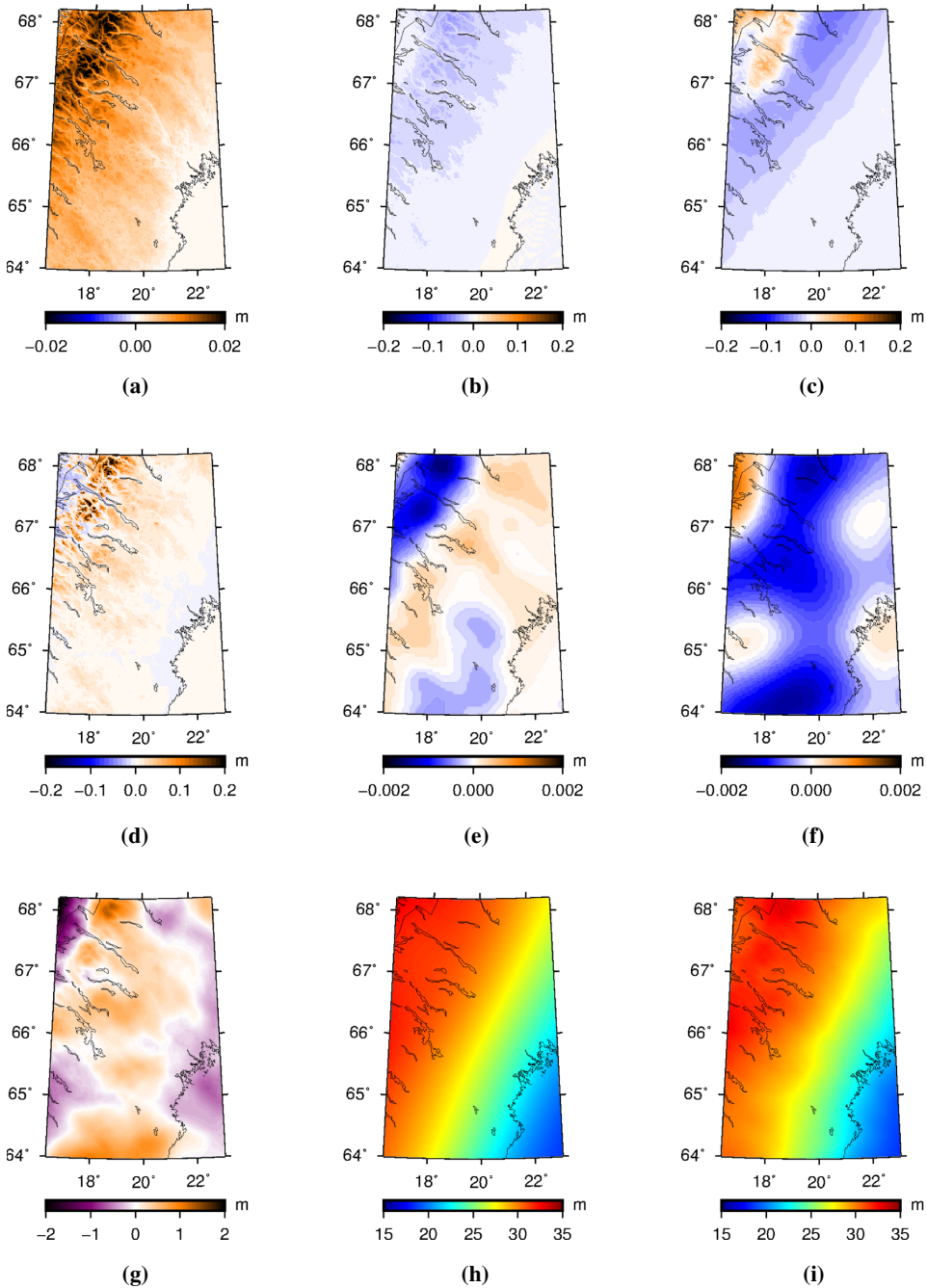
7 Comparison of the geoid modelling methods

In this section, the differences between geoid modelling by Stokes's or Hotine's formula and the various modifications thereof will be illustrated and discussed.
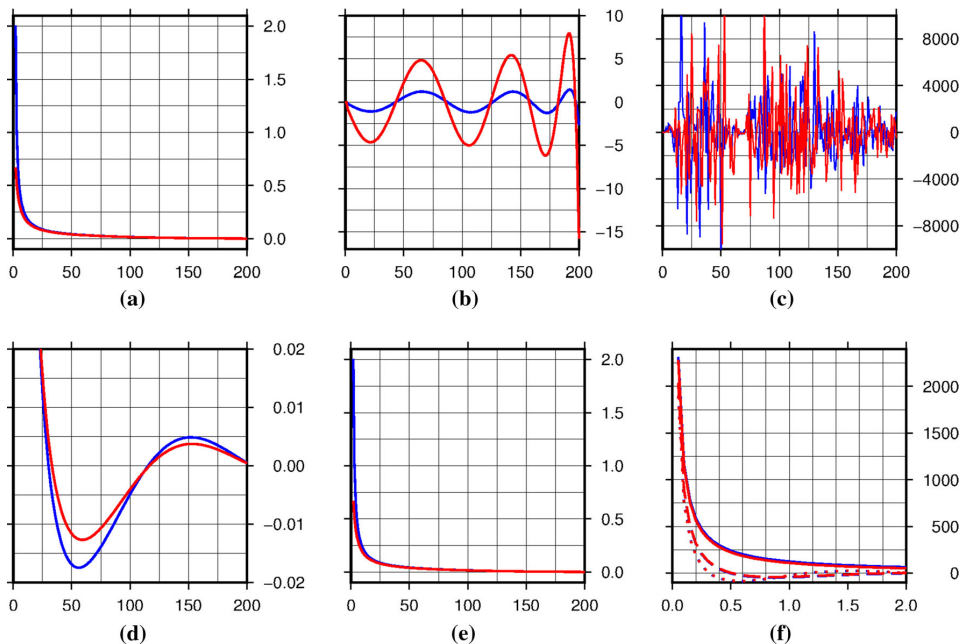
7.1 Modification parameters

First, the unmodified truncation coefficients of Eq. 12 evaluated by the recursive relations given in Jekeli (1979,

Fig. 3 Contributions of different computational steps of the Unbiased LSMHA procedure; min, max, mean and SD values in parenthesis, units: m. **a** $\delta\zeta_{DWC}^{(1)}$ (0.0000, 0.0293, 0.0055, 0.0043), **b** $\delta\zeta_{DWC}^{L(1),far} = \delta N_{DWC}^{L(1),far}$ (−0.0470, 0.0010, −0.0080, 0.0070), **c** $\delta\zeta_{DWC}^{L(2)} = \delta N_{DWC}^{L(2),far}$ (−0.0563, 0.1132, −0.0116, 0.0171), **d** $\delta N_{DWC}^{(1)}$ (−0.0382, 0.3664, 0.0115, 0.0223), **e** $\delta\zeta_{ATM} = \delta N_{ATM}$ (−0.0015, 0.0005, −0.0001, 0.0004), **f** $\delta\zeta_{ELL} = \delta N_{ELL}$ (−0.0014, 0.0012, −0.0005, 0.0005), **g** near zone (−2.121, 1.340, 0.077, 0.380), **h** far zone (18.511, 33.055, 27.770, 3.525), **i** final quasigeoid model (18.442, 33.093, 27.833, 3.599)

Fig. 4 Modification parameters for Hotine's (*red*) or Stokes's (*blue*) function (the *horizontal* axis of Fig. 4a–e depicts the degree n while that of Fig. 4f the spherical distance ψ). **a** s_n coefficients for the WG (and BLS) modifications, **b** s_n coefficients for the ULS (and OLS) modifica-tions, **c** s_n coefficients for the ULS modification obtained without SVD, **d** Unmodified truncation coefficients Q_n, **e** Modification parameters b_n, **f** the original (*solid*), WG modified (*dotted*), LS modified (*dashed*) Hotine or Stokes function

"Appendix C") are visualised in Fig. 4d. Compared to the traditional Molodensky truncation coefficients that can be evaluated by relations given in Paul (1973) or Hagiwara (1976), the Hotine counterparts have a slightly smaller ampli-tude, but similar shape.

What distinguishes the different modifications of Hotine's formula from each other, are the modification coefficients s_n. For the deterministic WG modification of Hotine's formula, the coefficients s_n steadily decrease from $\frac{2}{3}$ to 0, see Fig. 4a. Interestingly, s_n of the BLS modification follow the WG coef-ficients very closely. Compared to the Hotine versions, the original Stokes WG and BLS s_n coefficients start decreasing from 2.

While the WG and BLS s_n coefficients are steadily decreasing, those of ULS and OLS modification undulate, see Fig. 4b. For the same input parameters, the coefficients s_n of ULS and OLS are almost identical. Compared to the Stokes counterparts, the Hotine coefficients undulate with a larger amplitude (but roughly in the same phase).

As discussed in Sect. 2.5, the shape of ULS or OLS s_n coefficients depends strongly on the numerical method used to solve the system of equations given in Eq. 22. The solution presented in Fig. 4b has been obtained by Singular Value Decomposition as implemented in Press et al. (1992) with a singular value limit of 10^{-12}. A different solution is obtained

by straightforward inversion of the matrix **A**, see Eq. 33 and Fig. 4c. The undulation of this solution looks rather random and difficult to compare to the Stokes counterpart. However, the resulting quasigeoid models obtained by using the s_n coefficients depicted in Figs. 4b or c differ numerically by ± 0.3 mm only.

As seen from Eq. 15, the contribution of terrestrial data and the GGM is tuned by the combination of the modifica-tion parameters s_n, the modified truncation parameters Q_n^L and the parameters b_n, the latter two being functions of s_n. In fact, the modified truncation parameters Q_n^L determined by Eq. 11b work in conjunction with the corresponding s_n in such a way that the coefficients b_n become very similar regardless of the modification method used. That is, for all of the modifications, the b_n coefficients are close to the s_n val-ues of the Wong and Gore modification method, see Fig. 4e. Consequently, the Hotine b_n coefficients start from a smaller value than the Stokes counterparts. As seen from the sec-ond part of Eq. 15, smaller values of b_n result in a smaller contribution of the GGM to the geoid estimator.

The contribution of the terrestrial gravity data within the spherical cap σ_0 is determined by the modified Hotine func-tion (Eq. 6). As a result of different modification coefficients s_n, the modified Hotine function has a slightly varying shape, see Fig. 4f.

Table 3 Expected global RMS error of geoid modelling (based on different degree variance models for the Stokes and Hotine formula, see Sect. 5.2.2), units: mm

	n	Stokes				Hotine			
		WG	BLS	ULS	OLS	WG	BLS	ULS	OLS
$(\delta\widetilde{N})^2_{\mathrm{TR}}$	$2\ldots L$	0.00	0.20	0.00	0.04	0.00	0.24	0.00	0.04
	$L+1\ldots\infty$	2.79	2.01	2.16	2.16	2.78	2.00	2.24	2.24
	$2\ldots\infty$	2.79	2.02	2.16	2.16	2.78	2.02	2.24	2.24
$(\delta\widetilde{N})^2_{\mathrm{T}}$	$2\ldots L$	6.54	6.39	6.33	6.33	6.53	6.51	6.41	6.41
	$L+1\ldots\infty$	8.66	8.67	8.67	8.67	8.66	8.67	8.67	8.67
	$2\ldots\infty$	10.85	10.77	10.73	10.73	10.85	10.84	10.78	10.78
$(\delta\widetilde{N})^2_{\mathrm{GGM}}$	$2\ldots L$	1.74	1.77	1.80	1.80	1.73	1.73	1.77	1.77
	$L+1\ldots\infty$	–	–	–	–	–	–	–	–
	$2\ldots\infty$	1.74	1.77	1.80	1.80	1.73	1.73	1.77	1.77
$(\delta\widetilde{N})^2$	$2\ldots L$	6.76	6.63	6.58	6.58	6.76	6.74	6.65	6.65
	$L+1\ldots\infty$	9.10	8.90	8.93	8.93	9.09	8.90	8.95	8.95
	$2\ldots\infty$	**11.34**	**11.10**	**11.09**	**11.09**	**11.33**	**11.16**	**11.15**	**11.15**

Bold values represent the total expected error

7.2 Expected global mean square error

Although the expected global MSE of Eq. 16 is only a measure to propagate the assumed signal and error models to expected geoid model errors, it can be used to compare the different geoid modelling methods. In Table 3, the total and partial contributions of the global RMS error are presented for the different modification methods of Stokes's and Hotine's formula, again illustrating the similarities and differences of the modification methods.

All of the LS modifications of Hotine's formula yield very similar global error estimates. As the name suggests, the BLS modification yields a slightly larger truncation error (bias) for degrees $2-L$ than the ULS and OLS modifications that are numerically very similar to each other.

With the optimal modification limits $L1 = 50$ and $L2 = 200$, the WG modification of Hotine's formula shows rather similar error characteristics to the LS modifications. However, as seen from Table 1, this is highly dependent on the chosen modification limits. See for example how the terrestrial data error contribution lowers with decreasing $L1$ for fixed $L2 = 200$.

Although Table 3 suggests that the LS modifications of Hotine's formula yield a somewhat larger expected global RMS than the LS modifications of Stokes's formula, this result is dependent on the way the gravity disturbance degree variances were determined from those of gravity anomalies by Eq. 47. If the degree variances of gravity disturbance were assumed to be equal to those of anomalies (a case not presented in Table 3), the corresponding total expected error would be 11.01 mm which is in turn less than that of the Stokes modifications. Such theoretical superiority of Hotine's formula over Stokes's formula under the assump-

tion of equal (or smaller) degree variances has often been pointed out, see e.g. Sjöberg (1986b, Sect. 4) and Li (1991, Fig. 1).

8 Comparison of resulting geoid models

The differences of geoid models obtained by using the ULS and WG modifications of the Stokes or Hotine formula will be discussed below.

8.1 Approximate geoid models

First, the approximate geoid model $\widetilde{N}$ (Eq. 15) computed by the Hotine formula is compared to that computed by the Stokes formula, see Fig. 5.

While the contributions of the near and far zone of the ULS modified Stokes's or Hotine's formula differ on average by 7 cm, the sum of these i.e. the approximate geoid $\widetilde{N}$, is rather similar, see Fig. 5a. The maximum differences of 1.3 cm occur in the high topography region, while the SD of the differences is only 3 mm.

Since the LS modification can be sensitive to the input error estimates, the comparison of WG modifications is also shown, see Fig. 5b. The differences of the WG modifications are mostly within ±1 mm (SD, ignoring the edge effects).

8.2 Additive corrections

Second, the additive corrections for geoid or quasigeoid computations by the Stokes or Hotine formula are compared.

As discussed in Sect. 3.1, the combined topographic effect is the same for both approaches. The first part of DWC correc-
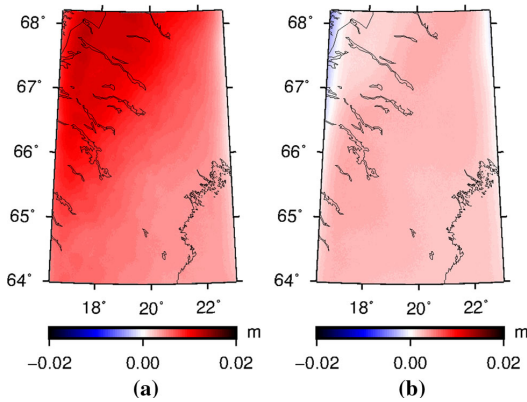
Fig. 5 Differences of approximate geoid models $\widetilde{N}$ computed by Stokes's or Hotine's formula. **a** ULS modification, **b** WG modification
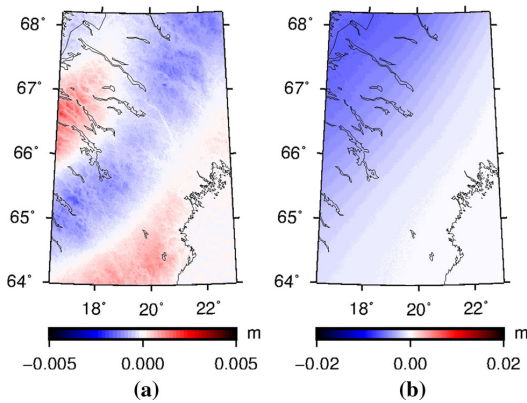
Fig. 6 Differences of partial contributions of the combined DWC effect computed for use with the Stokes or Hotine formula. **a** $\delta\zeta_{\mathrm{DWC}}^{L(1),\mathrm{far}} = \delta N_{\mathrm{DWC}}^{L(1),\mathrm{far}}$, **b** $\delta\zeta_{\mathrm{DWC}}^{L(2)} = \delta N_{\mathrm{DWC}}^{L(2)}$

tion for quasigeoid computation $\delta\zeta_{\mathrm{DWC}}^{(1)}$ (Eq. 43) does not differ either. Although $\delta N_{\mathrm{DWC}}^{(1)}$ (Eq. 39) differs from the Stokes counterpart by the factor 3 missing from the second term, the other two terms clearly dominate in $\delta N_{\mathrm{DWC}}^{(1)}$. As a result, $\delta N_{\mathrm{DWC}}^{(1)}$ is practically equal for the Stokes and Hotine case.

The differences in the other parts $\delta N_{\mathrm{DWC}}^{L(1),\mathrm{far}}$ (Eq. 40) and $\delta N_{\mathrm{DWC}}^{L(2)}$ (Eq. 41) can be significant, see Fig. 6. The total DWC contribution differences to geoid or quasigeoid models have an average of -0.2 mm, SD of 2 mm and an absolute maximum value of 7 mm with a clear NW–SE tilt, dominated by the contribution of $\delta N_{\mathrm{DWC}}^{L(2)}$.

With maximum ±0.1 mm, the differences of the combined atmospheric correction (Eq. 44) are negligible. The combined ellipsoidal correction (Eq. 45) has a mean difference of 0.3 mm with a SD of 0.1 mm.

From the above, it can be concluded that to adapt geoid or quasigeoid computation routines from the Stokes version to the Hotine version, it is in most cases sufficient to adapt only the DWC correction and more specifically, the $\delta N_{\mathrm{DWC}}^{L(1),\mathrm{far}}$ and $\delta N_{\mathrm{DWC}}^{L(2)}$ contributions only. Intuitively, the gravity disturbance gradient present in the DWC correction can safely be approximated with that of gravity anomaly.
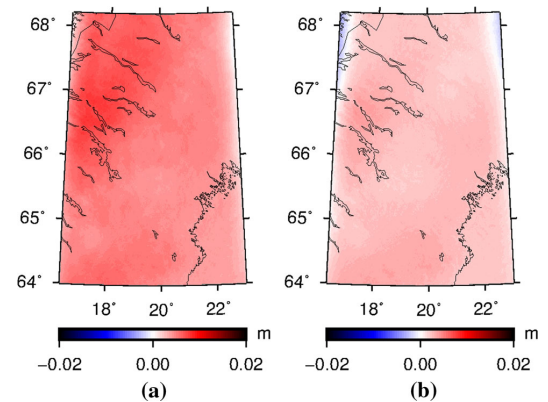
8.3 (Quasi)geoid models

Third, the final geoid/quasigeoid models computed by the Stokes or Hotine formula are compared. From the previous subsection, it follows that the differences are the same for geoid and quasigeoid models.

The models computed by ULS have an average difference of 5 mm, SD of 1 mm and the maximum differences reach 8 mm, occurring in the mountainous areas, see Fig. 7a. Together with the additive corrections, the differences of WG modifications of Stokes's or Hotine's formula are only slightly smaller than the ULS differences, see Fig. 7b.

These results may by somewhat affected by the input gravity disturbance grid being deduced from the anomaly grid using an existing quasigeoid model. For a more rigorous comparison, synthetic or specially collected gravity data could be used.

8.4 Evaluation by GNSS/levelling control points

Independent evaluation of geoid modelling is possible by comparison to co-located GNSS and levelling control points. However, it has to be acknowledged that both GNSS and levelling data contain errors that can be much larger in magnitude than the quasigeoid differences being evaluated (see e.g. Lysaker et al. 2007).

Fig. 7 Differences of (quasi)geoid models computed by Stokes's or Hotine's formula. **a** ULS modification, **b** WG modification
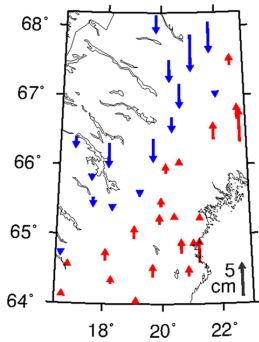
Fig. 8 Hotine ULS quasigeoid validation by GNSS/levelling points after mean removal, units: cm

Table 4 RMS values of the quasigeoid differences from GNSS/levelling control points after mean removal, unit: cm

	Stokes	Hotine
WG	2.34	2.38
BLS	2.44	2.43
ULS	2.42	2.40
OLS	2.42	2.40

In the current study area, there are 37 GNSS/levelling points available. These refer to the Swedish national ETRS89 realisation SWEREF99 (converted to the zero permanent tide system) and the national EVRS realisation RH2000 (c.f. Ågren et al. 2016; Häkli et al. 2016).

The differences of the quasigeoid computed by ULS modified Hotine's formula from the GNSS/levelling points after mean removal are presented in Fig. 8. The clearly systematic NW to SE trend is characteristic to GNSS/levelling comparisons made in this area (although not all over Sweden) possibly due to height data being inaccurate.

Existing control points are positioned mostly in areas of low elevation, which is likely a case for most study areas as accurate levelling lines are rarely available in high mountains. There the alternative quasigeoid models differ very little. Consequently, the validation results for other methods look very similar to Fig. 8. The variation in RMS values of quasigeoid differences from the GNSS/levelling control points of the alternative quasigeoid models are at the sub-millimetre level (see Table 4) which is statistically insignificant.

Although it was not the aim of this contribution, it was demonstrated that the deterministic WG solution can yield geoid models as accurate as the LS modification. However, to obtain such results, a considerable effort to find appropriate modification limits was required. With unsuitable limits (e.g. $L1 = L2 = 200$), the respective WG modified geoid models can differ by ± 25 cm from the best LSMHA models, yielding GNSS/levelling evaluation results that are 5 times worse.

9 Conclusions and discussion

This contribution adapted the (quasi)geoid modelling methods of Least Squares Modification of Stokes's Formula with Additive Corrections (LSMSA) as presented in Sjöberg (2003a) to the Hotine formula. Three versions (biased, unbiased and optimum) of the Least Squares modification were considered. Additive corrections were derived for both geoid and quasigeoid computations. The (quasi)geoid computation scheme presented is referred to as the Least Squares Modification of Hotine's Formula with Additive Corrections (LSMHA).

The methods of LSMHA were compared to each other and the LSMSA counterparts. As a reference, a deterministic Wong and Gore type modification was used. The modification parameters and the expected global root-mean-square error of resulting geoid models of each method were analysed.

The final (quasi)geoid model is the sum of the near- and far-zone contributions (the approximate geoid model) and the additive corrections that consider the downward continuation, topographic, atmospheric and ellipsoidal effect. The additive corrections differ slightly for geoid and quasigeoid modelling.

A case study was used to demonstrate the LSMHA methods for (quasi)geoid modelling. The results were compared to the LSMSA counterparts.

The approximate geoid models (used both in geoid and quasigeoid modelling) computed over the study area via the Stokes or Hotine formula differ by a few mm (in terms of SD) with maximum differences of 1.3 cm occurring in areas of high topography (up to 1900 m). The respective geoid or quasigeoid models computed have an average difference of 5 mm, SD of 1 mm and a maximum of 8 mm over the study area.

It was concluded that the differences between using the Stokes or Hotine formula are smaller than the general geoid modelling accuracy which is at the level of a few mm in the most suitable areas (e.g. flat landscape) to a few cm in more difficult areas (e.g. rugged terrain). The differences are therefore marginal and may be different under other circumstances.

As discussed in the introduction, gravity disturbances are now often available and could be used for geoid modelling without being converted to anomalies. It was demonstrated that the least squares modification principles can be applied to use gravity disturbances and the Hotine formula, yielding very similar geoid modelling results to those obtained by the Stokes counterpart. Therefore, either formula can be used in practical geoid determination tasks. All the necessary equations for the use of LSMHA were collected, derived and presented together in this contribution.

Stochastic modifications (of both the Hotine and Stokes formula), such as the LS modifications presented, depend on estimates of gravity signal and error properties. However, detailed analysis and improvement of degree variance modelling was considered to be outside the scope of this contribution. An advantage of the Hotine formula is the possibility of including the zero and first degree spherical harmonics in geoid modelling, although numerical analysis of their contribution was left for the future.

Although this contribution has presented the use of gravity anomalies and disturbances via the Stokes or Hotine formula as alternatives to each other, geoid modelling methods (such as Least Squares Collocation or various Radial Basis Functions) exist where the use of these can be combined. This is likely a direction for the future of geoid modelling.

References

Abbak RA, Ustun A (2015) A software package for computing a regional gravimetric geoid model by the KTH method. Earth Sci Inform 8(1):255–265. doi:10.1007/s12145-014-0149-3

Abbak RA, Sjöberg LE, Ellmann A, Ustun A (2012) A precise gravimetric geoid model in a mountainous area with scarce gravity data: a case study in central Turkey. Stud Geophys Geod 56(4):909–927. doi:10.1007/s11200-011-9001-0

Abdalla A, Fairhead D (2011) A new gravimetric geoid model for Sudan using the KTH method. J Afr Earth Sci 60(4):213–221. doi:10.1016/j.jafrearsci.2011.02.012

Abdalla A, Tenzer R (2011) The evaluation of the New Zealand's geoid model using the KTH method. Geod Cartogr 37(1):5–14. doi:10.3846/13921541.2011.558326

Ågren J (2004) Regional geoid determination methods for the era of satellite gravimetry: numerical investigations using synthetic earth gravity models. Ph.D. thesis, KTH Royal Institute of Technology, Stockholm

Ågren J, Barzaghi R, Carrion D, Denker H, Duquenne H, Grigoriadis VN, Kiamehr R, Sona G, Tscherning CC, Tziavos IN (2009a) Different geoid computation methods applied on a test dataset: results and considerations. In: VII Hotine–Marussi symposium on mathematical geodesy, Rome, 6–10 June. http://www.gfy.ku.dk/~cct/publ_cct/cct1988.pdf. Accessed 8 Sept 2017

Ågren J, Sjöberg LE, Kiamehr R (2009b) The new gravimetric quasigeoid model KTH08 over Sweden. J Appl Geod 3(3):143–153. doi:10.1515/JAG.2009.015

Ågren J, Strykowski G, Bilker-Koivula M, Omang O, Märdla S, Forsberg R, Ellmann A, Oja T, Liepinš I, Paršeliūnas E, Kaminskis J, Sjöberg L, Valsson G (2016) The NKG2015 gravimetric geoid model for the Nordic–Baltic region. In: 1st joint commission 2 and IGFS meeting international symposium on gravity, geoid and height systems. Thessaloniki, 19–23 September. doi:10.13140/RG.2.2.20765.20969

Alberts B, Klees R (2004) A comparison of methods for the inversion of airborne gravity data. J Geod 78(1–2):55–65. doi:10.1007/s00190-003-0366-x

Barthelmes F, Köhler W (2016) International centre for global earth models (ICGEM). J Geod Geod Handb 90(10):1177–1180. doi:10.1007/s00190-016-0948-z

Becker JJ, Sandwell DT, Smith WHF, Braud J, Binder B, Depner J, Fabre D, Factor J, Ingalls S, Kim SH, Ladner R, Marks K, Nelson S, Pharaoh A, Trimmer R, Rosenberg JV, Wallace G, Weatherall P (2009) Global bathymetry and elevation data at 30 arc seconds resolution: SRTM30_PLUS. Mar Geod 32(4):355–371. doi:10.1080/01490410903297766

Bruinsma SL, Förste C, Abrikosov O, Lemoine JM, Marty JC, Mulet S, Rio MH, Bonvalot S (2014) ESA's satellite-only gravity field model via the direct approach based on all GOCE data. Geophys Res Lett 41(21):2014GL062–045. doi:10.1002/2014GL062045

Daras I (2008) Determination of a gravimetric geoid model of Greece using the method of KTH. Master's thesis, KTH Royal Institute of Technology

Ellmann A (2004) The geoid for the Baltic countries determined by the least squares modification of Stokes' formula. Ph.D. Thesis, KTH Royal Institute of Technology, Stockholm

Ellmann A (2005) Computation of three stochastic modifications of Stokes's formula for regional geoid determination. Comput Geosci 31(6):742–755. doi:10.1016/j.cageo.2005.01.008

Ellmann A (2005b) On the numerical solution of parameters of the least squares modification of Stokes' formula. In: Sansò PDF (ed) A window on the future of geodesy, no. 128 in international association of geodesy symposia. Springer, Berlin, pp 403–408. doi:10.1007/3-540-27432-4_69

Ellmann A (2005c) Two deterministic and three stochastic modifications of Stokes's formula: a case study for the Baltic countries. J Geod 79(1–3):11–23. doi:10.1007/s00190-005-0438-1

Ellmann A, Vaníček P (2007) UNB application of Stokes–Helmert's approach to geoid computation. J Geodyn 43(2):200–213. doi:10.1016/j.jog.2006.09.019

Evans JD, Featherstone WE (2000) Improved convergence rates for the truncation error in gravimetric geoid determination. J Geod 74(2):239–248. doi:10.1007/s001900050282

FAMOS Consortium (2014) FAMOS (Finalising Surveys for the Baltic Motorways of the Sea). http://www.famosproject.eu/famos/. Accessed 5 Sept 2017

Featherstone W (2003a) Software for computing five existing types of deterministically modified integration kernel for gravimetric geoid determination. Comput Geosci 29(2):183–193. doi:10.1016/S0098-3004(02)00074-2

Featherstone WE (2003b) Band-limited kernel modifications for regional geoid determination based on dedicated satellite gravity field missions. In: Tziavos IN (ed) Gravity and geoid. Ziti Editions, Thessaloniki, pp 341–346

Featherstone WE (2013) Deterministic, stochastic, hybrid and band-limited modifications of Hotine's integral. J Geod 87(5):487–500. doi:10.1007/s00190-013-0612-9

Featherstone WE, Evans JD, Olliver JG (1998) A Meissl-modified Vaníček and Kleusberg kernel to reduce the truncation error in gravimetric geoid computations. J Geod 72(3):154–160. doi:10.1007/s001900050157

Forsberg R (1993) Modelling the fine-structure of the geoid: methods, data requirements and some results. Surv Geophys 14(4–5):403–418. doi:10.1007/BF00690568

Forsberg R, Tscherning CC (1997) Topographic effects in gravity field modelling for BVP. In: Sansó PDF, Rummel PDR (eds) Geodetic boundary value problems in view of the one centimeter geoid, no. 65 in Lecture Notes in earth sciences. Springer, Berlin, pp 239–272. doi:10.1007/BFb0011707

Guan Z, Li Y (1991) The determination of oceanic geoid using modified hotine integral. In: Rapp RH, Sansò F (eds) Determination of the geoid, no. 106 in international association of geodesy symposia. Springer, New York, pp 86–94. doi:10.1007/978-1-4612-3104-2_11

Hagiwara Y (1976) A new formula for evaluating the truncation error coefficient. Bull Géod 50(2):131–135. doi:10.1007/BF02522312

Häkli P, Lidberg M, Jivall L, Nørbech T, Tangen O, Weber M, Pihlak P, Aleksejenko I, Paršeliunas E (2016) The NKG2008 GPS campaign–final transformation results and a new common Nordic reference frame. J Geod Sci 6(1):1–33. doi:10.1515/jogs-2016-0001

Heck B, Grüninger W (1987) Modification of Stokes's integral formula by combining two classical approaches. In: Proceedings of the XIX IUGG general assembly, vol 2. Vancouver, pp 319–337

Heiskanen WA, Moritz H (1967) Physical geodesy. W. H. Freeman and Company, San Francisco

Hotine M (1969) Mathematical geodesy. US Environmental Science Services Administration, Rockville

ISG (2015) International Service for the Geoid: Baltic and Nordic Region (NKG2015). http://www.isgeoid.polimi.it/Geoid/Europe/NordicCountries/nordic_baltic_countries_g.html. Accessed 5 Sept 2017

Jekeli C (1979) Global accuracy estimates of point and mean undulation differences, gravity anomalies, and potential coefficients. Technical Report 288, The Ohio State University

Jekeli C (1980) Comparison of undulation difference accuracies using gravity anomalies and gravity disturbances. Bull Géod 54(2):137–147. doi:10.1007/BF02521243

Jekeli C (1981) Modifying Stokes' function to reduce the error of geoid undulation computations. J Geophys Res Solid Earth 86(B8):6985–6990. doi:10.1029/JB086iB08p06985

Kaula WM (1963) The investigation of the gravitational fields of the moon and planets with artificial satellites. Adv Space Sci Technol 5:210–226

Kiamehr R (2006) A strategy for determining the regional geoid by combining limited ground data with satellite-based global geopotential and topographical models: a case study of Iran. J Geod 79(10–11):602–612. doi:10.1007/s00190-005-0009-5

Kirby JF (2003) On the combination of gravity anomalies and gravity disturbances for geoid determination in Western Australia. J Geod 77(7–8):433–439. doi:10.1007/s00190-003-0334-5

Kuczynska-Siehien J, Lyszkowicz A, Birylo M (2016) Geoid determination for the area of Poland by the least squares modification of Stokes' formula. Acta Geodyn Geomater 13(1 (181)):19–26. doi:10.13168/AGG.2015.0041

Lysaker DI, Omang OCD, Pettersen BR, Solheim D (2007) Quasigeoid evaluation with improved levelled height data for Norway. J Geod 81(9):617–627. doi:10.1007/s00190-006-0129-6

Märdla S, Ågren J, Strykowski G, Oja T, Ellmann A, Forsberg R, Bilker-Koivula M, Omang O, Paršeliūnas E, Liepinš I, Kaminskis J (2017) From discrete gravity survey data to a high-resolution gravity field representation in the Nordic–Baltic region. Mar Geod. doi:10.1080/01490419.1326428

Märdla S, Ellmann A, Ågren J, Sjöberg LE (2017b) Regional geoid computation by least squares modified Hotine's formula with additive corrections. In: Joint scientific assembly of the international association of geodesy (IAG) and international association of seismology and physics of the earth's interior (IASPEI), July 30 to August 4, Kobe. doi:10.13140/RG.2.2.29154.63682

Meissl P (1971) Preparations for the numerical evaluation of second order Molodensky-type formulas. Technical Report 163, The Ohio State University

Molodenskii M, Eremeev V, Urkina M (1962) Methods for study of the external gravitation field and figure of the Earth. Translations from Russian, Jerusalem, Israel Program for Scientific Translations

Molodensky MS (1945) The principal problems of geodetic gravimetry (in Russian). TRUDY TsNIIGAiK 42

Moritz H (2000) Geodetic reference system 1980. J Geod 74(1):128–133. doi:10.1007/s001900050278

Nahavandchi H, Sjöberg LE (2001) Precise geoid determination over Sweden using the Stokes–Helmert method and improved topographic corrections. J Geod 75(2–3):74–88. doi:10.1007/s001900000154

Novák P (2003) Geoid determination using one-step integration. J Geod 77(3–4):193–206. doi:10.1007/s00190-003-0314-9

Novák P, Heck B (2002) Downward continuation and geoid determination based on band-limited airborne gravity data. J Geod 76(5):269–278. doi:10.1007/s00190-002-0252-y

Novák P, Kern M, Schwarz KP, Sideris MG, Heck B, Ferguson S, Hammada Y, Wei M (2003) On geoid determination from airborne gravity. J Geod 76(9–10):510–522. doi:10.1007/s00190-002-0284-3

Omang OCD, Forsberg R (2000) How to handle topography in practical geoid determination: three examples. J Geod 74(6):458–466. doi:10.1007/s001900000107

Paul MK (1973) A method of evaluating the truncation error coefficients for geoidal height. Bull Géo (1946–1975) 110(1):413–425. doi:10.1007/BF02521951

Press WH, Teukolsky SA, Vetterling WT, Flannery BP (1992) Numerical recipes in fortran 77, 2nd edn: the art of scientific computing. Cambridge University Press, Cambridge

Rexer M, Hirt C (2015) Spectral analysis of the Earth's topographic potential via 2D-DFT: a new data-based degree variance model to degree 90,000. J Geod 89(9):887–909. doi:10.1007/s00190-015-0822-4

Sansò F, Sideris MG (eds) (2013) Geoid determination, vol 110. In: Lecture notes in earth system sciences. Springer, Berlin

Serpas JG, Jekeli C (2005) Local geoid determination from airborne vector gravimetry. J Geod 78(10):577–587. doi:10.1007/s00190-004-0416-z

Sjöberg LE (1980) Least squares combination of satellite harmonics and integral formulas in physical geodesy. Gerlands Beitraege zur Geophysik 89:371–377

Sjöberg LE (1984) Least squares modification of Stokes' and Vening Meinesz' formulas by accounting for truncation and potential coefficient errors. Manusc Geod 9:209–229

Sjöberg LE (1986a) Comparison of some methods of modifying Stokes' formula. In: Bolletino Di Geodesia e Scienze Affini, vol 3. Florence

Sjöberg LE (1986b) The modification of Stokes' and Hotine's formulas: A comparison. In: Proceedings of international symposium on figure and dynamics of the earth, moon, and planets. Prague, pp 323–333

Sjöberg LE (1989) Integral formulas for geopotential coefficient determination from gravity anomalies versus gravity disturbances. Bull Géod 63(2):213–221. doi:10.1007/BF02519152

Sjöberg LE (1991) Refined least squares modification of Stokes formula. Manusc Geod 16:367–375

Sjöberg LE (2000) Topographic effects by the Stokes–Helmert method of geoid and quasi-geoid determinations. J Geod 74(2):255–268. doi:10.1007/s001900050284

Sjöberg LE (2003a) A computational scheme to model the geoid by the modified Stokes formula without gravity reductions. J Geod 77(7–8):423–432. doi:10.1007/s00190-003-0338-1

Sjöberg LE (2003b) A general model for modifying Stokes' formula and its least-squares solution. J Geod 77(7–8):459–464. doi:10.1007/s00190-003-0346-1

Sjöberg LE (2003c) A solution to the downward continuation effect on the geoid determined by Stokes' formula. J Geod 77(1–2):94–100. doi:10.1007/s00190-002-0306-1

Sjöberg LE (2004) A spherical harmonic representation of the ellipsoidal correction to the modified Stokes formula. J Geod 78(3):180–186. doi:10.1007/s00190-004-0378-1

Sjöberg LE (2005) A discussion on the approximations made in the practical implementation of the remove-compute-restore technique in regional geoid modelling. J Geod 78(11–12):645–653. doi:10.1007/s00190-004-0430-1

Sjöberg LE (2007) The topographic bias by analytical continuation in physical geodesy. J Geod 81(5):345–350. doi:10.1007/s00190-006-0112-2

Sjöberg LE, Bagherbandi M (2017) Gravity inversion and integration. Springer, Berlin

Sjöberg LE, Eshagh M (2009) A geoid solution for airborne gravity data. Stud Geophys Geod 53(3):359–374. doi:10.1007/s11200-009-0025-7

Sjöberg LE, Featherstone WE (2004) Two-step procedures for hybrid geoid modelling. J Geod 78(1–2):66–75. doi:10.1007/s00190-003-0367-9

Sjöberg LE, Hunegnaw A (2000) Some modifications of Stokes' formula that account for truncation and potential coefficient errors. J Geod 74(2):232–238. doi:10.1007/s001900050281

Sjöberg LE, Nahavandchi H (2000) The atmospheric geoid effects in Stokes' formula. Geophys J Int 140(1):95–100. doi:10.1046/j.1365-246x.2000.00995.x

Sjöberg LE, Nord T (1992) Geoidal undulation computation by modifying Stokes's kernel versus Hotine's kernel from gravity anomalies. Manuscr Geod 17:135–140

Sjöberg LE, Gidudu A, Ssengendo R (2015) The Uganda gravimetric geoid model 2014 computed by the KTH method. J Geod Sci. doi:10.1515/jogs-2015-0007

Stokes GG (1849) On the variation of gravity at the surface of the Earth. Trans Cambr Philos Soc 8:672–695

Tscherning CC, Rapp RH (1974) Closed covariance expressions for gravity anomalies, geoid undulations, and deflections of the vertical implied by anomaly degree variance models. Technical Report 208, The Ohio State University

Ulotu P (2009) Geoid model of Tanzania from sparse and varying gravity data density by the KTH method. Ph.D. Thesis, KTH Royal Institute of Technology, Stockholm

Vaníček P, Featherstone WE (1998) Performance of three types of Stokes's kernel in the combined solution for the geoid. J Geod 72(12):684–697. doi:10.1007/s001900050209

Vaníček P, Kleusberg A (1987) The Canadian geoid-stokesian approach. Manuscr Geod 12:86–98

Vaníček P, Sjöberg LE (1991) Reformulation of Stokes's theory for higher than second-degree reference field and modification of integration kernels. J Geophys Res Solid Earth 96(B4):6529–6539. doi:10.1029/90JB02782

Vaníček P, Changyou Z, Sjöberg LE (1992) A comparison of Stokes's and Hotine's approaches to geoid computation. Manuscr Geod 17:29–35

Vaníček P, Najafi M, Martinec Z, Harrie L, Sjöberg LE (1995) Higher-degree reference field in the generalized Stokes–Helmert scheme for geoid computation. J Geod 70(3):176–182. doi:10.1007/BF00943693

Wenzel HG (1983) Geoid computation by least squares spectral combination using integral kernels. In: Proceedings of the international association of geodesy general meeting, Tokyo, pp 438–453

Wessel P, Smith WHF, Scharroo R, Luis J, Wobbe F (2013) Generic mapping tools: improved version released. Eos Trans Am Geophys Union 94(45):409–410. doi:10.1002/2013EO450001

Wong L, Gore R (1969) Accuracy of geoid heights from modified Stokes kernels. Geophys J R Astron Soc 18(1):81–91. doi:10.1111/j.1365-246X.1969.tb00264.x

Yildiz H, Forsberg R, Ågren J, Tscherning C, Sjöberg L (2012) Comparison of remove-compute-restore and least squares modification of Stokes' formula techniques to quasi-geoid determination over the Auvergne test area. J Geod Sci 2(1):53–64. doi:10.2478/v10156-011-0024-9

Zhang C (1998) Estimation of dynamic ocean topography in the Gulf Stream area using the Hotine formula and altimetry data. J Geod 72(9):499–510. doi:10.1007/s001900050189

Paper B

2017 Taylor & Francis Group. Reprinted, with permission, from

Märdla, S., Ågren, J., Strykowski, G., Oja, T., Ellmann, A., Forsberg, R., Bilker-Koivula, M., Omang, O., Paršeliūnas, E., Liepinš, I., and Kaminskis, J. (2017). "From Discrete Gravity Survey Data to a High-Resolution Gravity Field Representation in the Nordic-Baltic Region". *Marine Geodesy* 40 (6), pp. 416–453. DOI: 10.1080/01490419.2017.1326428. **Paper B**.

Taylor & Francis
Taylor & Francis Group

Check for updates

From Discrete Gravity Survey Data to a High-Resolution Gravity Field Representation in the Nordic-Baltic Region

Silja Märdla [ID][a], Jonas Ågren[b], Gabriel Strykowski[c], Tõnis Oja[d], Artu Ellmann[a], René Forsberg[c], Mirjam Bilker-Koivula[e], Ove Omang[f], Eimuntas Paršeliūnas[g], Ivars Liepinš[h], and Jānis Kaminskis[i]

[a]School of Engineering, Tallinn University of Technology, Tallinn, Estonia; [b]Lantmäteriet, The Swedish Mapping, Cadastral, and Land Registration Authority, Gävle, Sweden; [c]National Space Institute, Technical University of Denmark, Lyngby, Denmark; [d]Department of Geodesy, Estonian Land Board, Tallinn, Estonia; [e]Finnish Geospatial Research Institute, National Land Survey of Finland, Masala, Finland; [f]Geodetic Institute, Norwegian Mapping Authority, Hønefoss, Norway; [g]Department of Geodesy and Cadastre, Vilnius Gediminas Technical University, Vilnius, Lithuania; [h]Geodesy division, Latvian Geospatial Information Agency, Riga, Latvia; [i]Faculty of Civil Engineering, Riga Technical University, Riga, Latvia

ABSTRACT

The deduction of a regularly spaced gravity anomaly grid from scattered survey data is studied, addressing mainly two aspects: reduction of gravity to anomalies and subsequent interpolation by various methods. The problem is illustrated in a heterogeneous study area and contrasting test areas including mountains, low terrains, and a marine area. Provided with realistic error estimates, Least Squares Collocation interpolation of Residual Terrain Model anomalies yields the highest quality gravity grid. In most cases, the Bouguer reduction and other interpolation methods tested are equally viable. However, spline-based interpolation should be avoided in marine areas with trackwise survey data.

Introduction

Although Global Geopotential Models (GGM) have become increasingly detailed and accurate, there is still a need for regional (quasi)geoid models that fulfil the needs of mapping and engineering applications, especially the conversion of Global Navigation Satellite System (GNSS)-derived ellipsoidal heights into conventional (physical) heights with respect to the sea level (as the geoid is a surface that roughly coincides with the mean sea level). Currently, the geodetic community has set the goal of achieving 5–10 mm accuracy in regional gravimetric (quasi)geoid modelling, imposing, thus, strict requirements not only on the modelling techniques but also on the input gravity data.

Even though there are (quasi)geoid determination methods that can be applied directly without prior gridding of input gravity data (such as Tscherning 1985), many modelling techniques (such as Haagmans, de Min, and Gelderen 1993; Forsberg and Sideris 1993; Li

---

and Sideris 1997; Sjöberg 2003; Ellmann and Vaníček 2007) need a regularly spaced gravity anomaly grid that has to be determined from the scattered survey data located from a few hundreds of meters up to a few tens of kilometres apart.

Importantly, geoid modelling is not the only application of gravity (anomaly) grids, these are also needed for other geosciences. For example, different gravity anomalies (free-air, simple Bouguer, complete Bouguer, slab-residual, mantle Bouguer etc., see e.g. Hackney and Featherstone 2003; Radhakrishna, Lasitha, and Mukhopadhyay 2008) are used in two- or three-dimensional inverse as well as forward modelling by various techniques to interpret variations in mass and density that reflect the structure of solid Earth. Gravity field derivatives such as gradients also reveal density contrasts (Elkins 1951). Numerous contributions similar to that of Mandal et al. (2015), Baptiste et al. (2016), and Klitzke et al. (2016) describe and interpret the gravity field and geophysical features of specific regions. For the user of a regularly spaced gravity anomaly grid, it is beneficial to be familiar with the basis upon which such a grid can be constructed and also be aware of limiting factors in grid accuracy.

Regional scale gravity database analysis and gridding are reported in Gil and Rodríguez−Caderot (1998), Hinze et al. (2005), Vergos et al. (2005), Jekeli et al. (2009), Martín et al. (2009), Saleh et al. (2013), and Véronneau (2013). Although gravity anomaly gridding is a task often performed, it is rarely discussed in detail. Generally a method is selected according to previous experience, popularity, or software availability. Sometimes the choice is based on further analysis which is not reported upon in scientific literature. Accordingly, this contribution will analyse various methods of gravity gridding to determine their advantages and shortcomings. A general remove-interpolate-restore (RIR) process is used. That is, the gravity anomaly point values are reduced, interpolated, and then restored to result in a surface gravity anomaly grid. In further text, the entire RIR process is referred to as "gridding" interchangeably.

A number of different aspects of gravity data processing are discussed. Most importantly, two different gravity reduction/restoration methods and four different interpolation methods will be described and compared. All of these methods are known and often used, see the reference list. However, this contribution aims at offering a consistent comparison and evaluation of some gravity reduction and interpolation methods that could be used over large and challenging study areas.

In addition, the entire work flow of gravity data processing together with the effect of some alternative processing choices (such as omitting/incorporating certain reduction options, data weighting or changing the degree and order of the GGM used) will be discussed in detail. The current status (coverage and quality) of the North European gravity data is reviewed, also illustrating the possible ways of solving gravity data unification issues in the context of a multi-nation geoid modelling study covering both land and marine areas.

The different methodological approaches and subsequent results achieved over the study area may be useful for any regional gravity gridding exercise worldwide. However, the quality of the actual result is dependent on many circumstances, including gravity data coverage, distribution, accuracy, and gravity field properties (rough vs. smooth). These issues will be discussed in appropriate sections of this contribution.

The research reported in this contribution is an input to the Nordic Geodetic Commission (NKG) geoid modelling project (Ågren et al. 2015, 2016) which aims at calculating a high-resolution and accurate regional gravimetric quasigeoid model over the Nordic and Baltic countries in Europe, embedding also the Baltic Sea, North Sea and a large portion of

the Arctic Ocean. Parts of the research area are topographically varying and data coverage is rather heterogeneous, challenging the choice of uniform modelling methods for the entire research area comprising of marine and dry land parts.

The specific area of interest has been subject to NKG geoid modelling projects since the mid 1980's. The succession of NKG geoid models include NKG-86 (Tscherning and Forsberg 1986), NKG-89 (Forsberg 1991), NKG-96 (Forsberg, Kaminskis, and Solheim 1997), NKG2002, and NKG2004 (Forsberg, Strykowski, and Solheim 2004). These regional geoid models were often adapted as national geoid models or height correction surfaces by fitting to a set of national GNSS/levelling points. In addition to NKG geoid models, parts of this region have been subject to other gravity field and geoid modelling studies such as Vermeer (1994), Noréus et al. (1997), Korhonen et al. (1999), Omang and Forsberg (2000), Omang and Forsberg (2002), Ellmann (2002, 2005), Jürgenson (2003), Nahavandchi et al. (2005), Lysaker et al. (2007), Ågren et al. (2009), Ågren (2009), Denker et al. (2009), Bilker-Koivula (2010), Ellmann et al. (2011), Omang et al. (2012), Bilker-Koivula (2014), and Märdla et al. (2015).

The NKG geoid modelling activities have contained extensive data improvements and preliminary computations. The NKG gravity database has been modernised, thoroughly updated, and quality checked. A new regional high-resolution Digital Terrain Model (DTM) and an ice thickness model have been compiled. The used datasets were, if possible and meaningful, transformed into common reference frames. Preliminary grid compilations were made independently by a number of geoid computation centres, using different methods, software packages and strategies (Ågren et al. 2015). It was decided that certain aspects of gravity gridding should be further investigated before the final geoid computations. This triggered the present study and also affected the choice of reduction and gridding methods tested.

This paper is organised as follows. First, the gravity reduction and interpolation methods together with data requirements for accurate geoid computation are explained. Second, the study area is introduced, leading to a description of experimental gravity gridding. The results are then analyzed and presented in the context of quasigeoid modelling. Finally, conclusions are drawn from the findings of this study.

Gravity reductions for interpolation

Interpolating the surface gravity values g directly is inaccurate as the gravity field contains high-frequency information due to the topography (or bathymetry), making it difficult for interpolation algorithms to estimate the correct gravity values at the grid nodes. A gravity reduction process converts the gravity point data values so that these are more reliable for prediction at the desired locations.

Thus, the surface gravity anomalies need to be first reduced. After reduction, the scattered point values are interpolated into a regular grid, leading to a reduced gravity grid. To obtain the surface gravity anomaly grid, there has to be a corresponding restoration process. Importantly, the restoration step adds to gravity data gaps either higher or lower frequency information from reference sources like the DTM, GGM or other relevant corrections.

The used anomaly types and applied corrections are reviewed below. Besides the two reduction schemes tested in this contribution, there are others that could be used. These include mainly isostatic reductions such as the Airy-Heiskanen or the Pratt-Hayford reduction that could improve the gridding outcome over land or ocean areas, respectively.

Free-air anomalies

It is assumed that the gravity value g on or above the topography at point P and the corresponding (normal or orthometric) height H_P are known. As a first step, the free-air or surface gravity anomaly Δg^{FAA} are computed by Heiskanen and Moritz [1967, (7) and (8)]:

$$\Delta g_P^{FAA} = g_P - \gamma_Q \tag{1}$$

where γ_Q is the normal gravity at point Q at the height H_P (reckoned from the reference ellipsoid) and is computed using standard formulas for the GRS-80 normal gravity field, cf. Moritz (2000).

Although reduced in magnitude (compared to the initial gravity value itself), the free-air anomaly field can still be quite rough and correlated with height. It is smoother in marine areas, but significant variations in the bathymetry (not considered in this study) may result in a comparatively rough field in these areas as well. Thus, a further reduction of gravity anomalies is often needed to yield a smoother anomaly field.

Simple and complete Bouguer anomalies

Removing the gravitational effect of an infinite planar Bouguer plate leads to the simple Bouguer anomaly Δg^{SBA} by Heiskanen and Moritz [1967, (3)–(19)]:

$$\Delta g_P^{SBA} = \Delta g_P^{FAA} - 2\pi G \rho H_P \tag{2}$$

where G is the gravitational constant and ρ is the topographic density (if approximated to 2670 kg.m^{-3} then the last term in the right-hand side becomes $0.1119 H_P$).

In areas of flat terrain, Δg^{SBA} can be a useful quantity for gridding. However, in mountainous regions the Δg^{SBA} field can be too biased for a meaningful interpolation (Janák and Vaníček 2005). Therefore, further reduction into planar complete Bouguer anomaly Δg^{CBA} is obtained by Heiskanen and Moritz [1967, (3)–(21)]:

$$\Delta g_P^{CBA} = \Delta g_P^{SBA} + \delta g_P^{T} |_{z_1 = H}^{z_2 = H_P} \tag{3}$$

where δg_P^T is the planar terrain correction and H is the height of the moving integration point (determined from a DTM). Note that the alternative spherical Bouguer anomalies (see e.g. Vaníček et al. 2001, 2004; Novák et al. 2001; Kuhn et al. 2009) are not considered in this contribution.

The terrain correction δg_P^T can be computed using different approximations. In the context of the RIR technique, there is no need to extend the integration too far from the computation point P. The terrain correction is thus calculated by summing the attraction of a finite number of prisms according to (Forsberg 1984):

$$\delta g_P^T = -G \times \sum \int_{x=x_1}^{x_2} \int_{y=y_1}^{y_2} \int_{z=z_1}^{z_2} \rho \times \frac{(z - z_P)}{\left((x - x_P)^2 + (y - y_P)^2 + (z - z_P)^2\right)^{3/2}} \, dx \, dy \, dz \tag{4}$$

where x_P, y_P, z_P and x, y, z are the local Cartesian coordinates of the computation point P and the moving integration element, respectively. The z coordinate is the 'up' direction, the limits x_1, x_2, y_1, y_2 are constants for each prism. Most commonly, only flat top prisms are

used, i.e. z_1 and z_2 are also constant for each prism. The way z_1 and z_2 are chosen is indicated by the type of notation used in (3). Again, due to lack of density information available, ρ is usually taken to be constant.

In the present study, the curvature of the Earth is taken into account by shifting each prism downwards by correcting the integration constants of (4) as (Forsberg 1984, p. 111):

$$z_1^* = z_1 - \frac{s^2}{2R}; \ z_2^* = z_2 - \frac{s^2}{2R} \tag{5}$$

where s is the distance between the computation point P and the integration point, R is the mean radius of the Earth. Admittedly, this is a crude way to take the Earth's curvature into account, but accurate enough in the context of the present study where the topographic corrections in question are used only for the RIR process.

Residual Terrain Model (RTM) anomalies

An alternative to the Bouguer reduction described in the previous section is to reduce the free-air anomaly field by a band-pass filter that attenuates signals above and below a desired frequency. The free-air anomaly values can be reduced in the long-wavelength spectrum by removing the gravity contribution of a GGM and in the short-wavelength spectrum by removing the contribution of a Residual Terrain Model (RTM) by:

$$\Delta g_P^{RTMA} = \Delta g_P^{FAA} - \Delta g_P^{GGM} - \delta g_P^{RTM} \tag{6}$$

where Δg_P^{GGM} is the gravity anomaly from a GGM evaluated to a suitable maximum degree and order (d/o), and δg_P^{RTM} is the topographic effect of the RTM reduction computed as (cf. Forsberg 1984):

$$\delta g_P^{RTM} = 2\pi G\rho \left[H_P - H_P^{ref} \right] - \left[\delta g_P^{T} \mid_{z_1=H_p}^{z_2=H} - \delta g_P^{T} \mid_{z_1=H_P^{ref}}^{z_2=H^{ref}} \right] \tag{7}$$

where H^{ref} is the height of a smooth reference surface; $\delta g_P^{T} \mid_{z_1=H_p}^{z_2=H}$ and $\delta g_P^{T} \mid_{z_1=H_P^{ref}}^{z_2=H^{ref}}$ denote the terrain correction for the topographic surface and the reference surface, respectively. Note that (7) does not demand the use of the so-called harmonic correction (Forsberg 1997, Section 2.3 and 2.4).

The reference elevation surface can be any smooth surface representing mean elevations in the area. It is often constructed by averaging the fine resolution DTM grid and then low-pass filtering this by taking moving averages of an appropriate number of adjacent blocks. Or alternatively, a spherical harmonic representation of either the regional or an independent global DTM is evaluated to a d/o that corresponds to the desired smoothness. For related studies, see e.g. Hirt (2010, 2013) and references therein.

Atmospheric and ice corrections

For both of the gravity reduction processes described above, the atmospheric and ice correction (denoted below by superscript A or I, respectively) can be applied. Again, these are applied before and removed after gridding.

The atmospheric correction accounts for the gravitational effect of the atmospheric masses, much as the terrain correction accounts for the topographic masses. This effect can be computed by an empirical formula of DMA [1987, (4)–(23)]:

$$\delta g^A = 0.87 \times e^{-0.116 \times H^{1.047}} \tag{8}$$

where $e \approx 2.718$, δg^A is in mGal and H is in km. The resulting numerical values are similar to the recommendations given in Moritz (2000). This correction cannot exceed 0.87 mGal, that is, the effect of atmospheric masses on the sea level.

δg^A is added to the surface gravity anomaly point values and subtracted (in gridded form) after interpolation.

The ice correction is needed since the Bouguer and RTM corrections are initially computed using topographic density and DTM heights that refer to the surface of glaciers. The ice masses are artificially filled up to reach topographic density ρ, at the same time as the Airy-Heiskanen isostatic compensation is taken into account (e.g. Sünkel 1986). After interpolation, the reduction is reversed, leading back to ice density (masses are moved back to where they originate from). To achieve this, a residual ice mass potential δV^I is defined as (e.g. Martinec 1998; Ågren 2004):

$$\delta V_P^I = V_P^I - V_P^{iso} \tag{9}$$

where V^{iso} is the corresponding compensating potential according to the Airy-Heiskanen hypothesis and V_P^I is the potential generated by the mass deficit of the glaciers, which is expressed by the Newton's integral in spherical coordinates as

$$V_P^I = G(\rho^I - \rho) \iint\limits_{\sigma^I} \int\limits_{z = R + H^I - T^I}^{R + H^I} \frac{z^2}{s} \, dz \, d\sigma^I \tag{10}$$

where ρ^I is the ice density, σ^I is the spatial domain covered with glaciers, H^I is the height to the (ice) surface, and T^I is the ice thickness. Note that the density difference in (10) is assumed to be constant and that it is negative. The ice effect δg_P^I on the surface gravity anomaly is then given by the standard boundary condition of physical geodesy:

$$\delta g_P^I = -\frac{\partial \delta V_P^I}{\partial r_P} - \frac{2}{r_P} \delta V_P^I \tag{11}$$

where r_P is the geocentric radius of point P.

Thereafter δg_P^I is subtracted from the surface gravity anomaly point values and added (in gridded form) after interpolation.

Interpolation methods

Most interpolation algorithms demand that the phenomenon described by the point data to be gridded could be regarded as a spatial stochastic process and the field to be

homogeneous: that is, stationary (the mean would be constant over space and the covariance would be position independent) and isotropic (the spatial dependence of values would be independent of direction). The reduction processes described earlier aim at fulfilling this requirement as rigorously as possible. However, in practice, the reduced gravity data are also somewhat non-stationary, anisotropic, and contain unavoidable observation errors, resulting in various deficiencies of grids obtained by different interpolation methods.

Numerous interpolation methods could be applied in gravity gridding. The four methods described below were selected as these have been demonstrated to yield reasonable gravity anomaly estimates and are also often used in similar studies.

Due to their varying nature, each method reveals different characteristics of the data. The first two of these methods are simple and fast deterministic methods that generate a spline-based surface. The latter two are stochastic methods that demand *a priori* information about the spatial correlation and quality of the data. In different ways, all four interpolation methods allow the resulting gravity anomaly surface to deviate from input data, thus accounting for inaccuracies of the input data.

Continuous curvature splines

According to this method, the gridded values z_P (functions of grid node co-ordinates x_P, y_P) are computed by solving:

$$(1 - T) \times L[L(z_P)] + T \times L(z_P) = 0 \qquad (12)$$

where $0 < T < 1$ is a tension factor and L is the Laplace operator. $T = 1$ results in a surface where maxima and minima are achievable only at data point locations while $T = 0$ results in a minimum curvature solution (Smith and Wessel 1990).

The continuous curvature splines interpolation method has been implemented in the Generic Mapping Tools (GMT, Wessel et al. 2013) sub-program *surface* and will hereafter be referred to as SURF. The default tension factor suggested by the program's manual for interpolation of potential field data is $T = 0.25$.

The SURF method is expected to generate a smooth gravity grid. However, it has previously shown some unreasonable undulation in larger data gaps, next to steep gradients and near the borders of input data area. It is possible to reduce the latter deficiency by setting the tension factor to 0 outside the research area. Another drawback of the SURF method is that it computes the z values on a planar surface. Thus the Earth's curvature-induced errors may become significant over larger research areas. Third, the uniformly chosen tension factor may not represent the behavior of the gravity field in all areas equally well. Note that, for practical purposes, the resulting grid has to be uniform and seamless. Therefore varying the tension factor manually according to different sub-areas is not a feasible option.

Spherical interpolation in tension

According to this method, a Delaunay triangulation on a sphere (e.g. Renka 1997a) is performed on input data. Then, given a certain tension factor (determined automatically from

local or global gradients) for each triangle side and arc containing the interpolation point and connecting a triangle vertex to the opposite side, a value is interpolated to the new point contained within that specific triangle, see e.g. Renka (1997b). Such a spherical interpolation in tension algorithm has been implemented in the GMT sub-program *sphinterpolate* and will hereafter be referred to as SPHI.

As this method is rather similar to the SURF method, it is expected to yield similar results, desirably improved by the high degree of automation in choosing the tension parameters and by accounting for the Earth's spherical geometry.

Least squares collocation

In the Least Squares Collocation (LSC) method, the gridded gravity anomaly values are obtained by solving the following matrix equation [Moritz 1980, (14.27)]:

$$\Delta \boldsymbol{g}_P = \boldsymbol{C}_{\Delta g_P \Delta g} \left(\boldsymbol{C}_{\Delta g \Delta g} + \boldsymbol{D} \right)^{-1} \Delta \boldsymbol{g} \tag{13}$$

where $\Delta \boldsymbol{g}$ is the vector of known (surveyed) anomaly point values, $\Delta \boldsymbol{g}_P$ is the vector of unknown (grid) values, $C_{\Delta g \Delta g}$ is the auto-covariance matrix of the $\Delta \boldsymbol{g}$ values, $\boldsymbol{C}_{\Delta g_P \Delta g}$ is the cross-covariance matrix of the $\Delta \boldsymbol{g}$ and $\Delta \boldsymbol{g}_P$ values, and $\boldsymbol{D}$ is the noise variance-covariance matrix. For further details, see Moritz (1980). LSC is implemented in the GEOGRID sub-program of the GRAVSOFT research software package (Forsberg and Tscherning 2008).

Importantly, for such an interpolation approach, the spatial dependence of the data in question is described by the covariance matrices and needs to be estimated from the survey data. This can be achieved by fitting a theoretical model to empirical covariance values. In this study, a second-order Markov model is used [Sansò and Sideris 2013, (9.34)]:

$$C(l) = C_0 \left(1 + \frac{l}{\alpha} \right) e^{-l/\alpha} \tag{14}$$

where $C(l)$ is the modelled covariance value over the distance l, C_0 is the signal variance, and α is a constant related to the correlation length $X_{1/2}$ approximately as $\alpha = 0.595 X_{1/2}$. The correlation length $X_{1/2}$ is here defined as the distance at which the covariance function reaches the value of $C_0/2$.

In addition, individual point weighting can be done using *a priori* standard deviation values supplied together with the gravity data, assuming that the variance-covariance matrix D in (13) is diagonal.

As an advantage, a formal error grid can be determined together with the LSC predictions. Being a powerful and flexible interpolation method, the LSC is expected to perform well in areas that correspond to the average correlation properties estimated. Unfortunately, a single covariance function is unable to fully describe a heterogeneous or anisotropic dataset, which is a rather common situation in gravity anomaly gridding. Research on the so-called non-stationary covariance function modelling is ongoing, see the detailed overview in Darbeheshti and Featherstone (2009).

Kriging

Kriging (Krige 1951, for a recent review see e.g. Cressie 2015) is an interpolation method that is similar to the concepts of LSC, for their differences see e.g. Dermanis (1984).

In the current study, Kriging is implemented using a different covariance function from LSC, namely, the spherical semi-variogram model $SV(l)$ [Isaaks and Srivastava 1989, (16.6)] is used:

$$SV(l) = \begin{cases} c_0 + [C_0 - c_0]\left[\dfrac{3l}{2A} - \left(\dfrac{l}{2A}\right)^3\right], & if \ l \leq A \\ C_0, & if \ l \ > \ A \end{cases} \tag{15}$$

where c_0 is the nugget effect and A is a length parameter corresponding to the range after which data are presumably no longer correlated. Note that the parameter A can be modified to account for the anisotropy effect. In the simplest case of the anisotropy angle being $0°$, A is divided by the anisotropy ratio. The semi-variogram values are related to the covariance values by

$$C(l) = C_0 - SV(l) \tag{16}$$

Kriging has many forms. In this study, Ordinary Kriging without a drift function implemented in the Surfer software (Golden Software LLC 2016) is used. This interpolation method will hereafter be referred to as KRIG.

Propagation of terrestrial gravity data errors into geoid modelling

The data-related error of a (quasi)geoid model comprises of omission errors (the lacking information with higher frequency than the model resolution) and commission errors (errors in the existing data). The latter can in turn be separated into uncorrelated (white noise) and correlated (systematic) parts.

The uncorrelated commission error has a relatively small effect as the positive and negative errors tend to cancel out. The most dangerous are long-wavelength systematic effects because the (quasi)geoid has most power in long wavelengths. This is illustrated by the spectral relationship of the geoidal undulation to gravity anomalies over the entire globe [e.g. Goos et al. 2003, (1)]:

$$N_n = \frac{R}{\gamma_0(n-1)}\Delta g_n \tag{17}$$

where N_n is the n-th degree surface spherical harmonic of the geoid height, R is the mean Earth radius, γ_0 is normal gravity on the surface of the reference ellipsoid, and Δg_n is the n-th degree surface spherical harmonic of the gravity anomaly.

In the simplified case of a sufficiently small spherical disc, the influence ε_N of a systematic gravity data error ε_g on the geoidal height N can roughly be estimated by Heiskanen and

Moritz [1967, (2)–(234)]:

$$\varepsilon_N = \frac{S}{g_P}\varepsilon_g \tag{18}$$

where g_P is the gravity value at the computation point and S is the polar distance. For instance, the presence of a 0.1 mGal gravity bias within a 100-km radius around the computation point yields a geoid error in the order of 1 cm.

Commonly, the Stokes (1849) formula is used to compute a gravimetric geoid from the gravity data. It can be modified so as to obtain the long-wavelength (global) information from a GGM (see e.g. Vaníček and Sjöberg 1991) that is more accurate than the terrestrial data in the long-wavelength spectrum. This alleviates the danger of having systematic errors in the regional gravity database. Nevertheless, since gravity data have usually been collected over long periods of time with varying accuracy and following different national conventions, it would be beneficial to analyse these in order to detect and eliminate systematic errors as much as possible, e.g. by a method in Saleh et al. (2013) or Wang et al. (2012).

Gravity point accuracy may currently be at the level of 5 μGal for absolute gravimetry (Niebauer et al. 1995) and 20–100 μGal for relative gravimetry surveys. However, as terrestrial gravity surveys are labour-intensive, a dense enough coverage of sufficient quality data is not available everywhere. Especially, the coastal and marine areas have gravity coverage of significantly lower quality and density (see e.g. Featherstone 2009).

A recent summary of the practical data requirements for a 1-cm geoid can be found in Denker (2013), see also references therein. It is concluded that gravity data need to be connected to a highly accurate gravity network (in the order of 0.01 mGal) while single observation accuracy of about 1 mGal is sufficient.

Ågren and Sjöberg (2014) show that a 5-mm geoid can be achieved within a medium-sized country (Sweden) if the gravity anomaly data with uncorrelated noise below 0.5 mGal and systematic errors below 0.1 mGal are available on at least 5 km resolution with no data gaps in the computation area or its vicinity. As this conclusion depends on the roughness of the gravity field, it is not necessarily general. For instance, the extremely rough gravity field in mountainous areas most likely requires a significantly denser gravity sampling.

Study area

In the NKG geoid modelling project the quasigeoid is computed for the area of 53° to 73° N, 0° to 34° E. This covers the territory of Denmark, Norway, Sweden, Finland, Estonia, Latvia, and Lithuania plus the surrounding areas, including the Baltic Sea, North Sea, and large parts of the Arctic Ocean (cf. Figure 1). The gravity data from the NKG database cover the area of 52° to 74° N, -2° to 36° E. It is a heterogeneous region covering both land and marine areas. Norway has a rugged terrain with deep fjords and heights exceeding 2 km while in Denmark and the Baltic countries (Estonia, Latvia, Lithuania) the topographic heights only reach a few hundred metrs, see Figure 1.

The NKG gravity database holds data submitted by participating countries for NKG geoid modelling purposes only. The information is stored as 'publications' (groups of observations submitted together) that have various amounts of meta data in the form of a report or short description. Most publications include a single approximate error estimate while some newer
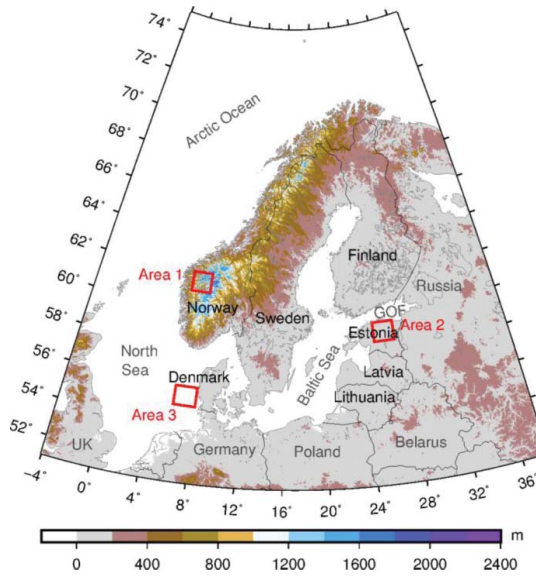
Figure 1. Terrain elevations of the NKG data area.

ones contain individual and well-reasoned error estimates for each data point. The distribution and estimated accuracy of gravity data in the NKG database are shown in Figures 2 and 3, relevant characteristics are summarized in Table 1.

According to the previous section, the average gravity coverage (that corresponds to a distance of about 3.5 km between neighbouring points) could be sufficient for computing a geoid model with an accuracy of 5–10 mm. However, the average *a priori* error esti-
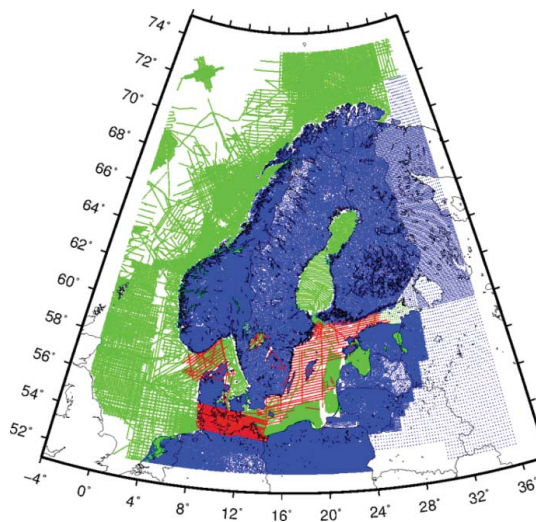
Figure 2. Distribution of the NKG gravity point data (blue—terrestrial, green—marine or sea bottom, red—airborne).
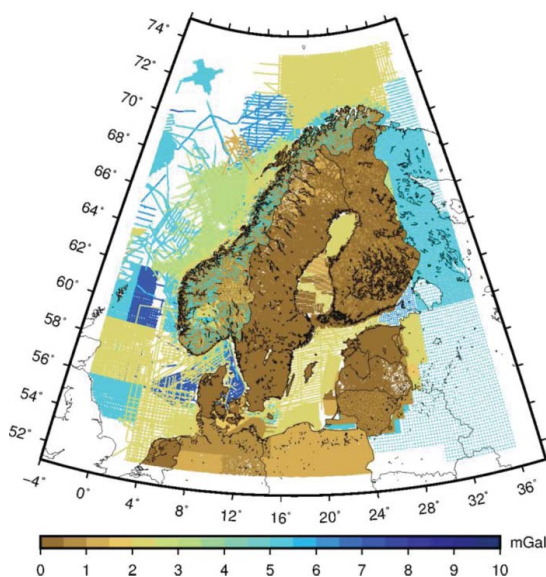
Figure 3. *A priori* error estimates of the NKG gravity point data.

mate of gravity data is about 2.3 mGal which does not meet the aforementioned requirements.

To illustrate the differences in gravity field modelling methods, three test areas of $1° \times 2°$ with contrasting characteristics that could commonly occur in any regional gravity field study were selected. Area 1 (61° to 62° N, 6° to 8° E, Figures 4a and 5a) was selected in the Sognefjord area, Norway. Sognefjord is a 200-km-long and, on average, 4.5-km-wide fjord

Table 1. Characteristics of the research and test area data.

		Full area	NKG area[a]	Area 1	Area 2	Area 3
No. of points		512772	172406	4509	8043	1819
(after selection)[b]		421108	141418	1609	5928	1518
1 point per no. of km²		11.9	8.1	2.7	1.5	6.7
(after selection)		14.4	9.8	7.5	2.0	8.0
Elevation (m)[c]	Mean	107	304	882	68	0
	StDev	196	305	481	23	0
	Min	0	0	0	0	0
	Max	2419	2419	1977	146	0
Free-air anomaly (mGal)	Mean	−0.48	0.97	−61.84	−12.92	5.71
	StDev	26.41	28.07	61.24	9.80	11.53
	Min	−307.79	−307.79	−117.70	−45.52	−19.10
	Max	210.46	210.46	145.59	18.18	35.91
(after selection)	Mean	−0.35	1.35	−16.62	−12.70	5.40
	StDev	24.65	27.48	75.33	9.90	10.97
A priori gravity	Mean	2.32	1.83	2.01	0.34	3.76
error estimate (mGal)	StDev	1.86	2.07	1.78	0.11	2.06
	Min	0.10	0.10	0.20	0.10	2.00
	Max	7.00	5.00	5.00	0.80	7.00
(after selection)	Mean	2.22	1.63	3.09	0.32	3.81
	StDev	1.84	1.99	2.09	0.12	2.10

[a]Dry land and inland water territory of the participating Nordic-Baltic countries.
[b]After preserving a single point with the lowest *a priori* error estimate in each 0.01° × 0.02° grid cell.
[c]Topographic elevation statistics are given from the 0.001° × 0.002° DTM.
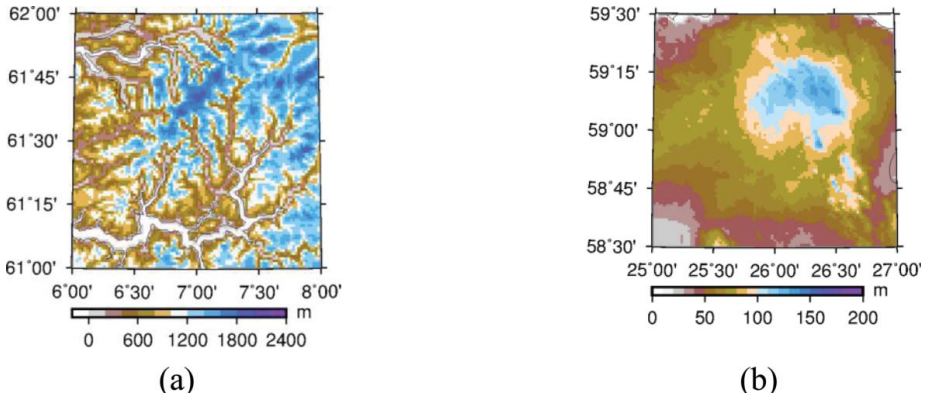
Figure 4. Terrain elevations in the test areas (note the different colour scales). (a) Area 1—Sognefjord area. (b) Area 2—central Estonia.

with depths up to 1300 m surrounded by rugged cliffs. Area 2 (58.5° to 59.5° N, 25° to 27° E, Figures 4b and 5b) was selected in central Estonia with flat terrain and unusually dense coverage of accurate gravity data. Area 3 (55° to 56° N, 6° to 8° E, Figure 5c) was selected in the marine area West of Denmark containing ship gravimetry tracks only. The data statistics for these test areas can also be found in Table 1. Area 2 is an example of very good gravity coverage and quality that comfortably fulfils the accuracy requirements discussed in above while Area 1 and 3 have similar statistics to that of the entire NKG area. The importance of eliminating systematic long-wavelength errors was also stressed. In the current study, it was assumed that, due to the great care taken in preparing the NKG database by representatives of the participating countries, such errors would be minimal, at least for the Nordic-Baltic countries. An example of examining national data for the presence (and elimination) of systematic errors within the current study area can be found in Ellmann et al. (2009).

For gravity data processing and evaluation, it is necessary to possess, in addition to the gravity survey values and positions, some supplementary information. First, a high-resolution DTM is necessary for terrain correction computation by (4). Second, a GGM is needed
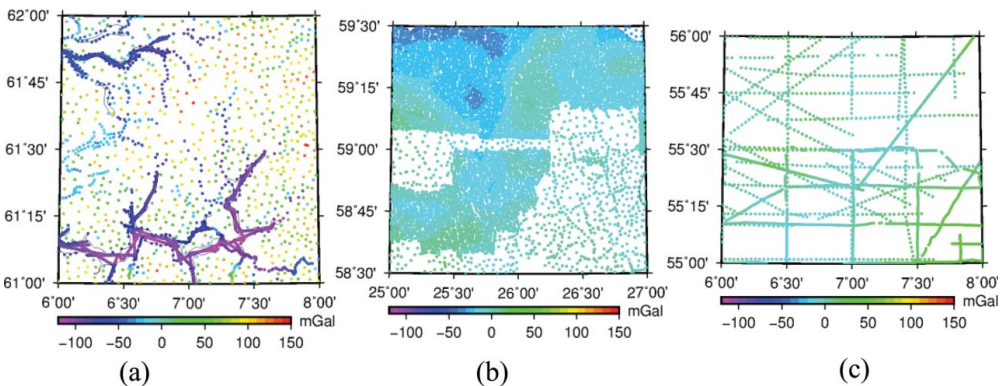
Figure 5. Free-air gravity anomaly point data available in the test areas. (a) Area 1—Sognefjord area. (b) Area 2—central Estonia. (c) Area 3—West of Denmark.

for generating a reference gravity field used in (6). Optionally, co-located GNSS and levelling points can be used for geometric geoid determination for comparison with the gravimetric geoid models derived from the gravity grids.

As the current research was aimed at the NKG2015 geoid modelling project, it made use of the $3'' \times 3''$ NKG DEM 2014, which in the present study was further averaged to $0.001° \times 0.002° \approx 3.6'' \times 7.2''$ (Figure 1) and 2538 GNSS/levelling points specially compiled by the participating countries. Additionally, the project specification allowed for the use of either the high-degree EIGEN-6C4 (Förste et al. 2015) or the satellite-only GO_CONS_GCF_2_DIR_R5 (Bruinsma et al. 2013) global geopotential model.

Preprocessing gravity data

In this section, numerous steps of data preprocessing are described. It illustrates possible ways of solving unification issues of a heterogeneous gravity dataset and could be of reference to other geoscientists working on similar tasks.

Reference systems

When working with gravity data from different sources, it is first necessary to make sure that their horizontal positions, heights, and gravity values are in the same reference frames and include the same, compatible corrections (e.g. tidal, atmospheric). In areas with significant geodynamic motions, like the postglacial land uplift in the Nordic-Baltic region, it is also important to choose a common reference epoch. Although small in magnitude, the errors introduced by inconsistencies in the above are systematic and widespread, thus of importance in geoid modelling [see (17) and (18)].

In the NKG2015 geoid modelling project, it was set as a goal to transfer datasets of different nations into uniform reference systems/frames. A common postglacial land uplift epoch of 2000.0 and the zero permanent tide system were selected. The gravity values are given in the official national gravity systems based on either modern absolute gravimetry or on the International Gravity Standardisation Net 1971 (IGSN71, Morelli et al. 1971), in the latter case, with a correction to convert from the mean tide to zero permanent tide system. Atmospheric corrections are not included in the NKG gravity database. Point positions are expressed in the national European Terrestrial Reference System (ETRS) 89 realisations and the normal heights in the national European Vertical Reference System (EVRS) realisations. More details on the NKG2015 geoid modelling project are available in Ågren et al. (2015, 2016).

Update and analysis of the NKG gravity database

Data updating for the NKG2015 geoid model project consisted of revising all the information in the NKG gravity database, cleaning or removing overlapping datasets and replacing or updating with new data in the correct reference systems/frames, permanent tide system and postglacial land uplift epoch. It was the responsibility of national representatives to decide which data to preserve and also to quality check all the remaining data within the country.

The above rather challenging requirements on reference systems, unintentionally, resulted in some large data voids. After extensive analysis, an exception was made for instance to parts of publication no. 345 that cover data void areas east of the Latvian border. The filling of this void affected the resulting quasigeoid model by around 2 cm in Eastern Latvia.

The Nordic and Baltic countries are surrounded by marine areas that possess significant variations in gravity signal which can affect the gridding result also in coastal areas. Therefore an effort has been made over the past decades to cover these areas with terrestrial, shipborne, airborne, and on-ice gravimetric data.

When updating the gravity database, a bias was found and corrected between two marine datasets in Skagerrak, the strait between Norway and Denmark. Another problematical area is the eastern part of Gulf of Finland (GOF) where there are practically no terrestrial/marine data available in an area of about 20000 km^2. It is not clear if there have ever been any surveys. Regardless, these are not available to the NKG community. Yet, information from this area directly affects the gravity gridding and subsequent quasigeoid modelling in Southern Finland and Northern Estonia, regions of intense shipping and economical activities. Therefore, to fill the data void in the eastern part of GOF, a patch was generated by evaluating the GO_CONS_GCF_2_DIR_R5 GGM up to d/o 240 at empty cells of $0.01° \times 0.02°$ in the area of 59° to 62° N and 25° to 30° E.

Further improvements in gravity coverage over the marine areas are expected within the frames of the ongoing Finalizing Surveys for the Baltic Motorways of the Sea (FAMOS Consortium 2014) international cooperation project.

In the context of gravity gridding, it is important to notice that the distribution of data varies on land and sea. Gravity points surveyed on land are rather uniformly distributed while marine data are gathered along ship tracks. For the optimum gridding results, these would demand different interpolation approaches. For example, the SURF and SPHI algorithms may generate unnecessary undulations or large extrema in the relatively large data gaps between tracks. This is likely a result of the selected tension factor allowing the spline surface to undulate with a larger amplitude than appropriate. The alternative statistical LSC and KRIG methods using a covariance function to model the spatial dependence of gravity values can also start undulating between tracks. Consider the following example: marine tracks are separated by 100 km and the spatial correlation goes to (nearly) zero in, say, 30 km, then the resulting gravity anomaly grid may contain artificial stripes. The actual performance of interpolation algorithms in marine areas will be analyzed in a later section.

Automatic blunder detection

Plotting and visual inspection of data and their derivatives (such as the reduced gravity field in this case) can help detect gross errors, see e.g. Vergos et al. (2005, Section 2.2). However, larger datasets need a more automatic approach. A simple, yet effective, method for automatic detection of outliers can be leave-one-out cross validation (CV). CV limits are, however, very dependent on the spatial variability of the modelled quantity. Therefore, it is best used after the reduction of gravity anomaly values to assure a minimally and homogeneously varying quantity across the entire research area.

Nevertheless, it is challenging to find a uniform CV limit suitable for a heterogeneous area. In the current research area, CV limits as high as 20–30 mGal remove as many as

0.1–1% of the total points. Most of these are located in the rugged landscape such as the Norwegian mountains and clearly represent the actual gravitational signal. Meanwhile, no points are removed over the other areas, where a much lower CV limit would be needed.

Certainly, automatic CV with a fixed limit across such a heterogeneous area is questioble. Recall that manual separation of the research area into sub-areas cannot be considered for practical reasons. Additionally, the reduced gravity fields computed as described earlier have different characteristics, again demanding for slightly different CV limits. Therefore, means to automatically differentiate CV limits between rougher and smoother parts of the (reduced) gravity field under consideration can be investigated in further studies. Meanwhile, it was decided that for the purpose of the gridding-related research reported in this contribution, no CV will be used. This will also ensure that the different gravity anomaly grids will be comparable. Fortunately, an effort has already been made by participating countries to remove obvious gross errors from the NKG database.

Downward continuation of airborne data

Airborne gravimetry has proved to be a useful and fast method for covering large, sometimes hard-to-reach, areas with gravity data, for connecting different terrestrial gravity surveys and for improving the gravity field models in areas of high gravity field variability or low terrestrial point density (such as coastal and marine areas), see e.g. Bae et al. (2012), Bolkas et al. (2016), Tscherning et al. (1998), Forsberg and Olesen (2010), and Hwang et al. (2007). Several low-elevation airborne gravity datasets are also available over the marine parts of the study area, see the red-coloured tracks in Figure 2.

Aerogravity values are measured at flight altitudes. Due to the attenuation effect, it is not sufficient to use the free-air gravity gradient (approx. $0.3086H$) to 'lower' these to the topographic surface. Instead, an additional downward continuation (DWC) correction needs to be added. After DWC, airborne data can be treated as terrestrial data. For the computation of the DWC correction, two different methods were tested.

Method 1: The DWC correction is taken to be equal to the free-air anomaly difference at the flight altitude and the surface by using a high-degree GGM (Ellmann 2011). The EIGEN-6C4 GGM was used in numerical computations.

A drawback of this method is that it is limited to the maximum spherical harmonic degree of the GGM, that is 2190. Also, the detailed gravity anomalies available for the regional geoid determination are not utilised. Instead, the unknown and possibly lower quality GGM-derived gravity anomalies are used.

Method 2: The vertical gradient of the reduced gravity anomaly (in this study, the RTM anomaly) is estimated and used to DWC the reduced airborne data. Such a method is limited to the first linear term in the Taylor expansion of the reduced gravity anomaly with respect to the height. Also, numerical problems might occur when estimating the gradient, although the reduced field should be suitable for such a task. As opposed to Method 1, there is no limitation of the maximum spherical harmonic degree, and the input information is of high quality.

The standard deviation and maximum value of the DWC corrections computed are 0.37 and 3.3 mGal for Method 1 and 0.47 and 8.7 mGal for Method 2, respectively. The standard deviation of the method differences is 0.38 mGal and the mean difference is 0.04 mGal. The larger differences occur over Denmark and Sweden, where the flight heights were much

higher than over the Baltic Sea (around 1000 and 250 m, respectively). Considering that the measuring noise of these airborne datasets is around 2 mGal, such differences between the methods can be considered negligible and either method can be used.

Covariance analysis

To provide LSC or KRIG interpolation with spatial correlation information, a covariance analysis was performed on the reduced (either Bouguer or RTM) gravity anomalies.

First, the entire research area was considered. Empirical covariance functions were computed for the RTM and Bouguer anomaly data, to which the second-order Markov covariance functions (14) were fitted, see Figure 6a and e. Similarly, spherical semi-variogram models (15) were computed. These were later used in the LSC or KRIG interpolations, respectively. For comparability, the semi-variogram models were then converted to covariance functions by (16) and also depicted in Figure 6a and e.

For reference, the empirical covariances of individual test areas were also estimated, see Figure 6b–d, and f–h. Note, that separate theoretical covariance functions were not fitted for the test areas as these would not be used in the interpolation process. For the Bouguer anomalies only, the three test areas were extended by 1° in the NS direction and 2° in the EW direction, to increase the reliability of covariance estimation (because Bouguer anomaly correlation length is in the same order as the test area size).

These figures illustrate the variability of spatial correlation of gravity anomalies between the test areas. Judging by the fit between empirical and theoretical covariance curves, a
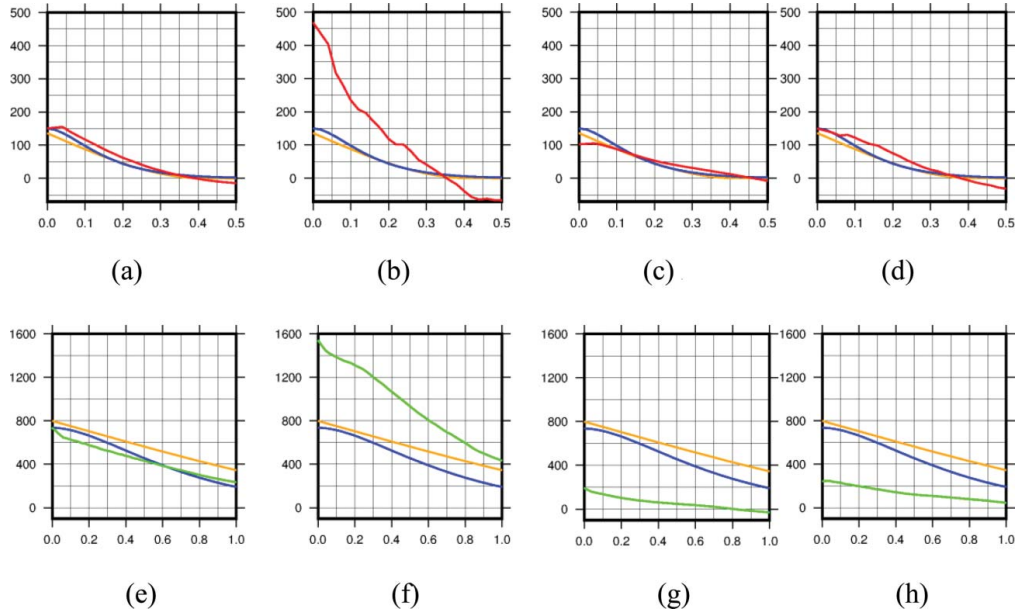
Figure 6. Covariance functions for the RTM (top row) and the Bouguer (bottom row) anomalies[*]. (a and e) Full area; (b and f) Area 1; (c and g) Area 2; and (d and h) Area 3. [*]The red or green lines depict the empirical covariance function, blue line the second-order Markov and orange line the spherical model. Spherical distance [°] and variance [mGal^2] are represented on the horizontal and vertical axes, respectively.

reasonable interpolation result can be expected in Areas 2 and 3 using the RTM anomalies. In case of the Bouguer anomalies, the theoretical covariance function either under or overestimates the spatial correlation in all the test areas.

Table 2 lists the estimated correlation lengths $X_{1/2}$ for both reduction methods. It is worth noting that the correlation lengths vary less for the RTM anomalies, while these of the Bouguer anomalies vary almost three times between the test areas. Another advantage of using the (relatively short correlation length) RTM anomalies for gridding is that in larger data voids, the underlying GGM and DTM will provide the missing information instead of the interpolation algorithm attempting to estimate the values based on spatial correlation.

As a result of covariance analysis, for practical computations, the following parameters were chosen (by rounding downwards): $X_{1/2} = 15$ km and $A = 1°$ for the RTM anomalies; $X_{1/2} = 70$ km and $A = 6°$ for the Bouguer anomalies.

Generating gravity anomaly grids

Before testing the different gravity reduction and interpolation processes on the NKG gravity data, the following practical steps were taken.

First, all data with *a priori* error estimates ≥ 8 mGal were excluded from the gridding. This limit corresponds to the highest realistic error estimates of the NKG gravity data.

Second, to improve interpolation quality along the edges of the area of interest, additional gravity data were derived (on a regular grid of $0.01° \times 0.02°$ not closer than $0.15°$ to any existing points) from EIGEN-6C4 GGM evaluated to its maximum d/o 2190 to fill all data gaps in the area of $51°$ to $75°$ N, $-4°$ to $38°$ E. This was considered sufficient for the purposes of this study. However, considering the convergence of the meridians, an even larger buffer area should be used for the actual geoid modelling in sub-polar latitudes. The error estimate of these fill-in points was set to 6 mGal to comply with the typical accuracy of GGMs over the oceans (see Förste et al. 2015; Andersen 2010) and to be larger than that of most observed data.

Third, the airborne observations were downward continued by Method 1. Fourth, multiple observations within a 50-m horizontal range were identified, arithmetically averaged, and the standard deviation of the resulting point was taken to be equal to the minimum standard deviation input value of the multiple-point cluster.

Fifth, the effect of using the atmospheric and ice corrections on the resulting surface gravity anomaly grid and the subsequent quasigeoid model were analysed. For this, a gravity

Table 2. Estimated correlation lengths of gravity anomalies[*].

Grid	Area	$X_{1/2}$ (°)	$\approx X_{1/2}$ (km)
$\Delta g^{CBA,A,I}$	Full area	0.65	71.5
	Area 1	0.63	69.3
	Area 2	0.23	25.3
	Area 3	0.49	53.9
$\Delta g^{RTMA,A,I}$	Full area	0.17	18.7
	Area 1	0.11	12.1
	Area 2	0.21	23.1
	Area 3	0.21	23.1

[*]Explanation of the symbols used in this and the following tables can be found in the text.

anomaly grid or corresponding quasigeoid with the atmospheric or ice corrections included in gridding was subtracted from an analogous product computed without these corrections.

The effect of using the atmospheric correction (8) in the RIR process has a distinct pattern that is correlated with height. However, it is in the order of only ± 0.1 mGal on the resulting surface gravity anomaly grid in the most rugged parts (Area 1) of the research area. The corresponding effect on the resulting quasigeoid model is certainly negligible with a standard deviation of 0.3 mm and the maximum difference reaching only 2 mm.

The effect of using the ice correction (11) in the gridding process is relevant only in the vicinity of Norwegian glaciers. In Area 1, it has a standard deviation of 1.4 mGal with maximum differences reaching 21 mGal, where the ice thickness reaches 440 m, see Figure 7a and b. Comparison of the resulting quasigeoid models reveals a systematic difference reaching 5 cm in the ice-affected area, see Figure 7c.

Although the atmospheric correction is very small and the ice correction is significant only in Norway, both were applied in all of the test computations of the current study. Recall, that a superscript A or I denotes quantities that are also corrected for the atmospheric or ice effect, respectively.

Grids computed via Bouguer anomalies

Grids computed via Bouguer anomalies were compiled in the following way:

(1) The free-air anomaly point observations Δg^{FAA} (Figure 8) were reduced to simple Bouguer anomalies Δg^{SBA} according to (2). For the result, see Figure 9a.

(2) The Δg^{SBA} were further converted to complete Bouguer anomalies Δg^{CBA} according to (3) by removing the terrain corrections δg^{T} (Figure 9b). The terrain corrections were computed according to (4) and (5), using the DTM grid of $0.001° \times 0.002°$ to a distance of 15 km and the DTM grid of $0.01° \times 0.02°$ to a distance of 200 km. Practical computations within the radius of 15 km were done using the GRAVSOFT sub-program TC. The DTM was locally spline interpolated to fit the given height of the gravity observation in the computation point P (Forsberg 1984, p. 114). The sub-program TCFOUR that speeds up the computation by Fast Fourier Transformation convolutions was used for the distance of 15–200 km.
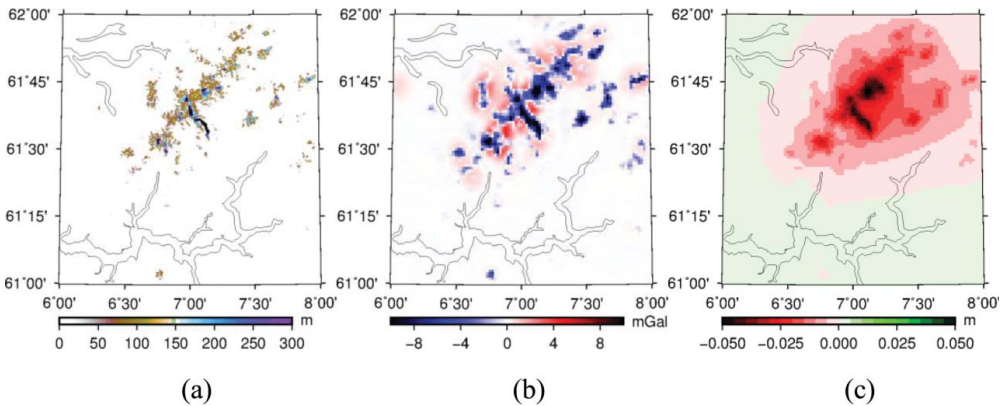
Figure 7. Ice thickness-related effects in Area 1. (a) Ice thickness. (b) Effect on the gravity field. (c) Effect on the quasigeoid.

(3) Since the atmospheric correction is not included in the NKG database, (8) was applied.

(4) The ice correction was applied as described earlier. In practice, it was computed exactly as in Ågren (2004, Chapter 6), using rectangular prisms (4) in the vicinity (closer than 0.1° in latitude and 0.2° in longitude) of each computation point P and spherical quadrature formulas with strict integration in the vertical (Martinec 1998, Section 3.8; Sjöberg 2000, Section 4) beyond the aforementioned limits. The ice density was set to 0.917 g.cm^{-3}, topographic density to 2.67 g.cm^{-3}, and the isostatic compensation depth was selected as 30 km.

(5) For practical implementation of most interpolation algorithms, the scattered point data should first be low-pass filtered or averaged according to the grid step of the final grid to reduce cluttering (or high frequency information) that results in aliasing. Therefore, the point data to use were then selected so that a single point with the smallest *a priori* error estimate was preserved in each 0.01° × 0.02° cell (c.f. Table 1).

(6) The resulting point values were interpolated to a regular grid using all the algorithms described previously; for a sample result, see Figure 11a.

For the SURF algorithm, the GMT default tension factor of $T = 0.25$ was used. Note that the research area is situated in sub-polar latitudes, around 60° N. Therefore, an aspect ratio of $\delta\varphi = \frac{1}{2}\delta\lambda$ (where φ is the latitude, λ the longitude, δ the grid step increment) was used for remedying the effect of the convergence of meridians.

For the SPHI algorithm, a smoothing interpolation with global gradient estimation was chosen with the -Q3 option in the GMT sub-program *sphinterpolate*, see Renka (1997b).

When computing a LSC solution in GEOGRID, the signal variance C_0 is automatically determined for the entire computation area, but for computational efficiency, only a limited number of (in this case 10) closest points in each quadrant are used in the prediction of each point. The second-order Markov model is always used with the user-specified length $X_{1/2}$. Importantly, in this research, a minimum limit of 0.5 mGal was set for point standard deviation values as a measure to dampen oscillations generated by closely located points that have a small standard deviation but a larger difference in values.

For the KRIG solution, the nugget effect c_0 was set to 1 mGal.

(7) The ice and atmospheric effects were removed on the grid, resulting in a complete Bouguer anomaly grid.

(8) The terrain correction of (4) and (5) was subtracted to yield the simple Bouguer anomaly grid.

(9) The simple Bouguer correction of (2) was added to the grid, yielding the final surface gravity anomaly grid.

The effect of reducing gravity values to Bouguer anomalies is illustrated in Table 3, Figure 8 vs. 11a and Figure 12c vs. 12a. Note, that this reduction did not reduce the overall amplitude of the anomalies. The standard deviation of Δg^{FAA} is 26 mGal while that of $\Delta g^{CBA,A,I}$ is 28 mGal. However, there is a significant effect in the rugged Area 1 where the standard deviation of $\Delta g^{CBA,A,I}$ is three times smaller than that of Δg^{FAA}, see Table 3. The figures show that the reduced gravity field is much smoother and less detailed than the surface gravity field, thus also more suitable for interpolation.
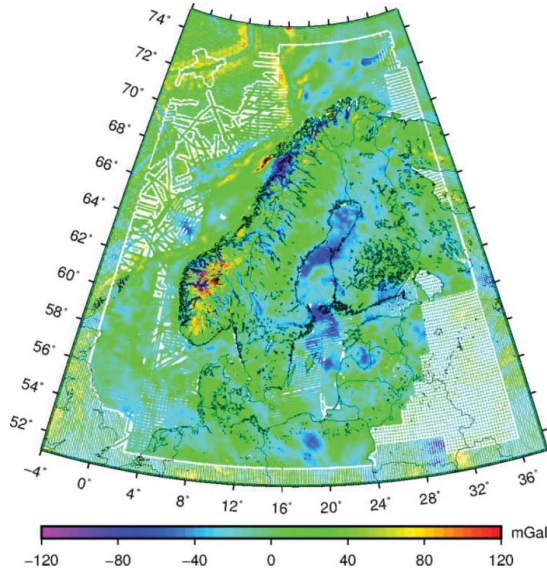
Figure 8. Free-air anomaly Δg^{FAA} data points.

Grids computed via RTM anomalies

Grids computed via RTM anomalies were compiled in the following way:

(1) The free-air anomaly point observations Δg^{FAA} (Figure 8) were first reduced by subtracting Δg^{GGM}, the second term on the right-hand side of (6). Δg^{GGM} was computed by evaluating the GO_CONS_GCF_2_DIR_R5 model up to its maximum d/o 300. For the result, see Figure 10a.

The computation of Δg^{GGM} at point P was simplified to computing two regular grids at different (minimum and maximum) altitudes and then interpolating both in horizontal

(a)

(b)
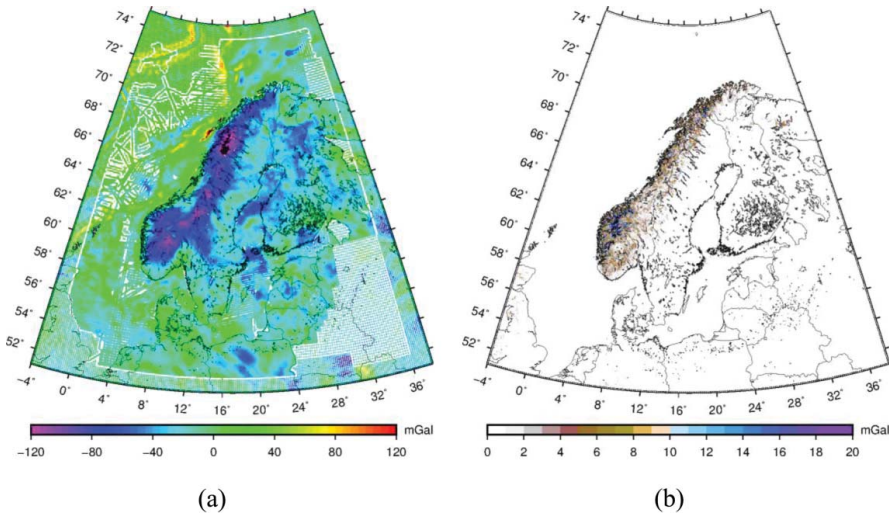
Figure 9. The Bouguer reduction. (a) Simple Bouguer anomalies Δg^{SBA}. (b) Terrain corrections δg^T.

Table 3. Statistics of the NKG gravity anomaly points.

Quantity	Full area[a]				Area 1			
	Mean	StDev	Min	Max	Mean	StDev	Min	Max
Δg^{FAA}	−0.48	26.41	−307.79	210.46	−61.84	61.24	−117.70	145.59
Δg^{SBA}	−9.91	29.03	−307.79	174.59	−85.54	19.40	−117.70	−25.91
Δg^{CBA}	−9.29	28.06	−255.31	176.50	−72.68	20.44	−108.77	−23.13
$\Delta g^{CBA,A,I}$	−8.44	28.07	−254.46	177.34	−71.97	20.41	−108.01	−22.43
$\Delta g^{CBA,A,I}$ (selected)[b]	−8.96	27.13	−254.46	177.34	−61.04	18.97	−107.80	−22.47
$\Delta g^{FAA} - \Delta g^{GGM}$	−3.68	20.95	−342.93	177.49	−109.44	59.95	−181.43	94.03
Δg^{RTMA}	−1.28	13.15	−242.55	194.26	−31.07	24.26	−79.26	30.82
$\Delta g^{RTMA,A,I}$	−0.42	13.15	−241.70	195.10	−30.36	24.23	−78.51	32.23
$\Delta g^{RTMA,A,I}$ (selected)	0.21	12.27	−241.70	195.10	−15.98	21.64	−78.51	31.23

[a]Including the EIGEN-6C4 GGM based fill-in on the edges, 524,274 points.
[b]After preserving only the point with the lowest *a priori* error estimate in each $0.01° \times 0.02°$ grid cell.

and vertical direction to specific point locations P (Forsberg 1997), thus reducing computational effort.

(2) The GGM-reduced point observations were further reduced by removing the RTM contribution (Figure 10b) computed according to (7). The integration to compute the RTM effect was again performed over a grid of $0.001° \times 0.002°$ to a distance of 15 km and a grid of $0.01° \times 0.02°$ to a distance of 200 km using the GRAVSOFT sub-programs TC and TCFOUR.

The height reference surface for the RTM reduction was computed by averaging the DTM to approximately the same resolution as the GGM. This was motivated by the fact that the GGM removal in the previous step also removes the topographic effect below the maximum d/o used and the aim of the RTM reduction is to remove the remaining topographic contribution beyond the maximum d/o used in the previous step.

(3) The atmospheric and ice correction were applied.

(4) The same selection process was applied.

(5) The resulting point values were interpolated. For a sample result, see Figure 11b.

(6) Again, the ice and atmospheric effects were removed on the grid, resulting in a RTM anomaly grid.

(7) The RTM contribution was restored on the grid.

(8) The GGM contribution was restored on the grid, yielding the final surface gravity anomaly grid.

The effect of reducing gravity values to RTM anomalies is illustrated in Table 3, Figure 8 vs. 11b and Figure 12c vs. 12b. Note, how the variability of the gravity field lowers: the overall standard deviation of Δg^{FAA} is 26 mGal while that of $\Delta g^{RTM,A,I}$ is only 12 mGal. The variability of the field in Area 1 again reduces about three times, see Table 3. The reduced gravity signal is of short wavelength and uniform across most of the research area.

It is worth noting that the standard deviation of $\Delta g^{RTM,A,I}$ is two times smaller than that of $\Delta g^{CBA,A,I}$ in the overall statistics, but slightly larger in Area 1 statistics. This suggests that RTM and Bouguer anomalies could be more suitable for gridding in low-elevation and rugged terrain areas, respectively.
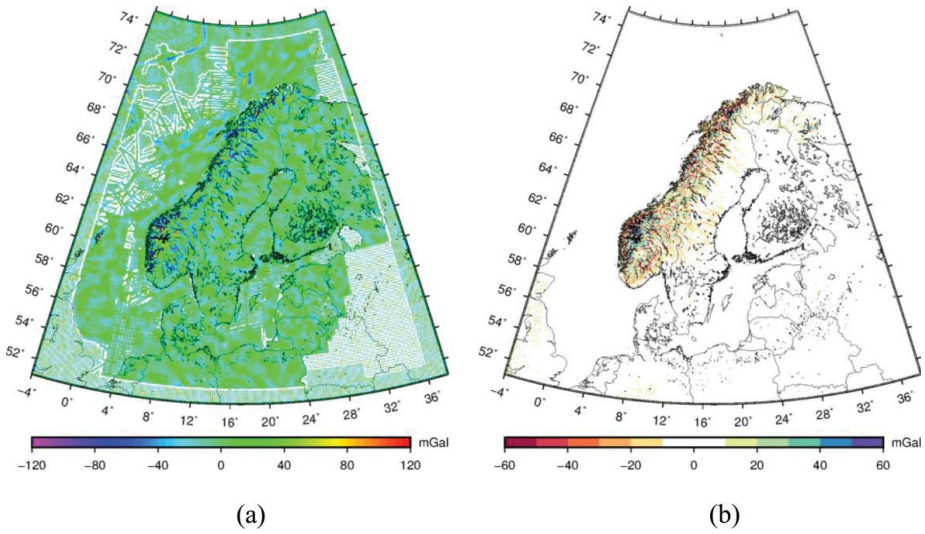
Figure 10. The RTM reduction. (a) Difference $\Delta g^{FAA} - \Delta g^{GGM}$. (b) RTM effect δg^{RTM}.

Test grids

Altogether, fourteen different free-air anomaly grids were computed, see Table 4. Grids named G1–G4 and G5–G8 were computed exactly as described previously, using the corresponding interpolation method in the first column of Table 4. Grids with the suffix B or C are special cases of the above.
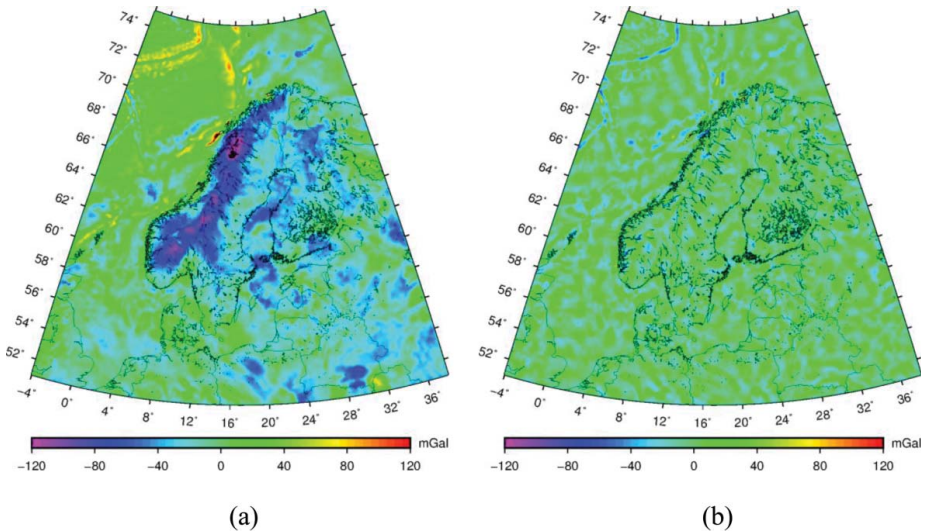
Figure 11. Reduced gravity anomaly grids (interpolated by LSC). (a) $\Delta g^{CBA,A,I}$ grid (G3). (b) $\Delta g^{RTMA,A,I}$ grid (G7C).
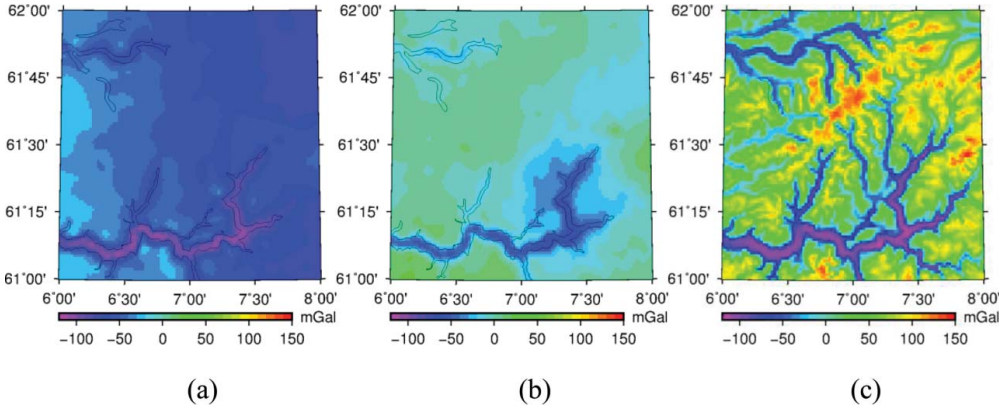
Figure 12. Reduced (a, b) and restored (c) LSC-derived gravity anomaly grids in Area 1. (a) $\Delta g^{CBA,A,I}$ grid (G3). (b) $\Delta g^{RTMA,A,I}$ grid (G7C). (c) Δg^{FAA} grid (G7C).

For instance, G3B and G7B denote LSC grids that were computed by not using *a priori* gravity error information from the NKG database, but a fixed value of 1 mGal instead. This was motivated by the varying quality of the *a priori* error estimates (see Figure 3). For example, most terrestrial gravity observations in Norway hold a pessimistic error estimate of 5 mGal while most error estimates of analogous data over the other participating countries

Table 4. Reduced gravity anomalies minus interpolated values from the reduced grid, units in mGal.

Interpolation method	Grid	Mean	RMS	Min	Max	Grid	Mean	RMS	Min	Max
		$\Delta g^{CBA,A,I}$					$\Delta g^{RTM,A,I}$			
				Full area						
SURF	G1	−0.0035	0.8667	−121.74	81.87	G5	−0.0034	0.8670	−121.71	82.31
SPHI	G2	−0.0062	0.5649	−71.60	82.47	G6	−0.0063	0.5667	−71.59	82.46
LSC	G3	−0.0052	2.5168	−141.87	137.37	G7	0.0260	2.0091	−164.22	236.20
KRIG	G4	−0.0029	0.9108	−127.91	120.11	G8	−0.0031	0.8873	−118.20	111.26
SPHI (no δg^T)	G2B	−0.0050	0.6737	−136.18	80.55					
SPHI (GGM d/o 240)						G6B	−0.0064	0.5641	−71.59	82.47
LSC (all 1 mGal)	G3B	−0.0129	1.7532	−228.46	176.31	G7B	−0.0030	1.2008	−186.71	155.08
LSC (Norw. 1 mGal)	G3C	−0.0404	2.1944	−227.25	176.31	G7C	0.0042	1.5158	−186.44	155.08
				Area 1 – Sognefjord area						
SURF	G1	−0.0747	2.5996	−20.72	21.76	G5	−0.0721	2.6112	−20.79	21.90
SPHI	G2	−0.3660	1.7543	−10.48	27.63	G6	−0.3695	1.7577	−10.46	27.66
LSC	G3	0.0430	6.2978	−25.22	39.69	G7	0.5041	5.3594	−21.33	40.51
KRIG	G4	−0.1750	2.8376	−10.78	29.36	G8	−0.2068	2.6996	−11.86	28.20
LSC (Norw. 1 mGal)	G3C	−0.5782	5.9242	−22.33	28.30	G7C	−0.2090	3.8518	−19.18	22.66
				Area 2 – central Estonia						
SURF	G1	0.0036	0.2073	−0.93	1.76	G5	0.0046	0.2078	−0.95	1.80
SPHI	G2	−0.0011	0.1335	−0.71	0.87	G6	−0.0008	0.1336	−0.71	0.87
LSC	G3	0.0006	0.3425	−1.94	2.01	G7	−0.0007	0.2007	−1.26	1.10
KRIG	G4	−0.0015	0.1983	−1.31	1.10	G8	−0.0008	0.1916	−1.24	1.04
				Area 3 – West of Denmark						
SURF	G1	0.0252	0.9318	−6.03	6.26	G5	0.0236	0.9311	−6.02	6.28
SPHI	G2	0.5608	0.5614	−3.37	4.01	G6	0.5606	0.5613	−3.37	4.01
LSC	G3	−0.4540	2.9997	−10.60	7.81	G7	0.2697	1.7776	−10.75	7.71
KRIG	G4	0.0153	0.8634	−5.37	3.70	G8	0.0088	0.8530	−5.16	3.55

have been set to represent the actual quality of the observations (typically less than 1 mGal) after careful analysis.

G3C and G7C denote LSC grids for the computation of which only the *a priori* error estimates of terrestrial points located in Norway were set to 1 mGal. Although the difference from grids G3B and G7B is numerically rather small, the C version grids allow to keep the error information in the other countries.

G2B represents a grid otherwise like G2 with the exception that the GGM contribution Δg^{GGM} was computed up to d/o 240 instead of the maximum d/o 300 of the satellite-only model used. The corresponding difference of the two gravity grids and the resulting quasigeoid models is rather insignificant: the standard deviation is 0.44 mGal and 0.6 mm, respectively. The absolute maximum deviation in the resulting quasigeoid models is 1.4 cm.

G6B represents a grid otherwise similar to G6, except that the removal and restoration of the terrain correction δg^T was omitted to illustrate its effect on the gravity field and the resulting quasigeoid model. As expected, the effect is small elsewhere, but significant in rugged terrains such as Norway. In terms of the resulting quasigeoid model, the standard deviation of differences over Norwegian territory is 1.8 cm and maximum deviations reach 30 cm.

Assessment of the gravity anomaly grids

Interpolation methods

First, the grids were analyzed to evaluate the different interpolation methods. One way to do so is to examine the differences of reduced anomaly point data and the resulting reduced grid values at the point locations, see Table 4. As an illustration, these are presented for G6, G7, and G7C in Figure 13. The residuals of SURF (G1, G5) and KRIG (G4, G8) methods appear to be numerically quite similar to those of SPHI (G2, G6).

The SPHI method shows by far the smallest residuals for the full area and test areas (see Figure 13a and Table 4), revealing that (with the selected parameter $T = 0.25$) it is a rather 'exact' interpolation method. SPHI does not account for the errors in point data values and in case these are large, like in the marine areas or Russian territory, the SPHI method appears to follow the point data values too rigorously.

The LSC method shows the largest residuals, especially over areas where the *a priori* standard error of gravity data is large (see Figures 3 and 13b). Over areas of high-quality gravity data and lower elevations (e.g. Area 2), the LSC residuals are larger than for other methods, but not as significantly, see Table 4. Considering that LSC accounts for observation errors and that the encountered residuals are in the same order of magnitude as the *a priori* error estimates, these residuals should not be interpreted as errors of the interpolation process. If data with large errors are situated close to each other, the optimal interpolation surface will be a smooth one with large residuals.

Using LSC without individual or only partially individual *a priori* error information (grids G3B, G7B, G3C, and G7C) also gives a more 'exact' interpolation of the input points, see Table 4. Thus, the choice of interpolation methods somewhat narrows down to whether the *a priori* error estimates should be trusted.

The grids' behavior near the especially challenging Area 1 (see Figure 12) was further analyzed by examining two profiles: one crossing a fjord (Figure 14a) and the other crossing an area where the computed grids showed large differences (Figure 14b). The profile plots
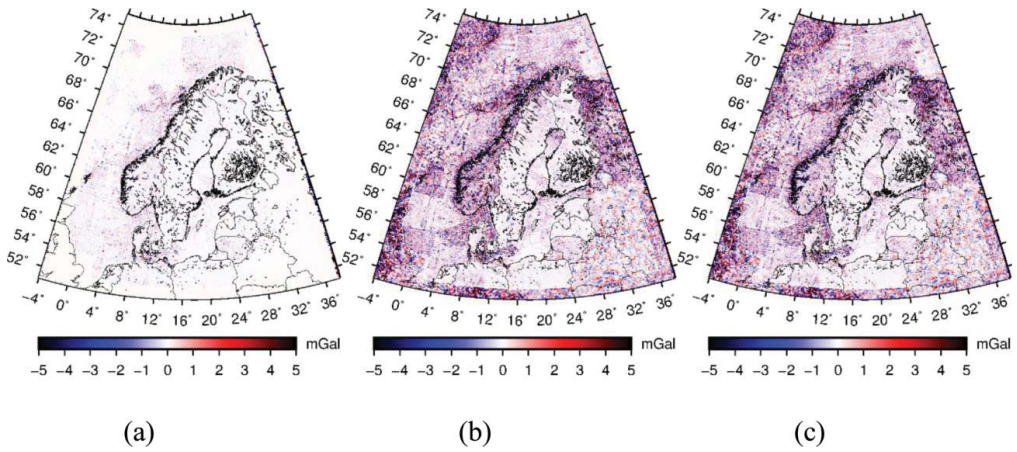
Figure 13. Reduced anomaly point values minus reduced grid values interpolated to point locations. (a) G6 − $\Delta g^{RTMA,A,I}$ grid interpolated by SPHI. (b) G7 − $\Delta g^{RTMA,A,I}$ grid interpolated by LSC. (c) G7C − $\Delta g^{RTMA,A,I}$ grid interpolated by LSC (Norway 1 mGal).

depict grids G3, G7, G7C, and, to demonstrate the violent change in the resulting grid depending on the chosen error estimate, an additional grid just like G7C except that the accuracy of gravity points in Norway was estimated to be even higher, 0.5 mGal. To visualize the input information available for grid generation, neighboring (selected) input points together with a linear (triangulated) grid from input point values are plotted as a reference.
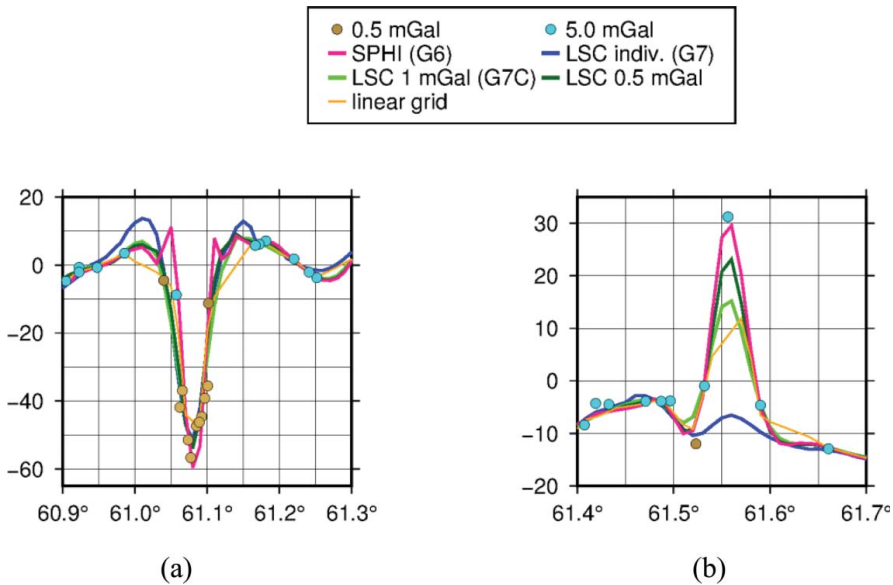
Figure 14. Profiles of free-air anomaly grids computed via RTM anomalies*. (a) 5.52° E. (b) 7.72°E. *The dots indicate input gravity data points coloured according to their *a priori* error estimates. RTM anomalies in mGal and latitude are depicted on the vertical and horizontal axis, respectively.

At the edge of the fjord, the SPHI grids often show an abrupt zigzag pattern while LSC generates a smoother transition. All of the gridding algorithms tested in this study overestimate the gravity field, the more so, the larger the data gap next to the steep gradient. It is a typical behavior of minimal curvature algorithms such as SPHI, but it also affects LSC depending on the covariance function. LSC with fixed (smaller) standard deviation values is affected the least, generating the most realistic gravity anomaly field model. This profile illustrates why gravity surveys in areas of a steep gravity gradient should always be planned so that the immediate neighborhood would also be covered rather densely.

On the fjord surface, the reference linear interpolation probably shows quite a realistic gravity field as the gravity data are dense and accurate. There, all of the tested algorithms underestimate the gravity field with SPHI usually going 5–10 mGal further down than the other algorithms.

In the future, gridding in such fjord areas can be improved by using bathymetric corrections which should reduce the extreme gradient currently present in the reduced gravity field.

A single point that stands out from the surrounding field (Figure 14b), that may or may not be erroneous, is expectedly reflected most in the SPHI grid and least in the LSC grid with individual weights (as in this particular case the *a priori* error estimates were large and the corresponding point weights thus small).

It is worth noting how large in magnitude are the differences in the grids on both of the profiles, also between the LSC grids. These differences do not correspond directly to the *a priori* error estimates supplied.

Another aspect discussed earlier is the behavior of different interpolation methods in data gaps that are often present in marine areas. Let us inspect the reduced gravity grids of Area 3 (Figure 15), starting with Figure 15b depicting the SPHI grid. Triangular patterns have formed, the most prominent one being at 55°5′ N, 6°30′ E. There is at least one area around 55°35′ N, 7°10′ E (depicted in purple) where an extreme minima is generated that most likely does not reflect the actual gravity signal. In addition, there were several other marine areas west of Norway, where the SPHI algorithm generated erratic maxima in the order of up to 100 mGal(!). In general, there is abundance of noise around and between the survey tracks. It is clear that SPHI does not qualify for interpolating track wise (marine gravity) data.

On the plot of the SURF grid (Figure 15a), and also the very similar KRIG grid, smaller anomaly values can be seen at the close vicinity of input gravity point tracks compared to the areas in between, thus generating unrealistic undulation between the tracks. The LSC grid (Figure 15c) is clearly the most physically meaningful grid in Area 3, although it also suffers slightly from similar undulation, see the NE-SW track close to which the gravity values are slightly larger than in the neighborhood.

Gravity reduction methods

Second, the grids were analyzed and compared to evaluate the suitability of the RTM or the Bouguer anomalies for interpolation. The differences in reduced point values from the grid values presented in Table 4 are very similar for both reduction schemes with neither of the methods showing significantly smaller RMS or extreme values.
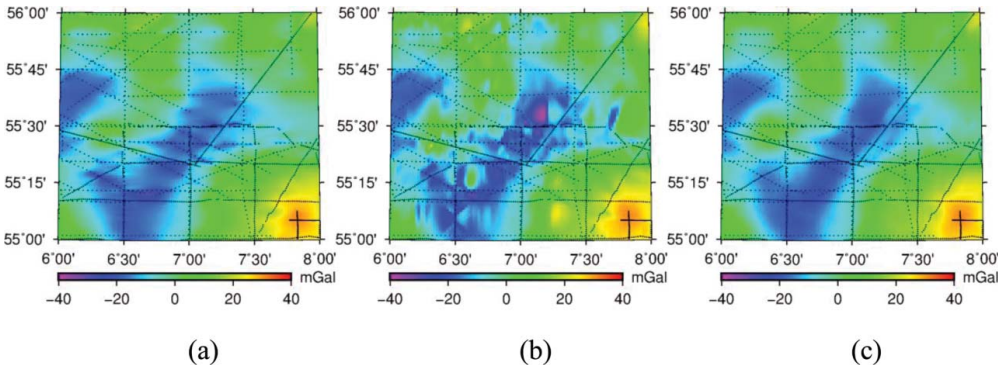
Figure 15. RTM anomaly grids in Area 3, black dots indicate the locations of input gravity data. (a) G5 – $\Delta g^{RTMA,A,I}$ by SURF. (b) G6 – $\Delta g^{RTMA,A,I}$ by SPHI. (c) G7 – $\Delta g^{RTMA,A,I}$ by LSC.

Although free-air anomalies are rough and maybe not best suited for evaluation, the final free-air anomaly grids were also compared to input free-air anomalies. The only interpolation method for which either of the reduction methods shows smaller residuals, is LSC, where the grid computed via RTM anomalies shows 9% and 11% better RMS values in the overall and Area 1 statistics, respectively.

The two reduction methods have different physical meaning, but the resulting surface gravity anomaly grids show a similar fit to the input data. It is difficult to prefer either of the reduction methods based on the test results obtained. A reason to prefer RTM anomalies could be their properties of shorter correlation length that are theoretically more suitable for gridding.

Overall gridding quality

Leaving aside the extreme examples represented by Areas 1 and 3, in most areas, especially where sufficiently high-quality data are available (e.g. Area 2), it seems clear that both of the reduction and all of the interpolation methods could in practice be considered for gravity gridding tasks. This is further supported by the GNSS/levelling evaluations of the corresponding gravimetric quasigeoid models presented in the next section.

Under this assumption of all the reduction and interpolation methods being equally plausible, the uncertainty stemming from the use of different gridding approaches is illustrated by the standard deviation of the values of the different test grids in each grid cell, see Figure 16. Thus, free-air gravity grid accuracy better than 0.5 mGal can only be reached in flat areas with high-quality gravity data such as Area 2, Denmark and Estonia, while the accuracy is limited to around 1 mGal in areas with slightly lower quality gravity data (Latvia and Lithuania) or higher terrains such as Sweden and Finland. Due to sparse data tracks, the marine areas are affected most by the choice of gridding methods, even if the spline-based grids are excluded from such an evaluation.

The research area is rather heterogeneous in terms of topography and data coverage, offering an overview of expected gridding results in varying conditions. However, in other similar computations, the results presented here can only be of general reference as the final grid is strongly dependent on the local situation – topography, bathymetry, gravity data coverage, distribution etc.
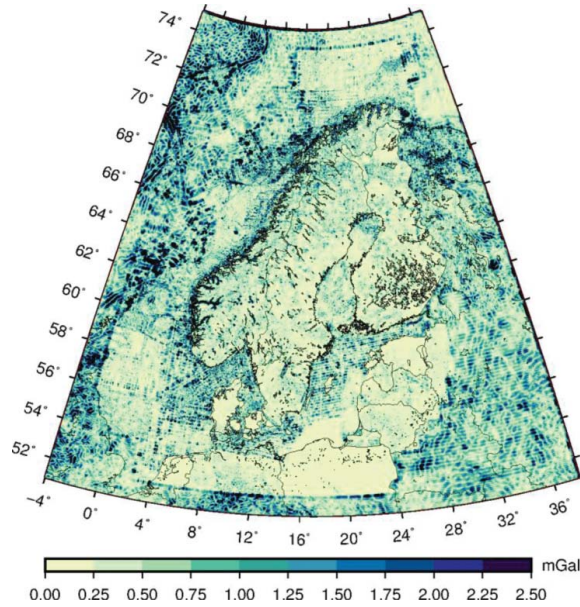
Figure 16. Standard deviation of G1 to G8 (with C versions of G3 and G7) surface gravity anomaly values in each grid cell.

Assessment by subsequent quasigeoid models

The main aim of the NKG project is to compute a quasigeoid model. Each gravity anomaly grid yields a preliminary quasigeoid model that is computed using Least Squares Modification of Stokes' formula with Additive Corrections (LSMSA, Sjöberg 1984, 1991, 2003). The LSMSA method is likely to be applied in the final NKG2015 quasigeoid computation (that will be reported upon in a separate publication, see also Ågren et al. 2016). These gravimetric quasi-geoid models were then compared with each other and to national GNSS/levelling datasets, i.e. to a geometric geoid determined from the difference of physical and ellipsoidal heights.

The physical (normal) heights are either in the national EVRS realizations with land uplift epoch 2000.0 (Nordic countries) or in the pan-European EVRS realization European Vertical Reference Frame (EVRF) 2007 (Baltic countries), which also has epoch 2000.0. The zero permanent tide system is used for the physical heights. The GNSS heights above the ellipsoid were first transformed into European Terrestrial Reference Frame (ETRF) 2000 with land uplift epoch 2000.0 using the NKG transformation parameters derived by Häkli et al. (2016) and then converted to the zero permanent tide system. It is important to note that the following results may also contain errors in GNSS/levelling control points used for the quasi-geoid validation.

The resulting RMS values of GNSS/levelling residuals (after mean removal) are reported in Table 5. In the NKG area, there are all together 2538 points, out of which 51 and 23 fall in test Areas 1 and 2, respectively. Again, the residuals are larger for the LSC grids, especially in the mountainous Area 1. However, the LSC-associated residuals in the NKG area result only from the algorithm generating an unrealistically smooth grid in Norway. Note that LSC yields the best fit in Area 2. Also, quasigeoid models computed from the B and C versions of

Table 5. RMS values of the quasigeoid differences from GNSS/levelling points after mean removal.

Interpolation	Quasigeoid via $\Delta g^{CBA,A,I}$ [cm]				Quasigeoid via $\Delta g^{RTMA,A,I}$ [cm]			
	Grid	NKG area	Area 1	Area2	Grid	NKG area	Area 1	Area 2
SURF	G1	2.92	4.94	2.04	G5	2.92	4.94	2.08
SPHI	G2	2.85	3.80	1.96	G6	2.85	3.82	1.96
LSC	G3	3.36	5.58	1.91	G7	3.16	5.37	1.94
KRIG	G4	2.90	4.93	1.97	G8	2.90	4.80	1.99
SPHI (no δg^T)	G2B	3.05	5.28	1.97				
SPHI (GGM d/o 240)					G6B	2.85	3.98	1.95
LSC (all 1mGal)	G3B	2.96	5.64	1.97	G7B	2.89	4.66	1.98
LSC (Norw. 1 mGal)	G3C	3.00	5.88	1.89	G7C	2.96	5.64	1.97

LSC grids show a better fit than the original LSC with individual error estimates. There is practically no numerical difference in the two reduction methods, except that LSC grids yield a slightly better fit to quasigeoid models in conjunction with RTM anomalies rather than the Bouguer anomalies.

Unfortunately GNSS/levelling data are not available over marine areas. Therefore, in specified computations the choice of gridding methods suitable for marine areas needs to rely on the gravity grid analysis above and the conclusions drawn from studying land areas with similar gravity field and data coverage characteristics.

The expected accuracy of quasigeoid models related to the used gravity gridding approach was analyzed, again, presuming that all the tested gridding methods are equally plausible in many practical cases. The expected accuracy for the NKG area is illustrated by the standard deviation of quasigeoid models computed using the different gravity grids, see Figure 17. Therefore, from the gravity data gridding point of view, it is possible to compute a 5-mm (quasi)geoid model over most of the Nordic-Baltic dry land. Again, the marine areas are
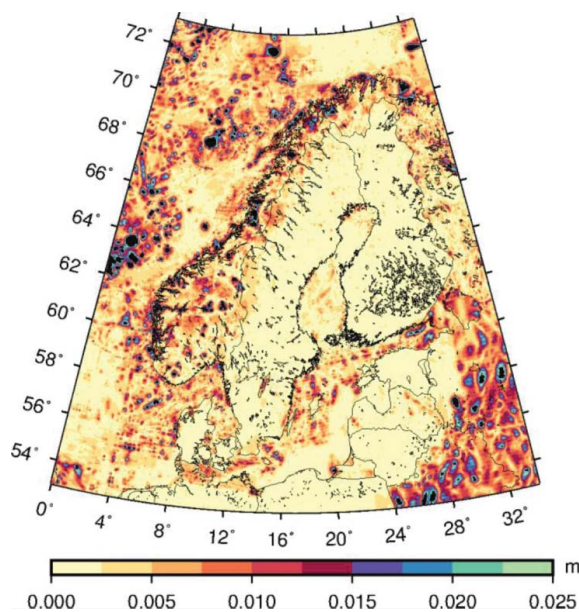
Figure 17. Standard deviation of quasigeoid models computed from G1 to G8 (with C versions of G3 and G7) in each grid cell.

affected most by the choice of gridding methods. If the spline-based grids are excluded from such an evaluation, a 1-cm accuracy can be expected over most of the Baltic Sea (except the Eastern part of GOF), but the situation does not improve much over remote parts of the Arctic Ocean. Thus, for optimum outcome, the data situation and gridding approaches still need to be improved in view of the desired 5-mm accuracy geoid model.

Conclusions

This contribution compared and analyzed methods of computing a surface gravity anomaly grid from scattered survey data. A general RIR method was used, that is, the surface gravity anomalies were reduced before and restored after the interpolation process. Two concurrent reduction and four interpolation methods were studied and assessed in the extended Nordic-Baltic area. The entire work flow of gravity data processing together with the effect of some alternative processing choices was discussed. The gravity field model was reduced to complete Bouguer or RTM anomalies; the interpolation methods analyzed include two spline-based (SURF and SPHI) and two statistical (LSC and KRIG) methods. LSC was the only method allowing points to be weighted according to individual *a priori* error estimates. The resulting gravity grids were assessed by comparison to input data and subsequent GNSS/levelling fit to the quasigeoid model.

Overall, it is not so crucial whether the surface gravity anomaly grid is computed via RTM or Bouguer type anomalies. The numerical results are similar in reasonably flat terrain areas containing high-quality observations. Due to their more homogeneous and isotropic property, in conjunction with statistical interpolation methods such as LSC, the RTM anomalies perform slightly better.

The spline-based interpolation methods SURF and SPHI generate a rather 'exact' grid that closely follows the input data. So does the KRIG method, at least when using the parameters fitted for the current dataset. The result of LSC interpolation depends significantly on the quality of the *a priori* error estimates: if these are not trustworthy, the benefits of using LSC with individual weights become disadvantages.

It is advisable not to judge an interpolation method only according to its ability to generate a grid matching the input data as closely as possible. If the residuals between the input point data and the resulting grid are within the limits of data error estimates, a smoother grid can in fact be physically more realistic and thus more appropriate. This is especially valid for marine areas where data points are often available along sparsely placed and rather inaccurate survey tracks, but the gravity field is usually quite smooth.

Both spline-based methods, especially SPHI, are best used in areas with many observations and no data gaps. Grids computed by SPHI displayed some uncontrolled behavior over marine areas with trackwise gravity coverage, data gaps and next to steep gravity gradients. In such areas, other methods, such as LSC, should be preferred for generating a physically meaningful gravity grid.

Based on the above, it was concluded that, provided that realistic error estimates are available, gridding RTM anomalies using LSC results in the highest quality gravity field representation.

It was also demonstrated that changing the maximum d/o (within reasonable limits of 240–300) to which the GGM is evaluated when computing RTM anomalies, has an insignificant effect on the resulting gravity field and subsequent quasigeoid models. As expected, the

use of simple instead of complete Bouguer anomalies in gridding has a notable effect on the resulting quasigeoid model in areas of rugged terrain and almost no positive effect elsewhere. Over the rugged Norwegian territory, these differences had a standard deviation of ± 2 cm.

The expected accuracy of quasigeoid models related to the used gravity gridding approach was analyzed in view of the geodetic community now aiming at 5-mm accuracy in (quasi) geoid modelling. The standard deviation of quasigeoid models computed from different gravity grids confirmed that a quasigeoid model with an accuracy of 5 mm could be computed in most areas with terrain elevations up to 2 km and gravity data with an average error estimate of 1.8 mGal available with a density of 1 point per 10 km^2. However, an accuracy of 5 mm has not yet been reached over more rugged terrain and most marine areas.

The main recommendations for the NKG2015 geoid modelling project that motivated this research are the following. First, both, Bouguer type or RTM anomalies may be used for gridding. Second, in general, any of the tested interpolation methods may be used. However, the SPHI method should be avoided due to unrealistic and extreme behavior in between the marine data tracks. Also, in Norway, where many of the *a priori* error estimates for contemporary terrestrial gravity data are set to be unrealistically large (i.e. 5 mGal), the usage of LSC with such individual *a priori* error estimates should be avoided. Attempts to provide more realistic error estimates should be encouraged.

Gravity gridding is of interest to other ongoing geodetic projects, for example the multinational GEOMED 2 (Barzaghi et al. 2016) and the EGG (Denker 2016) co-operation projects, or countries like Canada, USA, Russia, or Australia that have a large area covered with inhomogeneous gravity data. Also, accurate gravity field and geoid modelling is a key feature in the realization of the International Height Reference System (IHRS) reference stations and other datum unification tasks.

Although the gravity gridding procedure was analyzed in ample detail, further work outside the scope of this study can be conducted to elaborate the analysis reported above. Other gravity reduction methods, such as isostatic reductions, could be compared to the two methods tested. All of the gravity reductions could be improved by including density and bathymetry information, undoubtedly improving the accuracy of the resulting marine geoid model. Statistical interpolation could be improved by future research in non-stationary covariance function modelling (see e.g. Darbeheshti and Featherstone 2009). The KRIG solutions could be improved by including individual error estimates as it was done for the LSC method and the spline-based solutions of SURF and SPHI by tuning the tension factor according to some criterion to better fit the characteristics of the gravity field automatically in a specific area. The gravity data could benefit from automatically varying CV limits for gross error detection according to the field's roughness. Over the open oceans, it could be beneficial to include satellite altimetry data (in combination with terrestrial data) as these have been shown to reach accuracies of a few mGal, thanks to newer Cryosat and Sentinel satellite-related improvements (Andersen and Knudsen 2016). As for the specific area of the Nordic-Baltic region, improvements in the Baltic Sea gravity grid are expected due to the FAMOS project (FAMOS Consortium 2014) collecting new shipborne gravity data.

The recommendations and methodological approaches discussed above, together with the concerns and exceptions mentioned, are applicable to other gravity gridding tasks worldwide. A resulting surface gravity anomaly grid can serve as input to numerous geoscientific tasks. Other types of gravity anomalies, for example those used in geophysical studies or concurrent geoid modelling techniques, can then be derived from the surface gravity anomaly grid.

Acknowledgments

ORCID

Silja Märdla http://orcid.org/0000-0003-4140-9374

References

Ågren, J. 2009. Beskrivning av de nationella geoidmodellerna SWEN08_RH2000 och SWEN08_RH70 (Description of national geoid models SWEN08_RH2000 and SWEN08_RH70) (No. 2009:1). *Reports in Geodesy and Geographic Information Systems*. Gävle, Sweden.

Ågren, J. 2004. *Regional geoid determination methods for the era of satellite gravimetry: numerical investigations using synthetic earth gravity models*. KTH Royal Institute of Technology, Stockholm, Sweden.

Ågren, J., and L.E. Sjöberg. 2014. Investigation of gravity data requirements for a 5 mm-quasigeoid model over Sweden. *Gravity, Geoid and Height Systems: Proceedings of the IAG Symposium (GGHS'12)*. Venice, Italy, Springer International Publishing, pp. 143–150.

Ågren, J., L.E. Sjöberg, and R. Kiamehr. 2009. The new gravimetric quasigeoid model KTH08 over Sweden. *Journal of Applied Geodesy* 3:143–153. doi:10.1515/JAG.2009.015

Ågren, J., G. Strykowski, M. Bilker-Koivula, O. Omang, S. Märdla, R. Forsberg, A. Ellmann, T. Oja, I. Liepiņš, E. Paršeliūnas, J. Kaminskis, L. Sjöberg, and G. Valsson. 2016. The NKG2015 gravimetric geoid model for the Nordic-Baltic region. *1st Joint Commission 2 and IGFS Meeting International Symposium on Gravity, Geoid and Height Systems*. Thessaloniki, Greece, 19–23 September.

Ågren, J., G. Strykowski, M. Bilker-Koivula, O. Omang, S. Märdla, T. Oja, I. Liepiņš, E. Paršeliūnas, R. Forsberg, J. Kaminskis, A. Ellmann, L. Sjöberg, and V. Valsson. 2015. On the development of the new Nordic gravimetric geoid model NKG2015. *26th IUGG General Assembly*. Prague, Czech Republic, June 22–July 2.

Andersen, O.B. 2010. The DTU10 Global Gravity field and mean sea surface. *2nd International Symposium of the Gravity Field of the Earth (IGFS2)*. Fairbanks, Alaska.

Andersen, O.B., and P. Knudsen. 2016. Deriving and evaluating the DTU15 Global high resolution marine gravity field. *1st Joint Commission 2 and IGFS Meeting International Symposium on Gravity, Geoid and Height Systems*. Thessaloniki, Greece, 19–23 September.

Bae, T.-S., J. Lee, J.H. Kwon, and C.-K. Hong. 2012. Update of the precision geoid determination in Korea. *Geophysical Prospecting* 60:555–571. doi:10.1111/j.1365-2478.2011.01017.x

Baptiste, J., G. Martelet, M. Faure, L. Beccaletto, P.-A. Reninger, J. Perrin, and Y. Chen. 2016. Mapping of a buried basement combining aeromagnetic, gravity and petrophysical data: The substratum of southwest Paris Basin, France. *Tectonophysics* 683:333–348. doi:10.1016/j.tecto.2016.05.049

Barzaghi, R., G. Vergos, A. Albertella, D. Carrion, N.E. Cazzaniga, I. Tziavos, V. Grigoriadis, D. Natsiopoulos, S. Bruinsma, S. Bonvalot, L. Seoane, F. Reinquin, M.-F. LeQuentrec-Lalancette, C. Salaun, P. Bonnefond, P. Knudsen, O. Andersen, M. Simav, H. Yildiz, T. Basic, M. Varga, O. Bjelotomic, and A.J. Gil. 2016. Gravimetric geoid model development in the Mediterranean Sea within the Geomed2 project. *1st Joint Commission 2 and IGFS Meeting International Symposium on Gravity, Geoid and Height Systems*. Thessaloniki, Greece, 19–23 September.

Bilker-Koivula, M. 2014. Assessment of high-resolution global gravity field models and their application in quasi-geoid modelling in Finland. Marti, U. (ed.), *Gravity, Geoid and Height Systems: Proceedings of the IAG Symposium (GGHS'12)*, October 9–12:2012, Venice, Italy: International Association of Geodesy Symposia. Springer, pp. 51–58.

Bilker-Koivula, M. 2010. Development of the Finnish Height Conversion Surface FIN2005N00. *Nordic Journal of Surveying and Real Estate Research* 7:76–88.

Bolkas, D., G. Fotopoulos, and A. Braun. 2016. On the impact of airborne gravity data to fused gravity field models. *Journal of Geodesy* 90:561–571. doi:10.1007/s00190-016-0893-x

Bruinsma, S.L., C. Förste, O. Abrikosov, J.-C. Marty, M.-H. Rio, S. Mulet, and S. Bonvalot. 2013. The new ESA satellite-only gravity field model via the direct approach. *Geophysical Research Letters* 40:3607–3612. doi:10.1002/grl.50716

Cressie, N. 2015. *Statistics for Spatial Data*, 2nd ed. Hoboken, NJ: Wiley-Interscience.

Darbeheshti, N., and W.E. Featherstone. 2009. Non-stationary covariance function modelling in 2D least-squares collocation. *Journal of Geodesy* 83:495–508. doi:10.1007/s00190-008-0267-0

Denker, H. 2016. A new European Gravimetric (Quasi)Geoid EGG2015. *1st Joint Commission 2 and IGFS Meeting International Symposium on Gravity, Geoid and Height Systems*. Thessaloniki, Greece, 19–23 September.

Denker, H. 2013. Regional gravity field modeling: Theory and practical results. Xu, G. (ed.), *Sciences of Geodesy—II*. Berlin/Heidelberg: Springer, pp. 185–291.

Denker, H., J.-P. Barriot, R. Barzaghi, D. Fairhead, R. Forsberg, J. Ihde, A. Kenyeres, U. Marti, M. Sarrailh, and I.N. Tziavos. 2009. The development of the European gravimetric geoid model EGG07. Sideris, M.G. (ed.). *Observing Our Changing Earth: Proceedings of the 2007 IAG General Assembly*, Perugia, Italy, July 2–13, 2007, International Association of Geodesy Symposia. Berlin/Heidelberg: Springer, pp. 177–185.

Dermanis, A. 1984. Kriging and Collocation—A Comparison. *Manuscripta Geodetica* 9:159–167.

DMA. 1987. *Supplement to Department of Defense World Geodetic System 1984 Technical Report: Part II—Parameters, Formulas and Graphics for the Practical Application of WGS84 (Technical Report No. 8350.2-B)*. Defence Mapping Agency.

Elkins, T.A. 1951. The second derivative method of gravity interpretation. *Geophysics* 16:29–50. doi:10.1190/1.1437648

Ellmann, A. 2011. Downward continuation of airborne gravity data using high resolution global geopotentail models. Cygas, D. and K.D. Froehner (eds.), *Selected Papers of the 8th International Conference on Environmental Engineering*, Vilnius, Lithuania: Vilnius Gediminas Technical University press "Technika," pp. 1315–1320.

Ellmann, A. 2005. Two deterministic and three stochastic modifications of Stokes's formula: a case study for the Baltic countries. *Journal of Geodesy* 79:11–23. doi:10.1007/s00190-005-0438-1

Ellmann, A. 2002. An improved gravity anomaly grid and a geoid model for Estonia. *Proceedings of the Estonian Academy of Sciences, Geology*, 199–214.

Ellmann, A., T. All, and T. Oja. 2009. Towards unification of terrestrial gravity data sets in Estonia. *Estonian Journal of Earth Sciences* 58:229–245. doi:10.3176/earth.2009.4.02

Ellmann, A., T. Oja, and H. Jürgenson. 2011. Kosmosetehnoloogia rakendused geoidi ja gravitatsioonivälja täpsustamiseks Eesti alal (Application of space technologies to improve geoid and gravity field models over Estonia). *Geodeet* 41:22–25.

Ellmann, A., and P. Vaníček. 2007. UNB application of Stokes–Helmert's approach to geoid computation. *Journal of Geodynamics, Potential Fields in Geostatics and Geodynamics* 43:200–213. doi:10.1016/j.jog.2006.09.019

FAMOS Consortium. 2014. The FAMOS project. Available at http://www.famosproject.eu/famos/

Featherstone, W.E. 2009. Only use ship-track gravity data with caution: a case-study around Australia. *Australian Journal of Earth Sciences* 56:195–199. doi:10.1080/08120090802547025

Forsberg, R. 1997. Terrain effects in geoid determination. Sansò, F. (ed.), *Lecture Notes, International School for the Determination and Use of the Geoid*. Int. Geoid Service, DICA—Polytecnico di Milano. Rio de Janeiro.

Forsberg, R. 1991. A new high-resolution geoid of the Nordic area. Rapp, R.H., and F. Sansò (eds.), *Determination of the Geoid, International Association of Geodesy Symposia*. New York: Springer, pp. 241–250.

Forsberg, R. 1984. A study of terrain reductions, density anomalies and geophysical inversion methods in gravity field modelling (No. 355). Ohio State University.

Forsberg, R., J. Kaminskis, and D. Solheim. 1997. Geoid of the Nordic and Baltic Region from Gravimetry and Satellite Altimetry. Segawa, P.D.J., P.D.H., Fujimoto, and P.D.S. Okubo (eds.), *Gravity, Geoid and Marine Geodesy, International Association of Geodesy Symposia*. Berlin/Heidelberg: Springer, 540–547.

Forsberg, R., and A.V. Olesen. 2010. Airborne gravity field determination. Xu, G. (ed.), *Sciences of Geodesy I—Advances and Future Directions*. Berlin/Heidelberg: Springer, 83–104.

Forsberg, R., and M.G. Sideris. 1993. Geoid computations by the multi-band spherical FFT approach. *Manuscripta Geodaetica* 18:82–90.

Forsberg, R., G. Strykowski, and D. Solheim. 2004. NKG-2004 Geoid of the Nordic and Baltic Area. *Proceedings on CD-ROM from the International Association of Geodesy. Presented at the Gravity, Geoid and Satellite Gravity Missions*, August 30–September 3, Porto, Portugal.

Forsberg, R., and C.C. Tscherning. 2008. *An Overview Manual for the GRAVSOFT Geodetic Gravity Field Modelling Programs*. 2nd ed. Available at https://www.academia.edu/9206363/An_overview_manual_for_the_GRAVSOFT_Geodetic_Gravity_Field_Modelling_Programs.

Förste, C., S.L. Bruinsma, O. Abrikosov, J.-M. Lemoine, J.C. Marty, F. Flechtner, G. Balmino, F. Barthelmes, and R. Biancale. 2015. *EIGEN-6C4 The latest combined global gravity field model including GOCE data up to degree and order 2190 of GFZ Potsdam and GRGS Toulouse [WWW Document]*. GFZ Data Services. Available at http://doi.org/10.5880/icgem.2015.1

Gil, A.J., and Rodríguez−Caderot, G. 1998. Processing gravity data in the territory of Andalusia. *Marine Geodesy* 21:81–89. doi:10.1080/01490419809388123

Golden Software LLC. 2016. Surfer [WWW Document]. Available at http://www.goldensoftware.com/products/surfer. Last accessed 9.1.16.

Goos, J.M., W.E. Featherstone, J.F. Kirby, and S.A. Holmes. 2003. Experiments with two different approaches to gridding terrestrial gravity anomalies and their effect on regional geoid computation. *Survey Review* 37:92–112. doi:10.1179/sre.2003.37.288.92

Haagmans, R., E. de Min, and M. Gelderen. 1993. Fast evaluation of convolution integrals on the sphere using 1D FFT, and a comparison with existing methods for Stokes' integral. *Manuscripta Geodaetica* 18:227–241.

Hackney, R.I., and W.E. Featherstone. 2003. Geodetic versus geophysical perspectives of the "gravity anomaly." *Geophysical Journal International* 154:35–43. doi:10.1046/j.1365-246X.2003.01941.x

Häkli, P., M. Lidberg, L. Jivall, T. Nørbech, O. Tangen, M. Weber, P. Pihlak, I. Aleksejenko, and E. Paršeliunas. 2016. The NKG2008 GPS campaign—final transformation results and a new common Nordic reference frame. *Journal of Geodetic Science* 6:1–33. doi:10.1515/jogs-2016-0001

Heiskanen, W.A., and H. Moritz. 1967. *Physical Geodesy*. San Francisco: W. H. Freeman and Company.

Hinze, W., C. Aiken, J. Brozena, B. Coakley, D. Dater, G. Flanagan, R. Forsberg, T. Hildenbrand, G. Keller, J. Kellogg, R. Kucks, X. Li, A. Mainville, R. Morin, M. Pilkington, D. Plouff, D. Ravat, D. Roman, J. Urrutia-Fucugauchi, M. Véronneau, M. Webring, and D. Winester. 2005. New standards for reducing gravity data: The North American gravity database. *Geophysics* 70:J25–J32. doi:10.1190/1.1988183

Hirt, C. 2013. RTM gravity forward-modeling using topography/bathymetry data to improve high-degree global geopotential models in the coastal zone. *Marine Geodesy* 36:183–202. doi:10.1080/01490419.2013.779334

Hirt, C. 2010. Prediction of vertical deflections from high-degree spherical harmonic synthesis and residual terrain model data. *Journal of Geodesy* 84:179–190. doi:10.1007/s00190-009-0354-x

Hwang, C., Y.-S. Hsiao, H.-C. Shih, M. Yang, K.-H. Chen, R. Forsberg, and A.V. Olesen. 2007. Geodetic and geophysical results from a Taiwan airborne gravity survey: Data reduction and accuracy assessment. *Journal of Geophysical Research: Solid Earth* 112. doi:10.1029/2005JB004220.

Isaaks, E.H., and R.M. Srivastava. 1989. *Applied Geostatistics*. New York, NY: Oxford University Press.

Janák, J., and P. Vaníček. 2005. Mean free-air gravity anomalies in the mountains. *Studia Geophysica et Geodaetica* 49:31–42. doi:10.1007/s11200-005-1624-6

Jekeli, C., H.J. Yang, and J.H. Kwon. 2009. Using gravity and topography-implied anomalies to assess data requirements for precise geoid computation. *Journal of Geodesy* 83:1193–1202. doi:10.1007/s00190-009-0337-y

Jürgenson, H. 2003. *Eesti täppisgeoidi arvutus (Determination of Estonian Precision Geoid)*. Estonian University of Life Sciences, Tartu, Estonia.

Klitzke, P., J. Sippel, J.I. Faleide, and M. Scheck-Wenderoth. 2016. A 3D gravity and thermal model for the Barents Sea and Kara Sea. *Tectonophysics, Special Issue on GeoMod 2014 – Modelling in Geoscience* 684:131–147. doi:10.1016/j.tecto.2016.04.033

Korhonen, J.V., T. Koistinen, S. Elo, H. Säävuori, J. Kääriäinen, H. Nevanlinna, S. Aaro, L.Å. Haller, J. R. Skilbrei, D. Solheim, A. Chepik, A. Kulinich, L. Zhdanova, R. Vaher, T. All, and H. Sildvee. 1999. Preliminary magnetic and gravity anomaly maps of the Fennoscandian shield 1: 10 000 000. Special Paper—Geological Survey of Finland, 173–180.

Krige, D.G. 1951. *A Statistical Approach to Some Mine Valuation and Allied Problems on the Witwatersrand*. D.G. Krige.

Kuhn, M., W.E. Featherstone, and J.F. Kirby. 2009. Complete spherical Bouguer gravity anomalies over Australia. *Australian Journal of Earth Sciences* 56:213–223. doi:10.1080/08120090802547041

Li, J., and M.G. Sideris. 1997. Marine gravity and geoid determination by optimal combination of satellite altimetry and shipborne gravimetry data. *Journal of Geodesy* 71:209–216. doi:10.1007/s001900050088

Lysaker, D.I., O.C.D. Omang, B.R. Pettersen, and D. Solheim. 2007. Quasigeoid evaluation with improved levelled height data for Norway. *Journal of Geodesy* 81:617–627. doi:10.1007/s00190-006-0129-6

Mandal, A., S. Gupta, W.K. Mohanty, and S. Misra. 2015. Sub-surface structure of a craton–mobile belt interface: Evidence from geological and gravity studies across the Rengali Province–Eastern Ghats Belt boundary, eastern India. *Tectonophysics, Special issue on Comparative tectonic and dynamic analysis of cratons, orogens, basins, and metallogeny* 662:140–152. doi:10.1016/j.tecto.2015.01.016

Märdla, S., A. Ellmann, T. Oja, and H. Jürgenson. 2015. Improving and validating gravity data over ice-covered marine areas. Rizos, C., and P. Willis (Eds.), *IAG 150 Years: Proceedings of the 2013 IAG Scientific Assembly*, Potsdam, Germany, 1–6 September, 2013, International Association of Geodesy Symposia. Springer International Publishing, 263–270.

Martín, A., A.B. Anquela, J. Padín, and S. Baselga. 2009. Some notes and numerical comparisons on gravity anomalies interpolation. *Survey Review* 41:201–215.

Martinec, Z. 1998. *Boundary-Value Problems for Gravimetric Determination of a Precise Geoid, Lecture Notes in Earth Sciences*. Berlin/Heidelberg: Springer-Verlag.

Morelli, C., C. Gantar, T. Honkasalo, R.K. McConnell, T.G. Tanner, B. Szabo, U. Uotila, and C.T. Whalen. 1971. The international gravity standardisation network (IGSN71). *Bulletin Géodésique*, Special Publication No. 4.

Moritz, H. 2000. Geodetic reference system 1980. *Journal of Geodesy* 74:128–133. doi:10.1007/s001900050278

Moritz, H. 1980. *Advanced Physical Geodesy*. Wichmann. Tunbridge Wells, UK: Abacus Press.

Nahavandchi, H., A. Soltanpour, and E. Nymes. 2005. A new gravimetric geoidal height model over norway computed by the least-squares modification parameters. Jekeli, P.C., D.L. Bastos, and P.J. Fernandes (eds.), *IAG International Symposium on Gravity, Geoid and Space Missions: GGSM*, Porto, Portugal, August 30–September 3, 2004, International Association of Geodesy Symposia. Berlin/Heidelberg: Springer, 191–196.

Niebauer, T.M., G.S. Sasagawa, J.E. Faller, R. Hilt, and F. Klopping. 1995. A new generation of absolute gravimeters. *Metrologia* 32:159. doi:10.1088/0026-1394/32/3/004

Noréus, J.P., M.R. Nyborg, and K.L. Hayling. 1997. The gravity anomaly field in the Gulf of Bothnia spatially characterized from satellite altimetry and in situ measurements. *Journal of Applied Geophysics* 37:67–84. doi:10.1016/S0926-9851(97)00007-4

Novák, P., P. Vaníček, Z. Martinec, and M. Véronneau. 2001. Effects of the spherical terrain on gravity and the geoid. *Journal of Geodesy* 75:491–504. doi:10.1007/s001900100201

Omang, O.C., C.C. Tscherning, and R. Forsberg. 2012. Generalizing the harmonic reduction procedure in residual topographic modeling. Sneeuw, N., P. Novák, M. Crespi, and F. Sansò (eds.), *VII Hotine-Marussi Symposium on Mathematical Geodesy*, International Association of Geodesy Symposia. Berlin/Heidelberg: Springer, 233–238.

Omang, O.C.D., and R. Forsberg. 2002. The northern European geoid: a case study on long-wavelength geoid errors. *Journal of Geodesy* 76:369–380. doi:10.1007/s00190-002-0261-x

Omang, O.C.D., and R. Forsberg. 2000. How to handle topography in practical geoid determination: three examples. *Journal of Geodesy* 74:458–466.

Radhakrishna, M., S. Lasitha, and M. Mukhopadhyay. 2008. Seismicity, gravity anomalies and lithospheric structure of the Andaman arc, NE Indian Ocean. *Tectonophysics* 460:248–262. doi:10.1016/j.tecto.2008.08.021

Renka, R.J. 1997a. Algorithm 772: STRIPACK: Delaunay Triangulation and voronoi diagram on the surface of a sphere. *ACM Transactions on Mathematical Software* 23:416–434. doi:10.1145/275323.275329

Renka, R.J. 1997b. Algorithm 773: SSRFPACK: Interpolation of Scattered data on the surface of a sphere with a surface under tension. *ACM Transactions on Mathematical Software* 23:435–442. doi:10.1145/275323.275330

Saleh, J., X. Li, Y.M. Wang, D.R. Roman, and D.A. Smith. 2013. Error analysis of the NGS' surface gravity database. *Journal of Geodesy* 87:203–221. doi:10.1007/s00190-012-0589-9

Sansò, F., M.G. Sideris (Eds.). 2013. *Geoid Determination, Lecture Notes in Earth System Sciences*. Berlin/Heidelberg: Springer.

Sjöberg, L.E. 2003. A computational scheme to model the geoid by the modified Stokes formula without gravity reductions. *Journal of Geodesy* 77:423–432. doi:10.1007/s00190-003-0338-1

Sjöberg, L.E. 2000. Topographic effects by the Stokes–Helmert method of geoid and quasi-geoid determinations. *Journal of Geodesy* 74:255–268. doi:10.1007/s001900050284

Sjöberg, L.E. 1991. Refined least squares modification of stokes formula. *Manuscripta Geodaetica* 16:367–375.

Sjöberg, L.E. 1984. Least squares modification of Stokes' and Vening Meinesz' formulas by accounting for truncation and potential coefficient errors. *Manuscripta Geodaetica* 9:209–229.

Smith, W.H.F., and P. Wessel. 1990. Gridding with continuous curvature splines in tension. *Geophysics* 55:293–305. doi:10.1190/1.1442837

Stokes, G.G. 1849. *On the Variation of Gravity at the Surface of the EARTH*. Trans. Cambridge Philos. Soc. VIIII, 672–695.

Sünkel, H. 1986. Global topographic-isostatic models. Sünkel, H. (ed.), *Mathematical and Numerical Techniques in Physical Geodesy, Lecture Notes in Earth Sciences*. Berlin/Heidelberg: Springer, 417–462. doi:10.1007/BFb0010137

Tscherning, C.C. 1985. Local approximation of the gravity potential by least squares collocation. Schwarz, K.P. (ed.), *Proceedings of the International Summer School on Local Gravity Field Approximation*, Beijing, China, August 21–September 4, 1984. Calgary, Canada: University of Calgary, 277–362.

Tscherning, C.C., and R. Forsberg. 1986. Geoid determination in the Nordic countries from gravity and height data, in: Bolletino Di Geodesia E Scienze Affini. *Presented at the International Symposium on the Definition of the Geoid*, Florence, Italy, 21–43.

Tscherning, C.C., F. Rubek, and R. Forsberg. 1998. Combining airborne and ground gravity using collocation. Forsberg, P.D.R., P.D.M. Feissel, and P.D.R. Dietrich (eds.), *Geodesy on the Move - Gravity, Geoid, Geodynamics and Antarctica: Proceedings of lAG Scientific Assembly*, Rio de Janeiro, Brazil, September 3–9, 1997, International Association of Geodesy Symposia. Berlin/Heidelberg: Springer, 18–23. doi:10.1007/978-3-642-72245-5_3

Vaníček, P., P. Novák, and Z. Martinec. 2001. Geoid, topography, and the Bouguer plate or shell. *Journal of Geodesy* 75:210–215. doi:10.1007/s001900100165

Vaníček, P., and L.E. Sjöberg. 1991. Reformulation of Stokes's theory for higher than second-degree reference field and modification of integration kernels. *Journal of Geophysical Research* 96:6529–6539. doi:10.1029/90JB02782

Vaníček, P., R. Tenzer, L.E. Sjöberg, Z. Martinec, and W.E. Featherstone. 2004. New views of the spherical Bouguer gravity anomaly. *Geophysical Journal International* 159:460–472. doi:10.1111/j.1365-246X.2004.02435.x

Vergos, G.S., I.N. Tziavos, and V.D. Andritsanos. 2005. Gravity data base generation and geoid model estimation using heterogeneous data. *Gravity, Geoid and Space Missions*. Berlin/Heidelberg: Springer, 155–160.

Vermeer, M. 1994. A Fast Delivery GPS-Gravimetric Geoid for Estonia (No. 94:1). *Reports of the Finnish Geodetic Institute*. Finnish Geodetic Institute, Masala, Finland.

Véronneau, M. 2013. *The Helmert Gravity Grid Used for CGG2010. Geodetic Survey Division*, Natural Resources Canada, Ottawa, Canada (via pers. comm., 28.04.2016).

Wang, Y.M., J. Saleh, X. Li, and D.R. Roman. 2012. The US Gravimetric Geoid of 2009 (USGG2009): model development and evaluation. *Journal of Geodesy* 86:165–180. doi:10.1007/s00190-011-0506-7

Wessel, P., W.H.F. Smith, R. Scharroo, J. Luis, and F. Wobbe. 2013. Generic mapping tools: improved version released. *Eos Transactions American Geophysical Union* 94:409–410. doi:10.1002/2013EO450001

Paper C

Märdla, S., Ellmann, A., Oja, T., and Jürgenson, H. (2015). "Improving and Validating Gravity Data Over Ice-Covered Marine Areas". In: *IAG 150 Years: Proceedings of the 2013 IAG Scientific Assembly, 1–6 September, 2013*. Ed. by C. Rizos and P. Willis. International Association of Geodesy Symposia 143. Potsdam, Germany: Springer International Publishing, pp. 263–270. ISBN: 978-3-319-24603-1. DOI: 10.1007/1345_2015_163. **Paper C**.

Improving and Validating Gravity Data Over Ice-Covered Marine Areas

S. Märdla, T. Oja, A. Ellmann, and H. Jürgenson

Abstract

For accurate regional gravity field modelling it is vital to have dense and high quality data coverage. Ice gravimetry is a viable alternative to ship- and airborne gravimetry to help fill gaps over marine areas. A number of factors affect the accuracy of gravimetry on ice, thus special survey and data processing methods are needed. Nevertheless with appropriate methods an accuracy of ± 0.16 mGal was achieved on coastal ice. An efficient method for positioning of survey points is RTK GNSS which takes no more than a few minutes on each point and the accuracy achieved is at least ± 0.15 cm, while 10 min static surveys also yield acceptable results.

This study reports ice gravity surveys proceeded on shore-fast ice in the Väinameri Basin, Estonia. Acquired gravity data agree with existing airborne data while covering a larger area. As a result of the survey it was possible to confirm and specify the extents of an area of positive anomalies. An effort to determine the geoid heights over Väinameri Basin directly via using the GNSS data gathered during gravity surveys on ice was made. For now it proved to be less reliable than classical geoid determination from gravity data.

Keywords

Airborne gravimetry • Baltic sea • GNSS positioning • Gravity anomaly • Ice gravimetry • Relative gravimetry

1 Introduction

Satellite data have resolved the long-wavelength part of the global geoid with an accuracy of a few cm. In particular, thanks to dedicated gravimetric satellite missions (mainly GRACE and GOCE) there is now homogeneous global coverage of long wavelength gravity data with spatial resolution better than 100 km. However, in regional geoid modelling the satellite-only data need to be complemented with high quality and dense regional data across the entire study area. Therefore, when the gravity field is modelled in local scales for geoid computation, large lakes and coastal waters also need to be covered by gravity observations.

Filling gravity data gaps over water bodies is clearly more complicated than on land. Satellite altimetry can be used over open oceans. However, its usability in coastal waters is limited, see e.g. Fernandes et al. (2003), Deng et al. (2002) and references therein. Therefore a special vessel as well as equipment is needed for marine gravity surveys which make such observations expensive and time-demanding. Also, marine gravity data may often be contaminated with systematic errors due to factors of the moving survey environment, instrumental and navigational errors

S. Märdla (✉) • A. Ellmann
Tallinn University of Technology (TUT), Ehitajate tee 5, 19086 Tallinn, Estonia
e-mail: silja.mardla@ttu.ee

T. Oja
Estonian Land Board, TUT, Mustamäe tee 51, 10621 Tallinn, Estonia

H. Jürgenson
Estonian University of Life Sciences, Kreutzwaldi 1a, 51014 Tartu, Estonia

(Denker and Roland 2005), that need to be corrected via data processing methods, see e.g. Motao et al. (1999) and references therein.

During the past decade small aircraft have also been used for gravity data acquisition above water bodies, see Forsberg et al. (2001), Hwang et al. (2007) and references therein. However, acquisition of low-elevation airborne data near coasts may be complicated due to the turbulent environment caused by different temperatures of land and water. Therefore both coverage and quality of gravity data collected during marine and aerogravity surveys at shorelines could be quite heterogeneous, which affects subsequent geoid determination accuracy in the coastal regions.

Although not possible everywhere, gravity surveys on shore-fast ice with terrestrial gravimeters is an alternative to marine and airborne surveying. Modern equipment allows for accurate, relatively fast and therefore cost-efficient acquisition of gravity data over ice covered waters. Relative gravity surveys near the coast can easily be connected to the gravimetric network on land, which make them a valuable set of information for validating marine and airborne data.

Gravity surveys on ice were tried already in the 1950s, see a review in Lehmuskoski and Mäkinen (1978). Surveys have been proceeded in the Gulf of Botnia (Lehmuskoski and Mäkinen 1978), at Wanapitei Lake in Canada (Ugalde et al. 2006), Lake Vänern in Sweden (Ågren et al. 2015), on several large Estonian lakes and the Gulf of Riga (Oja et al. 2011). These studies reveal many issues related to mainly wind, ice oscillation and movement, positioning and data processing that affect the quality of gravity observations on ice and thus need to be investigated.

The main objective of this contribution is to assess and compare the quality of gravity data obtained by surveying on marine ice. Emphasis is on methods of evaluation: mainly comparison of gravity surveys on ice with airborne gravimetry, but also using the precise GNSS positioning on top of ice to validate possible geoid modelling improvements.

The paper is structured as follows. The introduction is followed by a review on problems concerning gravity surveys on ice alongside with methods of validating gravity surveys over water. The methods and results of a case study conducted on the Baltic Sea ice are presented. Brief conclusions summarize the contribution.

2   Problems of Gravity Surveys on Ice

According to previous studies (cf. references above) surveying gravity on ice is complicated by moving ice and weather conditions. One problem is the gravimeter tilting due to some compaction of snow as well as melting of ice under the tripod (occurring even with insulation) and the weight of equipment on ice. Modern gravimeters like Scintrex CG5 units have tilt

sensors which help correct for the inclination, but only as long as it remains within their working range, thus possible continuous measurement time is limited (Ugalde et al. 2006).

Another problem is strong wind above the ice that shakes the gravimeter (which was one of the main problems on Lake Vänern, see Alm et al. 2011) but also creates noticeable ice oscillation (Kiviniemi 1975). Ice moves and vibrates constantly: high frequency gravity records show peak-to-peak amplitudes of over 150 mGal occurring at frequencies of 0.05–0.35 Hz (at periods of 3–20 s), see Oja et al. (2011), which creates certain challenges for subsequent data processing. Similarly to surveys on land, to obtain reliable ice-gravity results a number of points need to be revisited to allow for gravimeter's drift calculation. A detailed discussion of other possible error sources in ice gravimetry is given in Lehmuskoski and Mäkinen (1978).

Fortunately, visual output of observed high-frequency signal on the screen of some modern gravimeters such as the Scintrex CG5 helps to estimate the quality of surveys on site and adjust the instrument and method accordingly. Hence it has been possible to achieve uncertainties of ±0.15 mGal in recent surveys (Oja et al. 2011; Ågren et al. 2015). The obtained results should be compared with existing gravity datasets.

3   Comparing Gravity Data from Different Sources

Comparing gravity anomaly values from different sources can not be proceeded directly. First, locations of different survey points do not coincide exactly. This can be overcome by interpolating gravity anomaly values of one campaign to the locations of the other. Second, survey altitudes can be different and need to be accounted for. Fortunately, in comparisons of ice gravity data to shipborne surveys the difference in heights is not significant. Conversely, in case of airborne surveys the results at flight level need to be downward continued (DWC) to the sea level.

The problem of DWC is visualized in Fig. 1 that describes comparison of gravity surveys on ice with airborne surveys. The corresponding free air anomalies (Δg) are calculated as follows:

$$\Delta g_{air}(\Omega) = g(r_{air}, \Omega) - \left[\gamma_0(r_e, \Omega) + \frac{\partial \gamma}{\partial h} \cdot H_{air}(\Omega) \right] \quad (1)$$

$$\Delta g_{ice}(\Omega) = g(r_{ice}, \Omega) - \left[\gamma_0(r_e, \Omega) + \frac{\partial \gamma}{\partial h} \cdot H_{ice}(\Omega) \right] \quad (2)$$

where g is measured gravity, γ_0 is the normal gravity on the surface of reference ellipsoid, r is the geocentric radius, Ω is the coordinate pair (latitude, longitude), H is the height with respect to the vertical datum, h is the geodetic
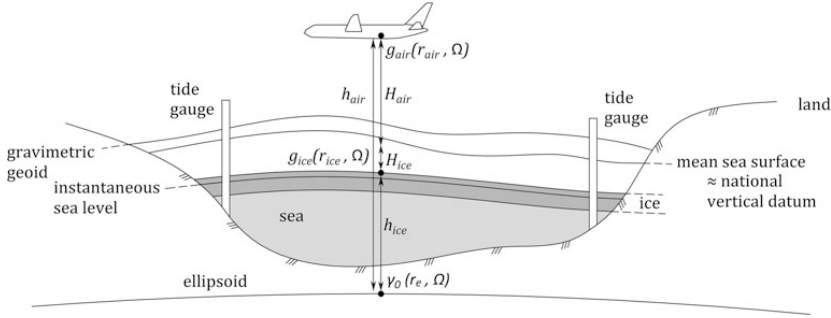
Fig. 1 Comparing gravity surveys on different height levels, the symbols used are explained in the text

height reckoned from the ellipsoid and $\partial\gamma/\partial h$ is the normal gravity gradient. Subscripts *ice* and *air* denote parameters acquired during ice and airborne gravity surveys, *e* refers to the surface of ellipsoid. Note that h can be measured by GNSS during surveys, H_{ice} can be obtained from the sea level data (nearby tide gauges) and H_{air} is conveniently derived in aerogravimetric data processing. To find the difference between gravity anomalies computed in air and on ice Eq. (1) is subtracted from Eq. (2):

$$\Delta g_{air}(\Omega) - \Delta g_{ice}(\Omega) =$$

$$g(r_{air}, \Omega) - g(r_{ice}, \Omega) - \frac{\partial\gamma}{\partial h} \cdot H_{air}(\Omega) + \frac{\partial\gamma}{\partial h} \cdot H_{ice}(\Omega) = \quad (3)$$

$$\frac{dg}{dH}(r_{air}(\Omega) - r_{ice}(\Omega)) - \frac{\partial\gamma}{\partial h}(H_{air}(\Omega) - H_{ice}(\Omega))$$

where dg/dH is the gravity gradient. Since

$$r_{air}(\Omega) - r_{ice}(\Omega) = H_{air}(\Omega) - H_{ice}(\Omega) \approx H_{air}(\Omega) \quad (4)$$

then

$$\Delta g_{air}(\Omega) - \Delta g_{ice}(\Omega) = H_{air}(\Omega) \cdot \left(\frac{dg}{dH} - \frac{\partial\gamma}{\partial h}\right) \quad (5)$$

Eq. (5) represents DWC correction for gravity anomaly and needs to be accounted for in rigorous comparisons of different gravity sets. There are a number of methods to estimate it, see Ellmann (2011) and references therein for an extended discussion.

4 Relation Between Gravity and GNSS Observations

Without accurate positioning all the care taken to measure the gravity signal becomes useless. Considering the gravity gradient of about 0.3 mGal/m: to achieve the accuracy of

± 0.05 mGal of gravity values a vertical positioning accuracy of about ± 0.15 m has to be achieved. Presently such an accuracy can in most cases be achieved by using RTK (Real Time Kinematic) GNSS positioning. For rapid positioning a reliable VRS (Virtual Reference Stations) service and a cellular data network can be used (where available), otherwise rapid static GNSS observations or other approaches are needed.

Gravity surveys are nowadays accompanied with precise GNSS positioning. The sea ice should reflect quite well the shape of a calm sea surface which in turn should reflect the shape of the geoid. Therefore GNSS positioning provides an additional dataset for validating the geoid model via comparison of heights of survey points situated directly on ice to the geoid model. For this it is important to consider variations of sea level heights during the surveys: ice may be above or below the national vertical datum (cf. Fig. 1 and Sect. 6.3).

5 Case Study on the Väinameri Basin

Due to the large number of islands and islets more than 85% of Estonian borderline is in fact waterfront. Therefore it is vital for Estonian gravity field (and consequent geoid) modelling to have sufficient data available over marine areas. For instance the historic (performed in the 1960s) Gulf of Riga seabottom gravity survey results and the 1999 Baltic Sea airborne gravity campaign (Forsberg et al. 2001) data have been used in earlier geoid modelling studies (Forsberg 2001; Ellmann 2005; Ellmann et al. 2011).

There was evidence however that there may be biases in existing datasets or some important features may be missing from the current gravity field model over marine areas. Since 2009 numerous winter campaigns of relative gravity surveys have been conducted on ice-covered lakes and coastal sea to evaluate the historic datasets and to fill gaps of gravity data in marine areas, the latest of these on the Väinameri Basin of the Baltic Sea in the West Estonian Archipelago.

5.1 Characteristics of the Study Area

The Väinameri Basin is a semi-closed (surrounded by an arc of islands and the mainland) and rather shallow water body with a mean depth of about 5 m. Its area is 2,200 km^2 and it contains hundreds of islets. Compared to the rest of the Baltic Sea the ice cover is formed more frequently and lasts longer (up to 4 months in cold winters). Väinameri, similarly to the rest of the Baltic Sea, is almost tide-less (tides are below a dm level). Instead, the sea level fluctuations are primarily forced by the wind stress and atmospheric pressure changes (Liibusk et al. 2013).

So far there were almost no gravity data except for a few (possibly poorly connected) measurements on the islets (Ellmann et al. 2009) and a single track of the 1999 airborne gravity campaign. Δg of these airborne data were the basis for compiling the anomaly field model used for calculating a recent national gravimetric geoid model GRAV-GEOID2011 (Ellmann et al. 2011), also for Märdla et al. (2015). Thus possible errors in the airborne data strongly affect resulting geoid models.

Indeed, a suspicious "lump" was detected in the anomaly field model over the sea surface of Väinameri (see its location on Fig. 4), showing anomalies up to 9 mGal larger than on surrounding islands. This was in fact one of the main reasons for conducting ice gravity surveys in this particular area. With new gravity data obtained in the surveys it would be possible to verify and improve the gravity anomaly field model.

In the winter of 2013 the Väinameri Basin became covered with a 20...50 cm thick layer of shore-fast ice. The adjacent marine areas were also covered with pack ice. Weather conditions were stable with prevailingly Southern winds well below 5 m/s and steadily high air pressure within the study area during the gravity surveys.

Surveys over the Southern part of the Väinameri Basin were carried out during 4 days in Feb–March 2013, covering about 1,000 km^2. The density (1 point/25 km^2) of surveys (altogether 41 points on ice, additionally 8 points on land) corresponds to that over land. The coverage of ice surveys, however, is more even since it is not constrained to existing roads.

Data collection consisted of relative gravity surveys and point positioning, additionally ice thickness and water depth were recorded (not used in data processing). On ice the team and equipment were transported by a lightweight amphibious crawler (Fig. 2).

5.2 Relative Gravimetry

Gravity measurements were performed relative to points on land using a digital Scintrex CG5 spring gravimeter no. 36

Fig. 2 Gravity surveys and GNSS positioning on Väinameri Basin, a lightweight amphibious crawler was used for transport

(hereafter S36). The benefit of using a CG5 gravimeter is its ability to record readings with a 6 Hz frequency, allowing for study of accelerations created by the vibration of ice surface.

The S36 used has been tested on the Pärnu and Tõravere-Haanja calibration lines in Estonia, an acceptable accuracy of about 200 ppm was concluded (Oja et al. 2010). Since the estimated gravity range in the study area was about 32 mGal, the calibration error of the S36 has an insignificant effect on the survey results (less than 10 μGal).

On each point at least three sets of 60 s readings were taken. Usually, the gravimeters readings in a set on ice were scattered a few mGal from the average (on land the scatter was 0.1...0.2 mGal), the sets agreed with each other within 50 μGal. In case the readings between sets deviated from the average by more than ±0.1 mGal the recording time was extended to 90 or even 120 s. Observations much longer than 120 s tend to be affected by the gravimeter's tilt and consume twice the time, hence were not used.

Gravity surveying was proceeded using loops so that every loop was closed within a day. The starting points on land and one or two additional points were repeated during the same day to estimate the drift parameters of the gravimeter in subsequent data processing. Moreover, on ice at least one point from a previously measured loop was repeated to estimate consistency between the results of different days. The starting points were connected with the national gravity network after the snow and ice melted and the network points were accessible again. Note that different time periods may introduce additional errors into survey results due to changing environmental conditions such as fluctuations in ground water level, sea level variations and so forth.

For gravity data processing and adjustment the GRAVS2 software package developed by the Estonian Land Board was applied. Points of the gravity network were used as reference for the adjustment. Gravity data was processed in much the same way and considering the same issues as in previous ice gravity campaigns in Estonia, see Oja et al. (2011) for more details.
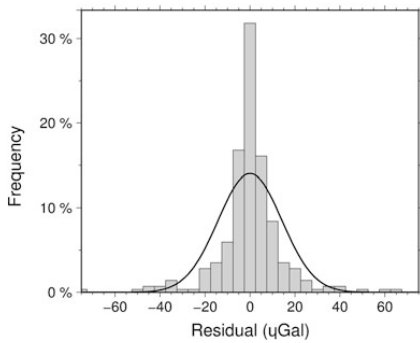
Fig. 3 Histogram of residuals of the adjustment of 286 readings, the bins near the edges and the misfit with the normal distribution curve are apparently connected to the effect of vibration noise on the readings

For comparison of gravity values on revisited points the results were reduced to the height level of the first measurement by applying a free air correction corresponding to the height difference obtained from GNSS data analysis (see Sect. 5.3). The gravitational attraction of changing volume of sea water nor the effect of changing air pressure were accounted for as the effects were estimated to be insignificant (both well below $10 \mu Gal$). After the reduction of gravimeter's drift effect on readings the discrepancies on revisited points were less than $20 \mu Gal$.

All in all the gravity data obtained on shore-fast ice was reasonably good: the expanded uncertainty multiplied by a coverage factor of k=2 (2-sigma) of ± 0.15 mGal was achieved from a least squares adjustment. It can be seen from the histogram of residuals of the adjustment of 286 readings (Fig. 3) that most of the residuals are within $25 \mu Gal$. However, the variation of readings on ice is much higher compared to land data, some residuals reach $40\ldots 65 \mu Gal$. Therefore ice gravity data was weighted down (decreased by a factor of 4) in the adjustment. In addition, the uncertainty of reference points (about $60 \mu Gal$) was considered.

Considering also the uncertainty of GNSS height positioning of ± 0.15 m (see Sect. 5.3) but neglecting a number of factors with smaller significance mentioned in Lehmuskoski and Mäkinen (1978) the final uncertainty estimation of gravity values amounts to

$$\sigma_g = \pm\sqrt{0.15^2 + (0.15 \cdot 0.3086)^2} = \pm 0.16 \text{ (mGal)} \quad (6)$$

Uncertainty of ± 0.16 mGal is close to that of modern gravity data collected on land and better than most data

currently available for gravity field modelling. The obtained accuracy is largely sufficient for calculating a geoid model with the accuracy below 1 cm (Ågren and Sjöberg 2015).

5.3 Survey Point Positioning

Positioning of the survey points at Väinameri was proceeded by GNSS methods using a GPS/GLONASS Trimble R8 receiver and a VRS service provided by a commercial CORS (Continuously Operating Reference Stations) network.

A combination of rapid static and kinematic surveys was tested for additional estimation of efficiency and accuracy, also because the availability of cellular network (necessary to obtain corrections via the VRS service) in such a remote area was uncertain before the campaign.

On 18 points a 10 min static measurement was conducted together with at least three kinematic readings of 5 s whereas towards the end of the campaign only kinematic readings were taken. In addition to three evenly distributed CORS 35–50 km away, a dual-frequency Trimble 5800 GPS receiver was set up on the coast about 5 km away and operated as a base point during 5 h of the campaign, covering the static measurement of 9 points in the Western part of the study area.

Data processing, which consisted primarily of baseline processing, was proceeded using a commercial software (Trimble Business Centre). It has to be mentioned that having an additional base point set up did not have a significant effect on the accuracy of positioning. This was revealed from varying baseline processing methods in which the base point position was fixed with different accuracy.

Discrepancies between static and kinematic height results at Väinameri reached $+0.03 \pm 0.04$ m. Although static measurements provided systematically larger height values, distribution of discrepancies does not reveal anything specific (except for a few larger ones in the NE being close to 10 cm).

Additionally differences of height values on revisited points were investigated. On land these were on a cm level, on ice as much as 15 cm. This reflects not only precision of GNSS positioning but also change in the water level during the survey.

In the light of GNSS quality assessment at Väinameri it can be concluded that an uncertainty of ± 15 cm can be expected in height values although most points are likely to have a smaller error than this. VRS RTK surveys should be preferred as they are faster, but readiness for static surveys needs to be maintained in case the cellular data network fails in such remote areas.
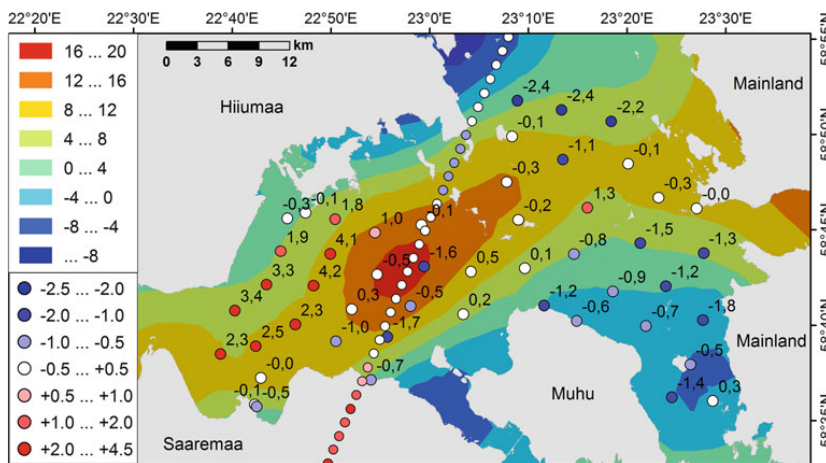
Fig. 4 Locations of air (*line-like sequence*) and ice (*scattered*) gravity points over the Väinameri Basin. The figure is contoured according to the Δg field used for calculating GRAV-GEOID2011, the colour range is explained in the *top legend*. Differences of $\Delta g_{ice} - \Delta g_{field}$ (shown as values on the figure) and $\Delta g_{air} - \Delta g_{field}$ in mGal are depicted by the *colours* explained in the *bottom legend*

6 Results and Comparisons

The results of the Väinameri campaign were compared to existing data that include (see also Sect. 5.1):

– Baltic Sea aerogravity survey from 1999
– The gravity anomaly field model used to calculate the official gravimetric geoid model of Estonia, GRAV-GEOID2011 (the existing gravity field model)
– The gravimetric geoid GRAV-GEOID2011 itself (the existing geoid model)

6.1 Evaluation of Aerogravity Data

In the Baltic Sea aerogravity survey a precision of ± 2 mGal was achieved (revealed from cross validation between tracks, Forsberg et al. 2001). Gravity anomalies from the Baltic Sea aerogravity data, downward continued to the sea level [see Eq. (1)...(5)] by an approach in Ellmann (2011), were used in this study.

As airborne data is very sparse in the Väinameri area (see the line-like sequence of points on Fig. 4), interpolation does not yield very good results. Therefore only a visual inspection of adjacent points of airborne and ice gravity data was made. Comparisons revealed that the air and ice gravity campaigns do not differ more than 2 mGal which confirms the initial accuracy estimation achieved from cross validation between tracks.

In marine areas off the NW coast of Estonia these airborne data are (and most likely will be for a while) the only data to describe the gravity field. Therefore knowing that airborne data are trustworthy in this area is very important.

6.2 Improvements to the Existing Gravity Field Model

Gravity data obtained in the Väinameri campaign was compared to the existing gravity field model. Although the average difference of ice gravity results from the anomaly field model is only $+0.09$ mGal the standard deviation is as large as ± 1.70 mGal (Fig. 4).

Looking at the distribution of these differences a number of features can be noted. Importantly, the new ice gravity dataset confirmed the existence and magnitude of the area of positive gravity anomalies (the "lump" in the anomaly field) estimated from airborne data. However, it reaches further West than expected. Also, the Eastern part of Väinameri has in fact slightly smaller anomaly values than previously known.

An initial comparison has revealed that the errors in the existing gravity field model in the Väinameri area have an effect of about a cm on the geoid model. Therefore a significant improvement has been made in the light of the attempts to calculate a geod model with an accuracy of 1 cm.

6.3 Evaluation of the Existing Geoid Model Using GNSS Surveys on Ice

The obtained geodetic heights of ice gravity points in the Väinameri Basin are a rather interesting source for verifying
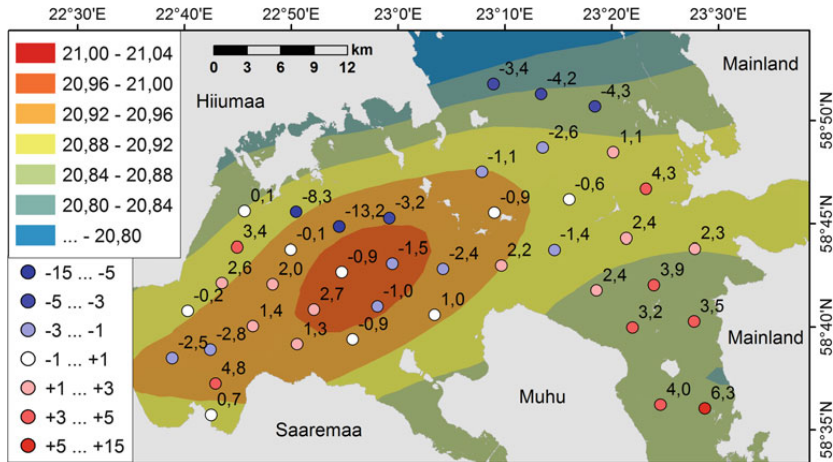
Fig. 5 Contoured GRAV-GEOID2011 model, the colour range in metres is explained in the *top legend*. Discrepancies of GNSS heights with respect to the GRAV-GEOID2011 model (in cm, GNSS-geoid, 1D offset removed) are depicted by *coloured circles* explained in the *bottom legend*

the shape of the marine geoid. In the following discussion RTK heights are used since they exist on all survey points and seem to be at least equally accurate as the static results.

To be able to compare GNSS heights obtained on survey points directly to the gravimetric geoid model heights in the Väinameri Basin some corrections need to be accounted for. During the surveys instantaneous sea level differed from the mean sea level by 30...45 cm (cf. Fig. 1). First, sea level corrections obtained from interpolating values from five surrounding tide gauges (from the online sea level system of Marine Systems Institute, TUT) were applied to surveyed heights. Second, the average difference of +0.375 m between survey point heights and the gravimetric geoid model in the study area was accounted for to simplify comparison. Note that variations in ice top and sea level difference were not accounted for, these could reach no more than 3 cm considering that ice thickness varied from 20...50 cm.

Difference of corrected heights of survey points from the GRAV-GEOID2011 model are depicted in Fig. 5. The standard deviation of differences was ±0.036 m. The largest differences (negative values in NW) appear where the discrepancy between static and kinematic GNSS results was also the largest (up to 10 cm), thus the comparison is not very reliable in that particular area. Although, large deviations could also be due to prevailing Southern winds raising the sea level above average in the area, therefore contradicting the assumption of the ice surface reflecting the geoid surface.

Although differences on adjacent points are similar and the results seem promising they do not match so well with the differences in the anomaly fields (Fig. 4). For example in the East, with addition of ice gravity data, free air anomalies

decreased and the height values in NE also decreased but in SE they increased. SE and NE were surveyed on different days which leads to suspect that the points in South could have a systematic error component in GNSS heights.

For now it seems like the GNSS positioning methods used are not accurate enough for direct geoid determination. Nevertheless, higher accuracy of height positioning on sea ice could allow for direct marine geoid determination using height data only.

7   Conclusions

Ice gravimetry is a viable alternative to ship- and airborne gravimetry in areas of shore-fast ice formation – with appropriate survey and data processing methods it is possible to achieve uncertainties of ±0.16 mGal. This is better than most gravity data currently available on land and satisfies easily the accuracy requirements needed for a 1 cm geoid determination.

One source of errors in collecting gravity data can be the positioning of survey points. A preferred method, where available, is RTK GNSS positioning using a VRS service.

Validation and comparison of ice gravimetry can be proceeded after reducing survey results to the same position in space. It was found that in the Väinameri Basin the Baltic Sea 1999 airborne gravity data agree reasonably well (±2 mGal) with new ice survey results.

The survey in Väinameri has revealed important information about the gravity anomaly field, confirming the existence of a local anomaly in the gravity anomaly field, specifying its magnitude and extents.

GNSS positioning on shore-fast ice could become an additional method of determining the shape of the marine geoid. However, the achieved uncertainty of ± 0.15 m in height determination seems insufficient for the method to improve the marine geoid model in Väinameri to the same accuracy as gravity data allow.

References

Ågren J, Sjöberg LE (2015, in print) Investigation of gravity data requirements for a 5 mm-quasigeoid model over Sweden. In: Rizos C, Willis P (eds) Gravity, geoid and height systems GGHS2012. IAG Commission 2: Venice, Italy, 9–12 October 2014, IAG symposia proceedings, vol 141. Springer, Berlin/Heidelberg, pp 143–150

Ågren J, Engberg LE, Alm L, Dahlström F, Engfeldt A, Lidberg M (2015, in print) Improving the Swedish quasigeoid by gravity observations on the ice of lake Vänern. In: Rizos C, Willis P (eds) Gravity, geoid and height systems GGHS2012. IAG Commission 2: Venice, Italy, 9–12 October 2014, IAG symposia proceedings, vol 141. Springer, Berlin/Heidelberg, pp 171–178

Alm L, Engberg LE, Dahlström F, Ågren J, Engfeldt A, Lidberg M (2011) Relative gravity measurements on the ice of lake Vänern. In: Symposium of the IAG subcommission for Europe (EUREF), Chisinau, Moldova, 25–28 May 2011. www.euref.eu/symposia/2011Chisinau/p-04-p-Engberg.pdf

Denker H, Roland M (2005) Consistent marine gravity data set surrounding Europe. In: Sansò F (ed) A window on the future of geodesy. In: Proceedings of the IAG general assembly, vol 128, Sapporo, 30 June–11 July 2003. Springer, Berlin/Heidelberg, pp 248–253

Deng X, Featherstone WE, Hwang C, Berry PAM (2002) Estimation of contamination of ERS-2 and POSEIDON satellite radar altimetry close to the coasts of Australia. Mar Geod 25:249–271

Ellmann A (2005) Two deterministic and three stochastic modifications of stokes formula: a case study for the Baltic countries. J Geodesy 79:11–23

Ellmann A (2011) Downward continuation of airborne gravity data using high-resolution global geopotential models. In: Cygas D, Froehner KD (eds) Selected papers of the 8th international conference on environmental engineering, 19–20 May 2011. VGTU Press, Vilnius, Lithuania, pp 1315–1320

Ellmann A, All T, Oja T (2009) Towards unification of terrestrial gravity data sets in Estonia. Estonian J Earth Sci 58(4):229–245

Ellmann A, Oja T, Jürgenson H (2011) Application of space technologies to improve geoid and gravity field models over Estonia (in Estonian). Geodeet 41:22–25

Fernandes MJ, Bastos L, Antunes M (2003) Coastal satellite altimetry – methods for data recovery and validation. In: Tziavos IN (ed) Proceedings of the 3rd meeting of the international gravity and geoid commission (GG2002), Editions ZITI, pp 02–307

Forsberg R (2001) Development of a Nordic cm-geoid with basics of geoid determination. In: Harsson BG (ed) Nordic Geodesy towards the 21st century. Lecture notes for Autumn School, Nordic Geodetic Commission 2001:1. Statens Kartverk, Hønefoss, pp 67–88

Forsberg R, Olesen AV, Keller K, Moeller M, Gidskehaug A, Solheim D (2001) Airborne gravity and geoid surveys in the Arctic and Baltic seas. In: Proceedings of international symposium on kinematic systems in geodesy, geomatics and navigation (KIS-2001), Banff, pp 586–593

Hwang C, Hsiao Y-S, Shih H-C, Yang M, Chen K-H, Forsberg R, Olesen AV (2007) Geodetic and geophysical results from a Taiwan airborne gravity survey: data reduction and accuracy assessment. J Geophys Res 112:B04407

Kiviniemi A (1975) Measurements of wave motion in the ice surface. Technical Report 75:4, Finnish Geodetic Institute

Lehmuskoski P, Mäkinen J (1978) Gravity measurements on the ice of Bothnian Bay. Technical Report, Finnish Geodetic Institute

Liibusk A, Ellmann A, Kõuts T, Jürgenson H (2013) Precise hydro-dynamic leveling by using pressure gauges. Mar Geod 36(2):138–163

Märdla S, Oja T, Ellmann A, Jürgenson H (2015, in print) Modelling the influence of terraced landforms to the Earth's gravity field. In: Rizos C, Willis P (eds) Gravity, geoid and height systems GGHS2012. IAG Commission 2: Venice, Italy, 9–12 October 2014, IAG symposia proceedings, vol 141. Springer, Berlin/Heidelberg, pp. 157–162

Motao H, Zheng G, Guojun Z, Yongzhong O (1999) On the compensation of systematic errors in marine gravity measurements. Mar Geod 22(3):183–194

Oja T, Türk K, Bloom A, Sulaoja M (2010) Gravity surveys on the ice of the Gulf of Riga in 2010 (in Estonian). Technical Report, Reasearch Project ETF7356, pp 71

Oja T, Türk K, Ellmann A, Gruno A, Bloom A, Sulaoja M (2011) Relative gravity surveys on ice-covered water bodies. In: Cygas D, Froehner KD (eds) Selected papers of the 8th international conference on environmental engineering, 19–20 May 2011. VGTU Press, Vilnius, Lithuania, pp 1394–1401

Ugalde HA, L'Heureux E, Lachapelle R, Milkereit B (2006) Measuring gravity on ice: an example from Wanapitei Lake, Ontario, Canada. Geophysics 71(3):J23–J29

Paper D

Märdla, S., Oja, T., Ellmann, A., and Jürgenson, H. (2014). "Modelling the Influence of Terraced Landforms to the Earth's Gravity Field". In: *Gravity, Geoid and Height Systems*. Ed. by U. Marti. International Association of Geodesy Symposia 141. Venice, Italy: Springer International Publishing, pp. 157–162. ISBN: 978-3-319-10836-0. DOI: 10.1007/978-3-319-10837-7_20. **Paper D**.

Modelling the Influence of Terraced Landforms to the Earth's Gravity Field

Silja Märdla, Tõnis Oja, Artu Ellmann, and Harli Jürgenson

Abstract

Medium resolution (1–3 arc-min) gravity anomaly grids do not reflect reality very accurately over terraced landforms, which in turn may affect the uncertainty of subsequent geoid modelling. This inaccuracy is due to many factors. The gravimetric datasets used in the gridding of gravity field models have a varying accuracy and coverage, especially in terraced and coastal areas. Further, the resolution of the terrain model used in the modelling of anomaly grids is usually too low to capture the complete gravimetric attraction of terraced landforms.

Since the values of free-air anomalies are strongly correlated with terrain heights, it is difficult to model the gridded surface over terraced landforms. Depending on the quality of existing gravity data and terrain height models, different procedures should be used. In the case of a terraced area that is densely covered by gravity data, if an accurate terrain model exists, free-air anomaly grids should be calculated on high resolution ($6'' \times 12''$) and using Bouguer anomaly values on grid nodes. If gridding is proceeded without Bouguer anomalies, triangulation based gridding methods should be preferred.

Keywords

Gravity • Anomalies • Gridding • Terrace • North-Estonian Klint

1 Introduction

The Earth's gravity field is varying, especially in areas of changing terrain surface. Today the global, long-wavelength features of the gravity field are relatively well known thanks to dedicated gravimetric satellite missions. A recent combined Earth's geopotential model EGM08 (Pavlis et al. 2012) has a resolution of 5 arc-min (corresponding to 9 km). Although it could correspond well with local gravity data within gravimetrically well studied areas (see e.g. Ellmann 2010), its spatial resolution or accuracy is still not sufficient for engineering applications, where 1–2 cm accuracy of geoid model is needed. Having better knowledge about the local nature of the gravity field would allow for more accurate regional geoid models, calculation of which is aided by the SRTM global topography model (Farr et al. 2007). In many countries, even more accurate airborne LIDAR-acquired data exist. Apparently, availability of detailed terrain heights helps improve gravity anomaly data.

The conventional and still often used source data for calculating a geoid model are the gravity free-air anomalies (FAA) deduced from gravity measurements. For some geoid computation methods (fast Fourier transform or Stokesian integration), anomalies need to be calculated into regular grids. This arises many questions about areas with sparse data, see e.g. Kirby et al. (1997), Goos et al. (2003) and references therein.

S. Märdla (✉) • A. Ellmann
Tallinn University of Technology, Tallinn, Estonia
e-mail: silja.mardla@ttu.ee

T. Oja
Tallinn University of Technology, Tallinn, Estonia

Estonian Land Board, Tallinn, Estonia

H. Jürgenson
Estonian University of Life Sciences, Tartu, Estonia

Usually, when compiling gravity anomaly models, no distinction is made between gridding over different landforms. It is, often optimistically, assumed that the selected gridding algorithm is universally suited for all landforms within the area of interest. In the past such simplification was often justified by computational constraints. In this study however, emphasis is on developing optimum gridding algorithms for areas with contrasting landforms.

The question arose since discrepancies between the results of different gridding methods seem to be especially large in areas with terraced landforms. Therefore, the behaviour of the gravity field in terraced areas, different methods for calculating gravity anomaly grids (without prior removal of any frequency based information such as EGM-based long-wavelength contribution) and the evaluation of the resulting models of gravity anomaly fields are discussed in this contribution.

First, different methods of gridding gravity data are introduced. Then, a numerical case study is described to evaluate these methods. The most suitable algorithm is found for gridding gravity data in the terraced study area. Obtained results are compared with existing models: the anomaly grids used for the latest Estonian gravimetric geoid calculation are evaluated. A discussion on practical uses of high resolution anomaly grids concludes this contribution.

2 Methods of Gridding Gravity Data

Gridding of gravity anomalies is a critical issue in geoid modelling, because any error committed at this stage will propagate into the geoid solution. There are a number of commonly used gridding methods. These include continuous curvature, triangulation or neighbouring points' based algorithms, among others. These are programmed into many software packages, including the free and open source Generic Mapping Tools (GMT; Wessel and Smith 1998), often used by geoscientists.

Continuous curvature is an algorithm that fits a curved surface between data points, allowing for a smooth and in a specific case even harmonic surface that either does or does not pass through all data points. Nearest Neighbour is an algorithm that considers only the very neighbouring points when calculating values. Triangulation gives a solution where the resulting surface passes through all data points. A grid can be produced from a triangulated surface by interpolation.

Due to free-air anomalies being strongly correlated with terrain heights, the FAA values can change quite rapidly in terraced areas. Therefore free-air anomalies are not very suitable for gridding. As discussed by many, e.g. Janák and Vaniček (2005), there are a number of different methods

Fig. 1 Detailed gravity measurement profiles Tabasalu1 and Tabasalu2 (depicted by *red dots*) crossing the North-Estonian Klint (depicted by the *brown line*) near seashore (Color figure online)

for compiling FAA grids, yielding remarkable differences in resulting anomaly models.

Instead of directly gridding the FAA values, the FAA grids can also be obtained through simple or complete Bouguer anomalies (denoted correspondingly as SBA and CBA) that have a much smoother behaviour in most cases. The grid is obtained by using a terrain model to calculate FAA values at every grid node of the Bouguer anomaly grid. Note that accurate height information at every grid node is needed for such a gridding approach. If heights are not well known, the free-air anomalies cannot be derived accurately through Bouguer anomaly grids.

Over the Canadian Rocky Mountains Janák and Vaniček (2005) calculated free-air anomalies through SBA and CBA. Systematic errors up to 20 mGal between corresponding FAA grids and 2 m in subsequent geoid models were detected. Therefore it is reasonable to believe that, in a terraced area, in addition to the gridding method, the way of obtaining free-air anomaly grids is also important.

3 Gravity and Terrain Data Within the Study Area

For the evaluation of gravity anomaly grids, detailed gravity surveys were conducted at a terraced area in Tabasalu, some 10 km west from Tallinn, the capital of Estonia. It is an area on the seashore with the North-Estonian Klint passing through, having a height of about 30 m there. Two gravity profiles (Tabasalu1 and Tabasalu2) were measured almost perpendicularly to the Klint, see Fig. 1.

Gravity data were measured about every 100 m with uncertainty of ±0.07 mGal. Coordinates and heights were deduced from GPS measurements with maximum uncertainty of about ±5–10 cm.

For the modelling of the gravity field, an existing gravity anomaly database of Estonia was used. The gravity data available in the study area mostly consist of gravity values with uniform uncertainty estimates (about ±0.2 mGal) from the surveys of Geological Survey of Estonia. For more details on the database, the evaluation of the gravity data in question and earlier use of the data see Ellmann et al. (2009) and references therein. Average gravity data density within the selected study area is 0.25 km in the North-south direction and 1 km in the East-west direction (see Fig. 5 for gravity points' placement).

From the gravity data measured, free-air, simple and complete Bouguer anomalies were calculated. For calculation of spherical terrain correction (e.g. Janák and Vaniček 2005) values, a LIDAR and SRTM combined digital terrain model (A. Gruno, *pers. comm.*) with $3'' \times 3''$ (approximately 90×45 m^2 in the study area) resolution was used. Discrepancies between the DTM and heights measured on profile points were found to reach up to 10 m. Apparently, even the $3'' \times 3''$ DTM does not have a high enough resolution or precise enough source data to reflect actual heights very accurately near a terrace.

Since the calculated spherical terrain corrections are less than 0.25 mGal the complete Bouguer anomaly values do not differ much from the simple Bouguer anomaly values. As the anomalies behave similarly, often no distinction is made between SBA and CBA in further discussion. Also, since both profiles showed similar gravity field behaviour, only Tabasalu1 is discussed hereafter.

As expected, the gravity increases with the height decreasing. Free-air anomalies are clearly correlated with height values with the change up to 6 mGal over the terrace. Bouguer anomalies (BA) however are smooth and not correlated with height values. Slight changes in the BA field near the terrace may be explained by complex variations of ground density underneath the terrace. See Talvik (2012) for a more detailed description of the gravity field in the area.

4 The Optimal Gridding Algorithm

As discussed in Sect. 2, there are many ways for gridding gravity anomalies. For this study, six different approaches were used to generate regular grids from the gravity anomaly database:

- GMT module *surface*, tension factors 0.25 and 1;
- GMT *triangulate*;
- Matlab *griddata*;
- GMT *nearneighbour* with 1′ search radius and four sectors (NN4);
- GMT *nearneighbour* with 1′ search radius and eight sectors out of which at least four must contain a point with a value that is not NaN (NN4/8).

Each time free-air anomalies were in turn calculated by the three different options described in Sect. 2. The resulting anomaly grids were denoted as following: FAAv (direct), FAAs (through SBA) and FAAc (through CBA).

In addition, six different grid resolutions were tested: $1' \times 2'$, $0.5' \times 1'$, $15'' \times 30''$, $6'' \times 12''$, $3'' \times 6''$ and $1.5'' \times 3''$. The lowest, $1' \times 2'$ (about 1.8×1.8 km^2) resolution corresponds to the resolution of the contemporary geoid and corresponding gravity (anomaly) field models of Estonia. The highest, $1.5'' \times 3''$ (about 45×45 m^2) resolution corresponds to the shortest distances between gravity points in the database and roughly to the distance between profile points.

The optimal gridding algorithm for the given terraced area proved to be the GMT *triangulate* with grid resolution of $6'' \times 12''$. This was determined by comparing the gridded anomaly data to the values obtained from the measurements on the profiles. For this, gravity anomaly values were interpolated from all the different grids to the profile points. Differences of the interpolated values and the measured values were depicted on one-dimensional profile graphs. The mean, root mean square (RMS), minimal and maximal discrepancies were found for each profile. The best algorithm was then chosen by the statistics of discrepancies.

The explanation to the optimal resolution lies in the average density of input gravity data in N-S direction (250 m $\approx 8''$). The advantage of the *triangulate* method is its ability to better reflect rapid changes in the modelled quantity, in this case, the anomaly field near the terrace's edge. Out of the modules available in GMT, the NN4 appeared to be almost as good as *triangulate* whereas the NN4/8 option was unable to estimate a value to many grid nodes. The GMT module *surface* with tension factor 0.25 distorts the gridded model unreasonably on resolutions higher than $6'' \times 12''$, which is something to take note of. When the tension factor was increased to 1, which gives a harmonic surface, the model was no longer distorted, statistical indicators however were still not as good as for the *triangulate* results.

Differences between methods were smaller for Bouguer anomaly fields as these have a much smoother behaviour. The best results were reached with the *surface* method, with other methods differing only by 0.1–0.2 mGal.

Discrepancies between the measured and interpolated (from the optimal *triangulate* $6'' \times 12''$ grid) anomaly values are shown on Fig. 2. The statistics of discrepancies between free-air anomalies are shown in Table 1, left hand side. On $6'' \times 12''$ resolution the free-air anomalies are considerably more accurate when gridded through Bouguer anomalies compared to when gridded directly.

In fact, the scheme of calculating the FAA grid through Bouguer anomalies instead of direct gridding yields a more

Table 1 Discrepancies of different type (FAA/FAAc) free-air anomaly grids from the profile data; units mGal

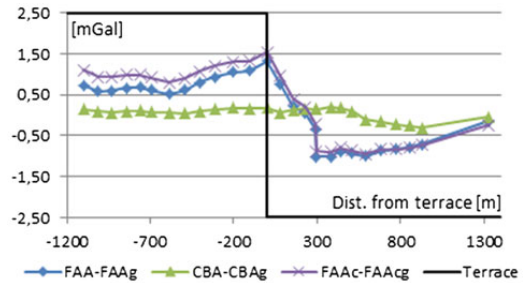| Profile	Optimal ($6'' \times 12''$)				GRAV-GEOID2011 ($1' \times 2'$)			
	Min	Max	Mean	RMS	Min	Max	Mean	RMS
Free-air anomaly (directly gridded)								
Tabasalu1	−1.74	+0.70	−0.34	±0.74	−1.02	+1.33	+0.10	±0.79
Tabasalu2	−2.06	+1.50	−0.41	±1.21	−1.65	+2.13	−0.16	±1.38
Free-air anomaly (using CBA)								
Tabasalu1	−0.39	+0.30	−0.04	±0.18	−0.95	+1.55	+0.28	±0.93
Tabasalu2	−1.17	+1.87	+0.29	±0.77	−1.22	+2.58	+0.25	±1.40
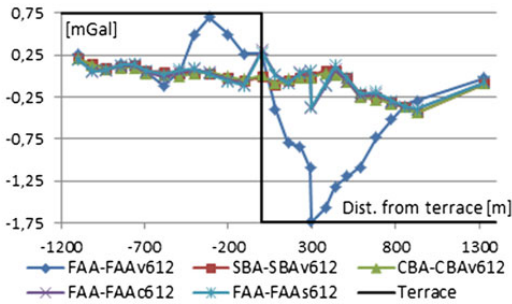
Fig. 2 Discrepancies between the gravity free-air (FAAv, FAAs and FAAc), simple Bouguer (SBA) and complete Bouguer (CBA) anomaly values calculated for the Tabasalu1 profile and interpolated from the optimal $6'' \times 12''$ *triangulate* grid (with suffix 612); the terrace is illustratively depicted by the *black line* (Color figure online)

Fig. 3 Discrepancies between the free-air (FAA and FAAc) or complete Bouguer anomalies (CBA) used for the GRAV-GEOID2011 (with suffix _g) and the profile measurements on Tabasalu1

accurate FAA grid only if the DTM resolution is as high as the resolution of the BA grid. If the DTM resolution is much lower than that of the BA grid, the resulting FAA grid is actually less accurate, which was noticed in the case of $1' \times 2'$ resolution (for calculations on each resolution the DTM was also sampled to that resolution).

5 Comparisons with Existing High-Resolution Gravity Anomaly Grids

The latest gravimetric geoid model of Estonia is GRAV-GEOID2011 (Ellmann et al. 2011). It has a resolution of $1' \times 2'$, which was also tested in this study. The free-air anomaly grids used for the geoid modelling had also been calculated directly from FAA values and through SBA or CBA.

The anomaly grids used for GRAV-GEOID2011 were compared to the profile measurements (Fig. 3). Discrepancies of the free-air anomaly values used for the GRAV-GEOID2011 from the measured data are shown in Table 1,

right-hand side. As mentioned, on low resolutions, gridding FAA through BA leads to no improvement of the FAA grid. That is why in case of the geoid modelling data, free-air anomalies obtained by gridding through CBA do not show a better agreement with the profile values.

Comparison of discrepancy graphs (cf. Figs. 2 and 3) and the statistics in Table 1 reveal that the $6'' \times 12''$ optimal grid corresponds better to profile measurements than the grids used for the geoid model.

Since the optimal $6'' \times 12''$ triangulate grids were found to have smaller discrepancies from the measured gravity anomaly values than those of the GRAV-GEOID2011, free-air anomaly grids of the geoid model were also compared to the corresponding optimal grids of the present study. To compare the free-air anomaly grids of GRAV-GEOID2011 to the optimal grid, the resolution of the first was increased to $6'' \times 12''$ by bicubic interpolation. Discrepancies between directly gridded free-air anomaly models did not exceed ±0.5 mGal and did not reveal any specific pattern.

However, discrepancies in free-air anomaly models obtained by gridding through complete Bouguer anomalies show a clear pattern with the optimal grid giving larger values on top of the terrace and smaller values on the foot than the grids used for the gravimetric geoid model (Fig. 4).
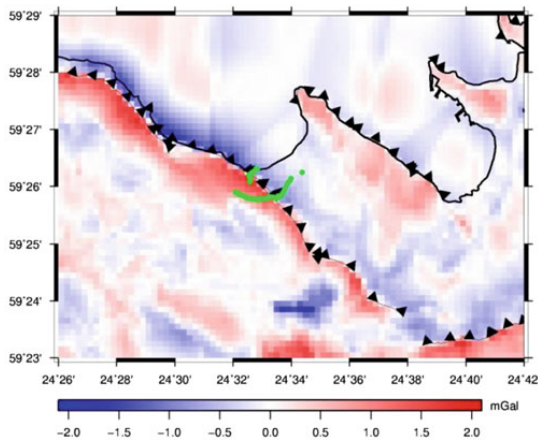
Fig. 4 Comparison of free-air anomalies gridded through complete Bouguer anomalies used for the GRAV-GEOID2011 model to the corresponding optimal $6'' \times 12''$ *triangulate* grid (optimal minus GRAV-GEOID); profiles depicted in *green*, the terrace by the aligned *black triangles* (Color figure online)
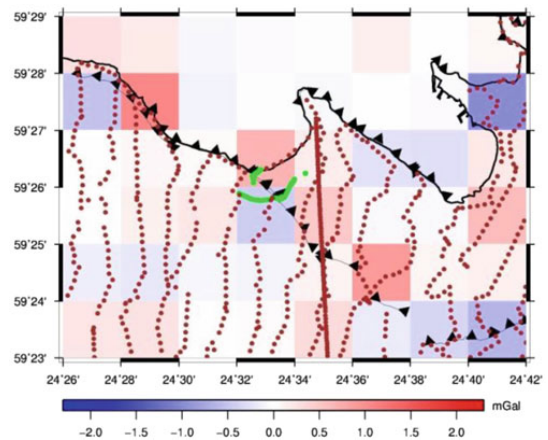
Fig. 5 Differences between the $1' \times 2'$ *triangulate* FAA grid and the $6'' \times 12''$ *triangulate* FAA grid averaged to $1' \times 2'$; profiles depicted in *green*, gravity data points in *brown* (Color figure online)

6   Averaging the Optimal $6'' \times 12''$ Anomaly Grid to $1' \times 2'$ Resolution

Using the optimal resolution of $6'' \times 12''$ in regional geoid modelling is computationally quite demanding (the number of cells increases two magnitude orders when using the resolution of $6'' \times 12''$ instead of $1' \times 2'$). Therefore, the reasonability of extracting areas that need specific attention, for example by selecting all cells that contain data points with height difference of more than 15 m or have a certain RMS value of heights within the grid cell, was investigated. In such areas, high-resolution gridding could be used. These grids could later be averaged back to $1' \times 2'$ resolution and substituted to the initial ($1' \times 2'$) anomaly grid.

In this study, $6'' \times 12''$ grid averaged to $1' \times 2'$ does not show superiority over the initial model calculated directly on $1' \times 2'$ resolution. This was determined by comparing the $6'' \times 12''$ *triangulate* grid averaged to $1' \times 2'$ resolution with the original $1' \times 2'$ *triangulate* grid (Fig. 5). Differences between free-air anomaly grids are not very significant (average difference is 0.06 ± 0.20 mGal), yet larger discrepancies occur near the terrace. Study of a longer strip along the coastline may reveal a clearer pattern.

Comparison of the averaged grid to profile values yields that the averaged grid is not necessarily more accurate than the original one; the discrepancies are just the same or slightly larger even. Similar results are seen for the free-air anomaly grids calculated using Bouguer anomalies.

Discussion and Conclusions

The $1' \times 2'$ resolution used for the gravimetric geoid model calculation appears to be too low to reflect short-wavelength changes in the gravity anomaly field near the terrace. One cell of the grid covers both the top and the foot of the terrace, thus assigning both the same gravity anomaly value which is a weighted average of the actual values, depending on the position of the cell. This implies that the magnitude of discrepancies from the actual value on top of or on the foot of the terrace may reach up to half of the actual change in the gravity (anomaly) field values on the terrace.

To reduce errors in the anomaly field models in terraced areas, the use of triangulation based gridding methods for free-air anomalies can be the most suitable approach. It would be best to increase the resolution of these models according to the average density of gravity data to get the most out of existing data. In case of North Estonia that would be up to $6'' \times 12''$. A significant improvement can be achieved in high resolution free-air anomaly grids if these are calculated using Bouguer anomalies which include height information via a DTM.

Within the study area the anomaly values were best reflected in the $6'' \times 12''$ resolution *triangulate* grid. Even if gravity data are gridded using the optimal algorithm, the result has some discrepancies from the measured data in terraced areas (cf. Fig. 2 and Table 1). This is due to the low resolution of both gravity data and the used DTM. It is therefore expected that LIDAR data will soon find its way into gravity anomaly field gridding, terrain correction calculation and geoid modelling [like the Stokes-Helmert

geoid determination approach, where estimation of related topographical effects may be quite demanding, for a review see Ellmann and Vaníček (2007)]. Discrepancies between gridded (using the optimal algorithm) and actual (measured) data may be larger in other areas (since gravity data as dense as data in the study area are rare both in Estonia and elsewhere), especially areas with much higher terraces.

The discrepancies between different models and also errors in the models (discrepancies of the models from the measured data) have a systematic pattern (cf. Figs. 2, 3 and 4). From the edge of the terrace to the bottom, the differences change sign. It is obvious that the terrace has a significant but short (1–2 km) wavelength effect on the gravity field and its models. In Estonia, the terraced Klint areas are narrow, but they continue along the coast for about a 100 km. These may cause noticeable errors in gravity anomaly models which may propagate to subsequent geoid models. Therefore it is necessary to note the existence of such areas, although the magnitude of the effect on geoid modelling needs to be tested in further studies.

It can be argued that gravity data with average distance of 5 km between data points is sufficient for a 5 mm quasigeoid solution (Ågren and Sjöberg 2012). In this study we have seen that gravity field models can be improved by using appropriate gridding methods, however in terraced areas the discrepancies are still significant (up to 0.8 mGal). If the terraces are high and their effect to gravity anomaly field models should also affect the geoid solution, some additional gravity data may be needed.

For gridding free-air anomalies directly, there is no remarkable difference between the optimal $6'' \times 12''$ *triangulate* grid and the $1' \times 2'$ grid used for the GRAV-GEOID2011. For gridding free-air anomalies through (simple or complete) Bouguer anomalies, the $6'' \times 12''$ grid is much more accurate than the grid used for the geoid model (cf. Table 1) confirming that anomaly grids can be calculated more accurately.

As the differences between the original $1' \times 2'$ grid and the $6'' \times 12''$ grid averaged to $1' \times 2'$ were insignificant (cf. Fig. 5), it can be concluded that using the optimal method is reasonable only if the gravity field model (and if necessary, the subsequent geoid model) can also be presented with the same resolution as the optimal one. If this is too demanding, an option of calculating one general model on a lower resolution and additional models on higher resolutions for specific areas could be considered.

The results of this study can also be applied to gridding the gravity field in other areas with terraced landforms. Much higher terraces are found in Europe and elsewhere, reaching more than 1,000 m. In these areas the effect of the terrace certainly demands attention. Gridding methods discussed here are well applicable to other areas; the optimal model resolutions however are dependent on existing gravity data density.

References

Ågren J, Sjöberg LE (2015) Investigations of the requirements for a future 5 mm quasigeoid model over Sweden. In: Gravity, geoid and height systems. IAG symposia 141. Springer International Publishing Switzerland

Ellmann A (2010) Validation of the new Earth Gravitational Model EGM08 over the Baltic countries. In: Mertikas SP (ed) Gravity, geoid and Earth observation. IAG symposia, vol 135, pp 489–496

Ellmann A, Vaníček P (2007) UNB application of Stokes–Helmert's approach to geoid computation. J Geodyn 43:200–213

Ellmann A, All T, Oja T (2009) Toward unification of terrestrial gravity data sets in Estonia. Est J Earth Sci 58:229–245

Ellmann A, Oja T, Jürgenson H (2011) Application of space technologies to improve geoid and gravity field models over Estonia [in Estonian]. Geodeet 41:22–25

Farr TG, Rosen PA, Caro E, Crippen R, Duren R, Hensley S, Kobrick M, Paller M, Rodriguez E, Roth L, Seal D, Shaffer S (2007) The Shuttle Radar Topography Mission. Rev Geophys 45

Goos JM, Featherstone WE, Kirby JF, Holmes SA (2003) Experiments with two different approaches to gridding terrestrial gravity anomalies and their effect on regional geoid computation. Surv Rev 37(288):92–112

Janák J, Vaníček P (2005) Mean free-air gravity anomalies in the mountains. Studia Geophysica et Geodaetica 49:31–42

Kirby JF, Featherstone WE, Kearsley AHW (1997) Geoid computations using ring integration: gridded vs. point data. Geomatics Res Aust 67:33–46

Pavlis NK, Holmes SA, Kenyon SC, Factor JK (2012) The development and evaluation of the Earth Gravitational Model 2008 (EGM2008). J Geophys Res 117, B04406

Talvik Silja (2012) Influence of terraced landforms to the Earth's gravity field and precise levelling results, with application to the North-Estonian Klint. Tallinn University of Technology. MSc. thesis. [in Estonian]

Wessel P, Smith WHF (1998) New, improved version of the Generic Mapping Tools released. EOS Trans AGU 79:579

Paper E

Liibusk, A., Talvik, S., Ellmann, A., and Oja, T. (2014). "Determining Regional Sea Surface Topography by GNSS Surveys on Ice". In: *Proceedings of the IEEE/OES Baltic International Symposium, May 27-29*. Tallinn, Estonia, pp. 1–9. DOI: 10.1109/BALTIC.2014.6887847. **Paper E**.

Determining Regional Sea Surface Topography by GNSS Surveys on Ice

Aive Liibusk[1], Silja Talvik[2], Artu Ellmann[2], Tõnis Oja[3]

[1] Estonian University of Life Sciences, Department of Geomatics, Kreutzwaldi 1, 51014 Tartu, Estonia
[2] Tallinn University of Technology, Department of Road Engineering, Chair of Geodesy, Ehitajate tee 5, 19086 Tallinn, Estonia
[3] Estonian Land Board, Mustamäe tee 51, 10621 Tallinn, Estonia

Abstract – **Sea surface topography (SST) – the difference between the geoid and sea surface height (SSH), is requested for many marine applications, e.g. for analyzing currents and variation of salinity. Globally, SST can be roughly determined by using satellite altimetry and oceanographic data. However, in coastal areas, the accuracy and spatial resolution of these methods are rather low. Accordingly, issues related to enhancing SST resolution and accuracy with GNSS (Global Navigation Satellite Systems) measurements are explored in this study.**

A practical case study that was carried out on the ice surface over a part of the Baltic Sea tackles profile- and point-wise GNSS measurements for determining SST. Profile-wise GNSS measurements were proceeded on official ice roads (altogether 50 km) between the mainland and the two major islands (Saaremaa and Hiiumaa). The GNSS profiles were complemented with GNSS point-wise measurements scattered (1 point per 25 km^2) all over the study area. The GNSS-derived SSH, which is the difference between the ellipsoid and the sea surface, was corrected with ice freeboard and corrections due to offsets of instantaneous sea level height values from the mean sea level. For calculating SST from the GNSS-derived and corrected SSH, a recent high-resolution (1' x 2') gravimetric geoid model GRAV-GEOID2011 was used. The estimated SST was compared to the global SST model DTU10MDT and with an earlier regional SST model.

Key words: sea surface topography, sea surface height, GNSS, geoid, Väinameri Basin, Baltic Sea

I. INTRODUCTION

Sea surface topography (SST) is affected by water velocity, currents, wind drag, water depth and bottom friction, water density, atmospheric pressure, the Coriolis force and gravity [1]. River discharge and seabed topography also contribute to the variability of SST in coastal regions [2, 3]. Globally, satellite altimetry has been used for more than 20 years (from the late 1980's) to observe sea surface height (SSH) changes. Using satellite altimetry, SSH can be detected with an accuracy of about 2 cm, at best. Additionally, for deriving SST from SSH, a geoid model is needed. However, the accuracy of global geoid models remains around 10 cm (in a regional scale). Thus the error of global geoid models is estimated to dominate in SST modelling in a regional scale. Therefore, the absolute accuracy of SST models based on

satellite altimetry remains within about 10…15 cm. In addition, the quality of satellite altimetry measurements in coastal and semi-enclosed marine areas is relatively poor, see e.g. [4, 5, 6]. Also, the precision of geoid models in coastal areas can suffer due to heterogeneity of regional gravity data. Therefore, the accuracy of SST models in such areas can be even lower.

Additional data sources used to calculate SST models include long-term oceanographic data [7, 8] and *in situ* sea surface measurements that are useful to improve and validate local SST models in the coastal areas. Third, geodetic measurements such as high precision levelling and GNSS observations at tide gauges are also used to detect SST, e.g. [9]. The accuracy of GNSS-based SST models is similar to satellite altimetry based models. The corresponding error budget comprises errors due to GNSS (~1…15 cm), local geoid model (~2…5 cm) and mean sea level determination (~1…2 cm) errors.

The point-wise GNSS observation method to determine SST is mainly used on shoreline tide gauges (TG). In countries of seasonal formation of sea ice however, the GNSS method could also be used over marine areas. Note that the sea ice follows the shape of a calm sea surface which in turn reflects, to a certain extent, the shape of the geoid. GNSS measurements on such "ice-tamed" sea surface can be carried out to detect SST by using both point-wise and profile-wise measurements [10]. GNSS measurements on ice can improve and/or validate the accuracy of SST models near coastal areas with relatively little effort.

This contribution presents the determination of SST on ice using point-wise and profile-wise GNSS measurements. First, principles of GNSS-based SST determination are explained. Next, methods of carrying out a case study in the Väinameri Basin are described. A GNSS-derived SST model is calculated using point-wise GNSS measurements on ice. The obtained results are compared with the global SST model DTU10MDT and with an earlier regional SST model of the Väinameri Basin. A brief summary concludes the paper.

II. PRINCIPLES OF SEA SURFACE TOPOGRAPHY DETERMINATION BY GNSS SURVEYS ON ICE

SST is derived from SSH that can be measured directly by GNSS methods. This can be proceeded either on sea ice or on board ships in open waters. Additionally, instantaneous absolute water level height (H_i, Fig.1) needs to be determined by nearby tide gauges. The antenna reference point (ARP) height (h_i) is computed with respect to the reference ellipsoid; vertical distance between the ARP and instantaneous water level (ΔH_{water}^{AH}) is measured. In the case of ice, the thickness of ice freeboard (ΔH_{FB}), also the distance between ARP and ice level (ΔH_{ice}^{AH}) are determined. Thus, the instantaneous SSH (h_{SSH}^{ins}) is computed as (cf. Fig. 1):

$$h_{SSH}^{ins}(\varphi,\lambda) = h_i(\varphi,\lambda) - \Delta H_{ice}^{AH}(\varphi,\lambda) - \Delta H_{FB}(\varphi,\lambda) + \Sigma\varepsilon(\varphi,\lambda) \quad (1)$$

where the geodetic coordinates φ and λ denote the location of measurements and the term ε comprises measurement errors.

Nevertheless, the h_{SSH}^{ins} at a location (φ,λ) is affected by wind direction and speed even in "ice-tamed" conditions. For the obtained h_{SSH}^{ins} to be comparable with the mean sea level (MSL), the absolute height H_i of the instantaneous water level needs to be accounted for:

$$h_{SSH}^{mean}(\varphi,\lambda) = h_{SSH}^{ins}(\varphi,\lambda) - H_i(\varphi,\lambda) + \Sigma\varepsilon(\varphi,\lambda) \quad (2)$$

where h_{SSH}^{mean} denotes mean sea level heights. H_i at a location (φ,λ) is obtained from TGs readings (for the same time-instant) at locations $(\varphi^{TG},\lambda^{TG})$ by interpolating over the marine area of interest using some interpolation function, e.g. a linear interpolation [11] between the TGs:

$$H_i(\varphi,\lambda) = H_j^{TG}(\varphi_j^{TG},\lambda_j^{TG}) +$$
$$+ \frac{(\varphi - \varphi_j^{TG})\cdot(H_{j+1}^{TG}(\varphi_{j+1}^{TG},\lambda_{j+1}^{TG}) - H_j^{TG}(\varphi_j^{TG},\lambda_j^{TG}))}{\varphi_{j+1}^{TG} - \varphi_j^{TG}} \quad (3)$$

where H_j^{TG} is instantaneous sea level height at j-th TG with coordinates $\varphi_j^{TG},\lambda_j^{TG}$. H_{j+1}^{TG} is instantaneous sea level height at other TG$_{j+1}$ with coordinates $\varphi_{j+1}^{TG},\lambda_{j+1}^{TG}$.

Considering Eqs. (1), (2) and the geoidal height from the gravimetric geoid model (N) (cf. Fig. 1), GNSS-derived SST (SST_{GNSS}) is calculated as:

$$SST_{GNSS}(\varphi,\lambda) = h_i(\varphi,\lambda) - \Delta H_{ice}^{AH}(\varphi,\lambda) -$$
$$- \Delta H_{FB}(\varphi,\lambda) - H_i(\varphi,\lambda) - N(\varphi,\lambda) + \Sigma\varepsilon(\varphi,\lambda) \quad (4)$$

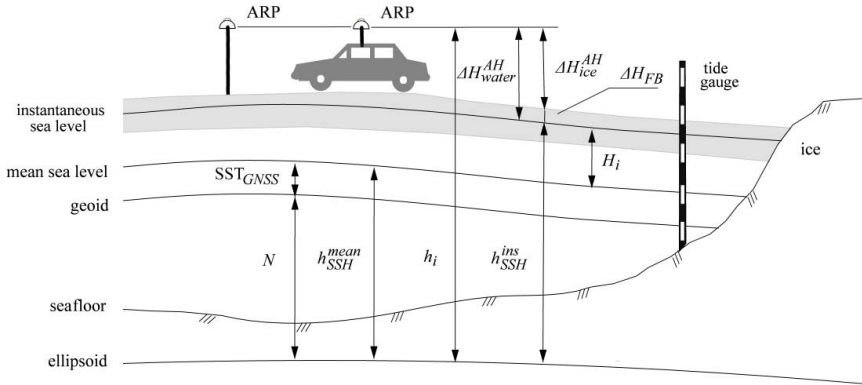Eq. (4) is used for calculating GNSS-derived SST values in the case study.

Figure 1. Point-wise (GNSS antenna on a rod) and profile-wise (GNSS antenna mounted on a vehicle) GNSS measurements on ice-covered marine areas with respect to mean sea level. ΔH_{FB} is the thickness of ice freeboard and ΔH_{ice}^{AH} is the distance between the antenna reference point (ARP) and the ice surface; in ship-borne surveys the ARP height is measured with respect to the water line (ΔH_{water}^{AH}). In all the cases, the ARP height is computed with respect to the reference ellipsoid (h_i). The mean sea level (MSL) is the sum of the gravimetric geoid model height (N) and the GNSS-derived sea surface topography (SST_{GNSS}). The absolute height (H_i) of the instantaneous sea surface height (h_{SSH}^{ins}) with respect to the MSL can be determined by nearby tide gauge(s).

III. CASE STUDY IN THE VÄINAMERI BASIN

The Väinameri Basin (surface area about 2200 km²) is surrounded by six precise high-frequency automatic TGs (Fig. 2 and [12]) for determining the absolute height (H_i) of the instantaneous SSH. Additionally, the study area is covered by a relatively accurate (±2…3 cm) regional gravimetric geoid model GRAV-GEOID2011 ([13], Fig. 2). Therefore, the selected study area appears to be a good test area for GNSS-derived SST determination.
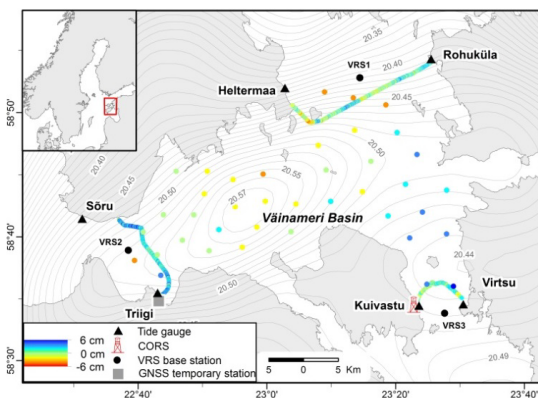

Figure 2. Locations of GNSS points and profiles over the ice covered Väinameri Basin. Their colours express detected discrepancies between the GNSS-derived SST surface and the GRAV-GEOID2011 model (cf. Eq. (4)). The CORS (Continuously Operating Reference Station) in Kuivastu, the temporary GNSS station at Triigi and the VRS base stations in the middle of the straits used as reference for post-processing of GNSS measurements are also depicted. The regional gravimetric geoid model GRAV-GEOID2011 (with a 40 cm offset) is placed in the background with a contour interval of 1 cm. Inset: Location of the study area in the Baltic Sea region.

Although Väinameri is a part of the Baltic Sea, its hydrodynamic conditions are slightly different from the rest of the Baltic Sea: wave heights are smaller, water is less saline, water temperature variations are larger, ice cover is formed more frequently and lasts longer. It is a semi-enclosed area surrounded by an arc of islands and mainland. The salinity of Väinameri remains mainly within 4…6‰ and thus could not have a large influence on the SST. The SST is mainly affected by water exchange processes and currents in the Väinameri Basin. Note that the Basin is a rather dynamic water body. Water exchange processes are forced by the nearby Baltic Proper and the Gulf of Riga. The main driver for water exchange and corresponding current speeds in the Väinameri straits is local wind speed and direction. Importantly, in Väinameri the currents can change their direction (and even become opposite) depending on wind direction and speed. A general description of the current system in the Väinameri is presented by Suursaar et al. [14]. Monthly SST changes in the Baltic Sea derived by satellite altimetry are studied by

Poutanen [15]. The results also demonstrate seasonal dependency of SST changes in the Väinameri Basin. Therefore, considering all of the above and the small size of the area it is reasonable to expect that in "ice-tamed" conditions the weather-induced sea level slope and instantaneous SST would be minimal.

Two very calm weather periods on February 2011 and on February-March, 2013 were selected for profile- and point-wise GNSS surveys on the Väinameri Basin ice to determine SST by Eq. (4).

A. Profile-wise GNSS measurements on ice, February 2011

Profile-wise GNSS measurements were carried out on February 22-23, 2011. In February 2011 the Väinameri Basin became covered with a 30…50 cm thick layer of shore-fast ice. The adjacent gulfs (the Gulf of Riga, the Gulf of Finland) were also covered with pack ice; open seawater was further than 10 km away from the study area (Fig. 3A). A high pressure continental weather system covered the Baltic Sea entirely during the second half of February. Thus the weather conditions were very stable within the study area. On February 20-25 the atmospheric pressure was almost the same and changed evenly over the Väinameri (cf. Table 4 in [12]). Recall that the instantaneous SST is mainly influenced by wind conditions in the Väinameri Basin. Therefore, it could be expected that the weather-induced sea level slope and instantaneous SST slope would be minimal.
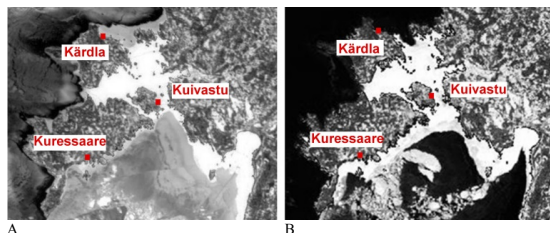

Figure 3. Ice conditions in the Väinameri and nearby areas on February 23, 2011 (A) and February 24, 2013 (B) as seen on MODIS satellite images. The white area between mainland and the islands denotes shore-fast ice at least 50 cm thick, the grey area denotes pack ice at least 10 cm thick; the darkest area denotes open water. The red dots indicate locations of Kuivastu, Kuressaare and Kärdla Continuously Operating Reference Stations used for post-processing static GNSS measurements. Photos: MSI

Two GNSS antenna/receivers (Trimble R8 and Spectra Precision Epoch 50) were mounted on the car roof (Fig. 1) for profile-wise GNSS measurements in kinematic mode. Tracking interval of 1 Hz was used in the receivers. Accordingly, profile points were positioned after every 7 meters with the car speed being 20…25 km/h. The profiles ran on the official ice roads between Virtsu–Kuivastu, Triigi–Sõru and Rohuküla–Heltermaa (Fig. 2). At the start of every profile the height of GNSS antennas (ΔH_{ice}^{AH}) was determined with

an accuracy of ±0.2 cm. Ice freeboard (ΔH_{FB}) was measured nearby every TG from bore holes before and after GNSS profile measurements. Because of currents and changing sea depths, the ice thickness was not homogenous along the routes. The ice thickness at shoreline reached 50 cm but was most likely less in the middle of the route (~30 cm, according to authorities maintaining the ice road). The separation between water and ice surface (i.e. the ice freeboard ΔH_{FB}) was determined indirectly. The density of ice is ~920 kg/m³ whereas that of brackish water is ~1004 kg/m³. Thus, approximately one-tenth of the ice volume floats above the water surface. Therefore, a 3 cm offset was used in Eq. (4) as the average ice freeboard.

Virtual GNSS reference stations (VRS) were used as reference for data post-processing and ARP height (h_i) calculations. VRSs were preferred as continuously operating reference stations (CORS) were situated farther than 20 km from the GNSS-profiles (cf. Fig. 3). Note that VRSs were artificially created from the VRS Network (at least three nearby CORS were used) in the middle of every route (Fig. 2). For more details about profile-wise GNSS data processing and working principles of VRS Networks see [10 and 16], respectively.

The GNSS profiles measured are located in the periphery of the Väinameri Basin, which makes them less suitable for SST interpolation across the Basin. For reasonable SST modeling, more homogeneously spaced profiles are needed over the area. However, profile-wise GNSS measurements are valuable for validating existing SST models.

B. Point-wise GNSS measurements on ice, February-March 2013

Point-wise GNSS measurements were carried out two years later – on February 21-22, March 12 and 14, 2013. The ice and weather conditions were similar to those of the 2011 campaign. The Väinameri Basin was covered in shore-fast ice with a thickness of 25...55 cm, see also Appendix I. However, open water was close to the east part of the Väinameri at the end of February (cf. Fig. 3B). Days with stable weather conditions were chosen as to minimize the effect of wind and air pressure on the SST. There were prevailingly Southern winds with speed well below 5 m/s and steadily high air pressure.

The point-wise survey covered an area of about 1000 km² with a density of 1 point/25 km². Altogether 41 points were measured on the sea ice (Fig. 2, see also [17]). An amphibious lightweight crawler was used for transport of the survey team and equipment on ice and a Trimble R8 GNSS receiver was used for point positioning. An additional GNSS receiver Trimble 5800 was temporarily set up on the coast near Triigi to serve as a reference station during some 5 hours of the beginning of the campaign on February 21.

Different GNSS survey methods were experimented with. Real Time Kinematic (RTK) GNSS measurements of at least 3 times 5 seconds using a VRS network based on nearby CORS were used on all the points. The CORS stations were located about 35...50 km away from the centre of the study area (Fig. 3) and should therefore allow for reasonably accurate real time positioning providing that it is possible to establish a mobile (GSM, EDGE or 3G) connection with the network. In addition, static measurements of 10 minutes were used on 18 points in the Western part of the Väinameri Basin to investigate the possibility of using rapid static GNSS measurements if there should be no mobile connection available for the use of VRS. Nine of these static measurements were linked to the reference station (RS) operating near Triigi to investigate if an additional reference station could improve the accuracy of static positioning. Such (rapid) static surveys, however, need post-processing to obtain accurate coordinates.

Data processing was proceeded according to different GNSS survey methods used. The 3 times 5 sec RTK measurements were averaged to get one result for each point. The accuracy of heights from RTK surveys in the area was estimated from measurements of a geodetic point and some temporary points on land. Discrepancies of 6...8 mm between repeated surveys as well as between the measured and the accurate height value of the geodetic point were found. Several points on ice were also revisited (points were found by their coordinates and marks on ice), the height discrepancies were much larger, reaching 70 mm after 6 hours in one case and 172 mm after 21 hours. Although TGs at shorelines only showed sea level change of a few cm it is most likely that such large discrepancies on ice heights in the middle of the Väinameri were caused by larger sea level changes in between revisiting such points.

Static GNSS survey data processing was proceeded in three different ways described below (cf. Table I).

Method 1: the coordinates of the RS near Triigi were first obtained by adjusting baselines to three CORS (Fig 3). Thereafter, the coordinates of the survey points measured within the same time frame were calculated with respect to the Triigi RS only.

Method 2: a joint adjustment was proceeded for all of the 18 static survey points – baselines from the RS near Triigi to the CORS and the baselines from the RS to the nine survey points covered by the RS operation time were processed together.

Method 3: first, the coordinates of the RS near Triigi were obtained by adjusting the baselines to the CORS. Then the coordinates of the nine survey points covered by RS operation time were calculated by fixing the coordinates of the CORS completely while those of the RS were fixed with an accuracy of 1 cm in the baseline processing.

TABLE I
COMPARISON OF STATIC SURVEY RESULTS WITH RESPECT TO
THE RTK DATA (STATIC MINUS RTK). UNIT IS METRE

	Method 1: With respect to Triigi	Method 2: Joint adjustment	Method 3: Stepwise adjustment
Number of survey points processed	9	18	9
Average difference and standard deviation from RTK results, 9 points	0.038±0.047	0.030±0.043	0.030±0.042
Average difference and standard deviation from RTK results, 18 points	-	0.027±0.039	-

The results of static data processing were checked against each other. Depending on the method used, the estimated height of a point could differ up to 6 cm. However, there was a static measurement on a known point on ground where the surveyed height value differed from the known value by 6 mm which is similar to that of RTK therefore it is not possible to tell which of the results are closest to the true value. It was decided to use RTK results as reference to judge the static data processing methods (cf. Table I). Method no. 2 performed best with the average height difference from RTK of +3.0±4.3 cm on nine points with the additional benefit of being able to give a result for all of the 18 points with the difference of +2.7±3.9 cm from RTK. Although static measurements provided systematically larger height values, the distribution of the discrepancies does not reveal any specific pattern (except for the two larger discrepancies near Hiiumaa being close to a dm, see Fig. 4). It is not clear as to why such a large discrepancy occurred. It seems however, that in this case the static results have a better fit with the neighbouring points.
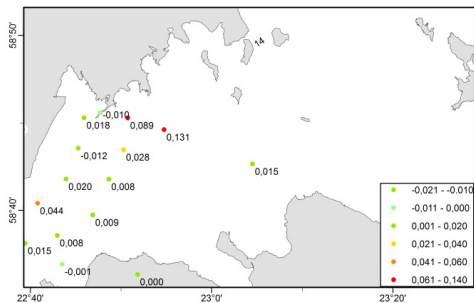

Figure 4. Comparison of heights measured by static and RTK GNSS methods (static minus RTK). Unit is metre.

As a conclusion from these tests with different GNSS survey methods it can be noted that a dm range uncertainty can be expected in height values, although most points are very likely to have smaller errors than this. RTK positioning

should be preferred as it is much faster while static measurements can be used if a CORS network is not available in such remote areas.

For calculation of ice freeboard correction (ΔH_{FB}) the ice thickness was measured from bore holes at all (except four) measurement points. Where thickness information was missing a similar value of nearby points was used.

C. GNSS-derived SST surface for the Väinameri Basin

The profile- and point-wise GNSS measurements were carried out in different years (2011 and 2013). Although the weather and ice conditions were similar in both cases, the absolute values of SST could be varied by several centimetres. In addition to weather and ice conditions, instantaneous SST is affected by several hydrodynamic processes not only in the Väinameri Basin but also in the surrounding areas (i.e. in the whole Baltic Sea). Therefore, the GNSS-derived SST surface for the Väinameri Basin was calculated based only on the point-wise GNSS measurements carried out in 2013. ARP heights (h_i) obtained by RTK GNSS were used for all points expect the two near Hiiumaa (cf. points with 0.089 and 0.131 m difference from static measurements in Fig. 4). These heights were replaced with the results of static measurements due to better agreement with nearby point heights. A recent gravimetric geoid model GRAV-GEOID2011 was used for the geoidal heights (N) in Eq. (4).

This geoid model has been computed by the least-squares modification of Stokes's formula, whereas the ESA's (European Space Agency) GOCE-satellite (Gravity field and steady-state Ocean Circulation Explorer) based geopotential model was used as the global reference. The resolution of the GRAV-GEOID2011 model is 1' x 2' (1.8 km x 1.8 km) and it covers the entire area of Estonia and surrounding waters of the Baltic Sea. Basically, this geoid model is a follow-up of an earlier geoid model [18], that uses a more complete set of gravity data. However, it should be noted that gravimetric data and their quality in the Väinameri Basin is heterogeneous, which could cause systematic errors in the marine geoid model [13, 19]. New gravimetric data that slightly changes the shape of the geoid model over the Väinameri basin has been collected since [17]. The accuracy of the regional gravimetric GRAV-GEOID2011 model has been estimated to be ±1.3 cm in the mainland of Estonia [20]. A recent study [21] validated the accuracy of the geoid model over the Väinameri Basin by using air-borne laser scanning profiles. Standard deviations of discrepancies between the gravimetric GRAV-GEOID2011 model and the Väinameri ALS-derived SSH profile remained within ±1…±2 cm [21].

In the present study a sea level corrected (Appendix I) GNSS-derived SST surface (Fig. 5) was calculated by using the ordinary kriging technique with a linear covariance model. A very clear NW-SE ward downslope of the modeled SST surface reaching up to 6 cm can be detected in the Väinameri

Basin (cf. Fig. 5). The SST model is more even in the Eastern part of the Väinameri, although some North-South downslope exists between the islands of Saaremaa and Hiiumaa as well. This could be an effect of the inaccuracy of GNSS measurements. However, it is more likely that two points in the SW (Fig. 4) were affected by nearby open water (cf. Fig 3B). Additionally, the enclosed Väinameri Basin is connected to the Baltic Proper through this strait. Therefore, the modelled SST could be less predictable in this area.
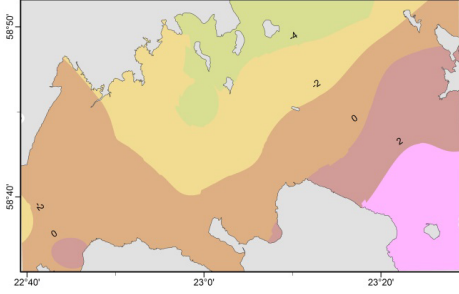

Figure 5. Sea level corrected GNSS-derived SST model in the Väinameri Basin in February and March 2013 (i.e. from point-wise surveys). Unit is centimetre.

For additional analysis, the sea level corrected GNSS-derived SST model was compared with the profile-wise SST values in the straits (cf. Fig. 2). The discrepancies between the modelled SST (cf. Fig. 5) and the profiles (cf. Fig. 2) are depicted with black dots in Fig. 6. Although the GNSS measurements on ice were carried out in different winters (2011 and 2013), the average SST discrepancy remains within ±4.3 cm in all straits (Table II). Such a difference may indicate the combined effect of the inaccuracy of GNSS measurements and ice freeboard estimates. The best SST coincidence is between Kuivastu–Virtsu. For illustration, the red trend lines depict the GNSS-derived SST surface from point-wise surveys (Fig. 6). Moving average filter with window $w = 30$ was used to calculate smoothed profile-wise GNSS data (see blue lines in Fig. 6). The length of along profile distance of each window is about 200 m. Both the point- and profile-wise results are sea-level corrected.

TABLE II
STATISTICS OF DISCREPANCIES BETWEEN THE POINT-WISE GNSS-DERIVED SST MODEL AND THE SST PROFILES (MODEL MINUS PROFILE). UNIT IS CENTIMETRE.

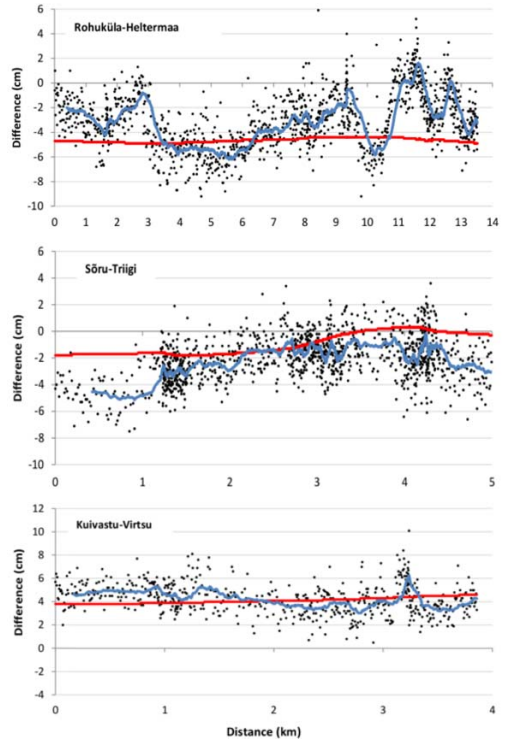| Profile-wise connection	Number of profile-points	Average	Minimal	Maximal	Standard deviation
Rohuküa-Heltermaa	1250	-3.0	-9.2	6.9	2.3
Sõru-Triigi	1316	-2.1	-7.5	3.6	1.7
Kuivastu-Virtsu	589	4.3	0.5	12.1	1.4

Figure 6. Discrepancies between the sea level corrected GNSS-derived SST model (red lines, from point-wise surveys) and the SST profiles (model minus profile). Blue lines indicate smoothed SST profiles calculated by using moving average filter.

D. *Comparisons with a global and a regional SST model*

The GNSS-derived instantaneous SST model (Fig. 5) is compared with two SST models based on long-term SSH observations. First, a global model DTU10MDT (Mean Dynamic Topography model) by Andersen [22] is used for comparison (Fig. 7A). The DTU10MDT model was obtained by combining the Mean Sea Surface model (DTU10MSS) and the global geoid model EGM2008 [23]. The DTU10MSS model was derived from 17 years of data from the ERS and ENVISAT altimetry missions. The resolution of the DTU10MDT model is 1 arc-minute (about 1.8 km x 0.9 km) and the accuracy remains mainly within 10 cm in the test area. Note that the TOPEX/Poseidon satellite altimetry mission ellipsoid is used as the reference for the DTU10MDT model. The TOPEX/Poseidon ellipsoid axis are ~70 cm shorter than GRS-80, which is used for the GRAV-GEOID2011. Therefore, for a better comparison with mean sea level a 40 cm offset has been removed from the DTU10MDT model in this study (Fig. 7A).
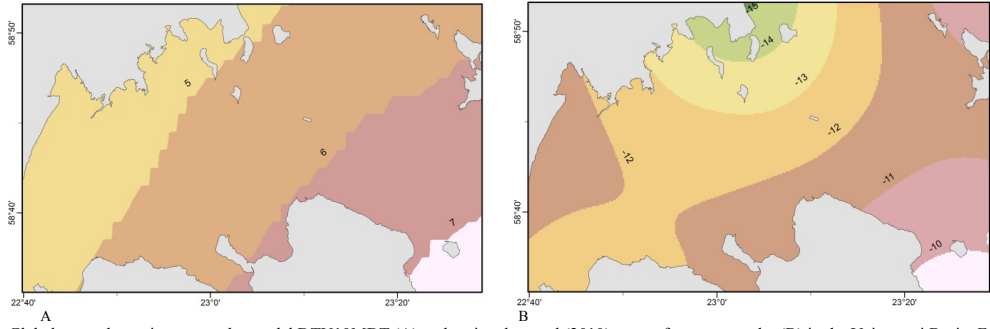
Figure 7. Global mean dynamic topography model DTU10MDT (A) and regional annual (2010) sea surface topography (B) in the Väinameri Basin. For a better comparison with mean sea level a 40 cm offset has been removed from the DTU10MDT model. Unit is centimetre.

Second, a regional SST model based on GNSS measurements in conjunction with the GRAV-GEOID2011 geoid model and annual (2010) mean sea level observations from six TGs around the Väinameri Basin (cf. Fig. 2) is used. The SST values at six TGs were calculated as:

$$SST_i(\varphi,\lambda) = h_i(\varphi,\lambda) - N_i(\varphi,\lambda) - \overline{T}_{msl} \quad (5)$$

where $h_i(\varphi,\lambda)$ is the geodetic height of the contact point on the top of TG, $N_i(\varphi,\lambda)$ is the geoidal height at the same point and $\overline{T}_{msl}$ denotes the vertical distance between the annual (2010) mean sea level and the contact point. The annual mean sea level is based on high-frequency (5 min) automatic

pressure gauge data series. More details about the data used for this model are presented by Liibusk [24]. By plotting the annual SST values at six TG stations a NW-ward downslope of up to 5 cm can be detected in the Väinameri Basin (Fig. 7B). From Fig. 7A and 7B it is obvious that in such small and enclosed areas the regional SST model from one year data series of TGs is more detailed than the global MDT model based on 17 years of satellite altimetry data. However, the same direction of downslope with a smaller magnitude of 3 cm is also visible in the global DTU10MDT model. Note however, that the spatial resolution of both models is much lower than that of the GNSS-derived SST model in the Väinameri.
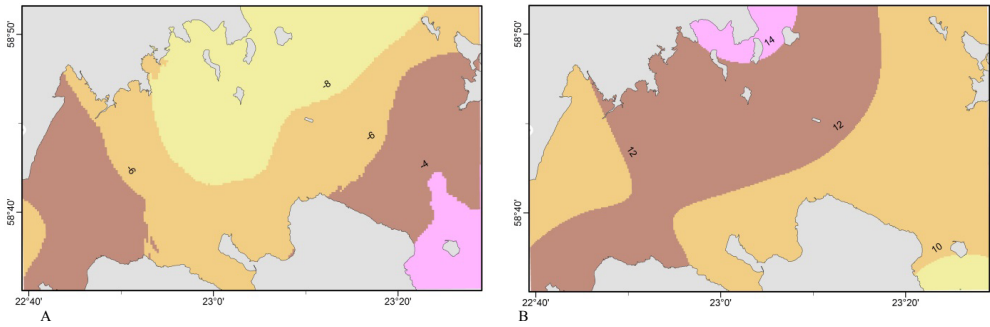

Figure 8. Differences between the GNSS-derived SST model and DTU10MDT model (GNSS minus MDT) (A) and between the GNSS-derived SST model and the regional annual (2010) sea surface topography (GNSS minus SST) (B). Unit is centimetre.

Relative differences between the GNSS-derived instantaneous SST and the DTU10MDT global model (Fig. 8A) or the annual SST model (Fig. 8B) remain within 4…5 cm in SE-NW direction in the Väinameri Basin. In both cases the larger differences occur in the Northern part of the Väinameri Basin (near Heltermaa). A local SST anomaly could exist in this area which is not detectable by global

models. However, it could also be an effect of the gravimetric geoid model GRAV-GEOID2011 used for the compilation of GNSS-derived SST (Fig. 5). All in all, the relative coincidence between SST models based on short-term (some days) and long-term (years) SSH observations is reasonable, remaining within the estimated accuracy of the measurements and the geoid model.

Moreover, this case study demonstrates the possibility of using short-term GNSS measurements on ice in combination with TG data to determine SST surface tilts with similar accuracy but better resolution to long term (years of) satellite altimetry observations in coastal regions.

IV. SUMMARY

The current paper introduced the principles of SST determination by GNSS surveys on ice. As a case study, two expeditions were carried out on the Väinameri Basin ice in the Baltic Sea. In the first campaign in 2011 profile-wise GNSS measurements in kinematic mode were used on the official ice-roads in the fringe areas of the Väinameri. In the second campaign in 2013 point-wise GNSS measurements were made all over the Väinameri Basin. An instantaneous SST model was calculated based on the point-wise measurements and it was compared with the GNSS profiles, DTU10MDT global model and a regional annual (2010) SST model in the Väinameri.

The comparisons of GNSS-derived SST model to the global and the regional SST models are not rigorous as the instantaneous SST was determined by GNSS measurements on ice during a few days whereas DTU10MDT is based on 17 years of satellite altimetry data and the regional SST model is based on annual sea level observations from TGs. However, the comparisons revealed a good agreement between the different models. The differences remained within 5 cm which is within the accuracy of GNSS measurements and the geoid model. The case study demonstrated that GNSS measurements on ice could be a good alternative to detect SST surface in coastal regions or to validate satellite altimetry-derived SST in small and semi-enclosed water areas.

ACKNOWLEDGMENTS

REFERENCES

[1] D. Pugh. „*Tides, Surges and Mean Sea-Level*". John Wiley, New York. 1987.

[2] J. R. Dunn and K. R. Ridgway. „Mapping ocean properties in regions of complex topography". *Deep-Sea Research Part I: Oceanographic Research Papers*, vol. 49(3), pp. 591-604, 2002.

[3] C. L. Merry and P. Vaníček. „Investigation of local variations of sea-surface topography". *Marine Geodesy*, vol. 7(1-4), pp. 101-126, 1983. DOI:10.1080/15210608309379477.

[4] D. Mantripp. Radar Altimetry, in: *The Determination of Geophysical Parameters from Space*. Institute of Physics Publishing, London, UK, pp. 119-171, 1996.

[5] C. K. Shum, M. E. Parke, B. E. Schutz, P. A. M. Abusali, R. Gutierrez, T. Pekker, B. D. Tapley, J. J. Martinez Benjamin, J. Blaha, G. Jacobs, G. A. Jeffress, K. J. Schaudt and D. J. Wingham. "Improvement of TOPEX/POSEIDON Altimeter Data for Global Change Studies and Coastal Applications". *AVISO Altimetry Newsletter* vol. 6, pp. 102-103, 1998.

[6] O. B. Andersen and P. Knudsen. „The Role of Satellite Altimetry in Gravity Field Modelling in Coastal Areas". *Physics and Chemistry of the Earth (A)* vol. 25(1), pp.17-24, 2000.

[7] M. Carlsson. „Mean Sea-Level Topography in the Baltic Sea Determined by Oceanographic Methods". *Marine Geodesy*, vol. 21, pp. 203-217, 1998.

[8] E. Lisitzin. „*Sea level hanges*". Oceanography, Vol 8. Amsterdam: Elsevier. 1974.

[9] J. Kakkuri and M. Poutanen. „Geodetic Determiantion of the Surface Topography of the Baltic Sea". *Marine Geodesy*, vol. 20, pp. 307-316, 1997.

[10] A. Liibusk and A. Ellmann. „Validation of Marine Geoid Models by Profile-wise GNSS Measurements on Ice Surface". (in review). Submitted to *Marine Geodesy* on February 20, 2014.

[11] W. Gautschi. „Numerical Analysis". Springer Science+Business Media, LLC 1997, 2012.

[12] A. Liibusk, A. Ellmann, T. Kõuts and H. Jürgenson. „Precise hydrodynamic levelling by using pressure gauges". *Marine Geodesy*, vol. 36(2), pp.138–163, 2013.

[13] A. Ellmann, T. Oja and H. Jürgenson. „Application of space technologies to improve geoid and gravity field models over Estonia". *Geodeet*, vol. 41(65), pp. 22-25, 2011 (in Estonian).

[14] Ü. Suursaar, T. Kullas and M. Otsmann. „The influence of currents and waves on ecological conditions". *Proceedings of the Estonian Academy of Sciences, Biology and Ecology*, vol. 50(4), pp. 231-247, 2001.

[15] M. Poutanen. „Sea surface topography and vertical datums using space geodetic techniques". Academic dissertation, Publications of the Finnish Geodetic Institute, Kirkkonummi. No 128. 2000.

[16] H. Landau, U. Vollath and X. Chen. „Virtual Reference Station Systems". *Journal of Global Positioning Systems*, vol. 1(2), pp. 137-143, 2002.

[17] S. Talvik, T. Oja, A. Ellmann, H. Jürgenson. „Improving and validating gravity data over ice-covered marine areas". International Association of Geodesy Symposia Proceedings, 143. 2014 (in print).

[18] A. Ellmann. „Two deterministic and three stochastic modifications of Stokes's formula: a case study for the Baltic countries". *Journal of Geodesy*, vol. 79, pp. 11-23, 2005.

[19] A. Ellmann, T. All and T. Oja. „Toward unification of terrestrial gravity datasets in Estonia". *Estonian Journal of Earth Sciences*, vol. 58(4), pp. 229-245, 2009.

[20] T. Oja, A. Ellmann, H. Jürgenson, T. Kall. „Differences between EST-GEOID2011 and EST-GEOID2003 models and the possible transition to the new height system in Estonia". *Geodeet*, vol. 41(65), pp. 31-37, 2011 (in Estonian).

[21] A. Gruno, A. Liibusk, A. Ellmann, T. Oja, A. Vain and H. Jürgenson. „Determining sea surface heights using small footprint airborne laser scanning". In SPIE Remote Sensing pp. 88880R1-88880R13, 2013.

[22] O. B. Andersen. *The DTU10 Mean Sea Surface for and with CryoSat-2*. Paper presented at CryoSat validation workshop, Italy, Rome, February 1-3, 2011.

[23] N. K. Pavlis, S. A. Holmes, S. C. Kenyon, J. K. Factor. „An Earth gravitational model to degree 2160: EGM2008". Presented at EGU-2008, Vienna, Austria, April 13-18, 2008.

[24] A. Liibusk. „Precise hydrodynamic levelling using pressure gauges with application to improvement of the Estonian National Levelling Network". Academic dissertation. Tartu. 2013.

RESULTS OF GNSS POINT MEASURMENTS ON ICE IN THE VÄINAMERI BASIN IN FEBRUARY AND MARCH 2013. UNIT IS METRE.

Point	Latitude (φ)	Longitude (λ)	Depth of water[1]	Ellipsoidal height (h_i) determined from RTK GNSS measurements (if not distinguished otherwise)	Interpolated instantaneous absolute sea level height H_i [4]	Ice thickness	Sea level and ice thickness-corrected ellipsoidal height h_{i_corr}
1	58.58972001	22.71961097	-	20.199	-0.341	0.400[5]	20.500
2	58.61507024	22.72549524	7.77	20.271	-0.335	0.400	20.565
3	58.64256399	22.7163806	7.88	20.237[2]	-0.333	0.500	20.520
4	58.67339708	22.68012816	4.22	20.200	-0.339	0.400	20.499
5	58.69647419	22.73227195	4.76	20.228	-0.340	0.530	20.514
6	58.72580901	22.75475000	3.56	20.226	-0.336	0.490	20.512
7	58.75483635	22.76541934	3.95	20.171	-0.337	0.440	20.464
8	58.75480355	22.84580877	5.02	20.221[3]	-0.324	0.540	20.491
9	58.74362765	22.91256828	7.76	20.256[3]	-0.319	0.570	20.518
10	58.72445453	22.83815804	8.18	20.238	-0.324	0.530	20.510
11	58.69631957	22.81109990	8.12	20.262	-0.327	0.530	20.536
12	58.66221430	22.78158426	8.19	20.260	-0.326	0.470	20.539
13	58.63509540	22.65743359	5.66	20.206	-0.321	0.470	20.480
14	58.64807495	22.85036889	7.64	20.281	-0.312	0.410	20.552
15	58.67645235	22.87574615	8.07	20.316	-0.304	0.500	20.569
16	58.70709685	22.91791985	8.02	20.290	-0.303	0.450	20.548
17	58.75103210	22.99043872	7.37	20.249	-0.301	0.500	20.500
18	58.71461004	22.99604086	6.49	20.281	-0.304	0.450	20.540
19	58.71092708	23.07515960	5.46	20.248	-0.304	0.410	20.511
20	58.67360937	23.06274982	4.77	20.252	-0.313	0.380	20.527
21	58.67983661	22.97410468	7.02	20.272	-0.310	0.390	20.543
22	58.65272554	22.93645302	6.84	20.253	-0.313	0.400	20.527
23	58.71431701	23.16522742	5.42	20.113	-0.455	0.410	20.527
24	58.75657249	23.15339077	2.23	20.116	-0.435	0.360	20.515
25	58.78942541	23.13301875	3.40	20.106	-0.430	0.450	20.491
26	58.86086608	23.14926309	5.30	19.988	-0.426	0.450	20.369
27	58.85312907	23.22383883	8.40	19.992	-0.437	0.400	20.389
28	58.84355047	23.30807354	8.80	19.994	-0.448	0.380	20.403
29	58.80973003	23.22721358	8.25	20.045	-0.448	0.350[5]	20.458
30	58.76802926	23.26925181	6.24	20.071	-0.453	0.350[5]	20.489
31	58.72726586	23.24738876	6.39	20.059	-0.454	0.350[5]	20.478
32	58.69495338	23.31361030	4.40	20.028	-0.496	0.310	20.493
33	58.73732262	23.35884854	4.52	20.045	-0.493	0.400	20.498
34	58.80667708	23.33702570	6.00	20.055	-0.469	0.360	20.489
35	58.77725574	23.38864891	6.05	20.087	-0.478	0.320	20.533
36	58.72933183	23.46535613	6.83	20.052	-0.477	0.470	20.482
37	58.69992525	23.40252627	5.43	20.063	-0.470	0.250	20.508
38	58.67064990	23.46493133	6.33	20.039	-0.472	0.350	20.476
39	58.60020158	23.48284695	2.95	20.068	-0.464	0.340	20.498
40	58.60297014	23.41421583	14.32	20.061	-0.451	0.290	20.483
41	58.66524909	23.36971815	12.00	20.076	-0.438	0.310	20.483
			Minimal:	2.23	19.988	-0.496	0.250	20.369
			Maximal:	14.32	20.316	-0.301	0.570	20.569
			STD:	2.30	0.102	0.071	0.076	0.042

[1] Water depth was measured from bore holes by lowering a flat metal weight with a ~10 cm diameter hanged to a cable until it touched the seabed and measuring the length of the cable submerged. Note that water depth is not sea level corrected in the table.

[2] This point was repeated; the second height value obtained was used as for the first one the height difference from static surveys was about a dm.

[3] Static GNSS height was used instead of RTK.

[4] Sea level values from TGs were interpolated over study area. TG data is measured by Marine System Institute (see: on-line.msi.ttu.ee/kaart.php).

[5] *In situ* ice thickness measurements were not carried out. The thickness is interpolated from nearby points.

DISSERTATIONS DEFENDED AT
TALLINN UNIVERSITY OF TECHNOLOGY ON
CIVIL ENGINEERING

1. **Heino Mölder**. Cycle of Investigations to Improve the Efficiency and Reliability of Activated Sludge Process in Sewage Treatment Plants. 1992.

2. **Stellian Grabko**. Structure and Properties of Oil-Shale Portland Cement Concrete. 1993.

3. **Kent Arvidsson**. Analysis of Interacting Systems of Shear Walls, Coupled Shear Walls and Frames in Multi-Storey Buildings. 1996.

4. **Andrus Aavik**. Methodical Basis for the Evaluation of Pavement Structural Strength in Estonian Pavement Management System (EPMS). 2003.

5. **Priit Vilba**. Unstiffened Welded Thin-Walled Metal Girder under Uniform Loading. 2003.

6. **Irene Lill.** Evaluation of Labour Management Strategies in Construction. 2004.

7. **Juhan Idnurm**. Discrete Analysis of Cable-Supported Bridges. 2004.

8. **Arvo Iital**. Monitoring of Surface Water Quality in Small Agricultural Watersheds. Methodology and Optimization of monitoring Network. 2005.

9. **Liis Sipelgas**. Application of Satellite Data for Monitoring the Marine Environment. 2006.

10. **Ott Koppel**. Infrastruktuuri arvestus vertikaalselt integreeritud raudtee-ettevõtja korral: hinnakujunduse aspekt (Eesti peamise raudtee-ettevõtja näitel). 2006.

11. **Targo Kalamees**. Hygrothermal Criteria for Design and Simulation of Buildings. 2006.

12. **Raido Puust**. Probabilistic Leak Detection in Pipe Networks Using the SCEM-UA Algorithm. 2007.

13. **Sergei Zub**. Combined Treatment of Sulfate-Rich Molasses Wastewater from Yeast Industry. Technology Optimization. 2007.

14. **Alvina Reihan**. Analysis of Long-Term River Runoff Trends and Climate Change Impact on Water Resources in Estonia. 2008.

15. **Ain Valdmann**. On the Coastal Zone Management of the City of Tallinn under Natural and Anthropogenic Pressure. 2008.

16. **Ira Didenkulova**. Long Wave Dynamics in the Coastal Zone. 2008.

17. **Alvar Toode**. DHW Consumption, Consumption Profiles and Their Influence on Dimensioning of a District Heating Network. 2008.

18. **Annely Kuu**. Biological Diversity of Agricultural Soils in Estonia. 2008.

19. **Andres Tolli**. Hiina konteinerveod läbi Eesti Venemaale ja Hiinasse tagasisaadetavate tühjade konteinerite arvu vähendamise võimalused. 2008.

20. **Heiki Onton**. Investigation of the Causes of Deterioration of Old Reinforced Concrete Constructions and Possibilities of Their Restoration. 2008.

21. **Harri Moora**. Life Cycle Assessment as a Decision Support Tool for System optimisation – the Case of Waste Management in Estonia. 2009.

22. **Andres Kask**. Lithohydrodynamic Processes in the Tallinn Bay Area. 2009.

23. **Loreta Kelpšaitė**. Changing Properties of Wind Waves and Vessel Wakes on the Eastern Coast of the Baltic Sea. 2009.

24. **Dmitry Kurennoy.** Analysis of the Properties of Fast Ferry Wakes in the Context of Coastal Management. 2009.

25. **Egon Kivi**. Structural Behavior of Cable-Stayed Suspension Bridge Structure. 2009.

26. **Madis Ratassepp**. Wave Scattering at Discontinuities in Plates and Pipes. 2010.

27. **Tiia Pedusaar**. Management of Lake Ülemiste, a Drinking Water Reservoir. 2010.

28. **Karin Pachel**. Water Resources, Sustainable Use and Integrated Management in Estonia. 2010.

29. **Andrus Räämet**. Spatio-Temporal Variability of the Baltic Sea Wave Fields. 2010.

30. **Alar Just**. Structural Fire Design of Timber Frame Assemblies Insulated by Glass Wool and Covered by Gypsum Plasterboards. 2010.

31. **Toomas Liiv**. Experimental Analysis of Boundary Layer Dynamics in Plunging Breaking Wave. 2011.

32. **Martti Kiisa**. Discrete Analysis of Single-Pylon Suspension Bridges. 2011.

33. **Ivar Annus**. Development of Accelerating Pipe Flow Starting from Rest. 2011.

34. **Emlyn D. Q. Witt**. Risk Transfer and Construction Project Delivery Efficiency – Implications for Public Private Partnerships. 2012.

35. **Oxana Kurkina**. Nonlinear Dynamics of Internal Gravity Waves in Shallow Seas. 2012.

36. **Allan Hani**. Investigation of Energy Efficiency in Buildings and HVAC Systems. 2012.

37. **Tiina Hain**. Characteristics of Portland Cements for Sulfate and Weather Resistant Concrete. 2012.

38. **Dmitri Loginov**. Autonomous Design Systems (ADS) in HVAC Field. Synergetics-Based Approach. 2012.

39. **Kati Kõrbe Kaare**. Performance Measurement for the Road Network: Conceptual Approach and Technologies for Estonia. 2013.

40. **Viktoria Voronova**. Assessment of Environmental Impacts of Landfilling and Alternatives for Management of Municipal Solid Waste. 2013.

41. **Joonas Vaabel**. Hydraulic Power Capacity of Water Supply Systems. 2013.

42. **Inga Zaitseva-Pärnaste**. Wave Climate and its Decadal Changes in the Baltic Sea Derived from Visual Observations. 2013.

43. **Bert Viikmäe**. Optimising Fairways in the Gulf of Finland Using Patterns of Surface Currents. 2014.

44. **Raili Niine**. Population Equivalence Based Discharge Criteria of Wastewater Treatment Plants in Estonia. 2014.

45. **Marika Eik**. Orientation of Short Steel Fibers in Cocrete. Measuring and Modelling. 2014.

46. **Maija Viška**. Sediment Transport Patterns Along the Eastern Coasts of the Baltic Sea. 2014.

47. **Jana Põldnurk**. Integrated Economic and Environmental Impact Assessment and Optimisation of the Municipal Waste Management Model in Rural Area by Case of Harju County Municipalities in Estonia. 2014.

48. **Nicole Delpeche-Ellmann**. Circulation Patterns in the Gulf of Finland Applied to Environmental Management of Marine Protected Areas. 2014.

49. **Andrea Giudici**. Quantification of Spontaneous Current-Induced Patch Formation in the Marine Surface Layer. 2015.

50. **Tiina Nuuter**. Comparison of Housing Market Sustainability in European Countries Based on Multiple Criteria Assessment. 2015.

51. **Erkki Seinre**. Quantification of Environmental and Economic Impacts in Building Sustainability Assessment. 2015.

52. **Artem Rodin**. Propagation and Run-up of Nonlinear Solitary Surface Waves in Shallow Seas and Coastal Areas. 2015.

53. **Kaspar Lasn**. Evaluation of Stiffness and Damage of Laminar Composites. 2015.

54. **Margus Koor**. Water Distribution System Modelling and Pumping Optimization Based on Real Network of Tallinn. 2015.

55. **Mikk Maivel**. Heating System Efficiency Aspects in Low-Energy Residential Buildings. 2015.

56. **Kalle Kuusk**. Integrated Cost-Optimal Renovation of Apartment Buildings toward Nearly Zero-Energy Buildings. 2015.

57. **Endrik Arumägi**. Renovation of Historic Wooden Apartment Buildings. 2015.

58. **Tarvo Niine**. New Approach to Logistics Education with Emphasis to Engineering Competences. 2015.

59. **Martin Thalfeldt**. Total Economy of Energy-Efficient Office Building Facades in a Cold Climate. 2016.

60. **Aare Kuusik**. Intensifying Landfill Wastewater and Biodegradable Waste Treatment in Estonia. 2016.

61. **Mart Hiob**. The Shifting Paradigm of Spatial Planning in Estonia: The Rise of Neighbourhood Participation and Conservation of Built-up Areas through the Detailed Case Study of Supilinn, a Historic Suburb of Tartu City, Estonia. 2016.

62. **Martin Heinvee**. The Rapid Prediction of Grounding Behavior of Double Bottom Tankers. 2016.

63. **Bharat Maharjan**. Stormwater Quantity and Quality of Large Urban Catchment in Tallinn. 2016.

64. **Nele Nutt**. The Restoration of Nationally Protected Estonian Manor Parks in the Light of the Florence Charter. 2017.

65. **Üllar Alev**. Renovation and Energy Performance Improvement of Estonian Wooden Rural Houses. 2017.

66. **Simo Ilomets**. Renovation Need and Performance of Envelopes of Concrete Apartment Buildings in Estonia. 2017.

67. **Argo Kuusik**. Determining Biogas Yield from Industrial Biodegradable Waste. 2017.

68. **Katri Pindsoo**. Spatio-Temporal Changes in the Components of Extreme Water Levels on Estonian Coasts. 2017.